Identification and Characterization of Novel Antivirals for Seasonal Influenza A Virus

By

Marnie Jean Willman

A thesis submitted to the Faculty of Graduate Studies of

The University of Manitoba

In partial fulfillment of the requirements of the degree of

Doctor of Philosophy

Department of Medical Microbiology and Infectious Diseases

University of Manitoba

Winnipeg

Abstract

Seasonal influenza viruses cause approximately 3-5 million cases of illness and 250,000-500,000 deaths globally annually, burdening the healthcare system. Currently, the best intervention against seasonal influenza is the annual vaccine, which protects against Influenza Type A subtypes H1N1, H3N2, and Type B viruses, all of which are endemic in humans. However, vaccine strains must be decided one year before the season, as the dominant seasonal strains may change year to year, which can lead to reduced efficacy. Typically, the first line of post-exposure defense for severe or complicated influenza infection is antivirals such as Oseltamivir. However, influenza quickly gains resistance against antivirals, limiting their value for sustained use during outbreaks. By utilizing DiscoveryProbe pre-aliquoted drug panels from ApexBio against a seasonal strain of H1N1 influenza, I aimed to discover novel antivirals to identify more options for emergency antiviral use in the case of future severe cases or seasonal IAV infection. *In vitro* screening of FDA-approved drug panel from ApexBio identified two compounds that provided protection against A/Canada/RV733/2007 H1N1 with limited cytotoxicity in MDCK and A549 cells. Screening of the Natural Product library panel from ApexBio identified 12 compounds that provided protection with limited cytotoxicity. Testing these compounds against seasonal and pandemic H1N1, A/Hong Kong/1/68 H3N2, a recombinant VSV, and a seasonal Rhinovirus showed that several of the compounds were effective against a wide range of infectious agents. Testing in both MDCK and A549 cell lines showed that the effectiveness of the compounds occasionally differed between cell lines. Further characterization using immunofluorescent assays to track viral proteins during infection in the presence of the compounds of interest showed that sodium aescinate, calycosin-7-glucoside, oridonin, dioscin, and kinetin reduced viral protein fluorescence 24 hours post-infection.

Hemagglutination inhibition assays, attachment and penetration blockades, and attachment immunofluorescent assays suggested that oridonin and dioscin may be inhibiting on IAV attachment, while sodium aescinate and calycosin-7-glucoside may be having a negative effect on IAV penetration. These novel antivirals could provide new possibilities for treatment of influenza infections, and provide additional options for the management of inevitable future IAV outbreaks.

Dedication

This dissertation is dedicated to my mother, Christine Hustins, who inspired me to pursue my dream of graduate studies. I am so glad that of all the mothers in the world, you are mine.

Acknowledgments

I would like to thank my supervisor, Dr. Darwyn Kobasa, and my committee members, Dr. Kevin Coombs and Dr. Janilyn Arsenio, for their contributions to the project. Thank you to Angela Nelson, Dr. Keith Fowke, and Dr. Denice Bay at the University of Manitoba for their guidance and encouragement.

To my lab-mates and co-workers in Special Pathogens, thank you for your advice and assistance throughout my program, particularly to Robert Vendramelli, who performed the initial screen of teriflunomide, antazoline, and domiphen bromide, and assisted with initial experimental design. Robert Vendramelli, Aaron Gartner, Anders Leung, Michael Chan, and Nikesh Tailor, your kind words, amusing jokes, and colorful stories got me though some of the hardest days of my PhD. Thank you to my fellow graduate students, particularly Nathan Glowach, Jessie Lynch, and Robyn Thorington. I am so grateful for your friendship, support, and advice during the many ups and downs of my program.

Thank you to my husband, Josh. I would not have endured the challenges that this journey has entailed without your wisdom, love, and encouragement. To my mother Christine and my daughter Isabelle, you were the shining lights that guided me to the shore during the storm. I love all of you dearly, and feel so blessed to call you my family.

"Here's to the strong women. May we know them. May we be them. May we raise them."

–Michelle Obama

Preface

All of the work described in this dissertation was conducted at the National Microbiology Laboratory (NML, PHAC) in Winnipeg, Manitoba.

Results from this work are original and unpublished. I would like to thank the Veterinary Technician Services staff whose guidance and support during my murine experiments was so appreciated. Also, thank-you to the DNA Core at NML, who assisted in primer design and genomics for my project. Thank you to Dr. Jing Cao's group who kindly donated HeLa cells, and Dr. Nathalie Bastien's group who generously gave an aliquot of seasonal Rhinovirus and red blood cells for the work. Thank you to Dr. Jonathan Audet, Dr. Logan Banadyga, and Dr. Babu Sajesh who assisted with statistical and confocal analyses for this dissertation, and to Robert Vendramelli who provided extensive guidance and support during the early stages of experimental setup.

Conception of all studies for this dissertation were by Dr. Darwyn Kobasa, Dr. Kevin Coombs, and myself. I performed all experimental procedures, data analysis, and writing of the manuscript, which was edited by Dr. Darwyn Kobasa, Dr. Kevin Coombs, and Dr. Janilyn Arsenio.

List of Tables

List of Figures

List of Abbreviations

A549 – human hypotriploid alveolar basal epithelial cells
ANOVA – Analysis of variance
ApexBIO – ApexBIO Technology, LLC
ATCC – American Type Culture Collection
BSA – Bovine serum albumin
CDC – Centers for Disease Control
CL2 – containment level 2
CPE – Cytopathic effects
cRNA – Complimentary RNA
DMSO – Dimethylsulfoxide
DAPI – 4',6'-diamidino-2-phenylindole
DMEM – Dulbecco's modified Eagle medium
DNA – deoxyribonucleic acid
dNTP – deoxyribonucleotide triphosphate
FCS – Fetal calf serum
FDA – Food and Drug Administration
HA – Hemagglutinin
HAI – Hemagglutination inhibition
HK68 - A/Hong Kong/1/68 pandemic H3N2 IAV
IAV – Influenza A Virus
IC50 – Half-maximal inhibitory concentration
ICTV – International Committee on Taxonomy of Viruses
LAIV – live attenuated influenza virus
M1 – Matrix protein 1
M2 – Matrix proton channel 2
MA-HK68 – Murine-adapted HK68
MDCK – Madin-Darby canine kidney cells
MEM – Minimum essential medium
MOI – Multiplicity of infection
mRNA – Messenger RNA
Mx10 - A/Mexico/INDRE4487/2009 pandemic H1N1 IAV
NA – Neuraminidase
NEP – Nuclear export protein
NES – Nuclear export signal
NML – National Microbiology Laboratory
NP – Nucleoprotein
NPC – Nuclear pore complex
NS1 – Nonstructural Protein 1
NLS– Nuclear localization sequences
PA – Polymerase acidic protein
PB1 – Polymerase Basic protein 1

PB2 – Polymerase Basic protein 2
PBS – Phosphate buffered saline
PCR – Polymerase chain reaction
PFU – Plaque-forming units
PFU_{eq} – Plaque-forming unit equivalency
pH1N1 – pandemic H1N1 virus from 2009 pandemic
RBC – Red blood cell
RdRp – RNA-dependent RNA polymerase
RNA – Ribonucleic acid
RNP – Ribonucleoprotein complex
RV733 - A/Canada/RV733/2007
R-1644 – seasonal Rhinovirus ATCC-VR1644
SEM – Standard error of the mean
sH1N1 – Seasonal H1N1 virus
SI – Selectivity index
SOP – Standard operating procedure
$TCID_{50}$ – Median tissue culture infectious dose
TPCK - Tosyl phenylalanyl chloromethyl ketone
XTT – 2,3-Bis-(2-Methoxy-4-Nitro-5-Sulfophenyl)-2H-Tetrazolium-5-Carboxanilide
Vero – African green monkey kidney cells
vRNA – Viral ribonucleic acid
vRNP – Viral ribonucleoprotein
VSV-MERS – VSV/MERS-spikeΔ16 VSV MERS Virus
VTS – veterinary technical services
WHO – World Health Organization

List of Symbols

μm – micron
mM – millimolar
μM – micromolar
nM – nanomolar
μL – microliter
mL – milliliter
g – gram
α – alpha
β – beta
Δ – delta
° - degrees

Table of Contents

Chapter One: Introduction

1.1: Influenza Virus Biology

The material presented in this dissertation is focused on influenza Type A virus (IAV), an endemic virus in the human population which also poses a pandemic risk. IAV contains many strains, some of which infect various animal species including humans. This section contains a brief overview of how influenza A viruses are technically classified, how their genome is arranged, virus particle (virion) structure, and the influenza A virus life cycle.

1.1.1: Classification of IAV

Influenza viruses are part of the family *Orthomyxoviridae*, and further categorized as genera *Influenzavirus* A, B, C, and D[1]. Influenza A, B, and C viruses cause the most human disease, while D tends to cause disease in animals. *Influenzavirus* D was the most recently discovered and was isolated from swine and cattle[2].

Type A Influenza viruses are further categorized by their hemagglutinin (HA) and neuraminidase (NA) surface proteins[1]. There are 18 known subtypes of HA and 11 known subtypes of NA. Full-length amino acid sequence differences form the basis of subtype categorization for influenza viruses[3]. While there are many variations and subtypes of IAV, influenza B viruses are divided into lineages Victoria and Yamagata, rather than subtypes like IAV[3].

The natural reservoir of IAV is waterfowl[4]. The two most recently discovered influenza viruses, H17N10 and H18N11, originate in bats[5,6]. A total of 16 HA and 9 NA subtypes have been identified in birds, and some of these IAVs can infect a variety of other species, including swine,

horses, dogs, and bats (see Figure 1). The many of IAVs identified to date and their source of isolation are described in Table 1.

1.1.2: Organization of the viral genome

Influenza A viruses have a negative-sense, single-stranded, RNA genome containing eight different gene segments[7]. The segmented genome is of particular evolutionary importance to IAV because it allows genetic reassortment, which can generate novel strains of IAV (see Figure 2)[8].

All eight gene segments are required for successful virus replication[7]. While it was originally believed that each gene segment encoded a single protein, we now know that mRNA splicing and alternative open reading frames generate differences in core and accessory proteins produced by IAV. Of the eight gene segments contained within IAV, the primary ORF of segments 1-8 encode polymerase basic II (PB2), polymerase basic I (PB1), polymerase acidic protein (PA), hemagglutinin (HA), nucleoprotein (NP), neuraminidase (NA), matrix protein (M1) and an ion channel (M2), and non-structural protein 1 (NS-1), respectively[7,9]. The NS gene also encodes Nuclear Export Protein (NEP) by alternative mRNA splicing, which is important for export of viral ribonucleoproteins from the nucleus[10]. M2 is also be generated by alternative splicing, whereas unspliced matrix protein remains M1. Recently, two new accessory proteins termed PB1-F2 (a proapoptotic virulence factor) and PB1 N40 (whose function remains unknown) have been discovered and are generated by an alternative open reading frame[11,12]. PA also has an alternative accessory protein termed PA-X, also generated via an alternative open reading frame[13].

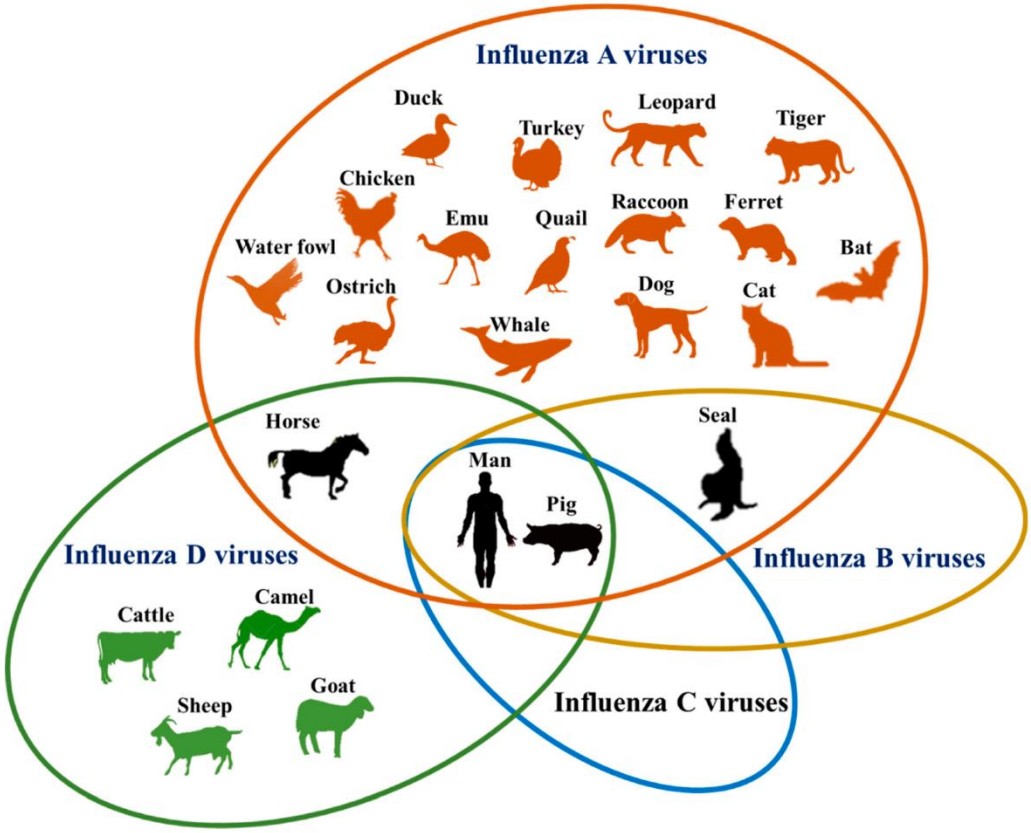

Figure 1. The many diverse hosts of influenza A, B, C, and D viruses with their potential overlaps of interspecies transmission. Image from Kuchipudi SV and Nissly RH. 2018. Vet. Sci. 5(3)[14].

Table 1. The subtypes of IAV isolated from various animal sources. Adapted from Sreenivasan et al. 2019, Viruses 11(6)[15].

IAV Subtype	Animal Host (Source of Isolation)
H1N1, H5N1	Tiger
H1-16, N1-9	Wild bird
H1-16, N1-9	Aquatic bird
H1-13, N1-9	Domestic bird
H10N7, H3N8	Seal
H13N2, H13N9	Whale
H1N1, H3N2, H5N1, H9N2, H10N4	Mink
H1N1, H3N2, H5N1, H5N6, H7N2	Cat
H1N1, H1N2, H3N2, H5N1, H3N8	Dog
H7N7, H3N8	Horse
H1N1, H1N2, H3N2, H4N6, H5N1	Pig
H3N2-like	Cow
H1N1, H2N2, H3N2, H5N1, H7N7, H9N2	Human

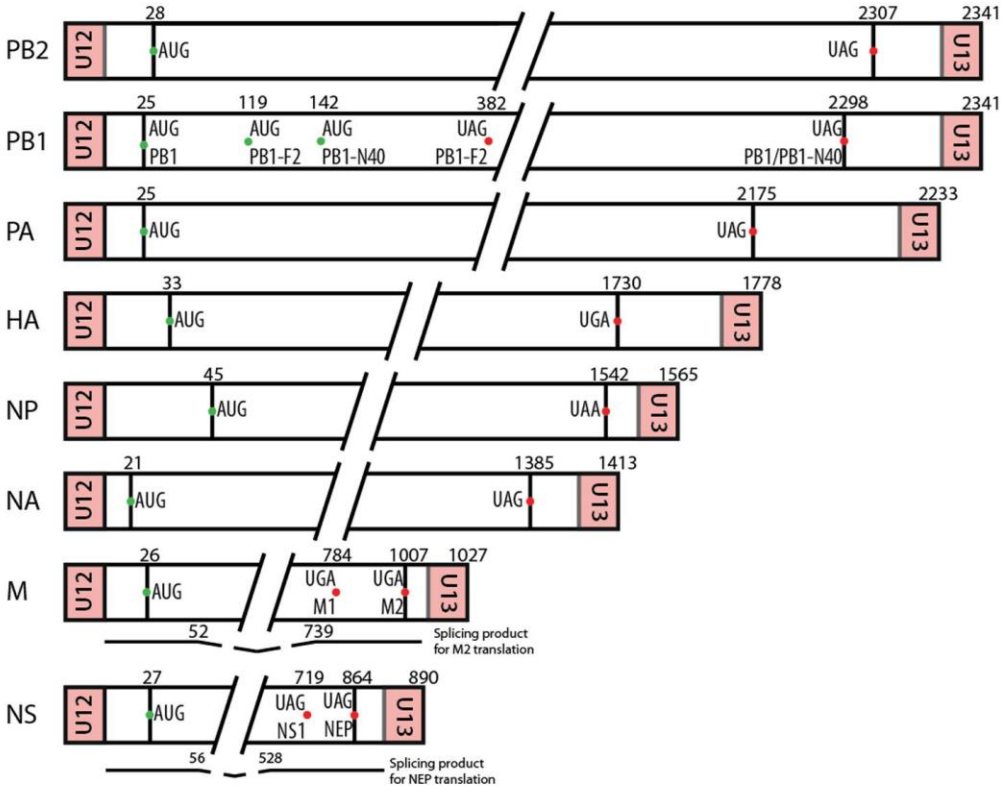

Figure 2. The structure of the IAV genome. The eight gene segments of IAV RNA during replication is a fundamental, unique construction that can form any of the below. The individual gene segments are pictured here, along with their start (AUG) and stop (UAA/UAG) codons. Image from Ferhadian D et al. 2018. Front. Microbiol.https://doi.org/10.3389/fmicb.2018.00559[16].

PB1, PB2, and PA are the largest proteins of IAV, which come together to form a polymerase, termed RNA-dependent RNA polymerase (RdRp), responsible for performing viral transcription and genome replication[17]. The complex of each viral RNA, a single copy of the RdRp, and NP forms the viral ribonucleoprotein (vRNP) complex. Transcription and genome replication are initiated by the entrance of vRNPs into the nucleus of an infected cell.

To summarize the roles of other essential proteins of IAV, HA, which is a surface protein of IAV, is required for attachment (receptor binding) to host cells, as well as entry and fusion into the host cell[18]. The M segment of IAV encodes two different viral proteins (yielded through RNA splicing), termed M1 and M2. The M2 proton channel facilitates virion uncoating and is responsible for the proton flux into the virus that triggers release of the viral contents into the cytoplasm, while the M1 forms a protein shell below the lipid bilayer and interacts with the vRNP during assembly. NS1 contributes to IAV pathogenicity and virulence, and NEP is associated with viral RNP complex export from the nucleus. NA removes sialic acid, triggering release of progeny virus from the host cell. Regions at the end of the IAV genome at the 5' and 3' ends of each segment are highly conserved and required for RNA packaging, acting as promoters for initiation of replication and transcription[19].

In addition to the individual gene segments, more variety can occur in IAVs through mutation acquisition. Lack of proofreading by IAV polymerase introduces additional mutations that can assist with immune escape, transmission, and subsequent adaptation to a novel host. IAV mutations can accumulate at a rate of 2.0×10^{-6} mutations per site per infectious cycle for human IAVs[20].

1.1.3: Structure of the IAV Virion

Influenza A viruses are pleomorphic, which means they are able to take on a filamentous or spherical shape (see Figure 3), with virion size averaging 80-120 nm in diameter, and can extend to a length of 20-50 μm[21]. The lipid membrane is derived from the host plasma membrane and contains membrane rafts assembled from cholesterol, sphingolipids, phospholipids, glycoproteins, and surface proteins HA, M2, and NA[22].

1.1.4: The Life Cycle of Influenza Virus

1.1.4.1: Receptor binding

Successful IAV infection of the respiratory tract epithelial cells is dependent on the viral HA protein binding to host sialic acid receptors (the most common being N-Acetylneuraminic acid in human and other mammalian cells) on epithelial cells. The human upper respiratory tract contains primarily α-2,6-linked sialic acid, while avian respiratory and gastrointestinal tracts contain primarily α-2,3-linked sialic acid, driving preferential binding of species-specific IAVs[23]. Pigs have historically been called a "mixing vessel" of IAV because their respiratory tracts contain both α-2,3- and α-2,6 sialic acid linkages, meaning they can be infected with both human and avian influenza viruses, though this has been challenged by some research groups[24]. Avian species can directly transmit to swine, and a swine mixing vessel can act as an intermediate adaptation host for IAV, allowing a shift in species preference, an event that could enable an avian IAV to infect a human host.

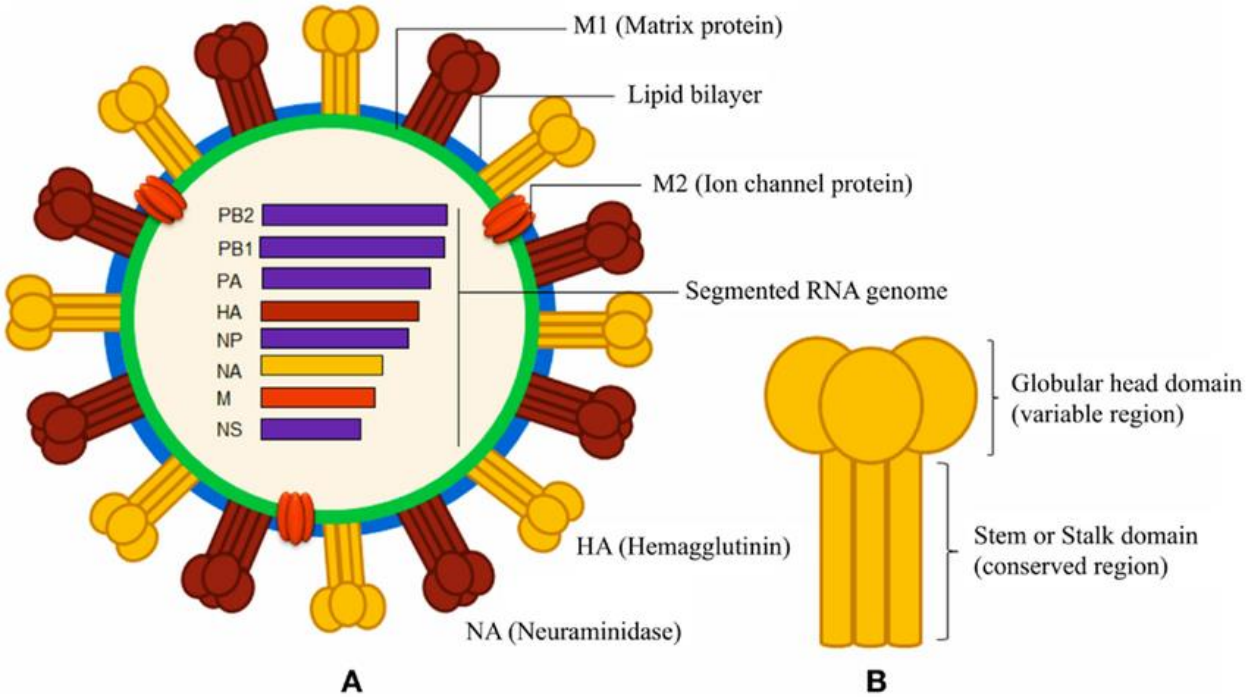

Figure 3. A schematic of the influenza A virion structure.The viral envelope is primarily composed of a lipid bilayer (seen in blue) and an M1 protein layer (seen in green), studded with glycoproteins, HA, and NA surface proteins (seen in yellow and brown, respectively). M2 ion channels (seen in orange) stabilize the pH, equilibrating it across the virus membrane. At the core are the eight gene segments (seen in red, purple, yellow, and brown), making up the RNPs (see section 1.2.3). Figure 3b shows the structure of hemagglutinin surface protein, which consists of a globular head and stalk domain. HA is a homotrimeric protein containing three identical monomers (HA0, HA1, and HA2) in the globular head domain and a conserved stalk. Image from Lofano G et al. 2015. Front. In Immun. DOI: 10.3389/fimmu.2015.00336[25].

HA is a homotrimeric surface glycoprotein with distinct head and stalk regions that undergoes several conformational changes during IAV infection[26]. The HA0 precursor is approximately 75 kDa and undergoes proteolytic cleavage to become products HA1 (58 kDa) and HA2 (26 kDa)[27]. Cleavage of HA0 into these subunits is required for fusion to the host endosomes to occur. The transmembrane domain of the stalk region of HA is buried in the viral envelope, and the rest of the stalk extends away from the envelope while the globular head attaches to the sialic acid receptor of the host cell.

1.1.4.2: Receptor-mediated endocytosis and membrane fusion.

Internalization of the IAV into the host cell is cell-type-dependent and can be achieved by clathrin-dependent or clathrin-independent endocytosis, caveolae, or macropinocytosis[28–30]. Upon fusing with the endosome, endosomal acidification triggers an irreversible conformational change in HA. This conformational change results in HA1 relocating and HA2 refolding, which allows the fusion peptide located on HA2 to insert into the viral and target membranes[31]. At the same time, the M2 ion channel moves protons into the interior of the virion which results in conformational changes that dissociate the RNP from the matrix protein, releasing the viral genome into the cytoplasm to initiate viral replication.

1.1.4.3: Transcription and translation of the viral genome

IAV vRNA replication has two distinct steps. In the first, complementary RNAs (cRNAs) are synthesized and are a replication intermediate which acts as a template for genome replication[31]. These cRNAs are templates for late transcription, which forms the negative sense

single-stranded RNA genome that becomes the final IAV genetic information, forming the second step of vRNA replication. cRNAs can be used as a template to produce more copies of viral RNA rapidly.

vRNP complexes are released into the cytoplasm and transported to the nucleus for transcription. Trafficking of the viral constituents for transcription is mediated by nuclear localization sequences (NLSs). NP is an important viral protein to note because the NLS on NP alone is sufficient to import vRNP to the nucleus[32]. The NLSs on vRNPs access the nucleus via the nuclear pore complex (NPC).

The viral RdRp, comprised of a single copy of PA, PB1, and PB2, is responsible for producing vRNA (viral RNA), cRNA (complimentary RNA), and viral mRNAs. For IAVs, the beginning of mRNA synthesis is marked by an event called "cap snatching". For eukaryotic gene expression, a 7-methylguanosine cap is added to mRNA for stability, export, and translation of the transcript. For RNA viruses, this is a problem because they are often unable to use cellular RNA capping machinery. While some viruses encode their own capping machinery, IAV uses a cap snatching method for viral mRNA synthesis[33]. To perform this process, the ribonucleoprotein complex takes 5'-capped transcripts produced by the cellular DNA dependent RNA polymerase II.

For cap snatching to begin, the PB2 subunit binds short capped oligomers (originally from the host pre-mRNA). These oligomers are cleaved by PA-contained endonuclease, after which the product is used by the PB1 subunit to prime mRNA synthesis[34]. Autopolyadenylation is caused by polymerase stuttering, which occurs at a unique oligo-U stretch at the 5' end of the vRNA[34]. This process avoids the need for viral-encoded capping enzymes and host polyadenylation machinery while producing translation-competent viral mRNAs. The poly(A) tail is added via a stuttering

mechanism of polyadenylation, triggered by viral polymerase slippage upon reaching a stretch of uridines followed by a double-stranded RNA barrier[35]. While this is occurring, the viral mRNAs for NA, HA, and M2 are transported by cytosolic ribosomes to the rough Endoplasmic reticulum for translation. Here, the host cell ribosomes translate the mRNA. Host cell ribosomes in the rough Endoplasmic reticulum then produce the final envelope proteins from the viral mRNA.

1.1.4.4: Assembly and Budding

Assembly and budding occur in four distinct stages; Assembly of viral components, bud initiation, bud growth, and pinching of the bud from the plasma membrane.

Once viral proteins have been folded into their final conformation in the Endoplasmic reticulum (ER), viral components (especially HA, NA, and M2, which are found in the viral envelope), are trafficked to the assembly site at the apical plasma membrane by Rab proteins such as Rab11[36]. Rab11 also plays a role in delivering M2 to the plasma membrane, allowing membrane scission and release to take place[37]. HA and NA are glycosylated in the Endoplasmic reticulum, an essential feature for IAV immune evasion and viral fitness[38]. Palmitoylation of HA and M2 (during which fatty acids are covalently attached to HA) assists in the trafficking and accumulation of viral constituents at these lipid rafts for assembly and budding[39].

Influenza utilizes lipid raft domains composed of cholesterol and sphingolipid-enriched regions as sites of assembly and budding[40]. While the complete mechanism of virus bud initiation is unknown, it is thought to be mediated by the HA and M2 proteins[41]. During budding, the amphipathic helix in the cytoplasmic tail of M2 targets M2 to the assembly site, which causes negative curvature because of the cholesterol rich environment caused by lipid raft presence[42].

This mechanism stabilizes the budding site so all viral proteins can be assembled for release. Some studies have shown that the negative curvature induced by the M2 may be enough to initiate budding, scission, and subsequent viral release, as mutations in M2 resulted in an absence of these events[42]. The budding process concludes with the membrane scission, which marks the end of the exit process of the newly made virion from the host cell. M2 has a cytoplasmic tail that is essential for this process, as some mutations in M2 result in prevention of scission and, ultimately, virion release[42,43]. The budded virion is then perched on the edge of the host cell in preparation for separation. To release the virion from the host cell, NA cleaves the sialic acids from the receptors near the budding site enabling the release of progeny viruses.

1.2: Animal Models for IAV Studies

There are a number of animal models that have different advantages and disadvantages with regard to studying IAV disease, pathology, transmission, immunology, and therapeutics. Some commonly used models for seasonal IAV research are mice (*Mus musculus)*, ferrets (*Mustela putorius furo*), and guinea pigs (*Cavia porcellus*).

1.2.1: Mice (Mus musculus)

Mice are one of the most commonly used models for IAV studies for a variety of reasons[44]. Mice are convenient and easy to house, are small in size, and low cost to purchase and maintain[44]. However, in some cases, the IAV must be adapted through serial infections or mutations to be pathogenic in mice. When using a mouse-adapted strain of IAV, IAV-infected mice develop lung

inflammation and immune changes that can be measured for overall response to IAV vaccines and viral infections, which can make them a good model for disease study[45].

1.2.2: Ferrets (Mustela putorius furo)

Ferrets are considered the "gold standard" for testing IAV vaccines and therapeutics[46]. Ferrets are available as "influenza-free" animals, which ensure experimental results are exclusively from introductions of experimental viruses. Ferrets are also naturally susceptible to human IAV, so adaptation is not required. Their clinical symptoms and progression very closely mimic human IAV infections, and transmissibility is similar as well. However, not all reagents for analysis (such as antibodies) are commercially available, limiting potential studies, and husbandry and purchasing are more expensive.

1.2.3 Guinea pigs: (Cavia porcellus)

Guinea pigs make a good model for IAV transmission. Similar to ferrets, the IAV does not need to be adapted for successful infection[47]. Two predominant reasons why guinea pig models are not as popular as murine and ferret models is that they do not show the same clinical signs of disease, and there is a lack of available reagents (limiting potential studies). Unlike mice, guinea pigs can be used for transmission studies because they can spread IAV via respiratory droplets, contact transmission, or small airborne droplets to their cage-mates when housed together[47].

1.3: The Significance of Past and Present Influenza A Viruses

1.3.1: Major influenza pandemics of recent human history (1918-present)

There have been four major IAV pandemic events in recent history (defined as the last ~100 years) (see Figure 4). Pandemic influenza refers to an outbreak of a new, often highly transmissible strain of influenza virus compared to the currently circulating strain due to lack of pre-existing immunity within the population. Pandemic viruses can be the outcome of major reassortment events or emergence from an animal reservoir.

The first and most devastating pandemic of the 20th century was Spanish Influenza, a pandemic H1N1 virus. The virus emerged in early 1918, with a second wave of infections occurring in the fall of 1918[48,49]. Spanish Influenza was the cause of over 50 million deaths worldwide and continues to be one of the most lethal biological events in human history. The virus has now been reconstructed, and studies using mice, ferrets, and non-human primates (NHPs) have successfully mimicked the morbidity and mortality seen during the 1918-1919 pandemic[50–55].

The next pandemic occurred in 1957, widely called "Asian Influenza", and was an H2N2 reassortant virus (genes between IAVs had been exchanged, generating a new pandemic virus). A reassortment of avian and human influenza viruses, this new virus had a backbone of previously circulating human H1N1 with avian H2N2 PB1, HA, and NA genes[56]. This outbreak was first reported in Singapore and proceeded to cause an estimated 1.1 million deaths globally[57]. Interestingly, as the H2N2 pandemic gained traction, previously rampant H1N1 influenza viruses disappeared from circulation[58].

In 1968, "Hong Kong flu" emerged. This H3N2 influenza virus killed an estimated 1 million people globally, with half of those victims being under the age of 65[59]. This virus contained

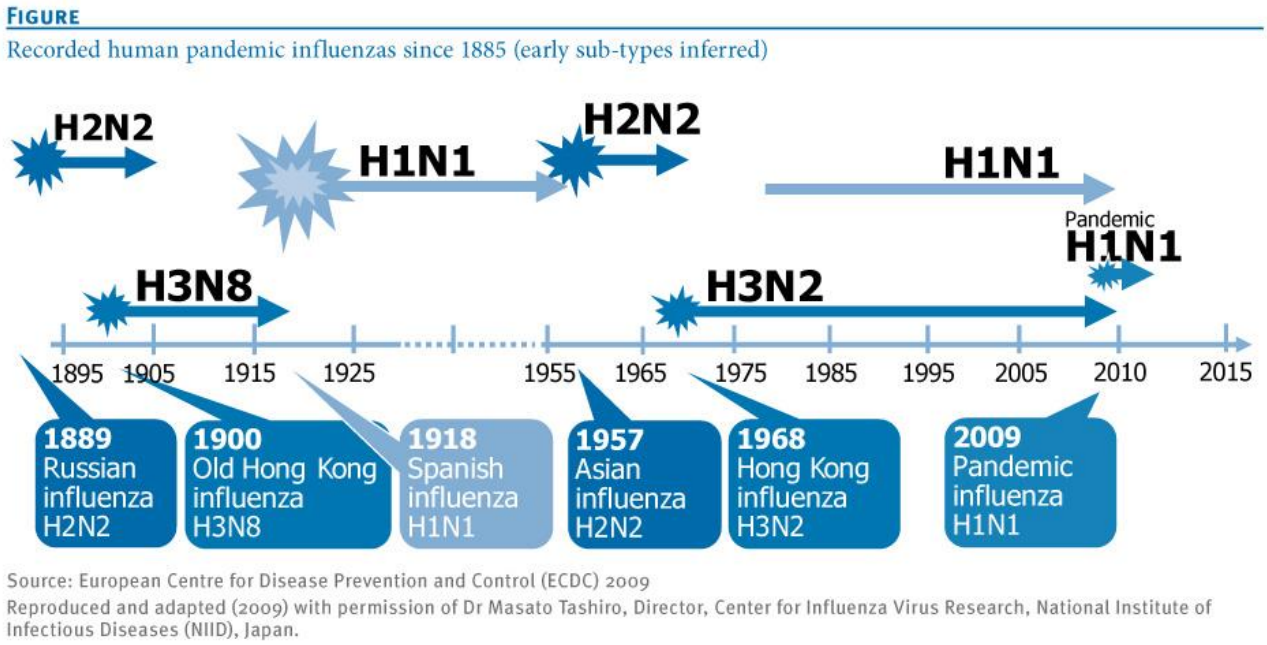

Figure 4. A timeline by the European Center for Disease Prevention and Controladapted by Dr. Masato Tashiro following the 2009 H1N1 outbreak. Image from ECDPC, 2010, https://www.eurosurveillance.org/content/10.2807/ese.15.01.19458en?crawler=true#html_fulltext.

an H3 HA from an avian virus which had previously adapted to attach to human cells[60]. The avian-derived PB1 gene segment improved transmissibility between humans, in addition to increasing viral growth by enhancing viral polymerase complex activity[61,62]. This pandemic occurred in two seasons, with the first spanning late 1968 to mid-1969 and the second occurring from late 1969 to mid-1970[63].

Chronologically, the next pandemic outbreak was caused by an H1N1 virus in 1977, but it is not technically considered a novel pandemic. Sequencing of the genes revealed that the virus was missing the evolutionary changes that naturally occur in IAVs over time[64]. Because of this interesting fact, and given that the virus was almost identical to 1950's H1N1 which was no longer in circulation, the virus was suspected to have been an accidental release of an experimental IAV strain from a laboratory, rather than a natural outbreak of a novel IAV[65]. The overall death toll is rarely estimated, but considered less than 5 per 100,000 individuals, less than the seasonal influenza causes in a typical year[66].

The most recent major IAV pandemic occurred in 2009 from a reassortment of circulating avian, porcine, and human IAVs[67]. This virus emerged from a 'triple-reassortant' lineage, containing avian-derived PB2 and PA, human-derived H3N2 PB1, NA and M from Eurasian avian-like swine H1N1, and classical swine HA, NP, and NS[68]. While the majority of cases were mild and self-limiting, the 12-month pandemic resulted in an estimated 284,500 deaths from overwhelming respiratory and cardiovascular symptoms[69].

As IAVs circulate and replicate, their genes continue to mutate over time. The 2009 H1N1 pandemic IAV replaced the previously circulating seasonal H1N1 virus and continues to circulate along with H3N2 and influenza B viruses in the human population. These influenza viruses are endemic in humans and are all included in the annual seasonal influenza vaccine.

1.3.2: Pandemic potential of IAV

IAV is a constantly changing virus with high genetic variability, many potential hosts, and a flexible genetic reassortment system. The two terms predominantly used for these genetic changes are "genetic drift" (see Figure 5A) and "genetic shift" (see Figure 5B). Genetic drift refers to the small genetic mutations that occur from general replication, while genetic shift refers to major changes that occur when gene segments from other IAVs are reassorted with current gene segments, forming an entirely new and distinct virus, compared to what was previously circulating. Genetic shift and drift may or may not lead to a subset effect called antigenic shift and drift, driven primarily by changes in HA and NA surface proteins, in which genetic changes are substantial enough to cause antigenic variability[70]. Antigenic changes can generate a novel virus (i.e., possession of a new HA and/or NA, and thus a new subtype of IAV), triggering the need for a new vaccine or a potential outbreak due to lack of existing immunity within the population. An example of this phenomenon occurred both in 1957 and 1968 when antigenic shift led to a new subtype that was antigenically distinct from the circulating human virus at the time of the pandemic[71]. These viruses were more readily able to cause a pandemic because the H1 HA was derived from an animal virus source.

Reassortments between the different HA and NA subtypes can also cause major genetic changes in IAV, triggering the emergence of new IAVs. There are a total of 18 HA and 11 NA subtypes currently known that can be reassorted between IAVs. Of these, two of the HA subtypes (H17 and H18) and two of the NA subtypes (N10 and N11) are not known to circulate outside of bats because of a species-specific residue in the PB2 gene[72]. These bat HA and NA proteins are canonically distinct from other types of HA/NA influenza viruses (for example, H17

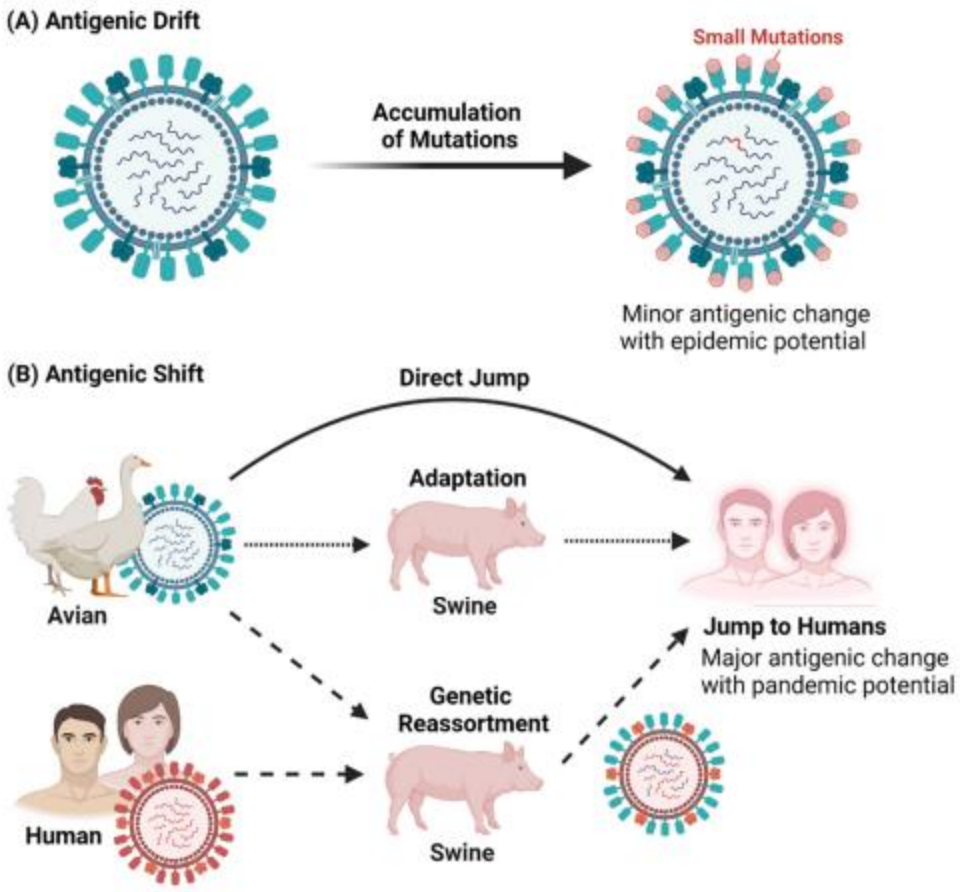

Figure 5. Depictions of antigenic drift (A) and shift (B), which result in genetic reassortments and can cause variations in circulating IAVs. Image from Yeo, JY and Gan SK. 2021. Viruses 13(2276)[74].

and H18 do not bind to sialic acid receptors), which limits the likelihood that they will infect other species, though there is always a possibility of this changing through adaptation[73]. The remaining 16 HA and 9 NA subtypes are found circulating in wild waterfowl and shorebirds, which are considered the primary reservoir of Type A influenza viruses.

1.3.3: Epidemiology and burden of influenza A virus (IAV)

Influenza viruses are a considerable healthcare burden, causing substantial global morbidity and mortality. In the United States alone, there were as many as 41 million cases of illness, 710,000 hospitalizations and 51,000 deaths annually from 2010 to 2023[75]. In Canada, influenza makes the list of "Top 10 Leading Causes of Death", averaging 12,200 hospitalizations and 3,500 deaths each year[76]. The general figure given by the World Health Organization (WHO) for the global burden of seasonal IAV is 3-5 million severe cases of illness and 290,000-650,000 deaths each year[76]. Seasonal IAV poses a serious problem for the economy, particularly when IAV infections cause children to miss school, absenteeism for all ages, and additional associated hospitalization costs[77]. IAV is easily transmitted via respiratory aerosols, droplets, or contact transmission, which can be a source of nosocomial or community-acquired infections[78].

Seasonal influenza estimates have improved over time with the establishment of the Global Influenza Hospitalization Surveillance Network (GIHSN), which conducts burden estimates and files reports on influenza cases[79]. FluView (CDC) and FluWatch (Government of Canada) are two examples of many other surveillance networks now in existence for proper monitoring and recording of seasonal influenza cases and outbreaks.

Seasonal IAV disproportionately affects children under two years of age and adults over 65 years of age[80,81]. In infants and young children, the immune system is still developing, often

leading to insufficient innate and adaptive responses that limit effective viral clearance. They exhibit reduced interferon responses, immature T cell populations, and limited immunological memory, all of which contribute to higher viral loads and prolonged illness[82]. Conversely, older adults experience immunosenescence, a gradual decline in immune competence characterized by reduced B and T cell diversity, impaired antigen presentation, and chronic low-grade inflammation[83]. This aging immune profile results in weaker vaccine responses and a higher likelihood of severe outcomes, including complications such as pneumonia. These immune system dynamics significantly influence the epidemiology of influenza, as both the very young and the elderly serve as vulnerable reservoirs for transmission and severe disease. Beyond age, sex differences also play a role in viral infection, transmission, and immune response. Biological sex influences immune regulation, with females generally producing stronger innate and adaptive immune responses[84]. These differences can impact both disease severity and response to therapeutics. In addition to this, adult cases add to these numbers, further increasing the economic and healthcare burden of IAV. Seasonal influenza is estimated to result in 11.2 billion dollars in healthcare and economic losses in the United States alone each year, with eight billion dollars of this being indirect economic losses[85].

1.3.4: Transmission

Three routes of human IAV transmissions have been identified: Droplets deposited in the upper respiratory tract from the air (these are inhaled but do not reach the lungs), droplet nuclei (small enough to be inhaled and reach upper and lower respiratory tracts), and contact transmission (particles from fomites or people are transferred to mucous membranes)[78]. Humidity and temperature have also been identified as factors that can affect transmission likelihood, because

higher humidity increases virus survival and lower temperatures increase the number of indoor gatherings[86]. Once IAV has successfully entered the upper respiratory tract, the virus attaches to glycan receptors with differing sialic acids on epithelial cells.

1.3.5: Clinical symptoms and disease progression

Seasonal influenza viruses have an incubation period of 1-4 days, on average[76]. Seasonal influenza is characterized by rapid onset of respiratory symptoms, including sore throat, coughing, sneezing, and nasal discharge[76]. In addition, fever, malaise, headache, myalgia, chest pain, and many other symptoms are common during active IAV infections[76]. Influenza is more dangerous for those with underlying conditions or comorbidities such as diabetes, asthma, and HIV, as well as those over 65 years of age and those under two years of age.

1.4: Current Therapeutics for IAV

Vaccines, also referred to as the "seasonal flu shot", are our best protection against the virus and the only preventative measure currently available. Severe IAV infections may require treatment with antivirals, though this can result in antiviral resistance.

1.4.1: Seasonal influenza vaccine: Our best protection against IAV

A seasonal vaccine designed to protect against predicted circulating strains is the best preventative measure we currently have for IAV. Twice per year, the WHO Consultation on the Composition of Influenza Vaccine is held to analyze this collected data and decide which strains

will be included in the seasonal vaccine platform in the coming year[87]. However, the flu shot requires 8-12 months to be made in a high enough volume for distribution. Emergence of a new IAV or incorrect prediction during this long manufacturing delay means that the differences between the predicted and circulating strains could cause a poor vaccine match[88]. A vaccine mismatch occurred 2021, when the H3N2 portion of the seasonal vaccine did not match the circulating strain, resulting in higher-than-normal rates of morbidity and mortality during the 2021/2022 flu season[89].

Once the virus strains have been chosen, manufacture of the vaccine can begin. To generate the embryonated-chicken-egg-based vaccine, the viruses selected for the upcoming flu season are injected into eggs to replicate. The virus is then purified from allantoic fluid and inactivated prior to adding it to the vaccine formulation[90]. This approach enables rapid growth of the virus and high enough titers to make the required number of doses of the vaccine. Some cell-only approaches are available for those who have egg allergies, but these vaccines cost more to produce due to the elevated cost of materials required, and are less desirable for mass distribution[90,91].

The currently available influenza vaccines come in a quadrivalent “flu shot”, which protects against two Influenza A subtypes and two Influenza B lineages, and a trivalent “flu shot”, which protects against two Influenza A subtypes and one Influenza B lineage[92]. These vaccines are typically inactivated viral particulates that boost immunity by stimulating B cells, thereby generating memory antibodies to be reactivated when an individual is infected[93]. There is also a nasal vaccine available in the form of a LAIV (live attenuated influenza virus). LAIVs are temperature-sensitive mutants that are selected because they only grow at lower temperatures than the infection site of influenza in humans, eliminating their ability to infect and replicate in host cells as they would in a typical infection[94,95]. LAIVs are desirable because they also have been

reported to boost preexisting cross-reactive T cells, primarily NP-specific responses, leading to an overall improved response to the vaccine and potentially better future protection[96].

However, despite best efforts, vaccine hesitancy remains a major barrier to widespread herd immunity against influenza, which occurs when enough people are vaccinated to protect those who cannot be vaccinated because of medical conditions or their age. Herd immunity protects the unvaccinated because it limits their exposure by ensuring those around them are protected, forming a "bubble" of protection. Hesitancy can occur due to risk perception, past behavior, personal experiences, or misinformation[97]. For this reason, along with the inconvenience and cost of requiring an annual influenza vaccine reformulation and distribution, the universal influenza vaccine remains highly sought after[98]. So far, no universal vaccine has been found, despite the best efforts of funding agencies, including the Bill and Melinda Gates Foundation and researchers in facilities around the world. Whether or not one will come to fruition remains a matter of debate[99].

1.4.2: Available antivirals against IAV: A last resort

Several antivirals are available for use against seasonal IAV infections, although they are considered a last resort and not a preventative measure. As described by Allen, *et al.,* practitioners are now trained and advised on the appropriate use of IAV antivirals, which includes testing for IAV prior to prescribing or administering an appropriate antiviral[100].

The first class of antivirals developed against IAV were adamantanes (including amantadine and rimantadine), which bound the M2 ion channel of IAV to prevent acidification of the interior of the virion in the endosome during entry, thus blocking hemagglutinin-mediated fusion[101]. Since then, mutations in the M2 gene of IAVs have appeared, causing resistance to these

antivirals[102]. Oseltamivir is an NA inhibitor that blocks IAV budding from infected cells by binding directly to NA[103]. However, the appearance of the H275Y mutation in IAV, which confers oseltamivir resistance, has resulted in reduced use[104]. Favipiravir was introduced shortly after, which targeted and bound to IAV polymerase, making it a potent polymerase inhibitor[105]. However, mounting resistance caused by a K229R mutations of the IAV PB1 gene in order to escape this mechanism of antiviral-induced arrest has made favipiravir a less desirable option for IAV treatment[106]. Zanamivir is another neuraminidase inhibitor that was highly effective against IAV in adults and children, but IAV later developed resistance during clinical trials by mutating the neuraminidase gene (termed the Q136K mutation) to avoid antiviral binding[107,108]. Peramivir is an NA inhibitor that can be used in tandem with oseltamivir or zanamivir and has been used occasionally against severe IAV but has still only been approved for emergency use[109,110]. The most recent IAV antiviral, Baloxavir, came to market in 2018 and targets the endonuclease function of the RdRp PA subunit[111]. However, this antiviral is now used sparingly, as polymerase subunit mutations (namely, PA I38T) have begun to appear in clinical cases, indicating the beginning of antiviral resistance by IAV[112].

The process of novel antiviral discovery and characterization from bench to practice takes a substantial amount of time and resources. The average pharmaceutical drug costs $314 million to $2.8 billion to produce and thoroughly test, and only a small proportion of drug hopefuls are successfully brought to market[113]. While it is evident that more antiviral options for influenza are needed, this process is expensive and time-consuming, which limits experimentation done to find new treatments.

The process of drug discovery, whether natural or synthetic in origin, begins with primary assays to determine potential effectiveness or target validation[114]. Following this, assays

that examine toxicity, cellular effects (e.g., metabolism), and confirmations of primary assays (such as initial antiviral efficacy assays) are performed. If these assays are successful, the candidates proceed along the drug discovery pipeline to more in-depth mechanistic testing, and *in vivo* efficacy animal testing before proceeding to clinical trials for further testing.

Existing IAV antivirals are excellent therapeutics, providing rapid, life-saving treatment for severe disease. However, antiviral resistance will continue to be a problem in great part because of the ability of IAV to mutate its genes and swap gene components, enabling improvement of viral fitness, transmissibility, and other aspects. The expense and time to generate treatments compared to the time IAV takes to mutate is long, and we must be prepared for the next imminent IAV outbreak. For these reasons, it is necessary to continue the search for novel IAV antiviral candidates.

1.4.3: Antiviral discovery: The search for novel candidates

One systematic approach to drug development involves targeting specific proteins of the virus based on their known effect on viral replication. If a novel antiviral can prevent the activity of a viral protein, it is likely to block viral replication. For example, many of the antivirals currently in use for IAV target the NA protein because NA is on the surface of IAV and thus is easily accessible[115]. The portion of the NA protein that antivirals bind (the residues involved in the catalytic function of the protein itself) is conserved and located on the surface, as well as being an essential viral protein for replication[115]. These features make NA a desirable target for novel antiviral discovery. By targeting these proteins, one can stop or limit specific stages of the replication cycle of IAV, reducing infectious and replicative potential.

Another way of discovering novel antivirals is to target host factors involved in viral processes such as attachment, entry, and release. Viruses by nature hijack host processes during infection because they lack the machinery required for successful replication. Using strategies like application of protease inhibitors, Hsp90 inhibitors, and lipid raft inhibitors, the virus can be stopped from replicating by barring non-viral but essential host functions, eliminating further infection[116].

With recent technological advancements, using computer-aided drug design programs for antiviral discovery is becoming more widely used. Testing and designing new antivirals for influenza has traditionally fallen into the crux between biology and chemistry. But, computer-aided drug design is a way to predict binding patterns and identify molecular targets within the virus for a new antiviral[117]. This approach tackles the problem by designing antivirals based on how the computer program predicts they will effectively bind and work against IAV[117]. Computer-aided drug discovery is a relatively new field, and there is optimization and algorithm improvement needed to perfect this method of antiviral discovery.

Discovery of novel antivirals can also be performed by repurposing existing compounds. To approach the primary assay portion of drug discovery, utilization of pre-existing FDA-approved compounds that can be repurposed for IAV treatment and natural products that can be used against IAV can be applied[118,119]. There are a number of benefits to using existing FDA-approved compounds for new purposes, including the fact that they have undergone toxicity testing in cell and animal models, and they may be readily available in the pharmaceutical market for purchase. They have also undergone human clinical trials for their specified application. Using previously approved compounds limits the need for early stages of availability, toxicity testing, and other preliminary analyses. As well, many extracts and natural

source compounds have been used to treat IAV-like symptoms including, malaise and fever, but few have undergone the testing required to make them an FDA-approved IAV antiviral. Given these promising compounds lack the stringent testing required for novel pharmaceuticals, they present an opportunity for further novel antiviral discovery.

No matter which strategy is adopted, identifying antivirals that are relatively effective against multiple subtypes of IAV is essential because many IAVs circulate seasonally at any given time. An antiviral that is only effective against a single subtype of IAV leads to limited potential and lowers usefulness. Selecting antiviral targets that will not quickly induce antiviral resistance but are also cross-protective against multiple seasonal IAVs are the primary goals of novel antiviral discovery. For a target to be a good one, it must be accessible by the antiviral (which is why surface proteins are a popular selection), relatively constant (continual changes in conformation or mutations can lead to antiviral resistance), and integral to the functioning of the virus (the antiviral must stop a process that the virus needs to survive such as attachment, transcription/translation, exit, etc.).

Influenza vaccination is our best defense against IAV infection, though there are drawbacks to this approach. Namely, the specificity of the vaccine to the strain of influenza the vaccine protects against, and the limited duration of protection the vaccine provides. While antivirals do exist for IAV, they are limited in number, and many options currently available have either caused widespread antiviral resistance and have been largely discontinued, or are beginning to cause resistance-associated mutations in IAVs. Discovery of novel antivirals would make us better prepared for the inevitable next IAV pandemic, and reduce morbidity and mortality from seasonal or pandemic outbreaks in the years to come.

1.5 Research Goals

1.5.1: Rationale

Because IAV gene mutations occur frequently due to errors in polymerase activity, selective pressure, a range of environmental factors, and other events, new antiviral options are needed to address the ever-increasing problem of antiviral resistance. With growing resistance against the limited number of approved antivirals currently available, alternative treatments for severe, life-threatening IAV infections are needed. By utilizing the DiscoveryProbe FDA-approved Compound Library, and DiscoveryProbe Natural Product Compound Library (both provided by ApexBio), I aimed to discover novel antivirals that can effectively reduce seasonal influenza virus titers with low cytotoxicity in cell culture assays. To ensure these effects were not virus or cell-line specific, I tested identified compounds against three different IAVs (seasonal H1N1, seasonal H3N2, and pandemic H1N1), in both Madin-Darby Canine Kidney cells (MDCKs) and A549 cells. I then confirmed that the compounds were not virucidal and identified a subset of compounds that appeared to be entry inhibitors. In the final *in vitro* portion of the project, I further examined attachment and penetration stages of IAV infection for the five candidates suspected to be entry inhibitors of IAV to further characterize their mode of action *in vitro*. The project was concluded with use of a murine model of influenza virus infection to determine *in vivo* potential.

1.5.2: Hypotheses

1. Existing libraries of FDA-approved and natural source compounds and therapeutics contain a variety of compounds that possess documented immune and antimicrobial

effects, making them excellent sources to identify novel drug candidates for reducing IAV titers *in vitro.*

2. The addition of compounds identified as IAV entry inhibitors from the library screens will partially or fully inhibit successful attachment or penetration of IAV *in vitro,* as measured by a reduction in viral titers or presence of viral protein over the course of viral replication.
3. Treatment with the compounds identified as entry inhibitors will effectively protect against lethal IAV infection *in vivo.*

1.5.3: Specific objectives

1. Identify compounds from the FDA-Approved and Natural Source Compound Libraries (provided by ApexBio) that are highly effective at reducing seasonal H1N1-induced cytopathic effects (CPE) and virus titers *in vitro,* while maintaining low host toxicity. Evaluate the specificity and cross-protective potential of these compound candidates toward distinct viruses and cell types.
2. Determine how the candidate compounds identified in the first objective may be having a negative effect on seasonal IAV infection. Discern how a subset of suspected entry inhibitors negatively impact the seasonal IAV entry process by looking specifically at viral attachment to and penetration of the host cell *in vitro.*
3. Test the suspected IAV entry inhibitors in a murine model to identify their *in vivo* potential.

Chapter Two: Materials and Methods

2.1: Tissue culture

All IAV experiments were performed using Madin-Darby canine kidney or A549 cells (hypotriploid alveolar basal epithelial cells) purchased from the American Type Culture Collection (ATCC). Cells were grown in Minimum Essential Medium (MEM) supplemented with 5% heat-inactivated (56° C for 30 min) Fetal Calf Serum (FCS) and 2 mM of L-glutamine (HyClone). For transfections, 293T (human embryonic kidney) cells were grown in Dulbecco's modified Eagle medium (DMEM, Hyclone) supplemented with 5% FCS and 2 mM L-glutamine.

For VSV-MERS experiments, I used Vero cells purchased from ATCC. Cells were grown in MEM supplemented with 5% heat-inactivated FCS and 2 mM of L-glutamine. Seasonal Rhinovirus (R-1644) experiments were performed with HeLa cells, kindly provided by Dr. Jing Cao located at the NML. The HeLa cells were grown in MEM supplemented with 10% heat-inactivated FCS and 2mM of L-glutamine.

Tissue culture maintenance was performed by passaging the cells every 3 days by removing the medium, rinsing the monolayer with Phosphate Buffered Saline (PBS), adding 2 mL of 0.25% trypsin EDTA (Hyclone), and incubating the flask at 37° C until all of the cells had detached. The cells were then resuspended in fresh culture medium. For routine maintenance, cells were split when they became 70-80% confluent using a 1:20 dilution for MDCK, A549, and Vero cells, and a 1:10 dilution for 293T cells. All cells were grown in a 37° C humidified incubator with 5% CO_2.

2.2: Viruses

2.2.1: Virus strains

Three strains of IAV were used for this dissertation project. The first was a seasonal A/New Caledonia/20/1999-like clinical isolate of H1N1 (sH1N1), A/Canada/RV733/2007 (RV733). The second was a 2009 pandemic H1N1 strain (pH1N1), A/Mexico/INDRE4487/2009 (Mx10). The last IAV strain used was an H3N2 virus, A/Hong Kong/1/68 (HK68). A murine-adapted HK68 virus that I generated using reverse genetics (see section 2.6) was used for the *in vivo* experiment in this dissertation.

A VSV MERS virus identified as VSV/MERS-spikeΔ16 (VSV-MERS) was also tested for this dissertation work, along with a seasonal Rhinovirus ATCC-VR1644 (R-1644). All viral work was carried out in the Containment Level 2 (CL2) facility at the National Microbiology Laboratory in Winnipeg, Canada following all approved guidelines and Standard Operating Procedures (SOPs).

2.2.2: Generation of murine-adapted HK68 virus using reverse genetics

2.2.2.1: Cloning

A murine-adapted HK68 virus was generated for the murine experiments, as the HK68 virus used in previous cell experiments is non-lethal in mice. The majority of the *in vitro* research for this dissertation was performed with RV733, which is a seasonal H1N1 virus. HK68 originated from a 1968 pandemic caused by an H3N2 virus. While these viruses are different subtypes, the compounds selected for testing in mice were effective against both RV733 and HK68. I used point mutations in specific gene segments (shown in Table 2) and PCR amplification to generate the

Table 2. Primers used for generation of murine-adapted HK68 gene segments.

HK68 Gene	Amino Acid Change and Position	Primers	Sequence (5' to 3')
PB2	Aspartic acid → arginine Position 701	HKPB2D701Nf	GGGTAAGGAAcAgAGAAGATATGGACC
		HKPB2D701Nr	CATATCTTCTcTgTTCCTTACCCAGAA
PB1	Arginine → Lysine Position 190	HKPB1R190Kf	GAAAAAGAAaAGTAAGAGACAACATGA
		HKPB1R190Kr	GTCTCTTACTtTTCTTTTTCTTTGGA
	Lysine → Theonine Position 578	HKPB1K578Tf	GCTAAAGAcGCTGTGGGAGCAA
		HKPB1K578Tr	CTCCCACAGCgTCTTTAGCTCGAA
HA	Glycine → Tryptophan Position 234	HKHAG234Wf	CCGAATATCtGGTCCAGACCCTG
		HKHAG234Wr	TGGACCaGATATTCGGGATTATAG
	Theonine → Asparagine Position 501	HKHAT501Nf	GAAATGGGAaTTATGACCATGATG
		HKHAT501Nr	GGTCATAAtTCCCATTTCTGATTG
NP	Aspartic acid → Asparagine Position 34	HKNPD34Nf	ATGATTaATGGAATTGGACGATTC
		HKNPD34Nr	CGTCCAATTCCATtAATCATCTTCCCGA
NA	Proline → Histidine Position 468	HKNAP468Hf	TTCATGCaTATATAAGCTTTCGCA
		HKNAP468Hf	CTTATATAtGCATGAAATTGATGTTC
M1	Aspartic acid → Asparagine Position 232	HKM1D232Nf	CTAAAAGATaATCTTCTTGAAAATTTG
		HKM1D232Nr	CAAGAAGATtATCTTTTAGACCAG
NS1	Valine → Alanine Position 23	HKNS1V23Af	CAAGTTGcAGACCAAGAACTAG
		HKNS1V23Ar	TCTTGGTCTgCAACTTGTTTTC

genetic components used to produce the virus, and reverse genetics to rescue the virus. Successful inclusion of mutations was confirmed using the primer sets shown in Table 3.

To generate the mutated genes required to generate the MA-HK68 virus, In-Fusion HD cloning (Takara, Clontech) was used to clone previously published point mutations into the gene segments of IAV, which were readily accessible in our laboratory[120]. Using PCR amplification PrimeSTAR Max DNA Polymerase (Takara, Clontech), the following PCR reaction was set up: 12.5 µL of PrimeSTAR Max Premix (2x), 1 µL each of 10 µM forward and reverse primer, and 2 ng of plasmid template were combined and topped up to 25 µL with HyClone™ water. The following thermal cycler conditions were then used: 98º C for 120 sec, followed by 35 cycles of 98º C for 10 sec, 55º C for 5 sec, and 72º C for 10 sec, concluding with 72º C for 45 sec. PCR products were then purified on a 0.7% agarose gel containing 0.35 g of UltraPure Agarose (Invitrogen, Thermo Fisher Scientific) that was dissolved in 50 mL of 1X TAE buffer and 1 µL of GelGreen™ DNA dye (Biotium, VWR). Samples were mixed with 10X FastDigest Green Buffer (Thermo Fisher Scientific) for loading into the gel along with a 1 kb DNA ladder (Invitrogen, Thermo Fisher Scientific). The gels were then run in an electrophoresis chamber (100V for 30 minutes) and visualized by UV light exposure using the InGenius gel documentation imager (Syngene). The identified bands of interest were then excised, and the QIAquick Gel Extraction Kit (Qiagen) was used to extract DNA, following the procedures described in the manual.

A digestion reaction was then set up to prepare the vector for gene insertion: 1 µg of pPol vector, 1 µL of BsmBI FastDigest (Thermo Fisher Scientific), 1 µL of 10X FastDigest Green buffer, 1 µL of Calf Intestinal Alkaline Phosphatase (New England Biolabs), and dH_2O to a final volume of 10 µL. Reaction mixtures were incubated at 37ºC for 1 hour, then the digested vector

Table 3. Sequencing primers used to confirm successful insertion of the correct HK68 gene segments to the pPol vector.

Gene	**Primers**	**Sequence (5' to 3')**
PB2	pPolF*	CTCCGTGTGTGGCTGCGA
	pPolR*	GGGGGACACTTTCGGACA
	PB2841F	GAGATGTGCCACAGCAC
HA	H3uni1641R	TGGCAAAGGAAATCCA
NP	S57NP536F	ACCAGAGGACAAGAGCTCTTG
NA	N2uni529F	GCATGGTCCAGCTCAAG-TTGTCACGATGGAAAAGC
PB1	S57PB1968F	ACCAGAGGACAAGAGCTCTTG

** Paired with all genes in addition to the above listed primers. Unlisted genes were sequenced with pPolF and pPolR primers, exclusively.*

was purified on a 0.7% agarose gel for final purification, and excised using the QIAquick Gel Extraction Kit (Qiagen), following the procedures described in the manual.

The In-Fusion HD Cloning Kit (Takara, Clontech) was then applied to enable fast cloning of the produced, purified DNA fragments into the vector. Primers were designed to contain a 15 base-pair overlap between insert and vector, as this is required for cloning to work. The fragments were inserted into the BsmBI cut site of pPol plasmid template using the following In-Fusion reaction: 2.5 µL of cut vector, 1 µL of each purified PCR fragment, 2 µL of 5X enzyme mix, and HyClone^{TM} water to a final volume of 10 µL. The mixed reaction contents were then incubated at 50° C for 15 min, then incubated on ice for immediate transformation into Stellar competent *E. coli* cells (Clontech).

For transformation, 50 µL of Stellar competent *E. coli* cells were thawed on ice in a 1.5 mL capped microtube (Corning). Once fully thawed, 2 µL of In-Fusion reaction was added to the cells. The mixed tubes were then incubated on ice for 30 min. Cells were then heat-shocked at 42° C for 45 sec, then immediately incubated on ice for 2 min. After incubation, 200 µL SOC medium (Thermo Fisher Scientific) was added to each tube. Cells and medium were then incubated at 37° C for 1 h with 1,000 rpm shaking using a Thermomixer (Eppendorf). After 1 h, the entire sample was then plated on pre-warmed (to room temperature) LB agar plates containing 100 µg/mL of Ampicillin, and incubated overnight at 37°C. The following morning, individual colonies were picked and grown in LB broth with 100 µg/mL of Ampicillin overnight at 37°C with 250 rpm shaking.

For plasmid isolation from the overnight bacterial culture, the QIAprep Spin Miniprep Kit (Qiagen) was used, following the procedure outlined in the manual. Extracted DNA was sent to the DNA Core Facility at the Public Health Agency of Canada for sequencing, to confirm successful insertion of the desired gene segment into the vector. All DNA samples were sequenced using the Sanger method of sequencing. Results were then verified by reference sequences using DNASTAR Lasergene 11 SeqMan Pro software.

2.2.2.2: Reverse genetics rescue of A/HongKong/1/68 virus

Once mutations were successfully incorporated into specified gene segments and amplified, I rescued the reverse genetics virus. The reverse genetics procedure used by our lab is based on the procedure described by Neumann *et al*. This method entails cloning the cDNA region of all genomic segments between the human RNA polymerase I promoter and mouse RNA polymerase I terminator of the pPol vector, then cloning the viral polymerase proteins PB1, PB2, and PA along with NP into a pCAGGS expression vector. pCAGGS is a mammalian expression vector with CAG promoter, developed for high expression of foreign genes produced by processes such as transfection[121]. In this process, RNA polymerase I transcribes the RNAs that do not contain a 5' cap and 3' poly(A)-tail, resulting in pPol constructing RNA code that mirrors viral RNA (vRNA). Thus, viral replication and transcription are able to occur because of vRNP production as a result of plasmid-driven expression of the three polymerase proteins and NP, combined with the artificial vRNA.

First, flat-bottom 6-well plates (Thermo Fisher Scientific) were coated with 0.5 mL per well of 0.1 mg/mL poly-D-lysine (Thermo Fisher Scientific). The plates were then incubated for

30 minutes at room temperature. Following incubation, the poly-D-lysine was removed, and the plates were washed 5 times with 0.5 mL per well of sterile PBS. Then, 293T cells were seeded in the poly-D-lysine coated flat-bottom 6-well plates the day before the reverse genetics procedure to reach a confluency of ~90%. To perform each transfection reaction, 200 µL of Opti-MEM (Gibco, Thermo Fisher Scientific) and 10 µL of TransIT™-LT1 transfection reagent (Mirus Bio, Thermo Fisher Scientific) was added to 1.5 mL capped microtubes (Corning) and incubated at room temperature for 5 min. Following incubation, 0.1 µg of the following mutated plasmids were added to the mixture: pPol-PA, PB1, PB2, NP, M, NS, NA, and HA. Following this, 1.0 µg of the following helper plasmids, supplemental plasmids encoding the following proteins, were also added to each tube: pCAGGS-PA, PB1, PB2, and NPThe DNA/transfection reagent mixture was then incubated at room temperature for 30 min. During the incubation period, the 6-well-plated 293T cells were washed with 2 mL per well of Opti-MEM (Gibco, Thermo Fisher Scientific). Then, 1 mL of Opti-MEM was added to each well prior to introduction of the incubated transfection mixture. The transfection mix was added to each well drop-wise by pipette. The plates were then incubated at 37°C in a humidified incubator with 5% CO_2 for 48 h.

Directly following the 48 h incubation, the transfection supernatants were blind passaged onto MDCK cells. To perform this step, MDCK cells were first seeded into flat-bottom 12-well plates (Thermo Fisher Scientific) to achieve a final confluency of 60-80% at the time of transfection. Supernatants from each of the transfection wells (6-well plates) were collected in a 2 mL capped cryovial (Corning) and centrifuged at 500 x g for 10 min to remove all cellular debris. Following this, a trypsin activation step was performed by adding 2 µL of Tosyl phenylalanyl chloromethyl ketone (TPCK)-trypsin (from a 1 µg/µL stock, Thermo Fisher Scientific) to each transfection tube. Trypsin activates the virus by proteolytic cleavage of the hemagglutinin and is

an essential addition for generation of an infectious virus. The tubes with TPCK-trypsin were then mixed thoroughly, and incubated for 15 min at 37° C.

The prepared MDCK cells were washed with neat MEM during incubation. Following this, 1 mL of MEM/0.1% BSA/L-glutamine/1 µg/mL TPCK-trypsin was added to each well. For each virus rescue, a range of transfection supernatant additions were tested: 10 µL, 100 µL or 1 mL of transfection supernatant was added to each well of the 12-well passage plate. MDCK cells were then incubated at 37° C for 48 h or until >90% CPE was observed. The well with the highest dilution of transfection supernatant added, but displaying nearly or entirely complete CPE was harvested. This was called the P1 passage of the rescued virus, and was stored in screw-cap cryovials (Corning) at -80°C until it was used to generate a P2 stock of the virus for general use. P2 passage of the viruses were generated as previously described in section 2.2.3. Final quantification of virus titer was performed by plaque assay.

2.2.3: Virus stock generation.

Virus stocks were prepared in T75 cm^2 flasks (Corning). MDCK cells were used for production of IAVs, while Vero cells were used for production of VSV-MERS, and HeLa cells were used for production of R-1644. Cells were grown according to section 2.1. For infection of IAV, 5 µL of virus stock (assuming a concentration of ~10^6 PFU/mL) diluted into 10 mL of MEM supplemented with 0.1% BSA, L-glutamine, and 1 µg/mL TPCK-treated trypsin (Sigma-Aldrich) is sufficient for 100% CPE of MDCK cells 48-72 hpi. Cells were first washed with unsupplemented medium to remove any FCS, which inhibits the trypsin required for IAV growth, and inoculated with virus. The flask was then incubated for 48 hpi when ~70-80% CPE was

observed. To harvest the virus, supernatant was centrifuged at 500 x g for 10 min to pellet cell debris. The remaining supernatants were aliquoted and stored at -80° C. Virus titer was determined by $TCID_{50}$ (see section 2.2.4).

For VSV-MERS, cells were grown according to section 2.1 prior to infection. First, 5 μL of virus stock was diluted into 10 mL of MEM supplemented with 2% FCS, L-glutamine, and incubated for 48 h. All other steps mirror IAV infection. R-1644 was handled and propagated using the same method as VSV-MERS, and peak CPE was observed after 72-96 h of incubation.

2.2.4: Virus titration methods

Virus titration by determination of the median tissue culture infectious dose ($TCID_{50}$)

$TCID_{50}$ is a standard method used to measure infectious viral titer in an *in vitro* model that represents a dilution at which 50% of the wells inoculated with that dilution are infected. MDCK cells were seeded 1:4 in flat-bottom 96-well plates (Thermo Fisher) with MEM/5% FCS/L-glutamine medium, 24 h before use. The following day, the growth medium was aspirated and cells were washed with 100 μL of PBS to remove residual FCS that would inhibit trypsin activation. Virus samples were serially diluted 1:10 starting at 10^{-2} to 10^{-9} in MEM/0.1% BSA/L-glutamine/1 μg/mL TPCK-trypsin using a 96-well dilution block (Nunc™ Polypropylene DeepWell™ Storage Plates, Thermo Fisher Scientific). Pipette tips during this step were changed between each dilution to avoid carry-over of viral supernatant, which would alter the reported $TCID_{50}$ titer. Wash medium was removed from the 96-well plates (Thermo Fisher Scientific), and 100 μL of each diluent from the dilution block was added accordingly. A single dilution replicate was passaged in triplicate on parallel 96-well plates of MDCK in this titration assay because the

minimal data set for $TCID_{50}$ calculation is 3 replicates for each single titer calculation. These sets of the 3 replicates required for the $TCID_{50}$ assay were then repeated twice more to form the three replicates reported. Plates were then incubated at 37° C with 5% CO_2 for 72 hpi. The Reed and Muench method was then used to determine the 50% endpoint ($TCID_{50}$/mL). VSV-MERS, and R-1644 were titrated the same way, but with their corresponding media as described in section 2.1.

The Reed and Muench method is a calculation used to determine the 50% endpoint in experimental biology. For the purposes of this dissertation, the numerical result indicates the titer of virus that produces CPE in half of the wells tested. As described by Lei, *et al.,* the Reed and Muench calculation can be performed in three steps[122]:

1. Proportionate distance = [(% infected at dilution immediately above 50%) – 50%] / [(% infected at dilution immediately above 50%) – (% infected at dilution immediately below 50%)]
2. $logID_{50}$ = log(dilution with > 50% positive) + PD x (-log(dilution factor))
3. Adjustment for ID per volume

If, for example, 6 of 7 replicates at a dilution of 10^{-7} were successfully infected (showing CPE), and 2 of 7 replicates at the 10^{-8} dilution were successfully infected, this is equivalent to 86% and 29%, respectively. Thus, the above calculation would yield:

$$\text{Proportionate distance} = (86 - 50)/(86 - 29) = 0.6$$

$$logID_{50} = -7 + 0.6 \times (-1) = -7.6$$

Thus $ID_{50} = 10^{-7.6}$, representing the end point dilution. To calculate the virus titer in terms of infection doses per volume used, taking the reciprocal and dividing by the volume (0.1 mL) yields the final value of $1/10^{-7.6}/0.1 = 10^{8.6}$ $TCID_{50}$/mL.

Virus titration by plaque assay

Two days prior to performing this procedure, MDCK cells were seeded into 12-well plates (Thermo Fisher Scientific) in MEM/5% FCS/L-glutamine so they reached a confluency level of 100% on the day of the assay. Cells were then washed with 1 mL of PBS. The experimental supernatant or mixture to be titrated was then serially diluted 1:10 starting at 10^{-1} to 10^{-6} in MEM/0.1% BSA/L-glutamine/1 µg/mL TPCK-trypsin. The wash was removed from plated cells, and 200 µL of the virus dilution was added to the wells in duplicate. Plates were incubated at 37°C in a humidified chamber with 5% CO_2 for 1 h. The plate was rocked every 15 min to prevent the cells from drying out.

During the incubation, prepared 2% SeaPlaque (Lonza) low melting point agar in tissue culture grade water was melted and kept warm at 37° C. A solution of 2X MEM/0.2% BSA/2X L-glutamine/2 µg/mL TPCK-trypsin was prepared and also kept warm at room temperature until use. After the 1 h incubation, the 2X MEM medium was mixed with an equal volume of 2% agar, resulting in a final concentration of 1% agar and 1X MEM/BSA/1 µg/mL TPCK-trypsin. The virus inoculum was removed from each well, and 1 mL of the agar mixture was added starting at the highest virus dilution to the lowest dilution by pipetting slowly down one side of the well. The agar was then allowed to harden before the plates were turned upside down and incubated at 37° C with 5% CO_2. Plaques were counted 48 hpi without staining by visually identifying plaques by their different contrast within the cell monolayer. The assay was performed in technical and biological duplicates.

2.3: Screening and Initial Testing of ApexBio Compound Panels

Initial compound stocks were obtained from the DiscoveryProbe libraries (ApexBio Technology LLC, Houston, Texas) and were received pre-dissolved to 100 mM in DMSO. The full list of the compounds included in each library totals 2,870 (the Natural Source library contains a collection of 550 natural products and the FDA-approved library contains a collection of 2,320 approved drugs with a variety of applications). These stocks were frozen at -80° C until use.

Subsequent analyses (post-initial screening) were performed using compound stocks in powder form ordered from Cedarlane Laboratories (Burlington, Ontario) from several different suppliers, such as Ray Biotech and Cayman Chemical Co, reconstituted in DMSO, and stored as per manufacturer instructions. The compounds were reconstituted to a concentration of 100 μM in DMSO, aliquoted into screw-cap cryovials (Thermo Fisher Scientific), and frozen at -20°C until the assay was performed. Aliquots were thawed a maximum number of two times to avoid freeze/thaw alterations.

2.3.1: Initial screening of ApexBio compound panels

Initial screening of antiviral candidates was performed in 96-well flat-bottom plates (Thermo Fisher Scientific), seeded with $3.2x10^4$ MDCK cells per well. The plates were incubated for 24 h at 37° C with 5% CO_2 in a humidified incubator until the monolayer had reached 70% confluency. Cells were then washed 2X with 100 μL of PBS. Then, 100 μL of MEM/0.1%BSA/L-glutamine/1 μg/mL TPCK-trypsin was added to each well.

To investigate the effect of antivirals on seasonal influenza, RV733 (sH1N1) was used for these experiments at a dose of 0.001 MOI. The pre-aliquoted compounds directly from ApexBio

were then thawed at room temperature, mixed thoroughly on an Analog Vortex Mixer (Thermo Fisher Scientific), and added to each well at a final concentration of 100 µM for testing the FDA-approved library and 10 µM and 100 µM for testing the natural source compound library. The plate containing only the compounds and cells was then incubated at 37° C with 5% CO_2 in a humidified incubator for 1 h, then 0.001 MOI of RV733 (100 µL) was added to each well. The plates were then incubated at 37°C with 5% CO_2 in a humidified chamber for 48 h, or until 100% CPE was observed in virus control wells.

Initial screening was performed in technical singlet and biological triplicate. For all experiments in this dissertation, technical replicates refer to those that were performed at the same time, contained in a single biological replicate, processed using the same experimental procedure, in parallel. Biological replicates refer to experiments performed using the same experimental procedure, but using different batches of cells and all required reagents from the first biological replicate, each of which contains its own set of technical triplicates. For example, an experiment reported to be performed in technical triplicate and biological duplicate was first performed in an experiment with three replicates at the same time, followed by a second experiment performed at a subsequent time with different cells and reagents, also containing three replicates. Compounds were identified as good candidates for antiviral activity against IAV if they showed no CPE compared to the virus-infected, untreated control. These candidates were carried forward to the inhibition assay.

2.3.2: Inhibition assay

This was performed using the same procedure as in section 2.3.1, but was performed in triplicate using a 1:2 dilution series resulting in a range of 100 μM to 19.5 nM tested for each compound of interest in a 96-well dilution block (Nunc™ Polypropylene Deep Well™ Storage Plates, Thermo Fisher Scientific). The experimental triplicate was performed using the same stock of diluted compound for all three replicates. Compounds were diluted in MEM/0.1%BSA/L-glutamine/1 μg/mL TPCK-trypsin, the medium used for this assay. Once the compound-containing medium was added to each well of the plate, 100 μL of 0.001 MOI of RV733 was added directly into each well. This additional volume was accounted for when calculating dilution of the compounds in the existing medium. RV733 was previously diluted in virus growth medium to reach the desired MOI. Pipette tips were changed between dilutions, to avoid supernatant carry-over.

The five controls used for this assay were diluted-DMSO-treated cells, RV733-infected cells, healthy cells (no compound or virus addition), and oseltamivir carboxylate addition with and without RV733 infection. In the case of the diluted-DMSO-treated cells, 10 μL of DMSO diluted in virus growth medium was added to the first well in the place of 100 μL of compound diluted in DMSO and virus growth medium, then serially diluted, like those wells containing diluted compounds. This volume matched the amount of DMSO in the first well of those columns containing serially diluted compounds. Purified oseltamivir carboxylate (Cayman Chemical Co.) with and without virus was added to show the result of the assay with a highly effective compound, known for its potent effect against IAV *in vitro* and *in vivo*. Uninfected cell controls received the same fresh medium as all other wells, but no was virus added. These three conditions allowed for direct comparison of compound-treated cells to a known effective treatment, DMSO content, and

healthy cells without compound or virus. The plates were then incubated for 48 h at 37° C with 5% CO_2. The supernatant from the wells containing the lowest effective concentration of compound was collected 48 hpi and frozen at -80° C until use. Viral titers were then determined by $TCID_{50}$ as in section 2.2.4, according to the Reed and Muench endpoint determination method.

The inhibition assay was carried out in technical duplicate and biological duplicate. Compounds were identified as good candidates for antiviral activity against IAV if they showed a minimum of a 2-$\log_{10}$ reduction in viral titers compared to the virus-infected, untreated control, and were carried forward for XTT cytotoxicity testing.

2.3.3: XTT cytotoxicity assay

The CyQUANT™ XTT Cell Viability Assay (Invitrogen™, Thermo Fisher Scientific) was used to measure metabolic activity as an indication of cell health. The wells in a 96-well flat-bottom plate (Thermo Fisher Scientific) were seeded with $3.2x10^4$ MDCK cells per well in 100 µL of MEM/10% FCS/L-glutamine. The following day, the cells were washed 1X with PBS, and 100 µL of FluoroBrite DMEM medium (Gibco, Thermo Fisher Scientific) per well with the same supplementation and diluted compounds (using a concentration range of 3.9-500 µM and 1:2 dilutions). FluoroBrite DMEM contains no phenol red, which can increase the absorbance reading by the plate reader, altering the interpretation of the XTT assay results.

After 48 h of incubation with the compound, 6 mL of XTT Reagent (2,3-bis[2-Methoxy-4-nitro-5-sulfophenyl]-2H-tetrazolium-5-carboxyanilide inner salt) and 1% PMS (phenazine methosulfate) was resuspended by briefly vortexing the vials, and mixing with 1 mL of the Electron Coupling Reagent, as per manual instructions. Following this, 70 µL of the "working

solution" of the two reagents was added to each well of the plate, which already contained the compounds diluted in Fluorobrite medium. The plate was then incubated at 37° C with 5% CO_2 in a humidified incubator for 4 h. After the incubation period, the absorbance of the plates was read at 450 and 660 nm on a BioTek™ Synergy™ Microplate Reader (Fisher Scientific, Thermo Fisher Scientific). Cytotoxicity was measured by quantifying a value called the specific absorbance using the following correction calculation, as described in the XTT Cytotoxicity Manual[123]:

$$\text{Specific Absorbance} = [\text{Abs}_{450\text{ nm(Test)}} - \text{Abs}_{450\text{ nm(Blank)}}] - \text{Abs}_{660\text{ nm(Test)}}$$

Measurement at 450 nm reads the maximum absorption of the XTT reaction product, while the 660 nm reading removes the background due to cell debris and excess coupling reagent. The data was then graphed using GraphPad 9 software utilizing a non-linear fit, variable slope with four parameters graph of $\log_{10}$(inhibitor) vs. response curve (see Figure 6). For example, in the case of teriflunomide at a concentration of 500 μM, the absorbance at 450 nm was 0.155, the absorbance at 660 nm was 0.043, and the blank absorbance was 0.04, which resulted in a specific absorbance of 0.072. The uninfected cell control gave an absorbance reading of 2.253 at 450 nm, and 0.049 at 660 nm, resulting in a specific absorbance of 2.164. Together, this means that the specific absorbance of teriflunomide was much lower than the cell control, which indicates cytotoxicity at this high concentration. As seen in Figure 6, teriflunomide becomes less toxic at a concentration of 31.25 μM. A lysed cell control, DMSO control, and uninfected cell control were included in each assay.

The assay was performed in technical duplicate and biological duplicate. However, final $TCID_{50}$ quantification experiments were always performed in triplicate due to the nature of the calculation, which requires three replicates. Using this experiment as an example, the experimental procedure was performed three times in parallel (used for three $TCID_{50}$ replicates each, totaling nine individual columns in the $TCID_{50}$ plate for quantification, representing three replicates) using the same cells and reagents on the day of the experiment. The full experiment was then repeated once more on a subsequent day using new reagents and cells (with the same number of replicates) to ensure reproducibility of results. This definition will be consistently used for the remainder of the dissertation. Numerical data points shown for experiments contained in this dissertation were consistently expressed as the mean ± the standard error of the mean (SEM) between replicates. Final results were analyzed using a log_{10}(inhibitor) vs. response variable slope with four parameters transformation using GraphPad Prism 9 software. This type of analysis is also called a "variable slope model". It is used in subsequent experiments in this dissertation because the compound response curves are performed on a log_{10} scale and are anticipated to be inhibitory (meaning higher compound concentrations are anticipated to lower the virus titer yield). The response was analyzed using a variable slope, meaning the program does not automatically assume a standard slope, which is preferable for a plot with many data points. This is the recommendation by GraphPad software for analyzing curves of this nature in which an inhibitory compound is being analyzed for an effect in a cellular or animal model with no (or limited) previously known results.

2.3.4: Yield assay

The yield assay quantified the viral load of the supernatant in an *in vitro* assay. This assay was performed in 12-well flat-bottom plates (Thermo Fisher Scientific) seeded with $4.2x10^5$ cells

per well and incubated for 24 h at 37° C with 5% CO_2 in a humidified incubator. Once the cells had reached ~70% confluency, the medium was removed, and the cells were washed 2X with sterile PBS. Fresh compound candidates were thawed for each experimental use, and diluted in MEM/0.1% BSA/L-glutamine/1 μg/μL TPCK trypsin in a dilution block to a range of 0.195 to 100 μM. From the dilution block, 1 mL of sample was added to the correct respective well in the 12-well plate containing cells. Then, 100 μL of 0.001 MOI of RV733 was added to each well of the 12-well plate. The plates were then incubated for 48 h at 37° C with 5% CO_2. Cell only and virus-infected controls were used to ensure integrity of results. The supernatant was collected 48 hpi and frozen at -80° C until use. Viral titers were then determined by $TCID_{50}$ as in section 2.2.4, according to the Reed and Muench endpoint determination method. The assay was performed in technical triplicate and biological duplicate.

2.4: Delineating the Effect of the Compounds of Interest on Seasonal IAV

2.4.1: Testing compounds against other IAVs, VSV viruses, and in A549 cells

To assess the specificity of the selected compounds, I tested a subset of the compounds of interest against two other types of IAVs, a VSV-MERS virus and in an A549 cell model. The compounds of interest were tested first against Mx10 and HK68 viruses (see section 2.2.1). The same experimental protocol, data analysis, and statistical analysis as the yield assay (see section 2.3.4) was used to determine reduction in virus titer and CPE 48 hpi in the presence of the compounds of interest. To test the compounds in A549 cells, which are distinct from MDCK cells and human in origin, the experimental protocol of the yield assay was also used (see section 2.3.4).

2.4.2: Virucidal assay

I performed a virucidal assay using a $TCID_{50}$ and a plaque assay method of quantification. For the purposes of this dissertation, virucidal activity is defined as an interaction with a virus that results in physical disruption of viral particles.

To perform this experiment, a screw-cap cryovial (Thermo Fisher Scientific) containing 100 µL of 20X the compound concentration determined to be toxic in the cytotoxicity assay (see section 2.3.3), diluted in DMSO, was combined with 100 µL $3.16x10^7$ $TCID_{50}$/mL of RV733 in MEM/0.1% BSA/L-glutamine/1 µg/mL TPCK-trypsin (virus growth medium). These were combined by vortexing and incubated together at 37° C for 2 h, mixing every 15 min for full immersion. After the incubation period, the compound/virus mixture was then diluted 1:50 in virus growth medium into a T75 cm^2 flask (Corning) containing a ~80% confluent monolayer of MDCK cells, and incubated at 37ºC with 5% CO_2 for 48 h. Following this incubation period, the flasks were observed for CPE, the presence of which would indicate a non-virucidal compound.

Subsequently, the same experimental setup was performed using a plaque assay to quantify residual virus. After the 2 h incubation period described above, the compound/virus mixture was then diluted 1:50 into virus growth medium in a 15 mL tube (Corning) and plated using the plaque assay procedure described in section 2.2.4. The 1:50 diluted compound/virus mixture was serially diluted for the plaque assay 1:10 starting at 10^{-1} to 10^{-6} in virus growth medium. Controls of hypochlorite (bleach) and Micro-Chem were used. Bleach compounds inhibit viral replication non-specifically (for example, hypochlorite denatures proteins, triggers enzyme destruction, and induces other destructive processes). Micro-Chem is a quaternary disinfectant that binds to the

outer membrane of microbes, killing or inactivating them. The virucidal assay was performed in technical duplicate and biological duplicate.

2.4.3: Time of addition assay

The time of addition assay was adapted from previous methods with some modifications[124]. This assay was performed in 12-well tissue culture plates (Thermo Fisher Scientific) seeded with $4.2x10^5$ cells and incubated for 24 h at 37°C with 5% CO_2 in a humidified incubator. Once the cells were ~70% confluent, the medium was removed, and the cells were washed 2X with PBS. Virus-containing medium (MEM/0.1% BSA/L-glutamine/1 µg/µL TPCK trypsin) supplemented with 0.001 MOI of RV733, was then added to the wells, 1 mL per well, over ice. Adsorption was allowed to proceed on ice for 60 min (considered -1 – 0 hpi for the purposes of this experiment), after which the monolayer was washed 2X with PBS and wells were incubated with 0.5 mL of virus growth medium until the designated compound addition time. The medium was then removed and 0.5 mL per well of viral growth medium containing $10IC_{95}$ of the compound was added at the indicated time points (-2 to 0, 0 to 2, 2 to 4, 4 to 6, 6 to 8, 8 to 10 hpi after original virus addition) to each well. A dose of 100 µM of oseltamivir was used as a control. In the case of the -2 hpi compound addition experiment, 0.5 mL of virus growth medium containing the compound was added 1 hour prior to virus adsorption over ice to the above described, washed monolayer. Following 1 hour of compound exposure, 0.001 MOI of virus was then directly diluted into the existing compound-containing medium for an additional hour (denoted as time point -1 – 0 hpi) during adsorption. After 2 hours of exposure to the compound, one of which being during viral adsorption, the monolayer was washed and incubated, as described above. In the case of the 0 hpi compound addition experiment, the compound was added when the viral growth medium

containing virus was removed following adsorption and the cells were washed 2X with PBS. The monolayer was then incubated with 0.5 mL of viral growth medium containing the compound, as described above, until the 2 h period (denoted as the 0-2 hpi time point) had concluded. All incubations following adsorption on ice were carried out at 37ºC with 5% CO_2.

Following the designated 2 h period in which cells were incubated with the compound, the monolayer was washed 2X with 0.5 mL of PBS, after which 0.5 mL of fresh viral growth medium was added to each well, and the plate was incubated until the 10 hpi time point had been reached. Controls containing virus and cells but no compound, and uninfected cells with no compounds present, were used to ensure integrity of results. These controls were designed to confirm that the virus infection proceeded as expected in the absence of the compounds, and that the cells were growing normally in the absence of the virus and compounds. The supernatant was removed after a total of 10 hpi had elapsed, regardless of compound addition time, and stored at -80°C until viral titer determination. Viral titers were then determined as in section 2.3.4, according to the Reed and Muench endpoint determination method. The time of addition assay was performed in technical duplicate and biological triplicate.

2.4.4: Immunofluorescence assays (IFAs)

To visualize three IAV proteins (HA/NA/NP), immunofluorescence assays were performed on MDCK cells. These antibodies were readily available for use in our research group, and had been used successfully for IAV IFA experiments previously. In 24-well plates (Thermo Fisher Scientific), glass coverslips were added to each well. To increase attachment of MDCK cells to the base of the plate, the plates were pre-coated with poly-D-lysine. To make a 0.1 mg/mL stock solution, 5 mg of Poly-D-lysine hydrobromide (Sigma-Aldrich) was

resuspended in 50 mL of commercial tissue culture grade water. To coat the base of the 24-well plate, 100 µL of stock solution was added to each well and incubated at 37°C for 15 min. Plates were then washed 2X with PBS before cells were seeded, and left to grow for 2 days before the assay was performed, until they had reached a confluency of 60-80%. Cells were first treated with the $10IC_{95}$ of the compound of interest dissolved in DMSO and diluted in MEM/0.1% BSA/L-glutamine medium without TPCK-trypsin, and incubated for 2 h. A dose of 100 µM of oseltamivir. Following this, cells were then infected with 3 MOI of RV733 in MEM/0.1% BSA/L-glutamine medium without TPCK-trypsin and incubated at 37°C for 24 h. The compound-supplemented medium was not removed prior to virus infection.

After incubation, virus was removed and cells were washed with 1 mL/well of PBS. All subsequent steps were performed in the 24-well plate containing glass coverslips. To achieve intracellular staining, cells were incubated with 10% formalin (containing methanol) in PBS for 10 min at room temperature. Incubating with formalin containing methanol achieves fixing while the methanol introduces holes in the cell membrane, allowing downstream staining to enter the cell. After fixation, cells were washed 3X with 1 mL/well of PBS for 3 min per wash. Cells were then blocked with PBS/1% BSA for 45 min at room temperature (1% BSA solution was prepared using PBS containing 0.1% Tween20). All primary antibodies were diluted in 1% BSA with 0.1% tween, and 500 µL of antibody was added to each well containing a coverslip (see Table 4). The plates containing antibody were then incubated for 1 h at room temperature in the dark.

After staining with respective primary antibodies listed in Table 4, cells were washed 3X with 1 mL/well of PBS. Secondary antibodies were diluted and applied to plates as before (see Table 4) and incubated for 1 h at room temperature in the dark. Cells were then washed 3X with PBS, and glass coverslips were removed with tweezers from the plate. After removal, each

Table 4. Antibodies and dilutions used for IFAs.

Antibody (company)	Source Species	Primary or Secondary Ab	Stock Concentration	Dilution
Monoclonal anti-H1N1 HA (Sino Biological Inc, cat# 11684-MM03)	Murine	Primary	0.51 μg/μL	1:1,000
Monoclonal NA (Sino Biological Inc, cat# 11058-R001)	Rabbit	Primary	1 mg/mL	1:1,000
Polyclonal NP (Sino Biological Inc, cat# 40205-R063)	Rabbit	Primary	1 μg/mL	1:1,000
Alexa Fluor 488 goat anti-murine (Sino Biological Inc, cat # SSA021)	Goat	Secondary	2 mg/mL	1:200
Alexa Fluor 568 goat anti-rabbit (Thermo Fisher, cat #A-11011)	Goat	Secondary	2 mg/mL	1:200
Alexa Fluor 647 anti-murine IgG (Invitrogen, cat # A32728)	Goat	Secondary	2 mg/mL	1:200

coverslip was dipped into dH_20 before being mounted onto glass microscopy slides. A drop (~20 µL) of ProLong Gold antifade reagent with DAPI (Invitrogen, Thermo Fisher Scientific) was then added to a glass slide to mount the coverslips on. Coverslips were placed with tweezers cell-side-down onto the drop of ProLong Gold, and left to dry for 15-30 min in the dark at room temperature. Slides were stored at 4°C and protected from light until analysis.

Fluorescence levels and contrast were adjusted using the same parameters, including initial capture of the image, for all IFA images in an experimental set. This makes the images directly comparable as they were read at the same time, on the same microscope, using the same parameters. As with other IFA images for this dissertation, these images have been adjusted and clarified as much as possible with the microscope used, given these images were taken at 60X with oil immersion, and further cropped and enlarged for added detail. The slides were imaged using a Carl Zeiss LSM20 confocal microscope at 20X zoom. Captured images were exported and analyzed using the free Zen 2009 Light Edition software (Zeiss). All IFAs were performed in technical duplicate initially, followed by an additional biological replicate. I also ran single dye controls (each virus-infected well and uninfected well was run on each dye channel to determine present background), which were used to remove any dye-related background. I removed dye-related background that was not bound to cells (host or viral) by using the linear unmixing function within the free Zen 2009 Light Edition software (Zeiss).

2.5: Analysis of Suspected Entry Inhibitors Identified by Screening

2.5.1: Hemagglutination Inhibition Assay (HAI)

Before completing the HAI assay, the HA unit value of RV733 was first determined. In a 96-well round-bottom plate (Thermo Fisher Scientific), 25 µL of cell-culture grade PBS was added to wells 2-12 in each row. Then, 50 µL of RV733 was added to the first well, and serially diluted 1:2 across the row. Next, 25 µL of PBS was added to each well followed by 25 µL of 0.5% turkey red blood cells (Innovative Research) prepared in cell-culture grade PBS. The resultant plate was then incubated at room temperature for 30 min before being read. The last well to show full hemagglutination contained the concentration designated as "1 HA Unit (HAU)", which was to calculate the 4 HAU value used in the HAI assay below.

In a 96-well round-bottom plate (Thermo Fisher Scientific), compound stocks were serially diluted in cell-culture grade PBS from 200 µM to 98 nM in 25 µL 1:2 dilutions. Next, 25 µL of 4 HA units of virus were then added to each well. The plates containing varying concentrations of the different compound stocks and virus were then incubated together for 45 min at 37°C with 5% CO_2, and the plates were rocked every 15 min. Following the 45 min incubation, 25 µL of PBS and 25 µL of prepared 0.5% red blood cells, as described in the previous paragraph, were added to the plates. The plates were incubated for 30 min at room temperature, and read for hemagglutination inhibition. Hemagglutination has occurred when the red blood cells become cross-linked by the virus and settle in a distribution across the bottom of the well instead of settling to the bottom center of the round-bottom well in a tight button. The HAI assay was performed in technical and biological triplicate.

2.5.2: Blockade of viral attachment assay

The procedure for this assay was adapted from a previous protocol outlining attachment assay procedures for viruses[125]. The assay was performed in 24-well flat-bottom tissue culture plates (Thermo Fisher Scientific) seeded with $1.7x10^5$ cells in cell culture medium (MEM/5% FCS/L-glutamine) and incubated for 24 h at 37° C with 5% CO_2. Once the cells were ~60% confluent, the plates were incubated in a 4ºC fridge for 1 h. Compounds were then prepared and stored at 4° C until used by diluting the stock solutions to $10IC_{95}$ as determined by the yield assay (see section 2.3.4) in virus growth medium (MEM/0.1% BSA/L-glutamine/1 µg/µL TPCK trypsin). This dilution took into account the final volume of the solution in each well, resulting in a final concentration of $10IC_{95}$ of compound per well. After adding 500 µL of the diluted compound to each well, 100 µL of 0.001 MOI RV733 virus (chilled to 4°C prior to use) was added to each well. The plates were then incubated in a 4º C fridge for 1 h. After incubation, the plates were washed 5X with chilled PBS. Virus growth medium (MEM/0.1% BSA/L-glutamine/1 µg/mL TPCK trypsin) was then added, 500 µL per well, and the plate was incubated for 8 h at 37º C with 5% CO_2 in a humidified incubator. After the incubation period, the supernatant from each well was harvested and stored at -80º C. Supernatant viral titers were determined by $TCID_{50}$, using the Reed and Muench endpoint determination method (see section 2.3.4). An infected, untreated virus control and cellular control containing only healthy cells (no virus or treatment) were included.

The attachment assay was performed in technical triplicate and biological duplicate. Final results were analyzed with a one-way ANOVA test with a significance level (p-value) of 0.05 or less considered significant using GraphPad Prism 9 software.

2.5.3: Blockade of viral penetration assay

The procedure for this assay was developed from a previous protocol outlining penetration assay procedures for viruses[125]. This assay was performed in 24-well tissue culture plates (Thermo Fisher Scientific) seeded with $1.7x10^5$ cells in cell culture medium (MEM/5% FCS/L-glutamine) and incubated for 24 h at 37°C. Once the cells were ~60% confluent, the plates were incubated in a 4º C fridge for 1 h. Following incubation, 0.001 MOI of RV733 diluted in virus growth medium (MEM/0.1% BSA/L-glutamine/1 µg/µL TPCK trypsin) and added to each well, 500 µL per well. The plate was then incubated for 1 h in a 4º C fridge. Following incubation, the plate was washed 3X with chilled PBS, and 2X with chilled cell culture medium. Virus growth medium (MEM/0.1% BSA/L-glutamine/1 µg/µL TPCK trypsin) containing $10IC_{95}$ of each experimental compound as determined by yield assay (see section 2.3.4) was then added to each well, 500 µL per well. The plate was then incubated for 1 h at 37º C with 5% CO_2 in a humidified incubator. The plate was then washed 5X with room temperature PBS, and 500 µL of virus growth medium (MEM/0.1% BSA/L-glutamine/1 µg/µL TPCK trypsin) was added to each well. The plate was then incubated for 8 h at 37ºC with 5% CO_2 in a humidified incubator. After the incubation period, supernatant from each well was harvested and stored at -80º C. Viral titers were determined from supernatants by $TCID_{50}$, using the Reed and Muench endpoint determination method (see section 2.3.4). An infected, untreated control and an uninfected, untreated control were included. The penetration blockade was performed in technical triplicate and biological duplicate. Final results were analyzed with a one-way ANOVA test with a significance level (p-value) of 0.05 or less considered significant using GraphPad Prism 9 software.

2.5.4: Attachment IFAs

To visualize attachment of the virus to the host cell, I used CellVue™ Maroon Cell Labeling Kit (Thermo Fisher Scientific) to stain the cell membrane. CellVue™ Maroon was chosen as it is excited at a very distinct wavelength from the other fluorescent antibodies used in this assay to label the virus itself (see Table 4), so the different dyes could be visually differentiated. MDCK cells were pre-treated with CellVue™ dye by first washing the cells with unsupplemented MEM. Washed MDCK cells were resuspended at $2x10^7$ cells/mL with Diluent C by pipetting slowly. Next, 1 mL of the "working dye" was added, which was made by combining 4 µL of 1 mM dye stock to 1 mL of Diluent C. Once uniformly mixed by pipetting slowly, cells were incubated for 2-5 minutes to ensure uniform labeling, then incubated with 2 mL of FCS at room temperature for 1 minute. Cells were then centrifuged, and the supernatent discarded. After washing the cells with complete media 3X, they were plated as normal (see section 2.1). CellVue™ is a lipophilic dye that labels the lipid membrane of MDCK cells, and the HA primary and secondary antibodies listed in Table 4 were used to fluorescently label the virus. All other procedures were carried out as per section 2.4.4, with the exception of sampling time. Instead of 24 h at 37°C in this previous section, the attachment assay was stopped, fixed, and processed at time points of 5 min post-infection (mpi), 30 mpi, 60 mpi, and 90 mpi. This allowed visualization of the attachment process by analyzing every 30 min. The pilot study analyzed images taken every 15 min, but there were seldom differences between every 15 and 30 min, so every 30 min was chosen as the final time point. The slides were imaged using a Carl Zeiss LSM20 confocal microscope at 60X zoom with oil immersion. Captured images were exported and analyzed using the free Zen 2009 Light Edition software (Zeiss). A Z-stack was attempted, but unsuccessful due to the thickness of the MDCK cells and limitations of the

equipment used. All IFAs were performed in technical duplicate initially, followed by a biological duplicate.

2.6: Testing the *in vivo* Potential of Suspected Entry Inhibitors

2.6.1: Virus stock generation by ultracentrifugation

To generate the MA-HK68 virus for the following murine experiments, ultracentrifugation was used to generate a high enough concentration of viruses to be used. Because 50 μL per mouse was required and had to reach $10LD_{50}$ for a lethal infection, the titer of the existing stock was too low without concentrating the virus from the supernatant to be used for this experiment. MDCK cells were prepared in 10 T150 cm^2 flasks (Corning) to 80% confluency in MEM/5% FCS/L-glutamine. Cells were then washed with PBS to remove residual FCS, which can inhibit trypsin activity required for successful IAV growth. The virus was then added to the T150 cm^2 flasks of cells in Minimum Essential Medium (MEM) containing 0.1% BSA and 1 μg/mL of TPCK-treated trypsin. I inoculated flasks with 5 μL of virus diluted in 10 mL of supplemented medium. The inoculated flasks were then incubated for 48-72 h in a 37°C humidified incubator with 5% CO_2 until >80% of the cells showed CPE. To harvest the virus, all supernatant was collected from the 10 T150 flasks and centrifuged at 500 x g for 10 min at 4°C to pellet cell debris. Aliquots of the supernatant post-centrifugation were taken and stored at -80°C for titration of pre-concentrated virus by $TCID_{50}$ (see section 2.2.4). To generate concentrated virus, the remaining supernatants were ultracentrifuged in a Beckman-Coulter L90-K with a SW-32 Ti rotor at 96,325 RCF (xg) for 1 h at 4°C. Supernatant was then discarded, and tubes were left to dry for 5 min upside down on the benchtop. Once dry, 200 μL of PBS was added to each virus pellet (per tube) and incubated at

4°C overnight, to soften the pellet and allow for easier resuspension the following day. Dissolved pellets were combined together post-incubation, aliquoted, and stored at -80°C until $TCID_{50}$ quantification was performed.

2.6.2: Evaluation of entry inhibitor candidate compounds in vivo

Experiments conducted with mice were approved by the Animal Care Committee (ACC) at the National Microbiology Lab in Winnipeg, Canada following procedures outlined in protocol H-22-018. All experimental work followed guidelines set out by the Canadian Council on Animal Care. Female and male 4–6-week-old BALB/c mice (Charles River Laboratories, Montreal, Quebec) were housed in BSL-2 facilities in HEPA filtered air caging units. The mice were housed in groups and fed standard chow diets with food and water provided ad libitum. Mice were housed in groups of 3 (separated by sex) per caging unit, following ACC protocols. Mice were monitored for health daily during the experimental period, cages were changed weekly, and the mice were euthanized once they had passed ACC-outlined guidelines for lethal illness (see section 8.1). Veterinary Technician Services (VTS) staff closely monitored animals in accordance with these rules throughout the experiment, and they were weighed daily and scored for symptoms and overall condition at least once daily.

On day -1 to 4 post-infection, groups of 6 mice (3 male, 3 female) per treatment compound and time point were treated daily with 200 µL of compound, as per Table 5. The compounds were diluted in DMSO at a concentration well below the LD_{50} of DMSO in mice. DMSO can be toxic at some concentrations in mice. For IP injections, the LD_{50} of DMSO is 6.2 mL/kg[126]. The mice received the equivalent of 0.1 mL/kg for the oridonin treatments and 0.02 mL/kg for sodium

Table 5. The dosing strategy for oridonin, dioscin, sodium aescinate, and calycosin-7-glucoside treatment of BALB/c mice.

Drug Treatment	**Dose (given on day -1 through 4 post-infection)**	**Delivery Route**	**Published LD_{50} in Mice**
Oridonin	10 mg/kg daily[130]	Intraperitoneal injection	35-40 mg/kg[127]
Dioscin	80 mg/kg daily[131,132]	Oral gavage	538.72 mg/kg[128]
Sodium aescinate	2 mg/kg daily[133]	Intraperitoneal injection	Unknown
Calycosin-7-glucoside	100 mg/kg daily[134]	Oral gavage	Unknown

aescinate treatments, which was well below the toxicity threshold of these compounds[127,128]. For oral gavage treatments, the LD_{50} of DMSO in mice is 16.5-21.4 mL/kg and they received the equivalent of 1.6 mL/kg of DMSO for the dioscin treatments, and 1 mL/kg of DMSO for the calycosin-7-glucoside treatments[129]. This means the mice did not receive the amount of DMSO expected to cause toxicity in this animal model. On day 0, mice were anesthetized with isofluorane and infected intranasally (dropwise) with 50 µL of inoculum containing $10LD_{50}$ of murine-adapted HK68. The LD_{50} was determined by Dr. Darwyn Kobasa to be $10^{4.6}$ $TCID_{50}$ per mouse. However, this stock of virus had been depleted by other experiments, and subsequent stocks had a lower concentration, which required ultracentrifugation for use in mice. All procedures were performed with the support of Veterinary Technical Services staff. Upon reaching a termination score, greater than 25% weight loss, or the end of the experiment (whichever occurred first), mice were euthanized by a lethal dose of isofluorane and cervical dislocation by VTS staff.

Chapter Three: Results

3.1: Screening Compound Libraries for Novel IAV Antivirals

3.1.1: Initial screening of compound libraries to identify potential novel seasonal IAV antiviral candidates

The libraries were screened at 100 μM for the FDA-Approved Library (containing 2,230 compounds) and 10 μM and 100 μM for the Natural Source Library (containing 550 compounds), the results of which are shown in in Table 6. The compounds from the libraries were tested against 0.001 MOI of RV733 and assessed for CPE reduction 48 hours post-infection. A DMSO-only control was included, which contained 1% DMSO. DMSO presence did not negatively impact cell integrity, as the cell monolayer remained intact. From the initial screen, 6 compounds from the FDA-Approved Library and 101 compounds from the Natural Source Library showed an estimated >80% CPE reduction on confluent MDCK cells 48hpi, determined visually. Nitolinib was eliminated at this stage because it has previously documented safety concerns or toxicity, reducing feasibility as an IAV antiviral[135,136]. Acacetin, alibiflorin, arctigenin, artesunate, benzethonium chloride, brucine, carnosic acid, diacerein, diltiazem HCl, echinacoside, gallic acid, ginsenoside Ro, harmine hydrochloride, isochlorogenic acid A, mycophenolic acid, nobiletin, patchouli alcohol, gensenoside Rh2, shikonin, ursolic acid, 6,7-dihydroxycoumarin, 8-methoxypsoralen, and α-estradiol were eliminated as they had already been tested in some capacity against influenza viruses[137–159]. The inhibition assay yielded 6 FDA-approved compounds (3 of which were from the FDA-approved Library, and 3 that were from the Natural Source Library), and 12 non-FDA approved natural products that notably reduced virus titer in confluent MDCK cells 48 hpi (see Table 7 and Table 8). A literature review

Table 6. Effective compounds identified during library screening*.

Compound	Library	100 µM screen of natural source and FDA-approved library	10 µM rescreen of natural source library**
Acacetin	ApexBIO Natural Source Compound Library	Not Effective	Effective
Alibiflorin	ApexBIO Natural Source Compound Library	Not Effective	Effective
Alisol B 23-acetate	ApexBIO Natural Source Compound Library	Effective	
Amentoflavone	ApexBIO Natural Source Compound Library	Effective	
Andrographolide	ApexBIO Natural Source Compound Library	Effective	
Antazoline HCl	ApexBIO FDA-Approved Library	Effective	
Arctigenin	ApexBIO Natural Source Compound Library	Not Effective	Effective
Artesunate	ApexBIO Natural Source Compound Library	Effective	
Asiatic acid	ApexBIO Natural Source Compound Library	Effective	
Aurantio-obtusin	ApexBIO Natural Source Compound Library	Effective	
Benzethonium Chloride	ApexBIO FDA-Approved Library	Effective	
Beta-Lapachone	ApexBIO FDA-Approved Library	Effective	Effective
Biochanin A	ApexBIO Natural Source Compound Library	Effective	
Bilirubin	ApexBIO Natural Source Compound Library	Effective	
Brazilin	ApexBIO Natural Source Compound Library	Effective	
Brucine	ApexBIO Natural Source Compound Library	Not Effective	Effective
Calycosin-7-Glucoside	ApexBIO Natural Source Compound Library	Effective	
Cantharanthine	ApexBIO Natural Source Compound Library	Effective	
Carnosic acid	ApexBIO Natural Source Compound Library	Effective	
Caudatin	ApexBIO Natural Source Compound Library	Effective	
Celastrol	ApexBIO Natural Source Compound Library	Effective	
Chelerythrine	ApexBIO Natural Source Compound Library	Effective	

Clinodiside A	ApexBIO Natural Source Compound Library	Effective	
Coptisine chloride	ApexBIO Natural Source Compound Library	Effective	
Dehydroandrographolide	ApexBIO Natural Source Compound Library	Effective	
Demethoxycurcumin	ApexBIO Natural Source Compound Library	Effective	
Diacerein	ApexBIO Natural Source Compound Library	Effective	
Dihydroartemisinin	ApexBIO Natural Source Compound Library	Effective	
Diltiazem HCl	ApexBIO FDA-Approved Library	Effective	
Dioscin	ApexBIO Natural Source Compound Library	Effective	
Diosmetin	ApexBIO Natural Source Compound Library	Effective	
Domiphen Bromide	ApexBIO FDA-Approved Library	Effective	
Doxycycline hyclate	ApexBIO Natural Source Compound Library	Effective	
Ecdysterone	ApexBIO Natural Source Compound Library	Effective	
Echinacoside	ApexBIO Natural Source Compound Library	Not Effective	Effective
Epiandrosterone	ApexBIO Natural Source Compound Library	Effective	
Fraxetin	ApexBIO Natural Source Compound Library	Effective	
Gallic acid	ApexBIO Natural Source Compound Library	Effective	
Genipin	ApexBIO Natural Source Compound Library	Effective	
Ginsenoside Ro	ApexBIO Natural Source Compound Library	Not Effective	Effective
Glucosyl-vitexin	ApexBIO Natural Source Compound Library	Effective	
Gracillin	ApexBIO Natural Source Compound Library	Effective	
Harmine hydrochloride	ApexBIO Natural Source Compound Library	Not Effective	Effective
Harpagoside	ApexBIO Natural Source Compound Library	Effective	
Helicid	ApexBIO Natural Source Compound Library	Effective	
Hydroxysafflor yellow A	ApexBIO Natural Source Compound Library	Effective	
Isoacteoside	ApexBIO Natural Source Compound Library	Effective	

Isochlorogenic acid A	ApexBIO Natural Source Compound Library	Not Effective	Effective
Isoliquiritin	ApexBIO Natural Source Compound Library	Effective	
Kinetin	ApexBIO Natural Source Compound Library	Effective	
Khasianine	ApexBIO Natural Source Compound Library	Effective	
Leonurine hydrochloride	ApexBIO Natural Source Compound Library	Effective	
Limonin	ApexBIO Natural Source Compound Library	Effective	
Linderane	ApexBIO Natural Source Compound Library	Effective	
Lithospermic acid	ApexBIO Natural Source Compound Library	Effective	
L-Theanine	ApexBIO Natural Source Compound Library	Effective	
Momordin Ic	ApexBIO Natural Source Compound Library	Effective	
Mycophenolic acid	ApexBIO Natural Source Compound Library	Not Effective	Effective
Momordin Ic	ApexBIO Natural Source Compound Library	Effective	
Mulberroside A	ApexBIO Natural Source Compound Library	Effective	
Nilotinib	ApexBIO FDA-Approved Library	Not Effective	Effective
Nobiletin	ApexBIO Natural Source Compound Library	Not Effective	Effective
Nordihydroguaiaretic acid	ApexBIO Natural Source Compound Library	Effective	
Oridonin	ApexBIO Natural Source Compound Library	Effective	
Oxybutynin chloride	ApexBIO Natural Source Compound Library	Effective	
Patchouli alcohol	ApexBIO Natural Source Compound Library	Not Effective	Effective
Parthenolide	ApexBIO Natural Source Compound Library	Effective	
Phloretin	ApexBIO Natural Source Compound Library	Effective	
Piperlongumine	ApexBIO Natural Source Compound Library	Effective	
Polyphyllin A	ApexBIO Natural Source Compound Library	Effective	
Polyphyllin B	ApexBIO Natural Source Compound Library	Effective	
Polyphillin VII	ApexBIO Natural Source Compound Library	Effective	

Progesterone	ApexBIO Natural Source Compound Library	Effective	
Protodioscin	ApexBIO Natural Source Compound Library	Effective	
Protopine	ApexBIO Natural Source Compound Library	Effective	
Psoralen	ApexBIO Natural Source Compound Library	Effective	
Pteryxin	ApexBIO Natural Source Compound Library	Effective	
Pulsatilla saponin D	ApexBIO Natural Source Compound Library	Effective	
Punicalagin	ApexBIO Natural Source Compound Library	Effective	
(R) Ginsenoside Rh2	ApexBIO Natural Source Compound Library	Effective	
Rutin	ApexBIO Natural Source Compound Library	Effective	
Saikosaponin A	ApexBIO Natural Source Compound Library	Effective	
Saikosaponin B	ApexBIO Natural Source Compound Library	Effective	
Salvianolic acid A	ApexBIO Natural Source Compound Library	Effective	
Schisantherin A	ApexBIO Natural Source Compound Library	Effective	
Sec-O-Glucosylhamaudol	ApexBIO Natural Source Compound Library	Effective	
Sinomenine Hydrochloride	ApexBIO Natural Source Compound Library	Effective	
Shikonin	ApexBIO Natural Source Compound Library	Effective	
Sodium Aescinate	ApexBIO Natural Source Compound Library	Effective	
Solamargine	ApexBIO Natural Source Compound Library	Effective	
Solasonine	ApexBIO Natural Source Compound Library	Effective	
Syringin	ApexBIO Natural Source Compound Library	Effective	
Tanshinone IIA	ApexBIO Natural Source Compound Library	Effective	
Teriflunomide	ApexBIO FDA-Approved Library	Effective	
Theophylline	ApexBIO Natural Source Compound Library	Effective	
Ursolic acid	ApexBIO Natural Source Compound Library	Not Effective	Effective
Vindoline	ApexBIO Natural Source Compound Library	Effective	

Yohimbine Hydrochloride	ApexBIO Natural Source Compound Library	Effective	
3,3'-Diindolylmethane	ApexBIO Natural Source Compound Library	Effective	
5-O-Methylvisammioside	ApexBIO Natural Source Compound Library	Effective	
6,7-Dihydroxycoumarin	ApexBIO Natural Source Compound Library	Not Effective	Effective
8-Methoxypsoralen	ApexBIO Natural Source Compound Library	Not Effective	Effective
10-Hydroxycamptothecin	ApexBIO Natural Source Compound Library	Effective	
12-O-tetradecanoyl phorbol-13-acetate	ApexBIO Natural Source Compound Library	Effective	
α-Cyperone	ApexBIO Natural Source Compound Library	Effective	
α-Estradiol	ApexBIO Natural Source Compound Library	Effective	
(-)-Epigallocatechin gallate (EGCG)	ApexBIO Natural Source Compound Library	Effective	

**Where "effective" indicates compounds that fully inhibited visible CPE in MDCK cells, 48 hpi.*
***Blank boxes indicate compounds that were only tested at 100 µM. Note that only compounds deemed were effective in the 100 µM or 10 µM screen are listed here. In some cases, toxicity at 100 µM may have initially been mistaken for CPE, but upon retesting at 10 µM, the effectiveness of the compound could be accurately noted.*

Table 7. The results of the inhibition assay performed with RV733 in MDCK cells*.

Compound	Lowest Effective Concentration (μM)**	Biological Replicate 1	Biological Replicate 1	Biological Replicate 2	Biological Replicate 2	Mean	Standard Deviation
Alisol β-23-acetate	10	$4.16x10^7$	$1.00x10^7$	$3.83x10^7$	$4.16x10^7$	$3.29x10^7$	$1.53x10^7$
alpha-estradiol	10	$1.00x10^7$	$2.54x10^7$	$3.83x10^7$	$3.83x10^7$	$2.80x10^7$	$1.35x10^7$
Amentoflavone	10	$1.85x10^7$	$3.83x10^7$	$1.47x10^7$	$1.85x10^7$	$2.25x10^7$	$1.07x10^7$
Andrographolide	10	$1.47x10^7$	$3.16x10^7$	$3.83x10^7$	$4.16x10^7$	$2.37x10^7$	$1.98x10^7$
Asiatic acid	10	$1.85x10^7$	$1.96x10^7$	$1.00x10^7$	$3.83x10^7$	$2.16x10^7$	$1.19x10^7$
Aurantio-obtusin	10	$1.00x10^7$	$1.85x10^7$	$4.16x10^7$	$1.85x10^7$	$2.21x10^7$	$1.36x10^7$
Bilirubin	10	$3.83x10^7$	$1.47x10^7$	$1.47x10^7$	$4.16x10^7$	$2.73x10^7$	$1.46x10^7$
Biochainin A	10	$2.54x10^7$	$4.16x10^7$	$1.00x10^7$	$3.83x10^7$	$2.88x10^7$	$1.44x10^7$
Brazilin	2.5	$1.00x10^7$	$4.16x10^7$	$3.83x10^7$	$1.00x10^7$	$2.50x10^7$	$1.73x10^7$
Calycosin-7-glucoside	1.25	$3.83x10^6$	$1.00x10^6$	$2.98x10^5$	$1.00x10^5$	$1.31x10^6$	$1.73x10^6$
Cantharanthine	10	$5.11x10^3$	$5.11x10^3$	$5.11x10^3$	$2.33x10^4$	$9.65x10^3$	$9.08x10^3$
Captisine chloride	10	$1.96x10^7$	$3.83x10^7$	$3.83x10^7$	$4.16x10^7$	$3.44x10^7$	$1.00x10^7$
Carnosin acid	5	$1.00x10^7$	$1.00x10^7$	$1.85x10^7$	$1.85x10^7$	$1.42x10^7$	$4.90x10^6$
Caudatin	10	$3.83x10^7$	$3.83x10^7$	$1.96x10^7$	$1.96x10^7$	$2.89x10^7$	$1.08x10^7$
Celestrol	0.625	$4.98x10^4$	$4.98x10^4$	$4.97x10^3$	$4.97x10^3$	$2.74x10^4$	$2.59x10^4$
Chelerythrine	2.5	$1.85x10^7$	$3.83x10^7$	$1.85x10^7$	$1.00x10^7$	$2.13x10^7$	$1.20x10^7$
Clinodisolide A	5	$2.54x10^7$	$3.83x10^7$	$3.16x10^7$	$1.00x10^7$	$2.63x10^7$	$1.21x10^7$
Corticosterone	10	$3.16x10^7$	$4.16x10^7$	$4.16x10^7$	$1.00x10^7$	$3.12x10^7$	$1.49x10^7$
Dehydroandrographolide	10	$1.00x10^7$	$3.83x10^7$	$3.83x10^7$	$1.00x10^7$	$2.42x10^7$	$1.63x10^7$
Demethoxycurcimin	5	$1.00x10^7$	$1.00x10^7$	$3.83x10^7$	$1.00x10^7$	$1.71x10^7$	$1.42x10^7$
Demethyliseylasterol	10	$3.16x10^6$	$1.00x10^6$	$1.47x10^7$	$1.00x10^7$	$7.21x10^6$	$6.29x10^6$
Dihydroartemisinin	5	$1.85x10^7$	$1.85x10^7$	$1.00x10^7$	$1.47x10^7$	$1.54x10^7$	$4.02x10^6$
Dioscin	0.156	$1.00x10^3$	$5.11x10^3$	$5.16x10^2$	$5.11x10^3$	$2.93x10^3$	$2.52x10^3$
Diosmetin	1.25	$2.01x10^5$	$2.01x10^5$	$4.30x10^5$	$2.01x10^5$	$2.58x10^5$	$1.14x10^5$
Doxycycline hyclate	0.313	$2.40x10^3$	$5.41x10^2$	$2.40x10^3$	$2.40x10^3$	$1.94x10^3$	$9.31x10^2$
Ecdysterone	10	$1.96x10^7$	$2.54x10^7$	$1.47x10^7$	$3.16x10^7$	$2.28x10^7$	$7.33x10^6$
ECGC	0.625	$3.16x10^5$	$1.00x10^5$	$3.16x10^5$	$3.35x10^4$	$1.91x10^5$	$1.47x10^5$
Epiandesterone	0.156	$5.11x10^3$	$5.11x10^3$	$2.40x10^3$	$5.11x10^3$	$4.43x10^3$	$1.35x10^3$
Fraxetin	5	$1.47x10^7$	$3.83x10^7$	$1.00x10^7$	$4.16x10^7$	$2.62x10^7$	$1.61x10^7$
Genipin	10	$1.47x10^7$	$1.00x10^7$	$3.83x10^7$	$1.47x10^7$	$1.94x10^7$	$1.28x10^7$
Germacrone	1.25	$4.30x10^6$	$2.01x10^6$	$4.30x10^6$	$4.30x10^6$	$3.73x10^6$	$1.14x10^6$
Glucosylvitexin	10	$3.16x10^7$	$3.16x10^7$	$1.47x10^7$	$1.96x10^7$	$2.44x10^7$	$8.61x10^6$
Gracillin	0.156	$4.16x10^7$	$1.47x10^7$	$1.85x10^7$	$1.00x10^7$	$2.12x10^7$	$1.40x10^7$
Harpagoside	10	$1.47x10^7$	$4.16x10^7$	$1.00x10^7$	$1.47x10^7$	$2.02x10^7$	$1.44x10^7$
Helicid	10	$4.16x10^7$	$4.16x10^7$	$1.96x10^7$	$3.83x10^7$	$3.53x10^7$	$1.06x10^7$
Hydroxysafflor yellow A	10	$1.00x10^7$	$3.83x10^7$	$4.16x10^7$	$3.16x10^7$	$3.04x10^7$	$1.42x10^7$
Isoacetoside	10	$3.83x10^7$	$1.47x10^7$	$4.16x10^7$	$2.54x10^7$	$3.00x10^7$	$1.24x10^7$
Isoliquiritin	10	$1.00x10^3$	$4.30x10^6$	$1.00x10^5$	$1.00x10^5$	$1.12x10^6$	$2.12x10^6$
Khasianine	0.313	$1.00x10^4$	$5.11x10^3$	$5.11x10^3$	$1.00x10^4$	$7.55x10^3$	$2.82x10^3$
Kinetin	1.5	$2.40x10^3$	$2.40x10^3$	$2.40x10^3$	$2.40x10^3$	$1.86x10^3$	$1.08x10^3$
Leonurine hydrochloride	10	$4.16x10^7$	$1.00x10^7$	$4.16x10^7$	$1.85x10^7$	$2.79x10^7$	$1.62x10^7$
Limonin	0.625	$4.98x10^4$	$4.98x10^3$	$4.98x10^4$	$4.98x10^4$	$3.86x10^4$	$2.24x10^4$
Linderane	10	$4.16x10^7$	$3.83x10^7$	$1.00x10^7$	$1.96x10^7$	$2.74x10^7$	$1.51x10^7$
Lithospermic acid	10	$1.47x10^7$	$4.16x10^7$	$4.16x10^7$	$1.00x10^7$	$2.70x10^7$	$1.70x10^7$
L-Theanine	10	$1.00x10^7$	$4.16x10^7$	$1.47x10^7$	$1.96x10^7$	$2.15x10^7$	$1.40x10^7$
Momordin Ic	2.5	$1.00x10^7$	$1.47x10^7$	$3.83x10^7$	$3.83x10^7$	$2.53x10^7$	$1.51x10^7$
Mulberroside A	1.25	$3.16x10^5$	$1.00x10^5$	$1.00x10^5$	$1.00x10^5$	$1.54x10^5$	$1.08x10^5$
Nordihydroguaiaretic acid	0.156	$5.41x10^2$	$1.00x10^3$	$1.00x10^4$	$1.00x10^3$	$3.14x10^3$	$4.58x10^3$
Oridonin	1.25	$2.61x10^2$	$1.00x10^4$	$3.83x10^5$	$1.00x10^5$	$1.23x10^5$	$1.79x10^5$

Oroxin B	10	$1.47x10^7$	$4.16x10^7$	$4.16x10^7$	$3.83x10^7$	$3.41x10^7$	$1.30x10^7$
Oxybutinin chloride	1.25	$1.96x10^7$	$2.99x10^6$	$1.00x10^7$	$1.00x10^7$	$1.06x10^7$	$6.81x10^6$
Pathenolide	5	$1.47x10^7$	$4.16x10^7$	$3.83x10^7$	$4.16x10^7$	$3.40x10^7$	$1.30x10^7$
Phloretin	0.313	$5.11x10^3$	$5.41x10^2$	$5.11x10^3$	$5.11x10^3$	$3.97x10^3$	$2.28x10^3$
Piperlogumine	1.25	$2.01x10^6$	$2.33x10^4$	$2.01x10^6$	$2.01x10^6$	$1.51x10^6$	$9.93x10^5$
Polyphyllin A	0.078	0	0	0	0	0	0
Polyphyllin B	1.25	$1.00x10^5$	$1.00x10^4$	$1.00x10^5$	$1.00x10^5$	$7.75x10^4$	$4.50x10^4$
Polyphyllin VII	0.078	0	0	0	0	0	0
Progesterone	10	$5.41x10^2$	$1.00x10^3$	$1.00x10^3$	$2.40x10^3$	$1.24x10^3$	$8.08x10^2$
Protodiscin	10	$1.00x10^7$	$1.85x10^7$	$1.85x10^7$	$3.83x10^7$	$2.13x10^7$	$1.20x10^7$
Protopine	10	$1.00x10^7$	$1.00x10^7$	$3.83x10^7$	$3.83x10^7$	$2.42x10^7$	$1.63x10^7$
Psoralen	10	$3.16x10^7$	$1.85x10^7$	$4.16x10^7$	$4.16x10^7$	$3.33x10^7$	$1.10x10^7$
Pteryxin	10	$4.16x10^7$	$1.47x10^7$	$3.83x10^7$	$4.16x10^7$	$3.41x10^7$	$1.30x10^7$
Pulsatilla saponin D	0.313	$5.11x10^3$	$2.40x10^3$	$5.11x10^3$	$5.11x10^3$	$4.43x10^3$	$1.35x10^3$
Punicalagin	10	$3.83x10^7$	$1.96x10^7$	$4.16x10^7$	$4.16x10^7$	$3.53x10^7$	$1.06x10^7$
Rutin	10	$1.47x10^7$	$1.96x10^7$	$1.85x10^7$	$1.47x10^7$	$1.69x10^7$	$2.54x10^6$
Saikosaponin A	1.25	$1.96x10^7$	$1.47x10^7$	$1.96x10^7$	$4.16x10^7$	$2.39x10^7$	$1.20x10^7$
Saikosaponin B	2.5	$1.00x10^7$	$1.00x10^7$	$3.83x10^7$	$1.85x10^7$	$1.92x10^7$	$1.34x10^7$
Salvanolic acid A	10	$1.00x10^7$	$1.00x10^7$	$4.16x10^7$	$1.85x10^7$	$2.00x10^7$	$1.49x10^7$
Schisantherin A	10	$4.16x10^7$	$3.83x10^7$	$1.00x10^7$	$3.83x10^7$	$3.21x10^7$	$1.48x10^7$
Sec-o-glucosylhammaudol	10	$3.83x10^7$	$1.85x10^7$	$1.47x10^7$	$3.16x10^7$	$2.58x10^7$	$1.11x10^7$
Shikonin	0.156	$1.00x10^7$	$1.47x10^7$	$4.16x10^7$	$4.16x10^7$	$2.70x10^7$	$1.70x10^7$
Sinomethine hydrochloride	10	$4.16x10^7$	$1.47x10^7$	$1.96x10^7$	$1.47x10^7$	$2.26x10^7$	$1.28x10^7$
Sodium aescinate	2.5	$1.00x10^6$	$1.47x10^6$	$3.84x10^5$	$1.00x10^5$	$7.38x10^5$	$6.15x10^5$
Solamargine	1.25	$4.16x10^6$	$1.96x10^6$	$4.97x10^3$	$4.97x10^3$	$1.53x10^6$	$1.98x10^6$
Solasonine	10	$1.96x10^7$	$1.00x10^7$	$3.16x10^7$	$1.96x10^7$	$2.02x10^7$	$8.86x10^6$
Syringin	10	$4.16x10^7$	$1.00x10^7$	$1.85x10^7$	$4.16x10^7$	$2.79x10^7$	$1.62x10^7$
Tanshinone 11A	10	$4.16x10^7$	$3.83x10^7$	$1.47x10^7$	$1.47x10^7$	$2.73x10^7$	$1.46x10^7$
Theophylline	10	$1.85x10^7$	$1.47x10^7$	$1.96x10^7$	$1.85x10^7$	$1.78x10^7$	$2.15x10^6$
Vindoline	5	$1.00x10^7$	$3.83x10^7$	$1.00x10^7$	$1.00x10^7$	$1.71x10^7$	$1.42x10^7$
Yohimibine hydrochloride	10	$1.00x10^7$	$1.85x10^7$	$3.83x10^7$	$1.00x10^7$	$1.92x10^7$	$1.34x10^7$
α-cyperone	10	$1.47x10^7$	$1.00x10^7$	$1.00x10^7$	$1.47x10^7$	$1.23x10^7$	$2.71x10^6$
10-hydroxycamptothecin	10	$3.83x10^7$	$3.83x10^7$	$1.00x10^7$	$1.47x10^7$	$2.53x10^7$	$1.51x10^7$
12-O-tetradecanoyl-phorbol-13-acetate	5	0	0	0	0	0	0
3,3-diindolylmethane	2.5	$2.61x10^2$	$5.41x10^2$	$1.00x10^3$	$2.61x10^2$	$5.16x10^2$	$3.49x10^2$
5-O-methylsivammioside	10	$3.83x10^7$	$4.16x10^7$	$1.96x10^7$	$1.47x10^7$	$2.85x10^7$	$1.34x10^7$
Oseltamivir	10	$1.00x10^5$	$1.85x10^5$	$4.16x10^6$	$1.47x10^5$	$1.00x10^1$	0
Virus control	N/A	$4.16x10^7$	$3.83x10^7$	$4.16x10^7$	$4.16x10^7$	$4.08x10^7$	$1.64x10^6$
Cell control	N/A	0	0	0	0	0	0

**In which viral titers were calculated by $TCID_{50}$ quantification using the Reed and Muench method, 48 hpi.*

***Note the lowest effective concentration was determined by CPE observation, representing the last well to show CPE in the presence of the compound.*

Table 8. Compounds found to be effective against RV733 in an MDCK cell model.

Compound Name	Original Source	Pharmaceutical Use	FDA-Approved	ApexBIO Library Source
Teriflunomide	Synthetic[160]	Anti-inflammatory that reduces proliferation of dividing cells which require *de novo* synthesis of pyrimidine to expand, used for treatment of Multiple Sclerosis[161]	Yes	FDA-approved Library
Antazoline	Synthetic[162]	Allergic conjunctivitis treatment (first-generation antihistamine)[163]	Yes	FDA-approved Library
Domiphen bromide	Synthetic[164]	A quaternary ammonium disinfectant compound used in sterilization solutions (e.g., mouthwash) and lozenges[164]	Yes	FDA-approved Library
Kinetin	Cytokinin found in *Cocos nucifera, Panax ginseng*, and *Carapichea I pecacuanha*	Plant growth hormone, used in cosmetics and anti-aging compounds[165]	Yes	Natural Source Library
Progesterone	A naturally occurring hormone found in animals[166]	Used for hormone replacement therapy and cancer treatment[167]	Yes	Natural Source Library
Sodium aescinate	Salt found in Rehd seeds from *Aesculus wilsonii*[168]	Used for wound healing in skin or lung injuries[168,169]	Yes	Natural Source Library

Epigallocatechin Gallate (EGCG)	Green tea leaves[170]	Suggested as a treatment for neudegenerative disorders[170,171]	No	Natural Source Library
3,3'-diindolylmethane	Cruciferous vegetables[172]	Used to treat gastrointestinal cancer and modulate estrogen levels in some disorders[172]	No	Natural Source Library
Phloretin	Apple tree leaves, and other fruits[173]	Claimed to be an antioxidant and anti-aging medication, used as an anti-inflammatory and neuroprotective compound[173,174]	No	Natural Source Library
Catharanthine	*Catharanthus roseus* plants[175]	Oncology compound, antioxidant, anti-microbial, wound-healing, and hypotensive properties[175]	No	Natural Source Library
Solamargine	Family Solanaceae plants (e.g., potatoes, tomatoes, eggplant)[176]	Oncology compound, particularly used for pancreatic and gastric cancer treatment[176]	No	Natural Source Library
Calycosin-7-glucoside	*Astragalus membranaceus*, a Chinese herb[177]	Used for prevention of apoptosis, oxidative stress, and neuronal apoptosis reduction[177]	No	Natural Source Library
Mulberroside A	White mulberry (Morus alba) root[178]	Nephroprotective, hypoglycemic, and neuroprotective properties[178]	No	Natural Source Library

Diosmetin	Citrus fruits[179]	Popular flavonoid, recently described to have anti-Alzheimer's properties[179]	No	Natural Source Library
Dioscin	Vegetables and herbs from the family *Dioscoreaceae*, among others[180]	Described to have antifungal, antiviral, anti-hyperuricemia, anti-tumor, and hepatoprotective properties[180]	No	Natural Source Library
Oridonin	*Rabdosia rubescens* herb[181]	Described to have anti-cancer, anti-inflammatory, and neuroprotective properties[181,182]	No	Natural Source Library
Polyphyllin B	*Paris formosana* Hayata plant[183]	Described tumor growth suppressant[183]	No	Natural Source Library
12-O-tetradecanoglyphorbol-B-acetate	The seed oil of the Croton tiglium L shub[184]	Used primarily as an oncology compound against liver and pancreatic cancer[184]	No	Natural Source Library

was performed at this stage, and celestrol, isoliquiritin, deoxycycline hyclate, and nordihydroguaiaretic acid were eliminated because they had already been identified as potential IAV therapeutics[185–188]. Khasianine was removed because its molecular weight of 720 kDa is higher than the threshold allowed by Lipinski's rule of five, suggesting poor metabolism and pharmacokinetic properties (including low permeability, solubility, and/or metabolic clearance)[189]. Limonin, pulsatilla saponin D and polyphyllin VII were removed because they had previously shown poor bioavailability, in the case of limonin, and toxicity concerns, in these cases[190,191]. Epiandesterone was not pursued further because it is a biologically active oxygenated metabolite of DHEA, which has been tested as a potential IAV therapeutic[192]. This impact was observed microscopically by noting damaged or floating cells as CPE from cytotoxicity or viral damage. The dose range of 19.5 nM to 100 μM was anticipated to result in a full S-curve of effectiveness showing both extremes of full effectiveness and lack thereof in an MDCK model. Compounds were considered "effective" and carried forward to later stages of testing if they reduced CPE and viral titers, compared to the infected, untreated control. If the observed CPE and viral titers were comparable to the virus-infected control, then these were considered "ineffective" and not carried forward into later testing.

3.1.2: Assessing cell viability by measurement of metabolic activity via XTT cytotoxicity assay

The XTT Cell Viability Assay indicates the toxicity of a compound, with higher readout values suggesting less toxicity after 48 hours of incubation with the compound. A higher readout result suggests that cellular metabolism was not negatively impacted by potential toxicity from the compound. The XTT cytotoxicity assay indicated that 14 of the 18 compounds carried forward from initial screening and the inhibition assay were categorized as being "effective",

suggesting that they showed low to no toxicity in MDCK cells (see Figure 6). Teriflunomide, polyphyllin B, solamargine, 12-O-tetradecanoylphorbol-B-acetate, disometin, and phloretin were toxic at lower concentrations than other compounds tested (see Figure 6) but were carried forward to determine the selectivity index of these compounds. Other compounds showed toxicity when 125 μM or higher concentration was tested. While oridonin showed toxicity above 15.6 μM, these are very high concentrations of compound, and was not considered problematically toxic at this stage of the project (see Figure 6). Despite six compounds showing toxicity at higher doses, all 18 compounds identified in the inhibition assay were carried forward for subsequent testing, which was performed below the toxic concentration identified for these compounds in the XTT cytotoxicity assay.

3.1.3: Quantifying RV733 titers in the presence of the compounds of interest

The yield assay aimed to quantify the amount of virus present in the supernatant after incubation in a cell model in the presence of the compounds of interest to determine if they reduced virus titers. The yield assay included a step of virus quantification by $TCID_{50}$ at the end of the incubation period with a range of compound dilutions (0.195 – 100 μM in 1:2 dilutions) (see Figure 7). The data were graphed using GraphPad 9 software utilizing a non-linear fit dose-response curve with variable slope and four parameters graph of $\log_{10}$(inhibitor) vs. response curve. While these experiments were performed to show effectiveness for follow-up studies, future studies may benefit from investigation into this specific concentration range at which effectiveness is lost to examine this effect and look into it mechanistically.

a)

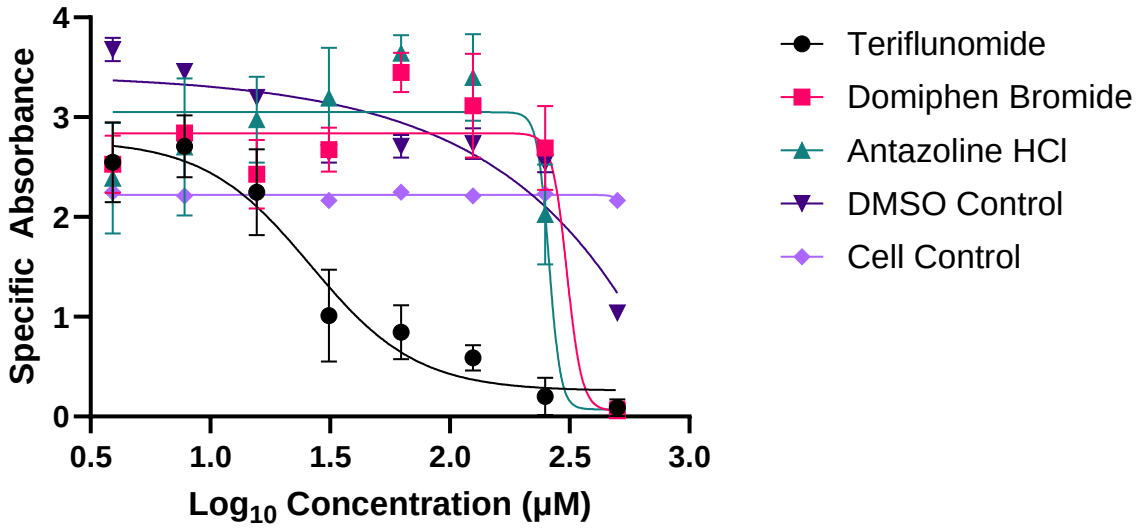
Specific Absorbance
4
3
2
1
0
0.5
1.0
1.5
2.0
2.5
3.0
Log10 Concentration (μM)
Teriflunomide
Domiphen Bromide
Antazoline HCl
DMSO Control
Cell Control

b)

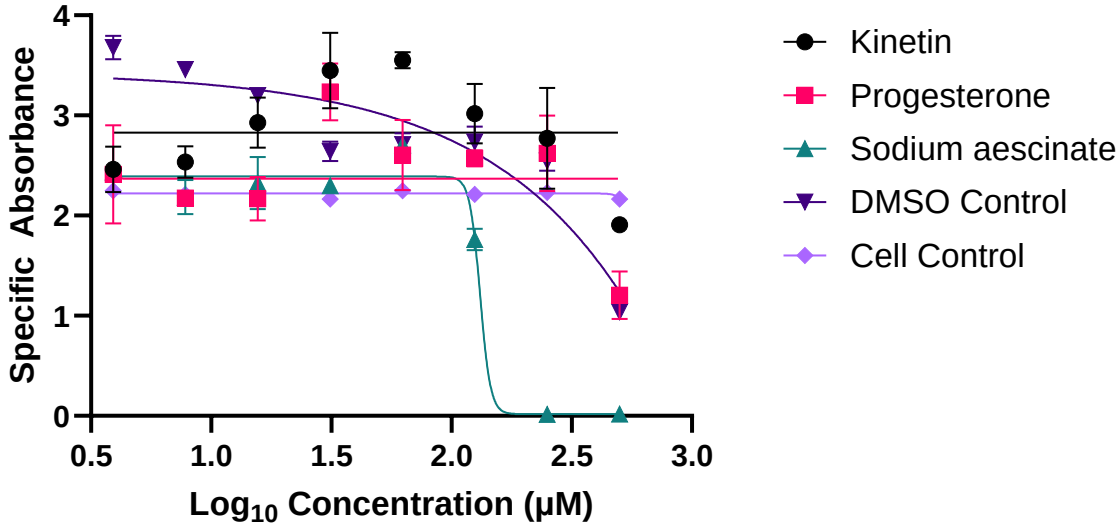
Specific Absorbance
4
3
2
1
0
0.5
1.0
1.5
2.0
2.5
3.0
Log10 Concentration (μM)
Kinetin
Progesterone
Sodium aescinate
DMSO Control
Cell Control

c)

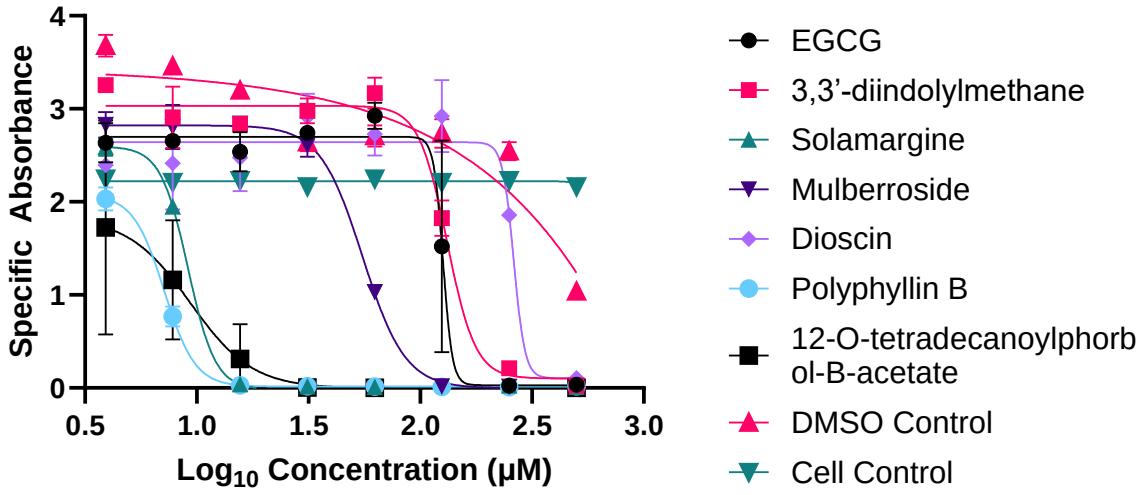

d)

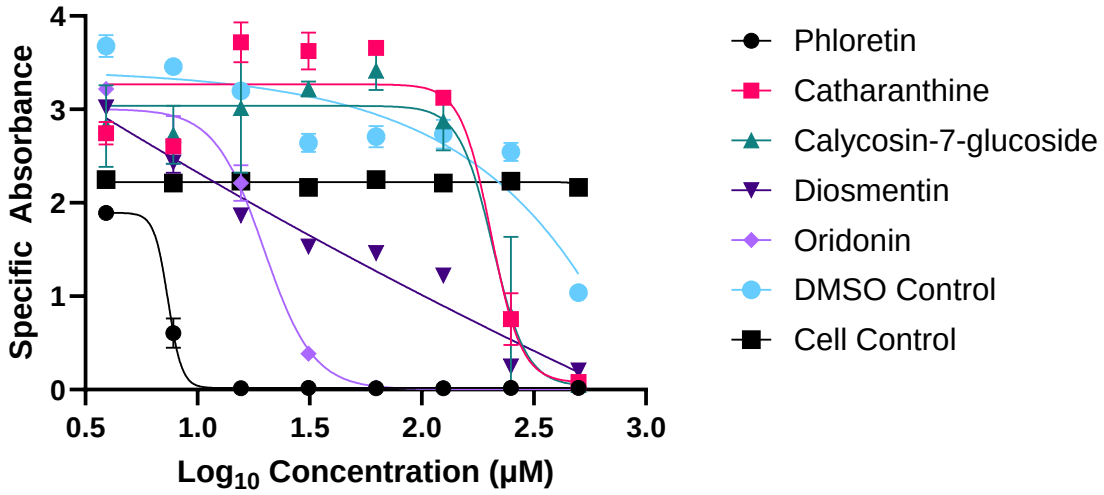

Figure 6. Corrected XTT quantification values for all FDA-approved and natural source compounds tested in MDCK cells. These results were quantified using GraphPad 9 Prism software, with each value representing the mean of the two biological with two technical replicates each. Error bars represent ±SEM. The assay was performed using a 1:2 serial dilution series ranging from 3.9 - 500 µM on MDCK cells. Cells were incubated at 37°C with 5% CO_2 for 48 h with diluted compound stock, and read for absorbance as per manual instructions.

a)

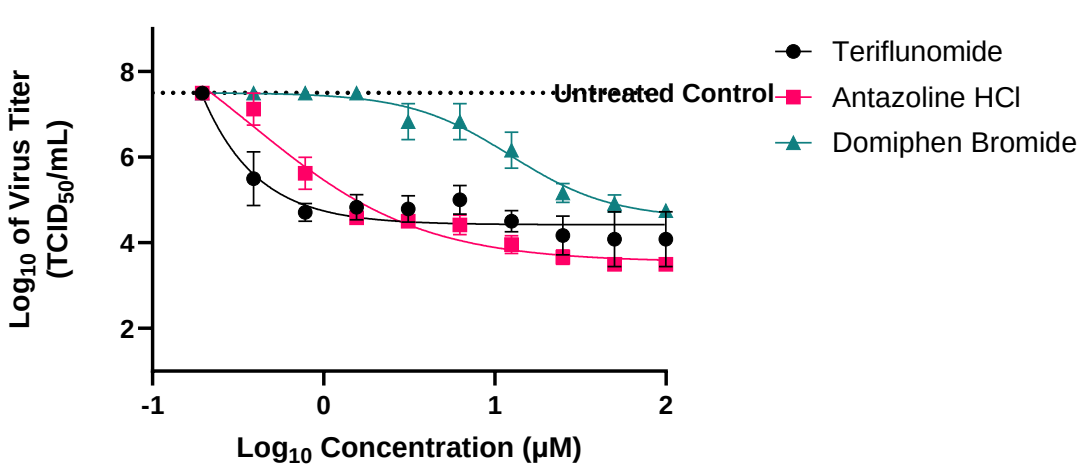
Log10 of Virus Titer (TCID50/mL)
8
6
4
2
-1
0
1
2
Log10 Concentration (μM)
Untreated Control
Teriflunomide
Antazoline HCl
Domiphen Bromide

b)

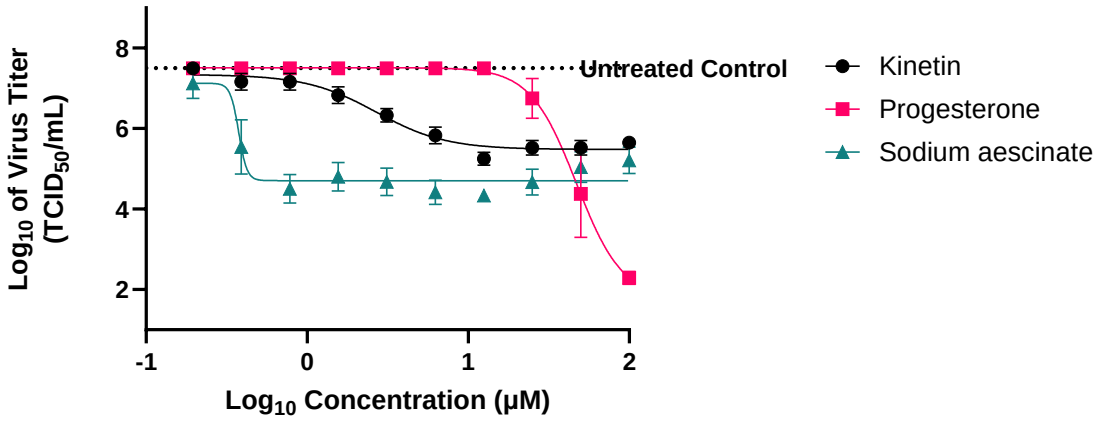
Log10 of Virus Titer (TCID50/mL)
8
6
4
2
-1
0
1
2
Log10 Concentration (μM)
Untreated Control
Kinetin
Progesterone
Sodium aescinate

c)

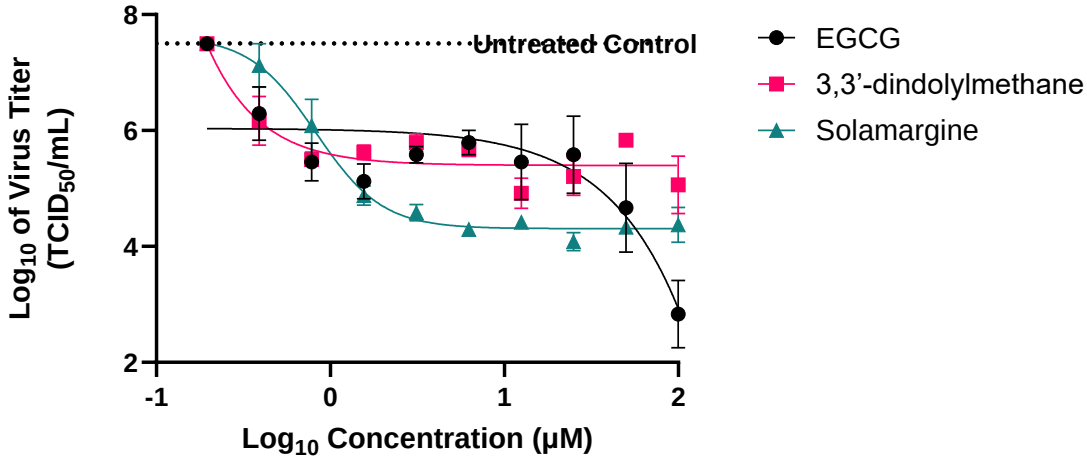
Untreated Control
EGCG
3,3'-dindolylmethane
Solamargine
Log10 of Virus Titer (TCID50/mL)
Log10 Concentration (μM)
8
6
4
2
-1
0
1
2

d)

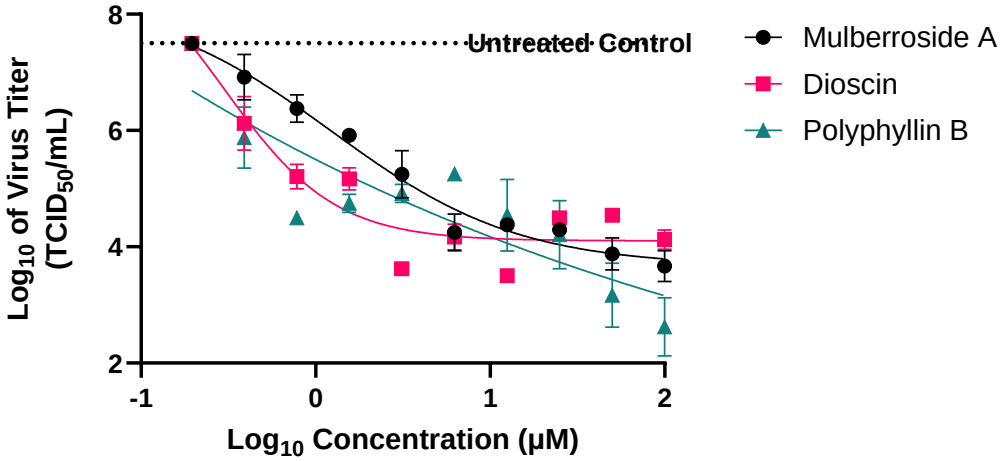
Untreated Control
Mulberroside A
Dioscin
Polyphyllin B
Log10 of Virus Titer (TCID50/mL)
Log10 Concentration (μM)
8
6
4
2
-1
0
1
2

e)

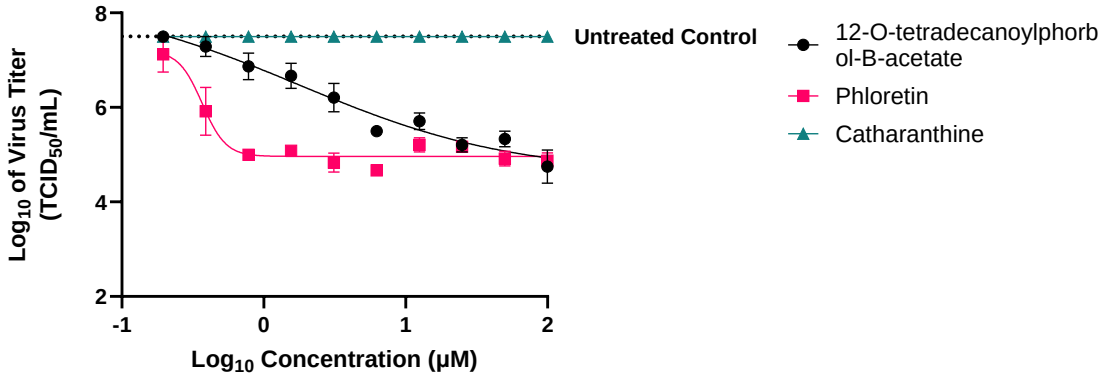

f)

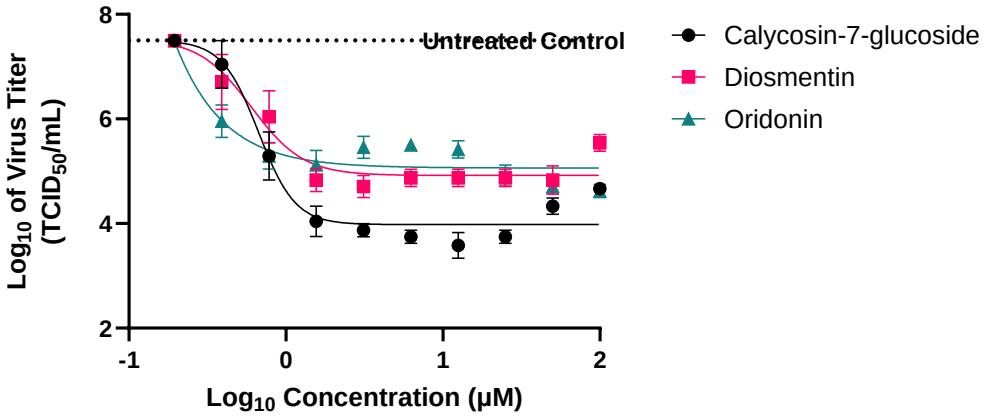

Figure 7. RV733 titer in the presence of FDA-approved and natural source compounds in MDCK cells. The compounds identified from the natural source library are seen, as previously described. Viral titers were determined by titration of samples in a standard $TCID_{50}$ assay, and titers were calculated using the method of Reed and Muench for estimating 50% endpoints[193]. Points shown indicate 2 biological replicates with 3 technical replicates in each. Error bars represent ±SEM. Cells were grown in a 12-well dish in a 1:2 dilution series ranging 195 nM - 100 μM of compound with 0.001 MOI of RV733 and ~70% confluent MDCK cells for 48 h at 37°C with 5% CO_2. Supernatants were collected at 48 hpi, then stored at -80°C until virus titers were quantified.

These results indicate that the initial screening process of using cytotoxicity assays and CPE reduction was an effective method of isolating compounds that effectively reduce IAV titers *in vitro*.

3.1.4: Calculating the selectivity index of the compounds of interest

Selectivity index (SI) is the ratio of a toxic concentration of a compound related to its effective bioactive concentration[194]. The SI is defined as the CC_{50} (the midpoint value from the XTT cell viability assay result curve for the compound) divided by the IC_{50} (the midpoint value from the yield assay result curve for the compound). These values represent the 50% mid-point of the curve between the highest level of "effect" (virus yield or toxicity) to the lowest. Given that higher SI indicates a compound that is highly effective at reducing viral titers but with low toxicity, compounds with high SI values are of interest for further study. The IC_{95} value represents the 95% inhibitory concentration, the concentration of compound that induced 95% of maximum viral titer reduction (i.e., the infected, untreated control), in the yield assay experiment.

The best candidates from these preliminary studies in MDCK cells (based on their high SI value compared to other compounds tested) were sodium aescinate, 3,3'-diindolylmethane, calycosin-7-glucoside, kinetin, ECGC, and dioscin (see Table 9). The least promising candidates from these studies (those that resulted in the lowest SI values) were progesterone, phloretin, solamargine, and 12-O-

Table 9. RV733 Selectivity Index (SI) values in MDCK and A549 cells calculated via XTT assay and yield assay, 48 hpi.

Compound/Compound Name	**CC_{50} in MDCK cells (µM)**	**IC_{50} in MDCK cells (µM)**	**IC_{95} in MDCK cells (µM)**	**SI in MDCK cells**	**CC_{50} in A549 cells (µM)**	**IC_{50} in A549 cells (µM)**	**SI in A549 cells**
Antazoline	259.2	0.55	5.06	471.27	135.1	1.003	134.70
Calycosin-7-glucoside	207.5	0.55	0.20	377.27	N/D	0.35	N/D
Catharanthine	203.9	N/D	N/D	N/D	N/D	-	-
Dioscin	261.9	0.35	0.96	748.29	N/D	N/D	N/D
Diosmetin	31.8	0.49	1.53	64.90	263.4	0.56	470.36
Domiphen bromide	308	8.21	6.56	37.52	10.35	1.1	9.41
EGCG	126.4	0.36	1.34	351.11	32.56	-	-
Kinetin	262.3	1.2	16.3	218.58	319.2	3.03	105.35
Mulberroside A	55.22	0.47	2.79	117.49	369.7	0.71	520.70
Oridonin	19.78	0.29	0.84	68.20	231.1	N/D	N/D
Phloretin	7.39	0.38	0.96	19.45	123.8	0.30	412.67
Polyphyllin B	7.15	0.37	1.23	19.32	118.8	N/D	N/D
Progesterone	497.1	40.04	43.41	12.42	562.7	0.10	5627
Sodium aescinate	131.5	0.38	1.42	346.05	171.1	0.56	305.54
Solamargine	9.133	0.63	4.08	14.50	194.7	0.74	263.10
Teriflunomide	26.25	0.36	1.19	72.92	137.6	N/D	N/D
3,3'-diindolylmethane	131.9	0.37	1.34	356.49	N/D	-	-
12-O-tetradecanoglyphorbol-B-acetate	9.35	0.73	19.08	12.81	N/D	-	-

** N/D values represent "not able to determine", i.e., curves for which the 50% midpoint could not be calculated*

***- values represent those compounds eliminated based on other criteria (e.g., toxicity) that were not pursued further*

tetradecanoglyphorbol-B-acetate (see Table 9). These results indicate that these compounds with high SI values, such as sodium aescinate, may be excellent novel antiviral candidates for seasonal IAV. Other compounds, such as 12-O-tetradecanoglyphorbol-B-acetate, resulted in very low SI values, which suggest they possess a limited ability to reduce viral titers, high toxicity in cellular models, or both, and are less optimal novel antiviral candidates for seasonal IAV.

3.2: Testing Compounds for Cell Line and Virus Specificity

While the effects noted in previous sections make these compounds of interest for further study, it was important to discern whether the potential antiviral effect noted was specific to the cell line or limited to one type of virus. Endemic seasonal IAVs often co-circulate in humans at a high rate during the peak season of fall through winter. Thus, identifying compounds that are effective against different strains of IAV and maintain their antiviral effects in across differing cell lines are ideal novel antiviral candidates.

3.2.1: Assessing the effectiveness of the compounds of interest in an A549 cell model

To test whether these compounds were effective in distinct cell lines, I used the same procedure as the yield and the cytotoxicity assays. Catharanthine was ineffective against RV733 in the past yield assay, and was not pursued in A549 yield assays (see Figure 7e). EGCG, 3,3'-diindolylmethane and 12-O-tetradecanoylphorbol-B-acetate were toxic in MDCK or A549 cells at the concentrations tested and were not pursued further (see Figure 6 and 8). I tested all remaining compounds of interest in A549 cells in addition to MDCK cells to more closely represent a human system, as A549 cells are human lung cells. The same compound

a)

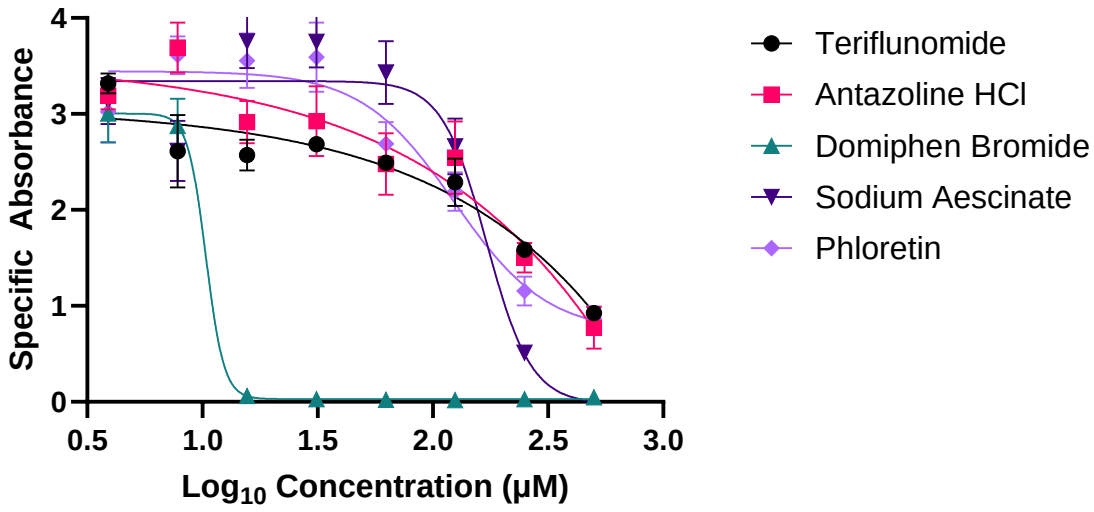
Specific Absorbance
0
1
2
3
4
0.5
1.0
1.5
2.0
2.5
3.0
Log10 Concentration (μM)
Teriflunomide
Antazoline HCl
Domiphen Bromide
Sodium Aescinate
Phloretin

b)

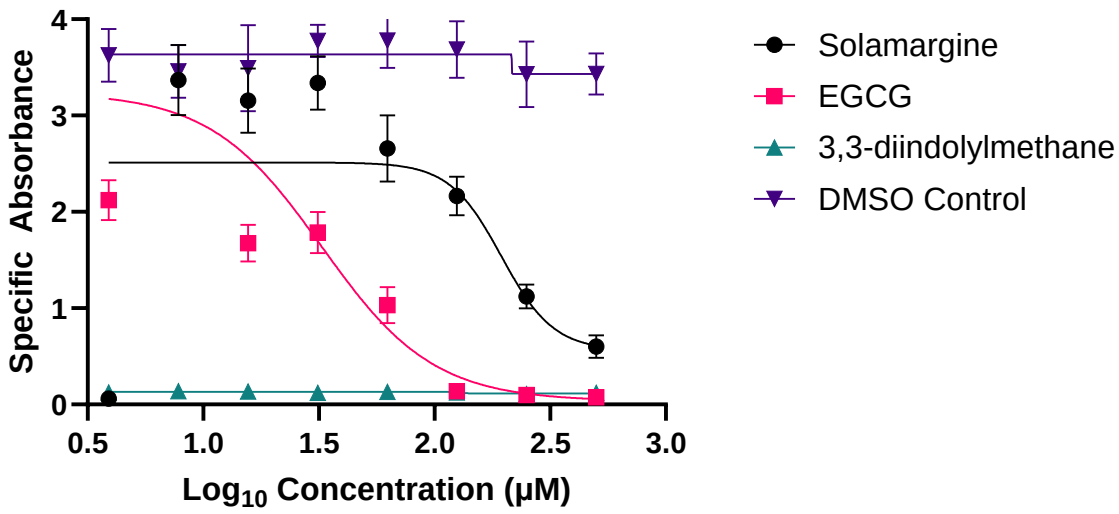
Specific Absorbance
0
1
2
3
4
0.5
1.0
1.5
2.0
2.5
3.0
Log10 Concentration (μM)
Solamargine
EGCG
3,3-diindolylmethane
DMSO Control

c)

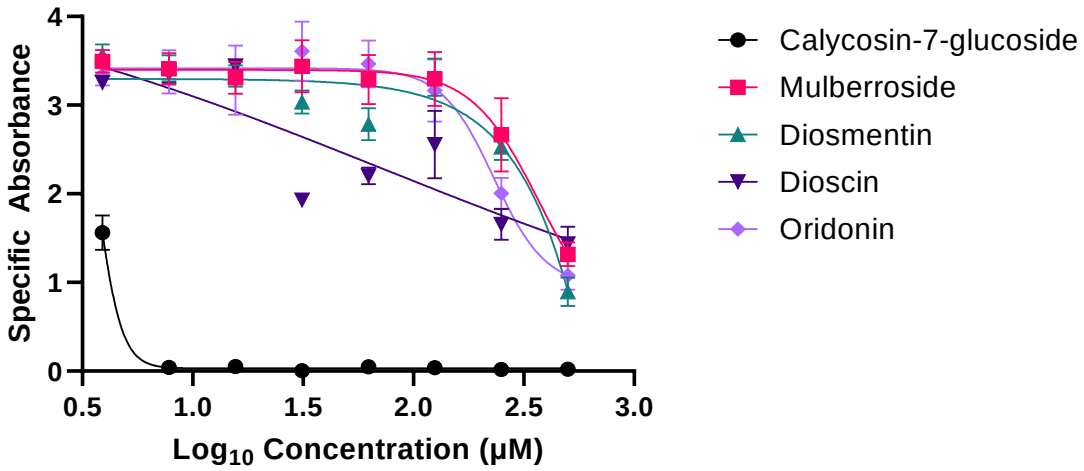

d)

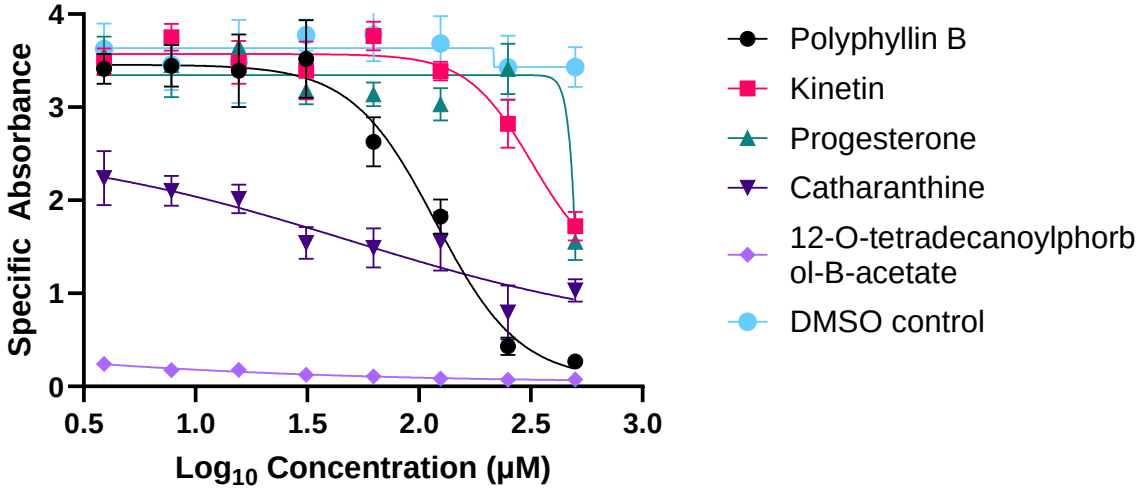

Figure 8. Specific absorbance values derived from the XTT cytotoxicity assay for all compounds tested in A549 cells. These results were quantified using GraphPad 9 Prism software, with each value representing the mean of the two biological replicates each with two technical replicates. Error bars represent ±SEM. The assay was performed using a 1:2 serial dilution series from 3.9-500 µM on A549 cells. Cells were incubated at 37°C with 5% CO_2 for 48 h with the diluted compound, then incubated for 4 h with XTT reagents and read for absorbance as per manual instructions[123].

concentrations were tested in the A549 model as in the MDCK model. The XTT cytotoxicity assay showed that 14 of the compounds tested were toxic only at the 3 highest doses tested in A549 cells (see Figure 8). Figure 8 shows that domiphen bromide, 3,3'-diindolylmethane, calycosin-7-glucoside, and 12-O-tetradecanoylphorbol-B-acetate were highly toxic at most or all concentrations tested, while solamargine, dioscin, and polyphyllin B showed marginal toxicity, particularly at higher concentrations tested. All other compounds except antazoline, EGCG, and phloretin, tested only showed toxicity at concentrations of 250-500 μM, or no toxicity at all (see Figure 8). In contrast, the yield assay showed almost all of the compounds tested were effective at reducing virus titers in A549 cells (see Figure 9). Compounds that were toxic in A549 cells were not tested further in a yield assay with this cell line. Calycosin-7-glucoside and domiphen bromide showed toxicity even at low doses, a notable difference between the results of the MDCK and A549 data for these compounds. As shown in Table 9, there were some SI differences between the results for these compounds when tested using an MDCK model compared to the A549 model. Kinetin, diosmetin, phloretin, progesterone, and solamargine showed higher SI values in A549 cells than in MDCK cells. The same concentration ranges as used for MDCK cells were applied to the A549 cell model in an effort to directly compare the differential effectiveness of the two cell lines. Some compounds, such as 12-O-tetradecanoylphorbol-B-acetate, were toxic at all concentrations tested, while other like catharanthine did not reach an endpoint (value of zero) in the range tested, and would have benefitted from a wider experimental concentration range (see Figure 8). While this range was used to be directly compared to MDCK experiments previously described, some compounds tested are known to be effective in the range on nM concentrations for their designated applications, and a future area of study described in section 5.2 would be expanding

a)

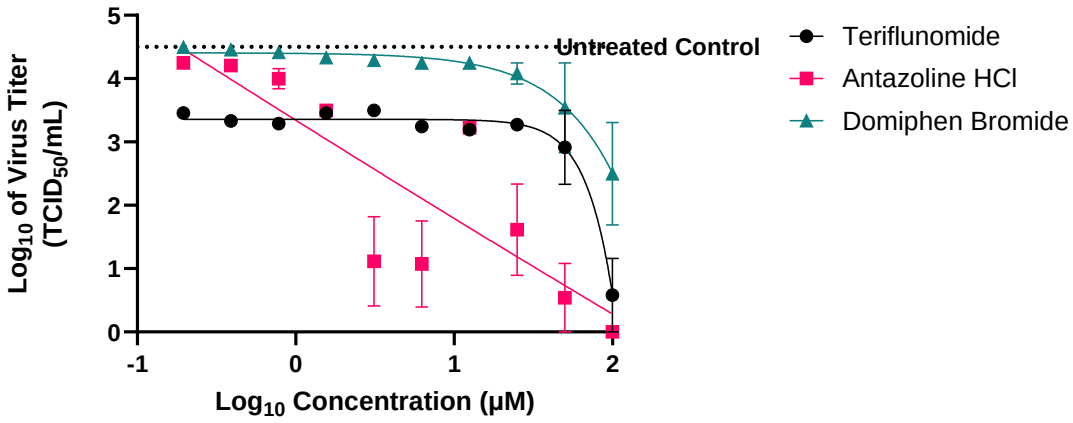
Untreated Control
Teriflunomide
Antazoline HCl
Domiphen Bromide
Log10 of Virus Titer (TCID50/mL)
Log10 Concentration (μM)
5
4
3
2
1
0
-1
0
1
2

b)

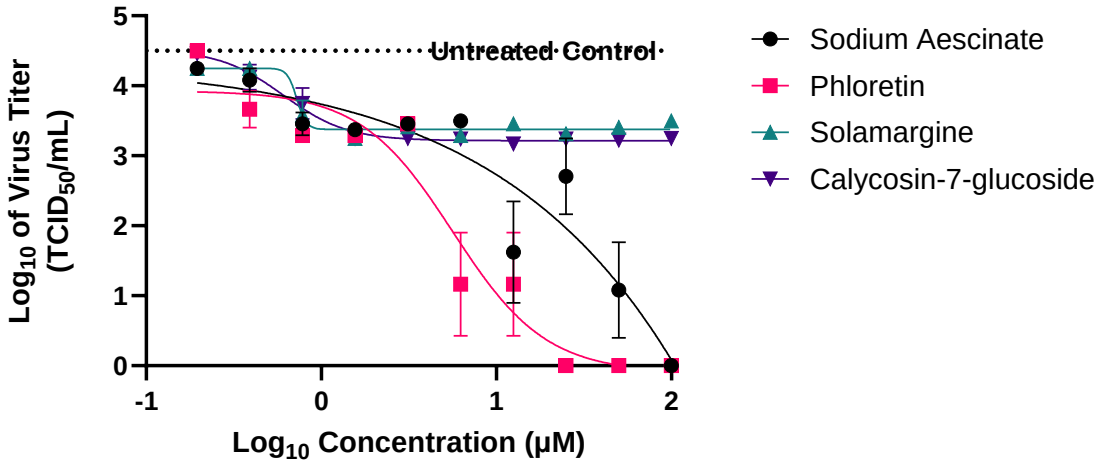
Untreated Control
Sodium Aescinate
Phloretin
Solamargine
Calycosin-7-glucoside
Log10 of Virus Titer (TCID50/mL)
Log10 Concentration (μM)
5
4
3
2
1
0
-1
0
1
2

c)

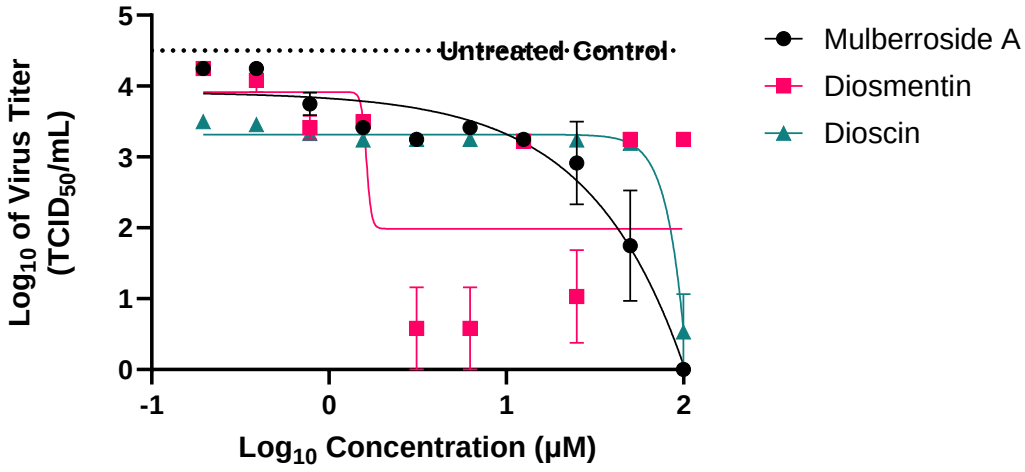

d)

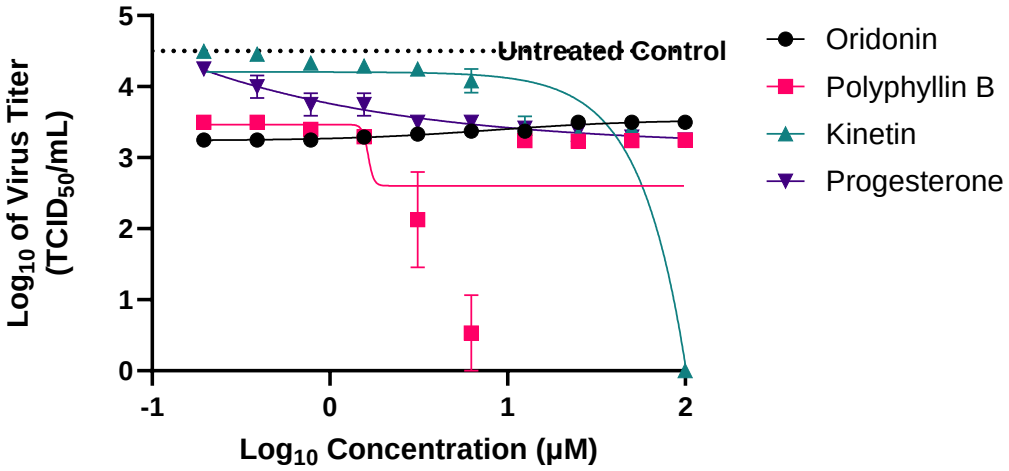

Figure 9. The antiviral activity of FDA-approved and natural source compounds against RV733 in A549 cells. Viral titers were determined by titration of samples in a standard $TCID_{50}$ assay and titers calculated using the method of Reed and Muench for estimating 50% endpoints[193]. Points shown indicate the mean of biological duplicates each containing technical triplicates. Error bars represent the mean±SEM. were grown in a 12-well dish in a dilution series ranging 195nM – 100 μM of compound with 0.001 MOI of RV733, and ~85% confluent A549 cells for 48 h at 37°C with 5% CO_2. Supernatants were collected at 48 hpi, then stored at -80°C until virus titers were quantified.

the range of concentrations tested. Selectivity calculations were performed where possible, given the data set available, by using both GraphPad Prism 9 $EC_{anything}$ function and a manual calculation, with N/D in Table 9 designating those compounds that did not have enough of an effectiveness range to be calculated. In future studies, these compounds require further dilution to reach an endpoint where activity was reduced.

Domiphen bromide, calycosin-7-glucoside, sodium aescinate showed lower SI values in A549 cells compared to MDCK cells (see Table 9). These results indicate that there are some differences between cell lines when it comes to toxicity and viral titer reduction, which could be due to differences in drug sensitivity, activity, pathway, or the amount of cellular drug target produced, among other differences.

3.2.2: Testing the effectiveness of the compounds of interest against Mx10 and HK68 viruses

I used the same procedure as the yield assay to test whether these compounds were effective against different IAVs. This experimental design was intended to determine if the dose of compounds used in the past RV733 experiments was effective against distinct strains of IAV, such as Mx10 (a pandemic H1N1 virus) and HK68 (a pandemic H3N2 virus). In the case of Mx10, with the exception of antazoline HCl, sodium aescinate, and solamargine, concentrations higher than 0.31 µM notably reduced viral titers (see Figure 10). In the case of HK68, with the exception of phloretin and progesterone, concentrations higher than 0.31 µM notably reduced viral titers, though the impact was not as drastic as it was for past viral yield assays (see Figure 11). Several compounds, such as phloretin and solamargine, had no activity at any concentration though they did in the presence of RV733 infections. This is a further demonstration of the many differences between subtypes of IAV and the mode of action of various antivirals compounds,

a)

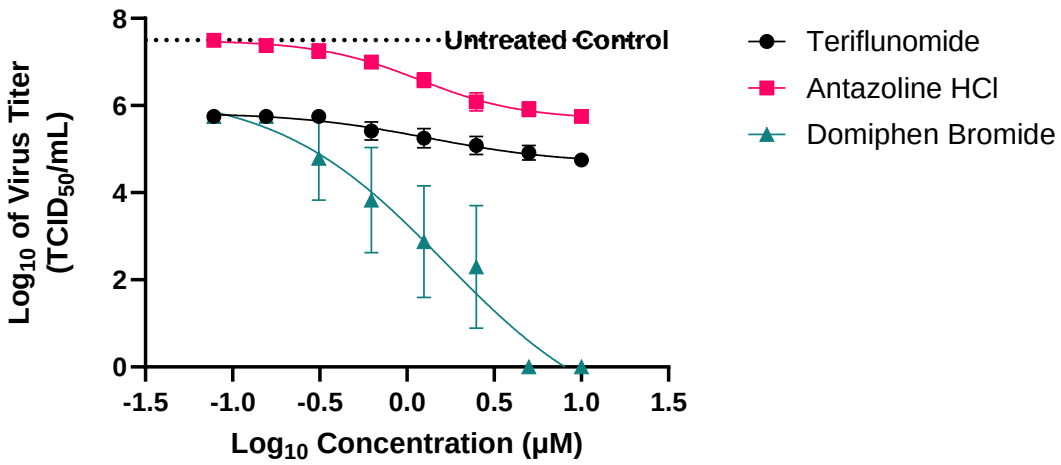
Untreated Control
Teriflunomide
Antazoline HCl
Domiphen Bromide
Log10 of Virus Titer (TCID50/mL)
Log10 Concentration (μM)
8
6
4
2
0
-1.5
-1.0
-0.5
0.0
0.5
1.0
1.5

b)

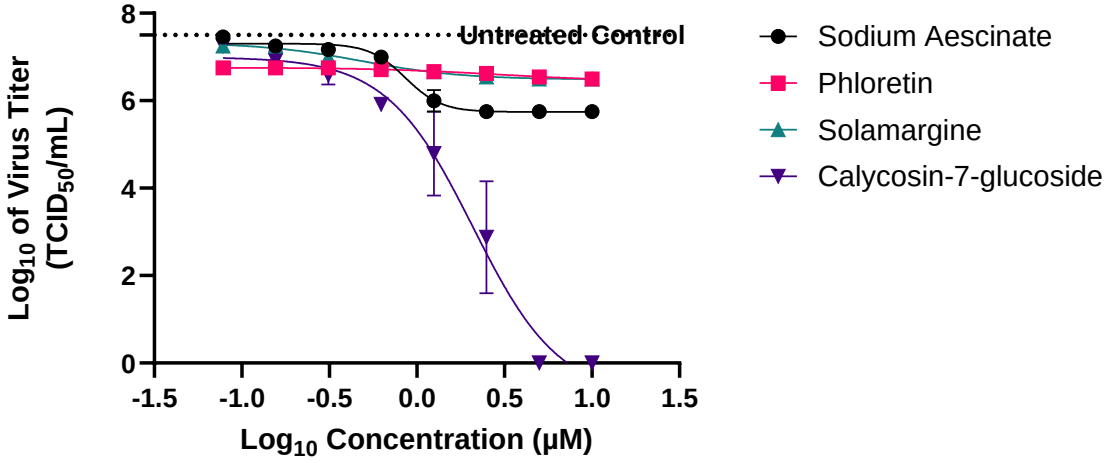
Untreated Control
Sodium Aescinate
Phloretin
Solamargine
Calycosin-7-glucoside
Log10 of Virus Titer (TCID50/mL)
Log10 Concentration (μM)
8
6
4
2
0
-1.5
-1.0
-0.5
0.0
0.5
1.0
1.5

c)

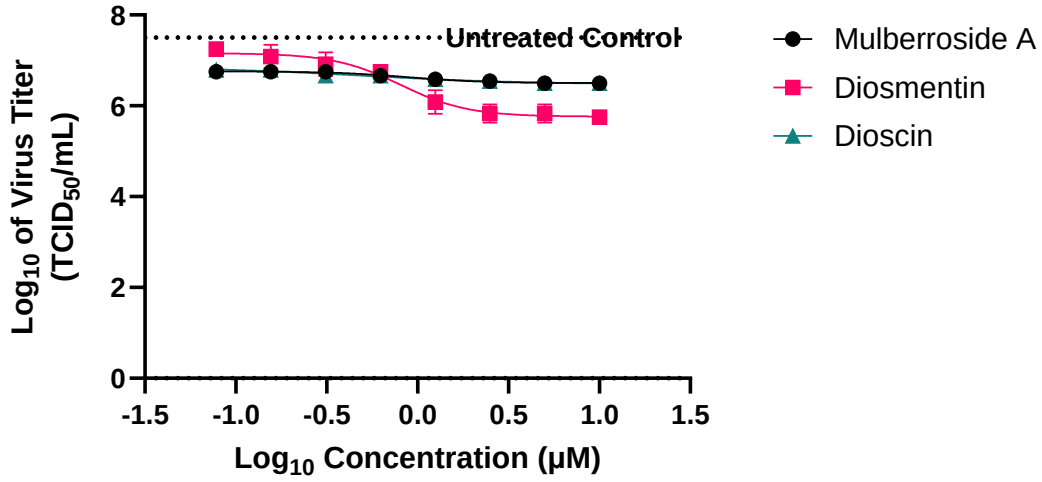

d)

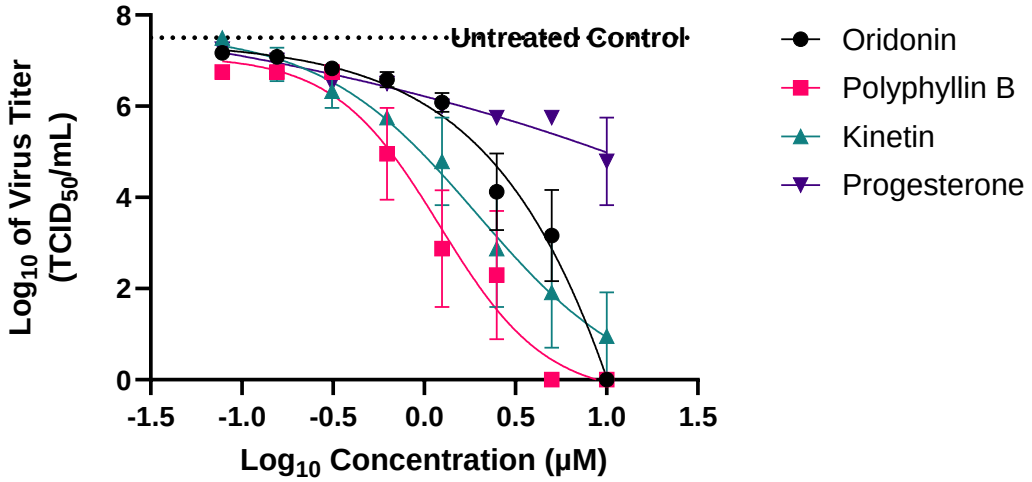

Figure 10. Mx10 titer in the presence of FDA-approved and natural source compounds in MDCK cells. Viral titers were determined by titration of samples in a standard $TCID_{50}$ assay and titers calculated using the method of Reed and Muench for estimating 50% endpoints[193]. Points shown indicate the mean of biological replicates (with 3 technical replicates each). Error bars represent ±SEM. Cells were grown in a 12-well dish until they were ~70% confluent, after which a dilution series ranging from 78 nM – 10 µM of the specified compound and 0.001 MOI of Mx10 IAV were added and incubated for 48h at 37°C with 5% CO_2. Supernatants were collected at 48 hpi, then stored at -80°C until virus titers were quantified.

a)

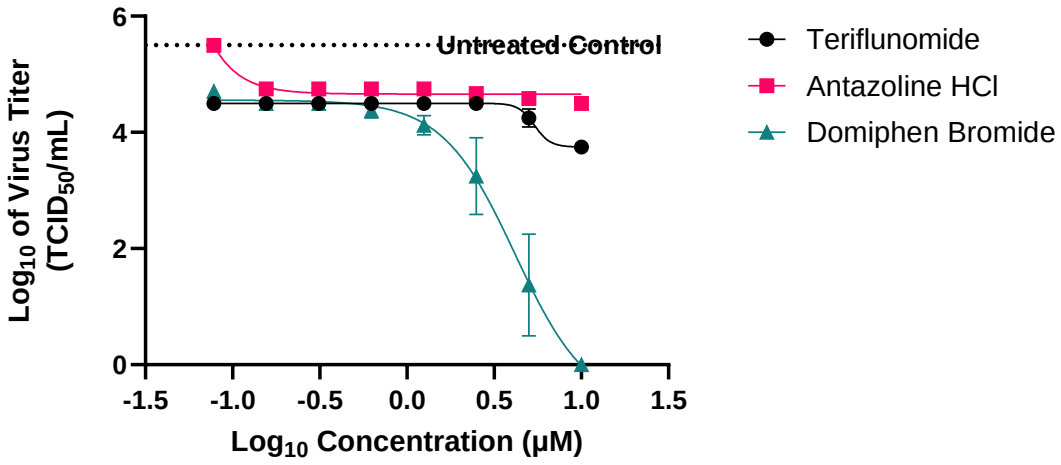
Untreated Control
Teriflunomide
Antazoline HCl
Domiphen Bromide
Log10 of Virus Titer (TCID50/mL)
Log10 Concentration (μM)
6
4
2
0
-1.5
-1.0
-0.5
0.0
0.5
1.0
1.5

b)

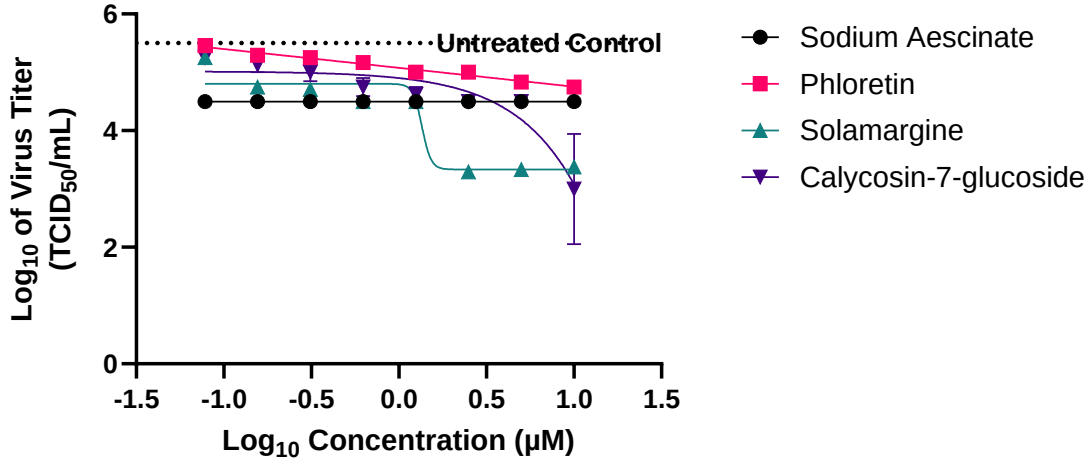
Untreated Control
Sodium Aescinate
Phloretin
Solamargine
Calycosin-7-glucoside
Log10 of Virus Titer (TCID50/mL)
Log10 Concentration (μM)
6
4
2
0
-1.5
-1.0
-0.5
0.0
0.5
1.0
1.5

c)

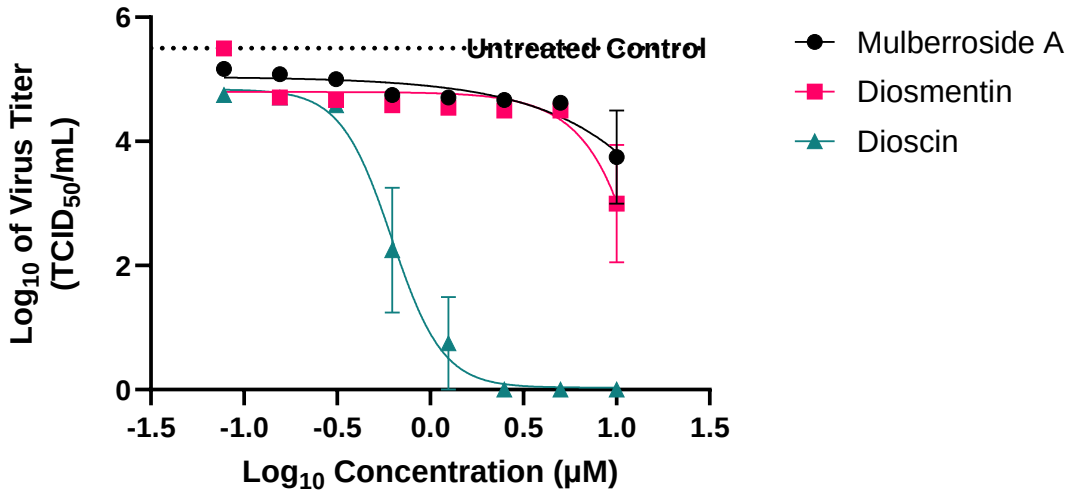

d)

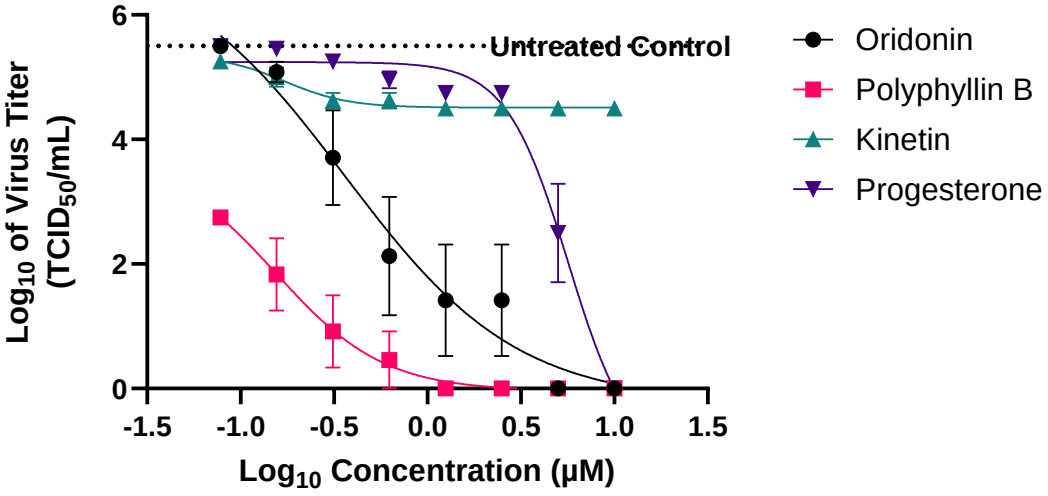

Figure 11. HK68 titer in the presence of FDA-approved and natural source compounds in MDCK cells. Viral titers were determined by titration of samples in a standard $TCID_{50}$ assay and titers calculated using the method of Reed and Muench for estimating 50% endpoints[193]. Points shown indicate the mean of technical triplicates and biological duplicates. Error bars represent ±SEM. Cells were grown in a 12-well dish in a dilution series ranging 78 nM – 10 μM of compound with 0.001 MOI of HK68 IAV, and ~70% confluent MDCK cells for 48h at 37°C with 5% CO_2. Supernatants were collected at 48 hpi, then stored at -80°C until virus titers were quantified.

two of many reasons why broad-spectrum antivirals for IAV are difficult to identify.

Catharanthine, ECGC, 3,3'-diindolylmethane, and 12-O-tetracanoglyphorbol-B-acetate resulted in curves that could not be used for 50% midpoint calculations because of their range or slope when testing Mx10 and HK68 viruses and are not shown in Table 10. Mulberroside A, kinetin, phloretin, polyphyllin, and solamargine resulted in curves that could not be used for 50% midpoint calculation for Mx10 or HK68, resulting in an "N/D" result shown in Table 10. The goal of the Mx10 and HK68 experiments herein described was as a direct comparative measure to previous RV733 work, so the same concentration range was used. This limitation is detailed in section 5.1. Because the CC_{50} value was the same for these differing compounds (all IAVs were grown on the same cell line), the factor resulting in different SI values was the IC_{50}. Calycosin-7-glucoside, sodium aescinate, and kinetin resulted in higher SI values and domiphen bromide resulted in much higher SI values when tested against Mx10, compared to RV733. Diosmetin resulted in a higher SI value when tested against HK68, compared to RV733. The final SI values were generated using GraphPad Prism 9 $EC_{anything}$ function and a manual calculation, where possible.

These results suggest differences between these IAVs that alter the antiviral effects of the identified compounds. Features of RV733 that resulted in high SI values for some compounds appear to have resulted in much higher or lower values when these compounds were tested against Mx10 or HK68. These results could be explained by differences in the HA or NA surface proteins which differ substantially between these viruses, or a differing internal protein, which also differ between these viruses, just to a lesser degree than the surface proteins. These changes

Table 10. RV733, Mx10, and HK68 Selectivity Index (SI) values calculated via XTT assay and yield assay, respectively, in MDCK cells, 48 hpi.

Compound/Compound Name	**CC_{50} in MDCK cells (µM)**	**RV733 IC_{50} (µM)**	**RV733 SI**	**Mx10 IC_{50} (µM)**	**Mx10 SI**	**HK68 IC_{50} (µM)**	**HK68 SI**
Antazoline	259.2	0.55	471.27	0.52	498.46	0.04	$6.48x10^3$
Calycosin-7-glucoside	207.5	0.55	377.27	0.21	988.1	0.43	482.56
Dioscin	261.9	0.35	748.29	N/D	N/D	N/D	N/D
Diosmetin	31.8	0.49	64.9	0.28	113.57	0.02	$1.59x10^3$
Domiphen bromide	308	8.21	37.52	N/D	N/D	N/D	N/D
Kinetin	262.3	1.2	218.58	0.20	1311.5	N/D	N/D
Mulberroside A	55.22	0.47	117.49	N/D	N/D	0.37	149.24
Oridonin	19.78	0.29	68.2	0.28	70.64	0.12	164.83
Phloretin	7.39	0.38	19.45	N/D	N/D	N/D	N/D
Polyphyllin B	7.15	0.37	19.32	N/D	N/D	N/D	N/D
Progesterone	3.41	40.04	0.09	0.19	17.95	0.39	8.74
Sodium aescinate	131.5	0.38	346.05	0.04	3287.5	N/D	N/D
Solamargine	9.133	0.63	14.5	0.37	24.68	N/D	N/D
Teriflunomide	26.25	0.36	72.92	N/D	N/D	N/D	N/D

** N/D values represent "not able to determine", i.e., curves for which the 50% midpoint could not be calculated*

in SI are not due to toxicity, as the same cell line was used for all three viruses. Thus, the differential results are due to the difference in effectiveness at reducing viral titers *in vitro*.

3.2.3: Determining the effectiveness of select compounds of interest against VSV-MERS

Our research group generated a virus termed VSV-MERS that was utilized in this dissertation. This virus is a recombinant Vesicular Stomatitis Virus (VSV) possessing a Middle Eastern Respiratory Syndrome Virus (MERS) spike expression in the place of the VSV G protein. VSV is a desirable vaccine platform because not only can it be easily propagated to high titers but can be manipulated using reverse genetics to adopt important virulence-factor proteins of other viruses, such as the spike protein of Coronaviruses, thus forming an excellent CL2 model of various pathogens without the dangers of working with the whole, wild-type virus, ensuring I could do this work myself[195]. By utilizing the spike protein of MERS, an antiviral effectiveness comparison between these two respiratory pathogens could be made for the antivirals noted as being effective in past IAV studies, adding a layer of respiratory virus interest to this study. In addition, basic information such as optimal growth conditions, favorable cell lines, and the general information about how infection would proceed, was already known. Because it is a level 2 pathogen, I was able to use it in the lab space available to me. Mx10 and HK68 are still IAVs, like RV733, and I aimed to test a virus that had a different replication cycle (including differing means of attachment and entry) and came from another viral family to determine whether there was any potential cross-virus protection provided by these compounds of interest. This experiment was performed later in the project, chronologically, when five compounds of interest had been identified as potential IAV entry inhibitors, so this subset was

tested against this VSV-MERS virus to determine whether they might be broadly protective beyond IAVs.

I used the same procedure and compound concentrations as the RV733 yield assay (see section 2.2.4). The results of the VSV-MERS experiment can be seen in Figure 12, which show that, when the virus was grown in the presence of sodium aescinate, calycosin-7-glucoside and oridonin, viral replication was inhibited, compared to the infected, untreated control. Dioscin addition resulted in moderately reduced viral titers, suggesting limited effects against VSV-MERS, and kinetin addition resulted in comparable viral titers to the infected, untreated control (see Figure 12). These results showed that sodium aescinate, calycosin-7-glucoside, and oridonin are cross-protective, effectively reducing VSV-MERS titers. This effect may be the result of similarities between attachment receptors or attachment processes of HA and MERS spike protein, among other reasons. That said, the numerous distinctions between VSV viruses (which provide the backbone of the VSV-MERS virus used) and seasonal IAV could also account for the varying results. Follow-up studies would be required to further clarify these contributing factors. Kinetin and dioscin were among the least effective against VSV-MERS and may have a mechanism restricted to IAVs. Oseltamivir also fully inhibited viral replication of VSV-MERS. While this phenomenon remains understudied, and the mechanism unknown, oseltamivir has been used as a treatment for Covid- 19 in some clinical settings, and whether its effects are due to spike protein interactions, as would be the case in this experiment, or another effect, this would be a fascinating area for further study[196]. For the purposes of this dissertation project, compounds that reduced viral titers by ~2 $\log_{10}$ or more were considered antiviral. A $2\log_{10}$ reduction in viral titers serves as a reasonable benchmark for preliminary antiviral studies, as further refinement of molecular structure, binding affinity, and related properties during ADME

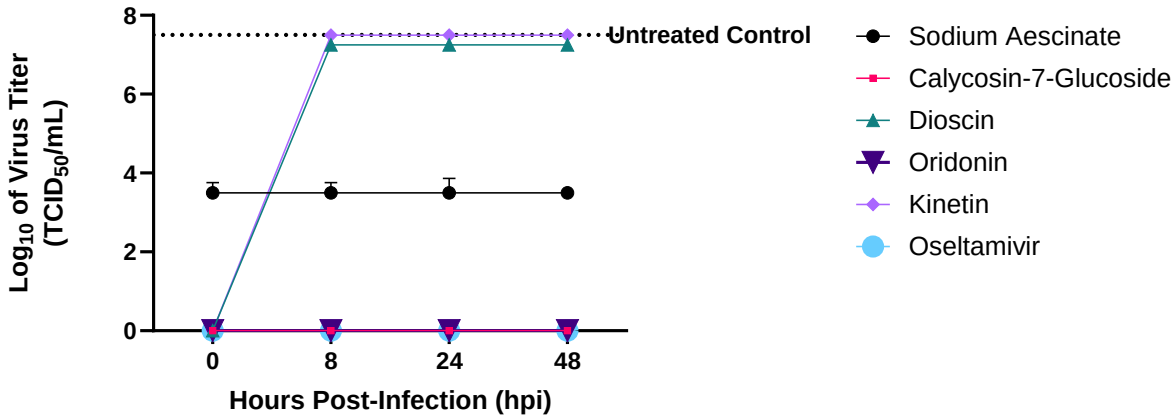

Figure 12. VSV-MERS titer in the presence of FDA-approved and natural source compounds in Vero cells. Viral titers were determined by titration of samples in a standard $TCID_{50}$ assay and titers calculated using the method of Reed and Muench for estimating 50% endpoints[193]. Points shown indicate the mean of technical triplicates and biological duplicates, and error bars represent ±SEM. Vero cells were grown in a 12-well dish and incubated for 24 h. Once ~60% confluent, 0.001 MOI of VSV-MERS was added to the cells, along with the compound dosage used in previous yield assay experiments. The infected and treated cells were then incubated for 48 h at 37°C. Supernatants were collected at 48 hpi, then stored at -80°C until virus titers were quantified.

optimization could potentially achieve the 3–4-$\log_{10}$ reduction typically required for effective antiviral agents. A dosage of 100 µM of oseltamivir has been identified in the literature as meeting these criteria for PR8 H1N1 influenza[197]. This concentration was thus carried forward as an antiviral control in several of the experiments shown in this dissertation to ensure a direct available comparison between the experimental compounds and a dosage of a known antiviral *in vitro.*

3.2.4: Determination of the effectiveness of select compounds of interest against seasonal Rhinovirus

Unlike IAV and VSV, Rhinoviruses like R-1644 do not have an envelope. They also have a vastly different life cycle from IAV, particularly in their attachment and entry mechanism. R-1644 was available to us, courtesy of Dr. Nathalie Bastien's group at the National Microbiology Lab, and its use was intended to determine whether the compounds of interest were effective against a non-enveloped virus with a different attachment mechanism from those tested previously. This experiment was also performed later in the project when five candidates of interest had been identified as potential IAV entry inhibitors, so this experiment exclusively tested these five candidates, at the same concentrations identified as effective against RV733. A full analysis including cytotoxicity in HeLa cells and dose range was not performed, as the purpose of this experiment was to evaluate whether the antiviral effect at the concentration used for past RV733 experiments in this dissertation could be noted in other viral models. As evidenced by Figure 13, this subset of compounds did not reduce viral loads or CPE in R-1644-infected HeLa cells. While some compounds (like sodium aescinate) were widely effective

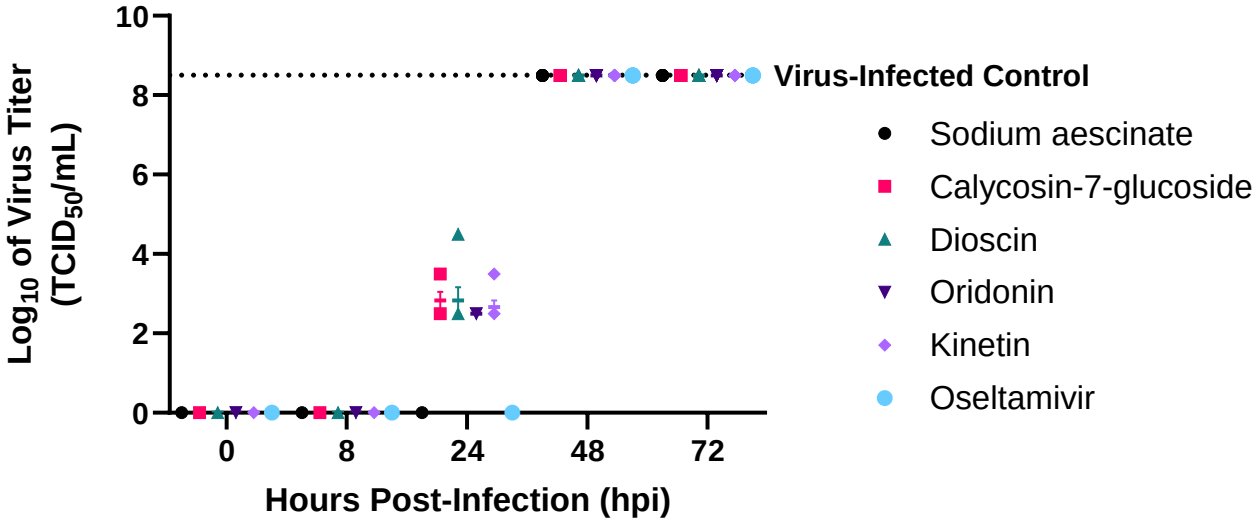

Figure 13. R-1644 titer in the presence of FDA-approved and natural source compounds in HeLa cells. Viral titers were determined by titration of samples in a standard $TCID_{50}$ assay and titers calculated using the method of Reed and Muench for estimating 50% endpoints[193]. Points shown indicate the mean biological replicates (each with 3 technical replicates). Error bars represent ±SEM. HeLa cells seeded in 12-well plates 24 h prior to the assay. The following day, once the cells were 80% confluent, 0.1 MOI of R-1644 was added to each well at 0 hpi. The compound dosage used in previous yield assay experiments was then added to corresponding wells. The plate was then incubated at 37°C with 5% CO_2 until the specified time point. Supernatants were collected at 48 hpi, then stored at -80°C until virus titers were quantified.

against IAVs and recombinant VSVs, none were effective against seasonal R-1644 at the doses previously used in yield assays (see section 2.2.4).

3.3: Delineating the Effect of the Compounds of Interest on Seasonal IAV

3.3.1: Identification of potentially virucidal compounds using a virucidal assay

Antiviral compounds tend to inhibit viral infection or replication, acting on a specific stage of the infection cycle or stimulating the immune system. Because the goal of this dissertation project was to identify compounds that are specifically antiviral, I used virucidal assays to remove any compounds that exhibited virucidal potential.

Virucidal compounds can have a range of effects such as inducing chemical alterations in lipids, proteins, and/or nucleic acids. They may also destroy membranes, and have other negative effects on virion structures and constituents (for example, hypochlorite denatures proteins, triggers enzyme destruction, and induces other processes that destroy cells). These negative, nonspecific effects would also impact host cells, making virucidal compounds unsuitable for future *in vivo* studies[198].

The experimental setup of the virucidal assay involved a high dose of compound ($10IC_{95}$, as determined by yield assay) with 10^5 $TCID_{50}$/mL of RV733 for 2 hours, then diluting the mixture 1:50 into fresh medium. By diluting the compound below the concentration known to induce toxicity and effectively reduce viral titers in fresh medium, any residual virus that had not been damaged by compound exposure would be able to replicate without compound-related inhibition. Amounts of compound remaining were far below the concentration previously determined to have any effect on viral titers (evaluated by $TCID_{50}$ and thus representing live,

replicating virus). The experiment was performed using both a flask (CPE) and plaque assay method to ensure quantification of both live, replicating virus and all residual virus was achieved. Known controls of 10% hypochlorite and 5% Micro-Chem were used to validate the experimental procedure.

In the initial CPE-based experiment, none of the results indicated complete virucidal effects, as 50% or more CPE was observed in all cases (Table 11). Some experimental compounds, such as domiphen bromide, appeared to be partially virucidal (Table 11). This could be the result of inhibition of viral replication in the absence of toxicity. The largest reductions in viral viability were seen with incubation of the virus with sodium aescinate and virus with oridonin. However, other compounds showed little to no impact on plaque production after being incubated with $10IC_{95}$ of the compound (Table 11). The 10% hypochlorite, and 5% Micro-Chem controls showed the expected 100% reduction of CPE after the 2 h incubation of the virus and compound. This result indicates that the compounds of interest being investigated were not virucidal in that they did not kill or inactivate the virus on contact, compared to the known disinfectant controls used. 3.3.2: Evaluating the effect of differential addition timing to identify compounds effective at specific stages of IAV infection

3.3.2: Time of addition assays

Time of addition assays were adapted from previously described methods, and performed to determine where the compounds of interest may be acting in the virus life cycle by adding the compound at various stages of infection[124,199]. IAV has a replication cycle spanning approximately 8 hours (see section 1.1.4). As a general estimate, attachment and entry occur

Table 11. Virucidal assay results for selected compounds of interest.

Compound Used	CPE*	% of Virus-Infected, Untreated Control (±std)**	Inactivating/Neutralizing Effect Noted
Teriflunomide	Yes	97±22	No
Antazoline HCl	Yes	103±27	No
Domiphen Bromide	Partial	57±21	Mild
Sodium Aescinate	Partial	49±7	Mild
Phloretin	Partial	62±18	Mild
Solamargine	Yes	104±14	No
Calycosin-7-Glucoside	Yes	88±9	No
Mulberroside A	Yes	101±26	No
Diosmetin	Yes	104±19	No
Dioscin	Yes	98±28	No
Oridonin	Partial	63±11	Mild
Polyphyllin B	Partial	77±14	Mild
Kinetin	Yes	96±25	No
Progesterone	Partial	63±4	Mild
Controls:			
Cells only, no virus	No	0	N/A (no compound added)
Cells with virus	Yes	100±19	N/A (no compound added)
5% Micro-Chem	No	0	Yes
10% hypochlorite	No	0	Yes

Percent CPE was determined visually, where yes indicates full CPE, no indicates no CPE, and partial indicates a partially intact monolayer (more than 50% remaining).
**% CPE determined by viral growth on MDCK cells in a flask.*
***Viral titers determined by plaque assay, where std = the standard deviation (measured by number of plaques) of technical and biological duplicates.*

starting at 0 hpi, and can last until 2 hpi, depending on the kinetics of infection. How long it takes the virus to attach to the host cell are affected by factors such as the time a virus takes to travel through the medium to reach the host cells. Once attached, movement into endosomes occurs during the stage of minutes after infection to 2 h post-infection. Transcription and translation can occur as early as 2 hpi and as late as 4-6 hpi. The final stage of exit via budding occurs at approximately 8 hpi, at the latest.

In this way, rough estimates of where an antiviral may be acting in the replication cycle of IAV can be interpreted by differential timing of addition of the compounds in question. For example, if the compounds are most effective at reducing viral titers (as quantified by $TCID_{50}$ assay) when present at -2 hpi (2 hours before virus addition) or 0 hpi (2 hours after virus addition) until infection, they may be acting as an entry or fusion inhibitor, or inhibiting HA activity, as it is not effective when added after this stage of the life cycle. Compounds that are maximally effective at reducing viral titers when present at 4-6 hpi (which is when the virus is undergoing transcription/translation in the host cell) may be acting as transcription or translation inhibitors. Finally, those most effective when present at 6 hpi or later (the stage at which the virus is exiting the host cell via budding) may be affecting the budding/egress process. Interpretation of the assay assumes that if the compound is not present for the stage of the virus replication cycle that it impacts, the compound will not reduce viral titers resulting in titers similar to a virus-infected but untreated control. However, it is essential to take caution in these estimates, as viral kinetics of infection vary, and only rough estimates can be made.

Titers are compared to untreated controls (shown as dotted lines in the graphs), which was the result of a virus-infected cell monolayer treated the same way as the compound-treated experimental groups (including harvest and incubation conditions and times) but not treated with

any compounds. These results provide an excellent direct comparison to virus titers when cells are infected without the experimental compound treatment.

Oseltamivir acted as the control because its mechanism of action as a neuraminidase inhibitor is well known[200–202]. However, neuraminidase is thought to play a role in the entry process of some IAVs[203,204]. While it is unclear whether this is a factor for the assays used in this dissertation, it is important to consider that this may occur. Of note, the IC_{95} was derived from previous assays, as were those for other compounds tested in this section. The result of the time of addition assay for oseltamivir showed inhibition at the early stages of addition, predominantly before virus addition (see Figure 14o). While this would suggest a potential entry inhibitor, there may be some additional complexity caused by the complex activity of neuraminidase.

Teriflunomide, antazoline HCl, domiphen bromide, sodium aescinate, phloretin, solamargine, calycosin-7-glucoside, mulberroside A, dioscin, and polyphyllin B showed reduced RV733 titers, compared to the infected, untreated control, only when present before virus addition (see Figure 14a-h, 14j, and 14l, respectively). These results suggest the specified compounds may be acting as IAV entry inhibitors. Oridonin showed no time of addition-specific effect, but the overall virus titers were lower than the untreated control (see Figure 14k). However, subsequent testing using a higher MOI showed a potential entry inhibition effect (see section 8.2). Thus, it was carried forward as a novel antiviral candidate to further explore its potential. This difference in virus titer reduction between the two MOIs tested was noted for several compounds. Given that all other experimental parameters were kept the same between the two experiments, the compounds demonstrating a lower virus titer reduction in the higher MOI experiment may have been unable to exert their effects on a higher dose of virus. In the case of oridonin, where an effect was only seen in the higher MOI experiment, perhaps the ratio

a) Teriflunomide

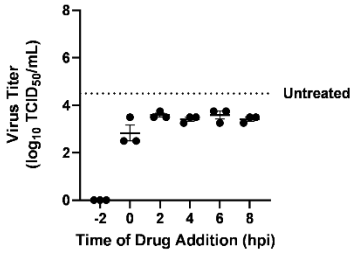

b) Antazoline HCl

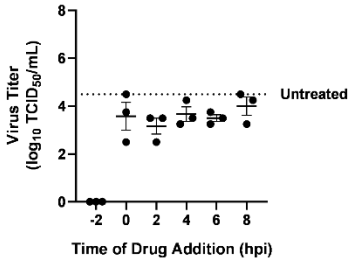

c) Domiphen bromide

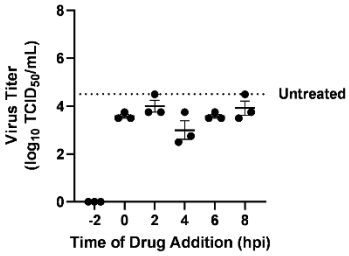

d) Sodium aescinate

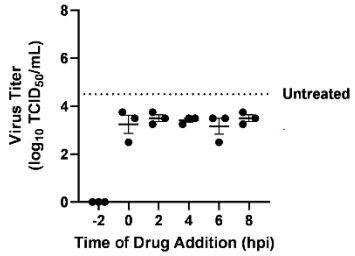

e) Phloretin

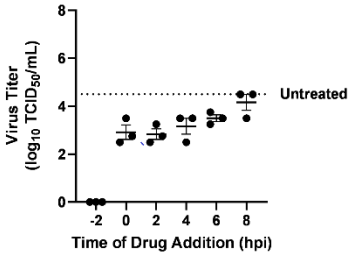

f) Solamargine

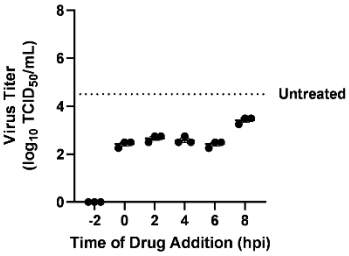

g) Calycosin-7-glucoside

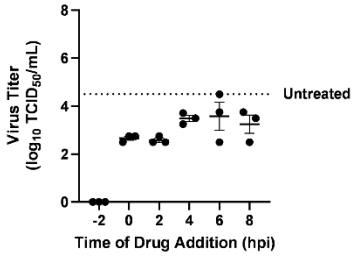

h) Mulberroside A

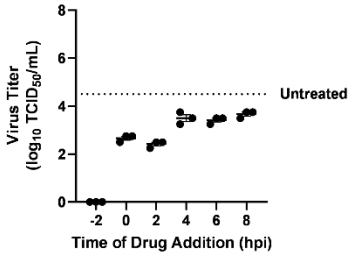

i) Diosmetin

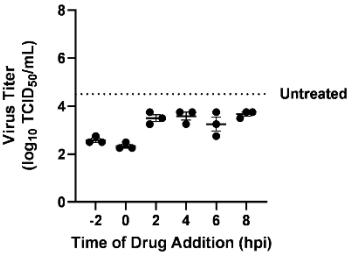

j) Dioscin

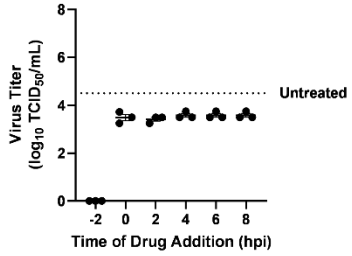

k) Oridonin

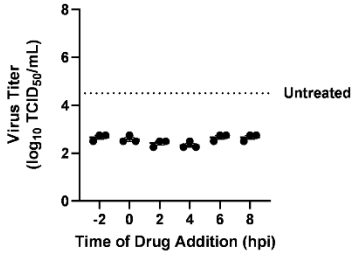

l) Polyphyllin B

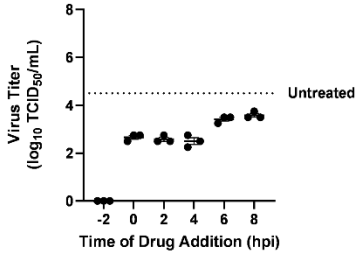

m) Kinetin

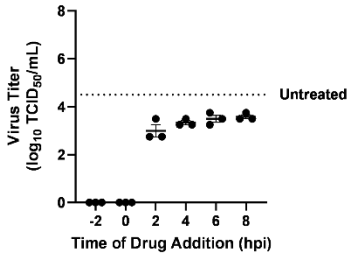

n) Progesterone

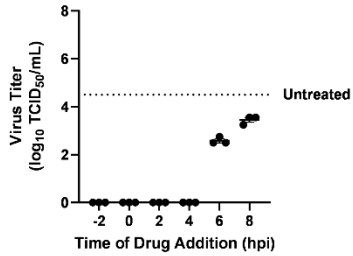

o) Oseltamivir

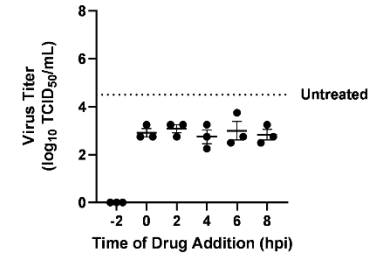

Figure 14. Time of addition assay results for teriflunomide (a), antazoline HCl (b), domiphen bromide (c), sodium aescinate (d), phloretin (e), solamargine (f), calycosin-7-glucoside (g), mulberroside A (h), diosmetin (i), dioscin (j), oridonin (k), polyphyllin B (l), kinetin (m), progesterone (n), and oseltamivir (o). Points shown indicate the mean of technical duplicates and biological triplicates. Error bars represent ±SEM. MDCK cells grown to ~80% confluent were seeded in 12-well plates 24 h prior to the assay. The following day, 0.001 of RV733 IAV was allowed to pre-adsorb on ice for 1 h, after which the cells were washed 3X with PBS and incubated at 37º. Subsequently, $10IC_{95}$ of the specified compound (determined by yield assay results) or 100 µM of oseltamivir was then added at the specified time point (-2 to 0, 0 to 2, 2 to 4, 4 to 6, 6 to 8, 8 to 10 hpi), after which the well was washed with PBS and incubated until 10 hpi had been reached. The supernatants were then harvested, and stored at -80°C until quantification. Viral titers were determined by titration of samples in a standard $TCID_{50}$ assay and titers calculated using the method of Reed and Muench for estimating 50% endpoints[193]. Virus control wells contained virus added for an adsorption step of -1 – 0 hpi, as previously described, as was the case in the above-described experimental setups.

of virus to compound was better suited to the antiviral mode of effect. A pre-absorbance stage was used for this experiment, and the higher MOI paired with $10IC_{95}$ of oridonin was observed to be optimal for viral titer reduction. Generally, the 1 MOI experiment observed after 24 h indicated entry inhibition results that matched subsequent results shown in section 3.4 (see section 8.2). Having seen these later experimental results, the 0.001 MOI experiment indicated more compounds of interest which were later followed up as potential entry inhibitors, but the 1 MOI experiment more accurately predicted compounds that were later deemed to be potential entry inhibitors with other assays (see section 8.2).

Diosmetin also showed no time of addition-specific effect, yielding an inconclusive result regarding infection cycle impact (see Figure 14i). Kinetin reduced viral titers, compared to the infected, untreated control, when present up to 2 hours post-infection, suggesting that this compound may be acting early in the infection cycle (see Figure 14m). Progesterone was effective at reducing viral titers at multiple stages of infection, compared to the infected, untreated control (see Figure 14n). These results indicate an effect at multiple stages of addition or the final stage of exit. Since progesterone is a hormone with many cellular effects, it may be acting on multiple portions of the virus replication cycle.

The results of the time of addition assay (Figure 14) identified teriflunomide, antazoline HCl, domiphen bromide, calycosin-7-glucoside, sodium aescinate, dioscin, phloretin, oridonin, mulberroside A, polyphyllin B, solamargine, and kinetin as likely IAV entry inhibitors because the reduction in IAV titers only occurred when they were present during or before the virus addition. Only compounds that remained feasible as novel antiviral candidates (i.e., reduced viral titers and were not virucidal) were carried forward for subsequent testing. These were sodium

aescinate, phloretin, calycosin-7-glucoside, kinetin, solamargine, mulberroside A, polyphyllin B, dioscin, and oridonin.

3.3.3: Visualizing viral HA, NA, and NP protein presence during infection in the presence of the compounds of interest via IFA

IFAs enabled visualization of the infection process in the presence of the experimental compounds showing whether viral protein production was reduced in the presence of the compounds. Anti-HA, anti-NA, and anti-NP monoclonal antibodies were selected in part because they had been previously used and validated for RV733 IAV microscopy studies in our research group. The first protein selected for fluorescent targeting was HA, as it is vital for the entry and fusion of the virus to the target host cell. HA is a surface protein that binds to the sialic acid receptors of the host cell, allowing viral entry[205,206]. By determining if this protein was accumulating on the surface of the host cell, I could visualize whether the compound may have had a negative impact on entry through direct HA interactions. For example, if the compound blocked entry by binding to HA, limiting binding to sialic acid of the host cell, accumulation on the host cell surface could result. The second protein selected, NA, also a surface protein, and is essential for the exit of the viral progeny from the host cell via cleavage of the sialic acid receptor binding between the host cell and virus in a process called budding[207]. Staining for this protein may be able to show if production of NA was impacted by the compound, or that NA is accumulating without assembling into virions at the surface of the host cell, suggesting the compound could be negatively affecting viral release. NA accumulation would indicate an effect to be followed up on for future mechanism of action study, rather than offering a finite answer. The third and final protein selected, NP, is crucial for encapsidating the genome in preparation

for RNA transcription, replication, and packaging [208–210]. These IFA results indicate that many of the compounds reduced the level of virus protein produced during the infection process, indicated by only limited staining of antiviral proteins shown in green, compared to the bright fluorescent green staining of the virus control. This assay confirmed the complete or partial reduction of the selected viral protein content during infection, reinforcing their applicability for treating seasonal IAV infections. Figure 15a shows the progression of virus replication in the absence of an inhibitor for direct comparison.

Sodium aescinate, phloretin, calycosin-7-glucoside, and kinetin showed lower CPE and viral titers compared to RV733-infected controls in past screening and yield assays. However, HA, and NP proteins were brightly stained in the IFAs by 24 hpi in the presence of these compounds, but the monolayer appeared to be present and, while somewhat compacted, morphologically intact by 24 hpi (see Figure 15b, Figure 15c, Figure 15d, and Figure 15e, respectively). In the case of sodium aescinate, the 24 hpi panels of HA and NA panels showed possible cellular toxicity, while the NP panel appeared largely intact, though variability between panels could be responsible for this observation (see Figure 15b). This suggests that toxicity could be appearing between 8 and 24 hpi, which agrees with the XTT cytotoxicity results (see section 3.1.2) and a reduced dosage of compound in future confocal experiments with sodium aescinate may be beneficial. However, the presence of monolayer at 24 hpi in the NA and NP channels compared to absence of monolayer in the virus-infected, untreated control (see Figure 15a) in addition to previous reductions in viral titers noted for this compound suggested possible antiviral effects (see sections 3.1.1 and 3.1.3).

a)

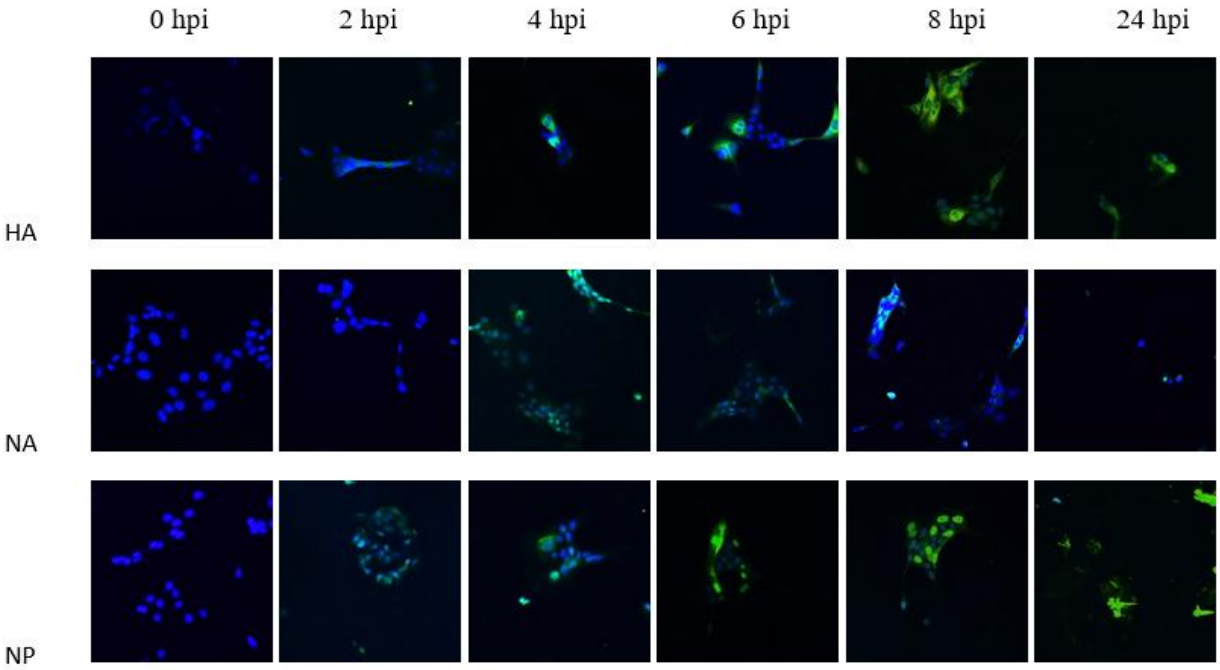

Figure 15a. Immunofluorescence assay results for the virus-infected, untreated control. Infection was performing using 3 MOI of RV733. Blue represents DAPI, and green represents the viral protein indicated in the left margin. Images were taken on a Zeiss Confocal microscope at 20X, showing a field of view of approximately 0.9 mm. The result shown is of one independent representative experiment from a set of 2 biological replicates with 2 technical replicates in each.

b)

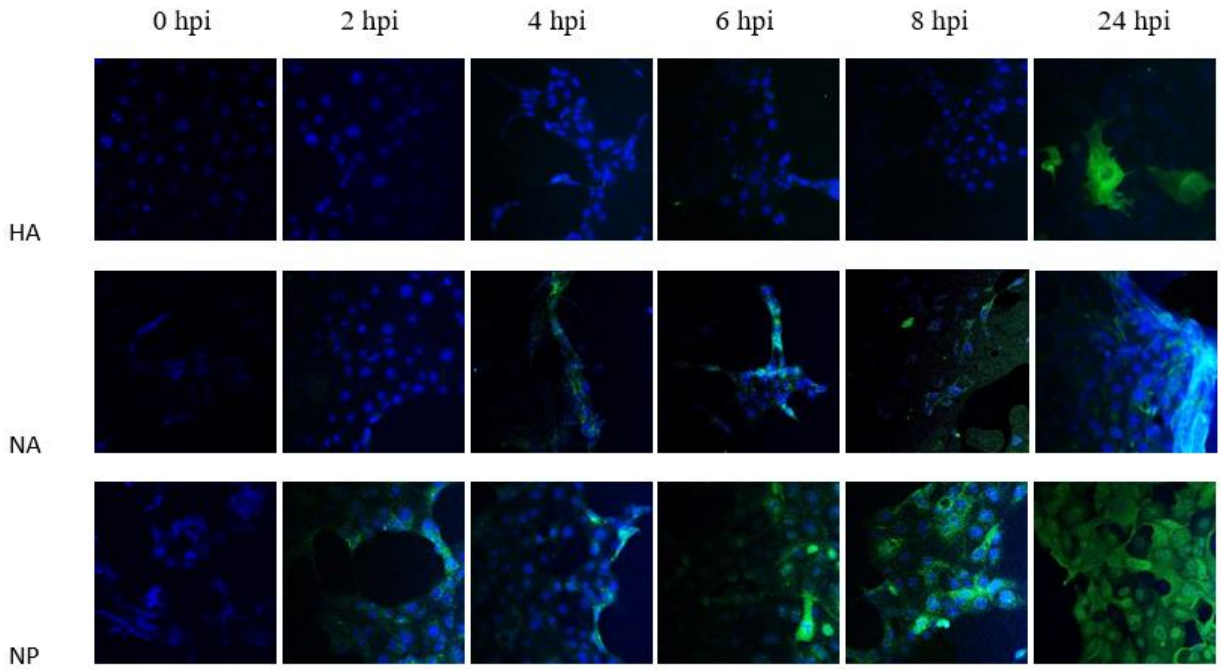

Figure 15b. Immunofluorescence assay results for the sodium aescinate treated, infected cells. Infection was performing using 3 MOI of RV733, and treatment of $10IC_{95}$ was used. Blue represents DAPI, and green represents the viral protein indicated in the left margin. Images were taken on a Zeiss Confocal microscope at 20X, showing a field of view of approximately 0.9 mm. The result shown is of one independent representative experiment from a set of 2 biological replicates with 2 technical replicates in each.

c)

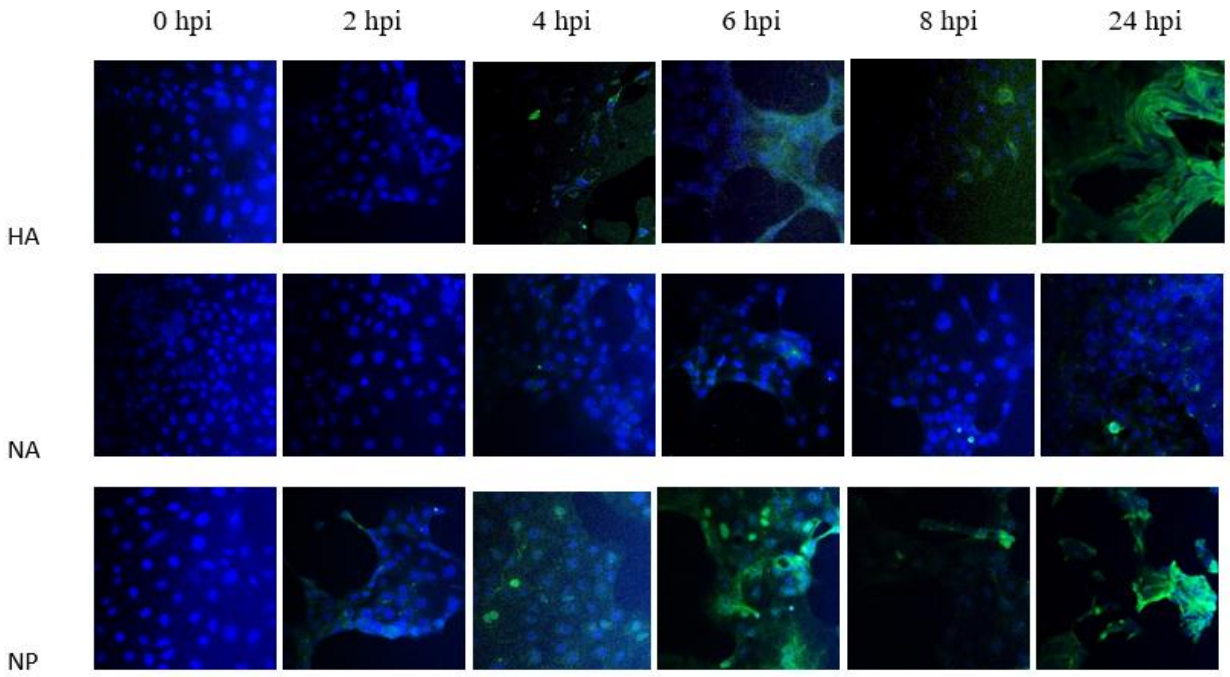

Figure 15c. Immunofluorescence assay results for the phloretin treated, infected cells. Infection was performing using 3 MOI of RV733, and treatment of $10IC_{95}$ was used. Blue represents DAPI, and green represents the viral protein indicated in the left margin. Images were taken on a Zeiss Confocal microscope at 20X, showing a field of view of approximately 0.9 mm. The result shown is of one independent representative experiment from a set of 2 biological replicates with 2 technical replicates in each.

d)

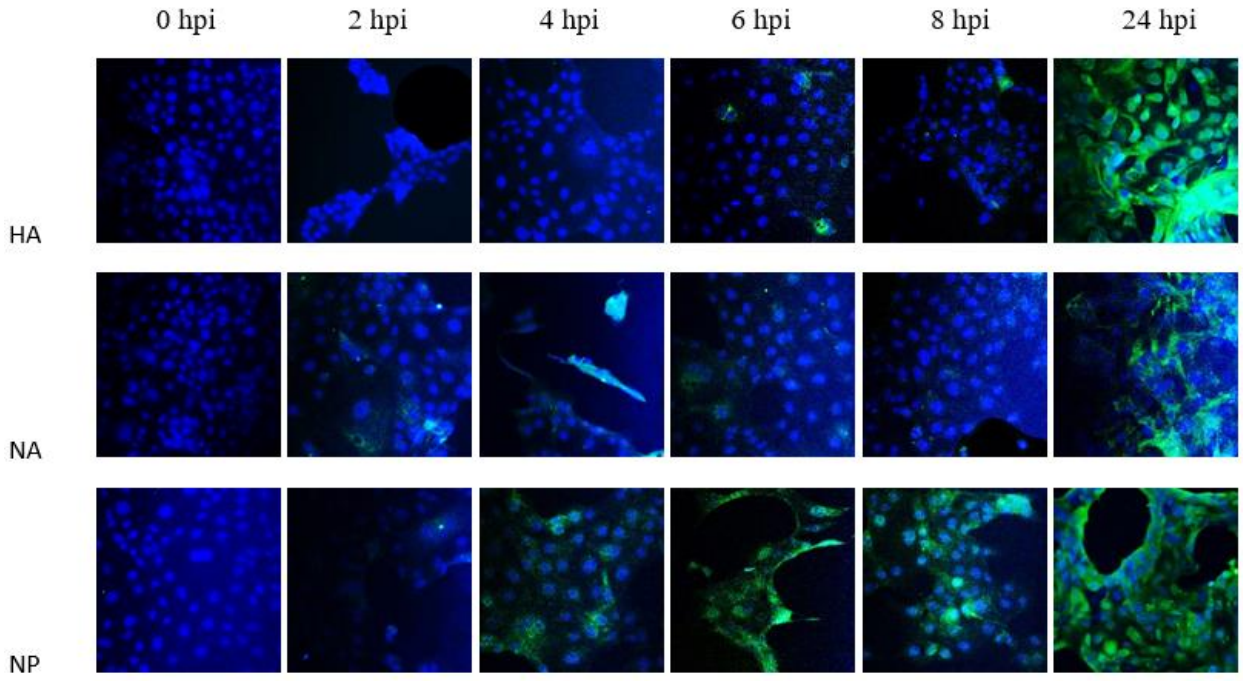

Figure 15d. Immunofluorescence assay results for the calycosin-7-glucoside treated, infected cells. Infection was performing using 3 MOI of RV733, and treatment of $10IC_{95}$ was used. Blue represents DAPI, and green represents the viral protein indicated in the left margin. Images were taken on a Zeiss Confocal microscope at 20X, showing a field of view of approximately 0.9 mm. The result shown is of one independent representative experiment from a set of 2 biological replicates with 2 technical replicates in each.

e)

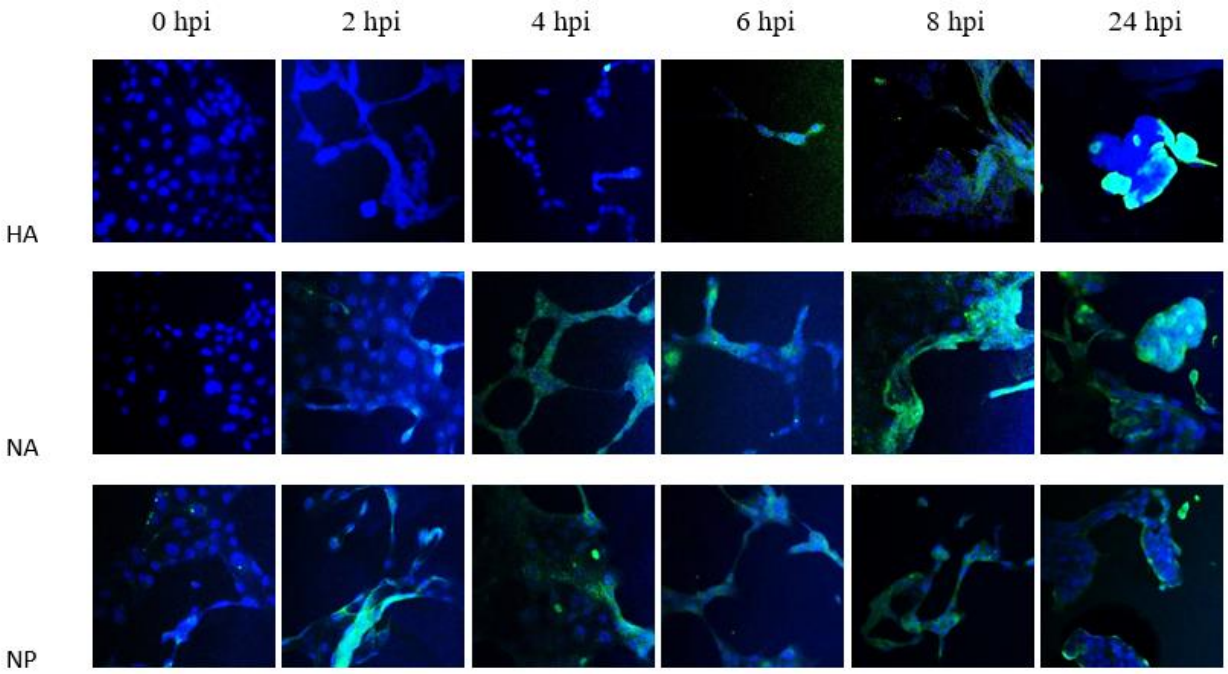

Figure 15e. Immunofluorescence assay results for the kinetin treated, infected cells. Infection was performing using 3 MOI of RV733, and treatment of $10IC_{95}$ was used. Blue represents DAPI, and green represents the viral protein indicated in the left margin. Images were taken on a Zeiss Confocal microscope at 20X, showing a field of view of approximately 0.9 mm. The result shown is of one independent representative experiment from a set of 2 biological replicates with 2 technical replicates in each.

The phloretin panels showed a similar result to sodium aescinate with increasing viral protein staining observed between 6 hpi and 24 hpi, but visible DAPI-stained cell membranes at the end of the time course (see Figure 15c). This result indicated a lack of CPE compared to the virus-infected, untreated control, but potential toxicity exhibited by compacting of the cells and loss of an even monolayer between 6-8 hpi, compared to the appearance of the monolayer between 0-4 hpi. It is difficult to tell from this experiment whether these effects were due to infection or toxicity, so this compound was pursued as a potential antiviral because past screening and yield assays also identified a reduction in viral titers, but the XTT assay result would suggest toxicity at $10IC_{95}$ was likely occurring (see section 3.1.2).

Calycosin-7-glucoside showed a drastic increase in viral protein fluorescence in addition to an intact monolayer, which was a peculiar result (see Figure 15d). While no evident toxicity was present, viral HA, NA, and NP were bright and prevalent by the end of the time course. However, in a typical infection like the virus-infected, untreated control, cell lysis has occurred by 24 hpi, and the monolayer is no longer intact. This lysis and absence of intact monolayer did not occur in the presence of calycosin-7-glucoside. The morphologically intact monolayer combined with reductions in viral titers observed in past screening and yield assays justified the continuation of testing with this compound as a potential antiviral to further delineate possible antiviral mechanisms of action.

Kinetin showed sporadic fluorescence of viral proteins between 2 and 24 hpi, which was unexpected (see Figure 15e). This effect may be due to kinetin's ubiquitous effects on cells including impacts on cell division, microtubular structure, and cell cycle arrest, resulting in differential results across time points depending on interaction kinetics between kinetin, the host cells, and virions. Kinetin showed sporadic and disparate results in past experiments seen in past

screening and yield assays, in which viral titers showed high SEM rates because results differ more substantially between replicates than was observed for other compounds. Kinetin, therefore, was pursued as a potential antiviral, but the lack of reproducibility and differential effects the compound were noted.

While most of the compounds tested showed some viral protein staining by 24 h, solamargine showed only blue DAPI staining indicating the cell nucleus with no green stain indicative of the viral HA, NA, and NP protein at all time points, but the cells appeared lysed and dead by 24 hpi (see Figure 15f). This result indicates toxicity rather than virus-induced cell death. Because of the limited effectiveness in viral titer reduction noted in past screening and yield assays, the combined lack of antiviral effect at the concentration which formed the crux between toxicity and CPE and viral titer reduction eliminated this compound from future study in favor of other compounds which resulted in greater viral load reduction quantified by $TCID_{50}$ (see sections 3.1.1 and 3.1.3) and an intact monolayer observed in this experiment.

Mulberroside A and polyphyllin B showed very limited HA, NA, and NP staining, but the cells appeared largely lysed and dead by 24 hpi (see Figure 15g and Figure 15h). This also indicates toxicity, due to lack of viral protein fluorescence. In the case of mulberroside A, the monolayer was destroyed at 8-24 hpi, indicated that rather than acute toxicity, long-term compound exposure may have caused destruction of the monolayer (see Figure 15g). Polyphyllin B treatment showed lack of viable monolayer beginning at 2 hpi until 4 hpi, suggesting more acute toxicity, and the XTT cytotoxicity assay result also suggests this concentration may have induced toxicity (see section 3.1.3). Because these compounds also showed marginal reductions in viral titers in past screening and yield assays were ineffective in the 1 MOI time of addition

f)

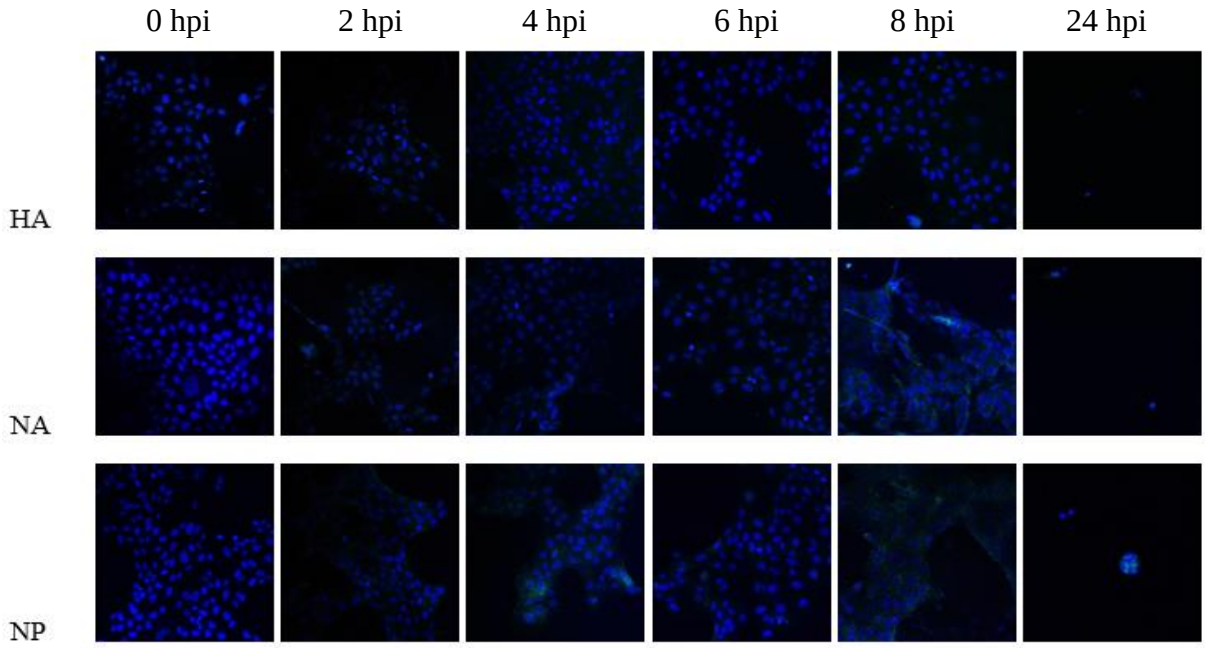

Figure 15f. Immunofluorescence assay results for the solamargine treated, infected cells. Infection was performing using 3 MOI of RV733, and treatment of $10IC_{95}$ was used. Blue represents DAPI, and green represents the viral protein indicated in the left margin. Images were taken on a Zeiss Confocal microscope at 20X, showing a field of view of approximately 0.9 mm. The result shown is of one independent representative experiment from a set of 2 biological replicates with 2 technical replicates in each.

g)

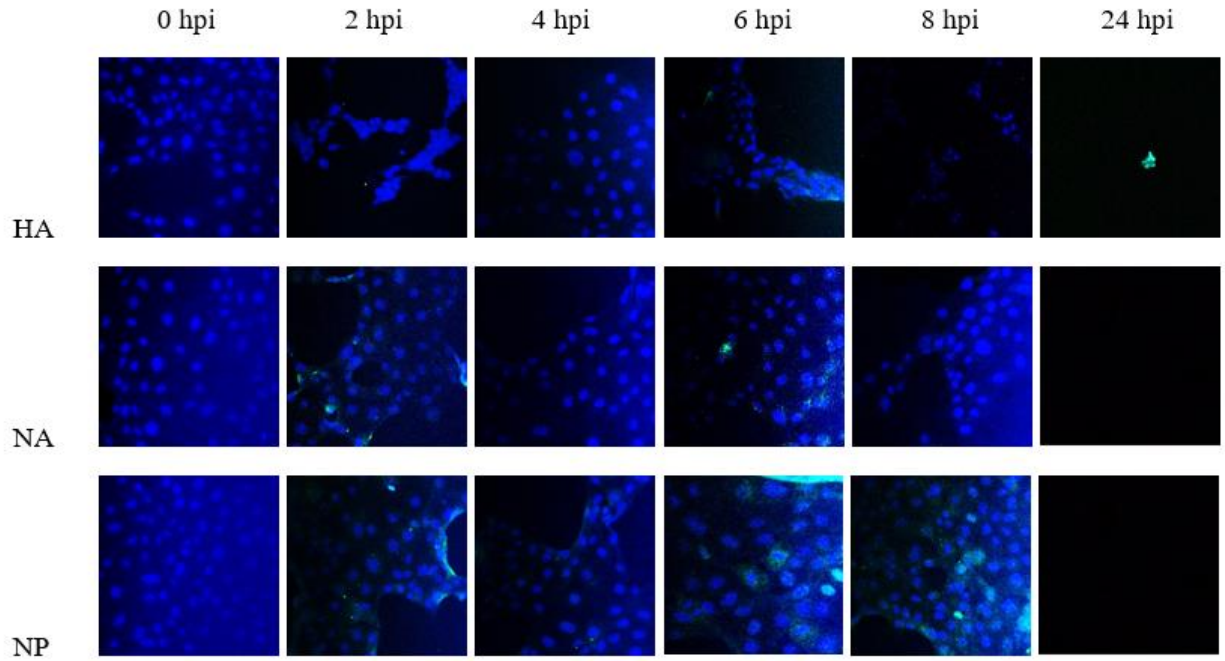

Figure 15g. Immunofluorescence assay results for the mulberroside A treated, infected cells. Infection was performing using 3 MOI of RV733, and treatment of $10IC_{95}$ was used. Blue represents DAPI, and green represents the viral protein indicated in the left margin. Images were taken on a Zeiss Confocal microscope at 20X, showing a field of view of approximately 0.9 mm. The result shown is of one independent representative experiment from a set of 2 biological replicates with 2 technical replicates in each.

h)

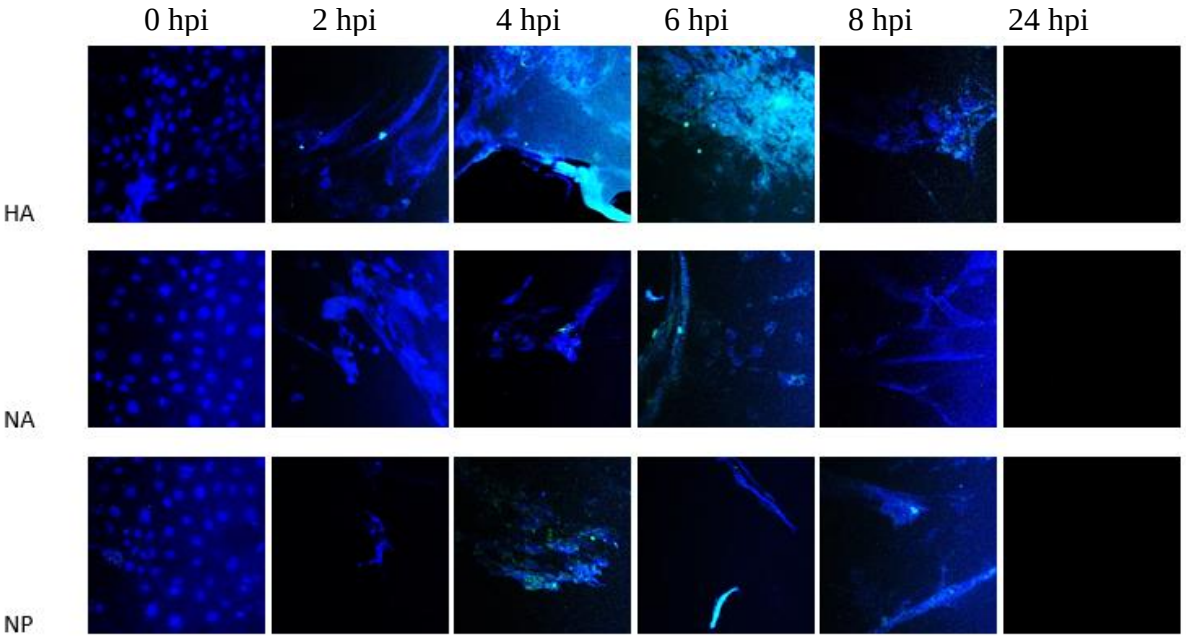

Figure 15h. Immunofluorescence assay results for the polyphyllin B treated, infected cells. Infection was performing using 3 MOI of RV733, and treatment of $10IC_{95}$ was used. Blue represents DAPI, and green represents the viral protein indicated in the left margin. Images were taken on a Zeiss Confocal microscope at 20X, showing a field of view of approximately 0.9 mm. The result shown is of one independent representative experiment from a set of 2 biological replicates with 2 technical replicates in each.

experiment (see section 8.2), they were discontinued from further analyses as feasible and effective potential IAV antivirals.

Dioscin and oridonin showed no virus presence but evident cellular damage from acute toxicity occurring early in the time course (see Figure 15i and Figure 15j, respectively). In addition to reducing viral titers without showing toxicity in earlier screening and yield assays these compounds were also effective in early time additions in both the 0.001 MOI time of addition experiment (see section 3.3.2) and the 1 MOI time of addition experiment (see section 8.2). These compounds had also been recently identified in the literature as reducing acute lung injury and inflammatory pathways, making them of great interest for further study[211,212]. Given the potential of dioscin and oridonin in past assays performed in this dissertation and reports in the literature, I carried these compounds forward for further analysis to delineate their effect, while being aware that toxicity using $10IC_{95}$ may occur, requiring lower concentrations of the compounds be used for future experiments. Evaluating the IFA and time of addition results together, sodium aescinate, calycosin-7-glucoside, kinetin, dioscin, and oridonin were most effective at reducing viral titers/protein presence and appeared to be potential IAV entry inhibitors. These five compounds were carried forward for further analysis.

i)

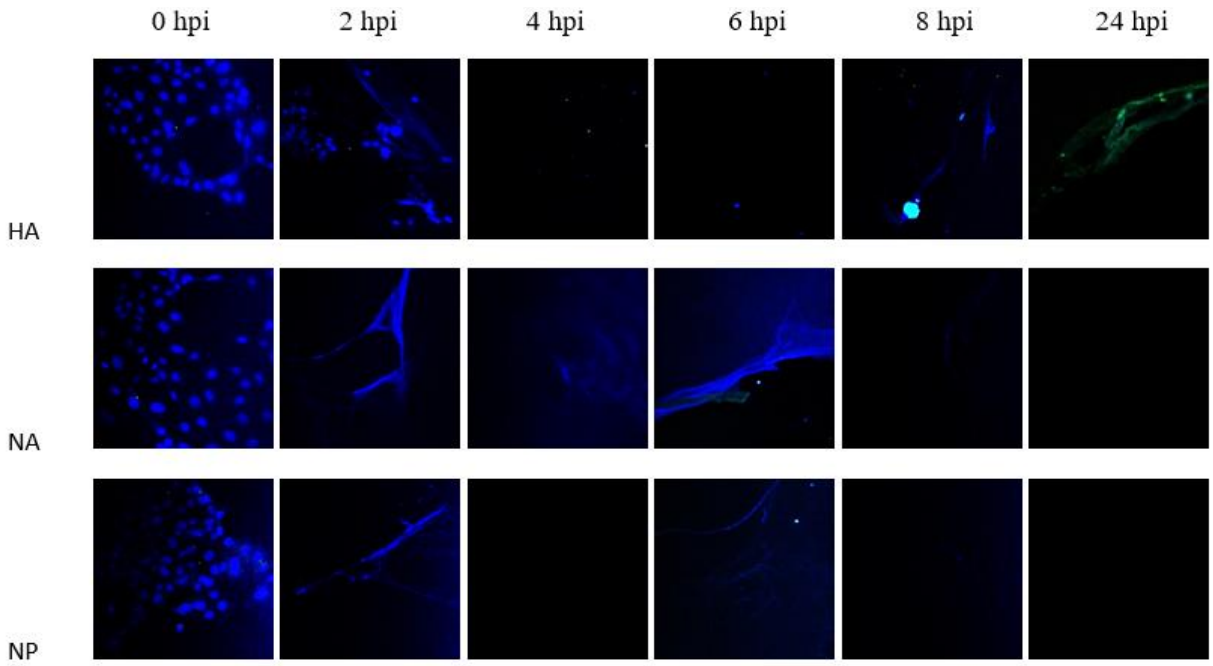

Figure 15i. Immunofluorescence assay results for the dioscin treated, infected cells. Infection was performing using 3 MOI of RV733, and treatment of $10IC_{95}$ was used. Blue represents DAPI, and green represents the viral protein indicated in the left margin. Images were taken on a Zeiss Confocal microscope at 20X, showing a field of view of approximately 0.9 mm. The result shown is of one independent representative experiment from a set of 2 biological replicates with 2 technical replicates in each.

j)

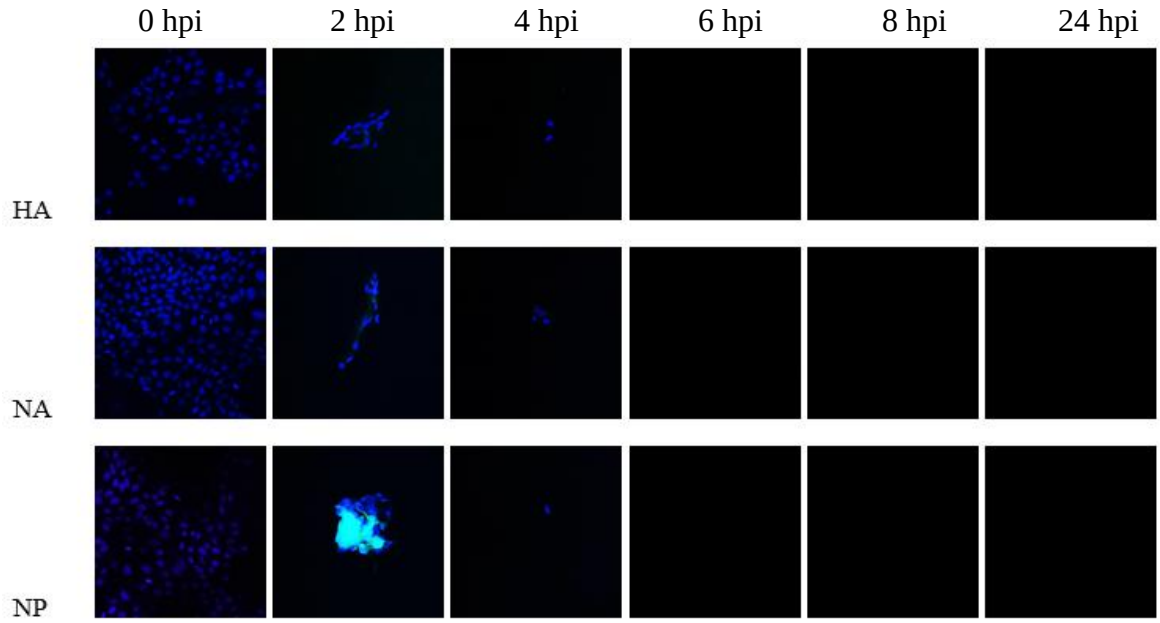

Figure 15. Immunofluorescence assay results for the virus control (a), sodium aescinate (b), phloretin (c), calycosin-7-glucoside (d), kinetin (e), solamargine (f), mulberroside A (g), polyphyllin B (h), dioscin (i), and oridonin (j). MDCK cells grown to ~80% confluent were seeded on poly-D-lysine-coated glass coverslips in 24-well plates 24 h before the assay. Each well contained 1 glass coverslip on which cells were grown. The following day, 10IC_{95} of the compound (determined by yield assay results) was added to all the wells at time -2 hpi, and 3 MOI of RV733 IAV was added to each well at time 0 hpi. The infection was then paused by removing the supernatant and washing the plate twice at the specified time point (0, 2, 4, 6, 8, 24 hpi), followed by fixation with formalin. Plates were then stored at 4°C with PBS until use. Blue represents DAPI, and green represents the viral protein indicated in the left margin. Images were taken on a Zeiss Confocal microscope at 20X, showing a field of view of approximately 0.9 mm. The result shown is of one independent representative experiment from a set of 2 biological replicates with 2 technical replicates in each.

3.4: Analysis of Suspected Entry Inhibitors

I further examined suspected entry inhibitors sodium aescinate, calycosin-7-glucoside, dioscin, kinetin, and oridonin in this section. By using HAI assays and experiments designed to examine whether attachment or entry were inhibited by the presence of the compounds of interest, I aimed to determine the stage of entry being negatively affected by the proposed novel entry inhibitors identified thus far in the dissertation. Examining these compounds in action in a timecourse spanning the first round of viral replication under high magnification on a confocal microscope, staining for HA, further delineated the potential mode of action.

3.4.1: Measuring the impact of the compounds of interest on virus binding using an HAI assay

In the presence of IAV, the virus binds the sialic acid receptors on the surface of red blood cells (RBCs) and forms a mix of RBCs crosslinked by virus in a process referred to as hemagglutination. Hemagglutinated RBCs will settle to the bottom of a round-bottom well in a plate in a crosslinked lattice, distributing evenly across the base of the well, resulting in a fuzzy or hazy appearance of RBCs evenly distributed across the bottom of the well, which is readily distinguished from the compact button of RBCs that is seen in the absence of hemagglutination. This compact button is the result RBCs settling to the bottom of the well, which occurs when the RBCs are in solution exclusively. If the compounds of interest are actively blocking the attachment of the virus to red blood cells, they will stop this hemagglutinating effect, again forming the small button[213]. Seeing the small button of red blood cells appear in the presence of a compound and virus infection suggests that the compound stopped IAV from attaching to the sialic acid receptors on the red blood cells, indicating an attachment inhibitor. The red blood

cells used for this assay were also washed to remove serum clotting factors making them form a small button at the bottom of a round-bottom well when they settle in medium or PBS.

I used turkey red blood cells for this assay because these are reactive to the hemagglutinin of more recent H1N1 IAVs. In addition, turkey RBCs are nucleated and settle quickly due to their higher density than non-nucleated RBCs, providing the advantage of a more rapid assay readout. Hamster and guinea pig RBCs have historically been used for hemagglutination assays, but are not nucleated, so they do not settle as quickly as avian red blood cells[214]. Chicken red blood cells were originally used for hemagglutination-style assays, but IAV strains after 1990 also do not agglutinate chicken red blood cells.

The experiment was performed in a dilution series of experimental compounds across the rows of wells, with all wells containing the same viral titer. This readout produced two pieces of information. The first result indicated whether hemagglutination inhibition had occurred, and the second indicated the compound concentration at which this effect ceased. Sodium aescinate, calycosin-7-glucoside, and kinetin showed no hemagglutination inhibition, indicating that the added seasonal IAV readily binds to the red blood cells. Dioscin and oridonin showed a low hemagglutination inhibition (HAI) titer, meaning they were effective at blocking the virus from binding red blood cells causing hemagglutination until less than 98 nM or 195 nM, respectively, of the compound was present (see Table 12). The value below, defined as the HAI titer, was the and lowest concentration in the dilution series to show hemagglutination inhibition, as described in section 2.5.1. These results suggest that sodium aescinate, calycosin-7-glucoside, and kinetin are not blocking virus attachment, but dioscin and oridonin are, even at low concentrations of 98 nM and 195 nM, respectively (see Table 12). Because the process of the viral HA binding to RBC sialic acid utilizes the same mechanism as natural IAV infections binding to epithelial cells,

Table 12. HAI titers of the experimental compounds and the interpretation of the result (technical and biological triplicates per condition).

Compound	HAI titer (last dilution to show hemagglutination inhibition)	Potential attachment inhibitor?
Sodium aesincate	No inhibition	No
Calycosin-7-glucoside	No inhibition	No
Dioscin	98 nM	Yes
Oridonin	195 nM	Yes
Kinetin	No inhibition	No
Virus-only control	No inhibition	N/A
Cell-only control	No inhibition	N/A

this result indicates a potential inhibitory action against the ability of HA to bind to the host receptor during infection in the presence of the compound.

3.4.2: Utilizing attachment and penetration blockades to further delineate the potential mechanism of the compounds of interest

I performed attachment and penetration blockade assays, which were adapted from a previously published protocol utilized for several viruses, including IAV[125]. The virus attachment blockade works for IAV because attachment can occur at 4°C, but penetration cannot proceed until the temperature is above 15°C. Virus and compound were added at the same time for this assay. By allowing attachment to occur at this lower temperature for an hour, then removing the virus-and-compound-containing supernatant and washing several times, then incubating the plate at 37°C, only the virions that were able to attach in the presence of the compound would be allowed to penetrate and replicate in the host cells. After the 24 h incubation period, there should be very little to no virus replication if the compound was very effective at blocking attachment. If the compound did not negatively impact the virus attaching to the host cell, the result should be similar to the untreated control in which all virions could attach and would remain to penetrate and infect the cells.

Dioscin addition resulted in no virus detected by $TCID_{50}$ (see Figure 16). Oridonin addition resulted in little detectable virus, resulting in an estimated 2-$\log_{10}$ reduction in viral titers (see Figure 16). Sodium aescinate, calycosin-7-glucoside, and kinetin showed no significant difference in viral titer compared to the virus control. A significance of $p<0.0001$ for both dioscin and oridonin results against the infected, untreated control was determined by one-

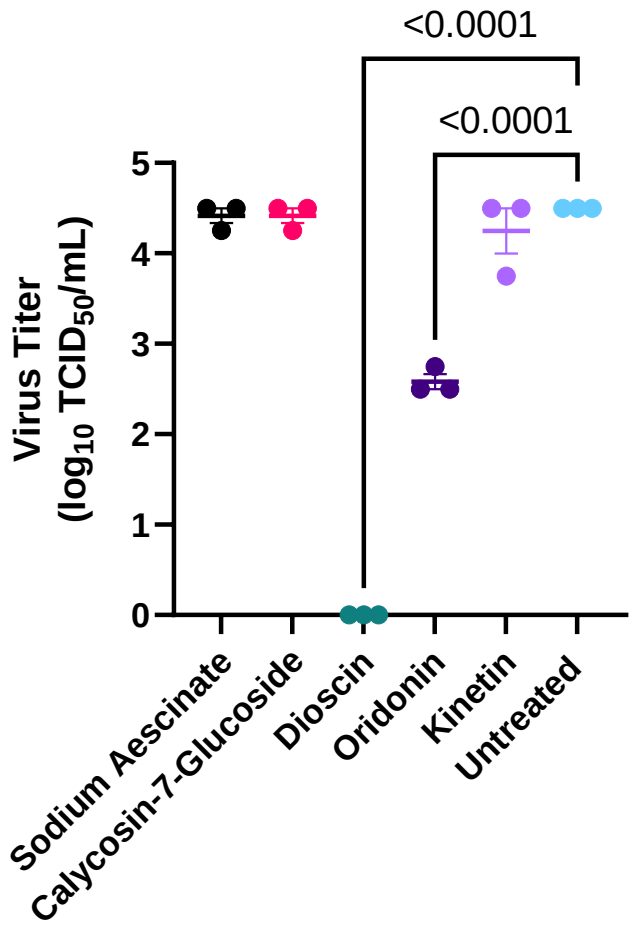

Figure 16. Attachment blockade assay results. Points shown indicate the mean of technical triplicates and biological duplicates (n=6) with bars showing the mean and error bars representing ±SEM. MDCK cells grown to ~60% confluent were seeded in 24-well plates 24h prior to the assay. The cells were then treated with $10IC_{95}$ of the compound of interest, infected with 0.001 MOI of RV733, and incubated at 4º C for 1 h. Following incubation, the plates were thoroughly washed with PBS, and the virus growth medium (MEM/0.1%BSA/L-glutamine/1 µg/mL TPCK-trypsin) was added to each well. The plates were then incubated at 37ºC in a 5% CO_2 incubator for 8 h. The plates were then read for CPE, and the supernatant was harvested and stored at -80º C until virus titration was performed. Viral titers were determined by titration of samples in a standard $TCID_{50}$ assay and titers calculated using the method of Reed and Muench for estimating 50% endpoints[193]. P values determined by one-way ANOVA indicating the level of statistical significance of samples significantly different from the virus-infected, untreated control are indicated by numerical values above bars in the image.

way ANOVA GraphPad Prism software (see Figure 16). These results indicate that the oridonin and dioscin may be acting as attachment inhibitors, while sodium aescinate, calycosin-7-glucoside, and kinetin may be having effects on other stages of the infection cycle.

The penetration blockade is an adaptation of the above attachment blockade with the difference being that the compound is added at a later time. The virus was allowed to attach at 4°C for 1 hour as before, but there was no compound added until the temperature was raised to 37ºC, marking the beginning of viral penetration. If the compound effectively blocked penetration, then the virus attached to the cellular receptors would have been unable to penetrate the host cell, despite the temperature and other conditions being ideal.

The penetration blockade showed no quantifiable virus presence when sodium aescinate was present. In contrast, calycosin-7-glucoside showed a 2.25-$\log_{10}$ reduction in viral titers, and kinetin showed a 1-$\log_{10}$ reduction in viral titers (compared to the untreated, virus-infected control) (see Figure 17), but was not significant. A significance of $p<0.0001$ for sodium aescinate and calycosin-7-glucoside results against the virus-only control was determined by one-way ANOVA GraphPad Prism software (see Figure 17). Quantifiable viral titers were present in these blockade experiments for oridonin and dioscin, despite $10IC_{95}$ being the concentration used in both these and the IFA experiments. This suggests that the experimental setup of the IFAs may have induced higher toxicity than the other in vitro assays utilized in this dissertation. Because the result was unclear for kinetin, it was not examined further in this dissertation, shifting the focus to sodium aescinate, calycosin-7-glucoside, oridonin, and dioscin as potential novel IAV entry inhibitors.

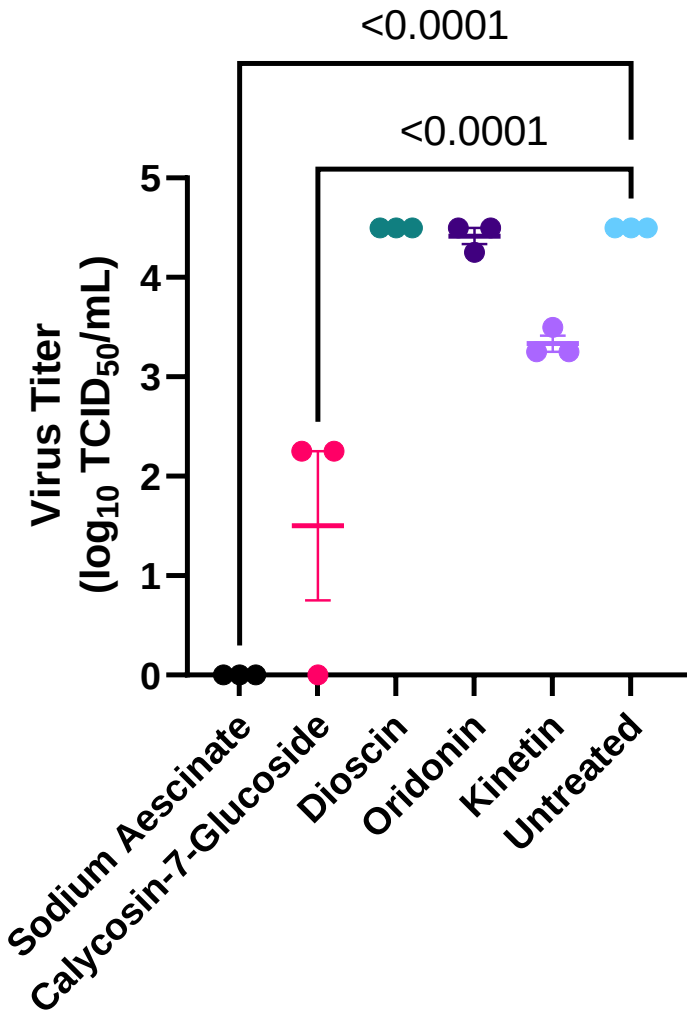

Figure 17. Penetration blockade assay results. Points shown indicate the mean of technical triplicates and biological duplicates, with bars showing the mean and error bars representing ±SEM. MDCK cells grown to ~60% confluent were seeded in 24-well plates 24 h prior to the assay. The plates were then washed and treated with 0.001 MOI of RV733 and incubated at 4º C for 1 h. The plate was then washed and treated with $10IC_{95}$ of the compound of interest and incubated at 37ºC for 1 h in a 5% CO_2 incubator. Following incubation, the plates were thoroughly washed with PBS, and the virus growth medium (MEM/0.1%BSA/L-glutamine/1 µg/mL TPCK-trypsin) was added to each well. The plates were then incubated at 37º C in a 5% CO_2 incubator for 8 h. The plates were then read for CPE, and supernatant was harvested and stored at -80º C until virus titration was performed. Viral titers were determined by titration of samples in a standard $TCID_{50}$ assay and titers calculated using the method of Reed and Muench for estimating 50% endpoints[193]. P values determined by one-way ANOVA indicating the level of statistical significance of samples significantly different from the virus-infected, untreated control are indicated by numerical values above bars in the image.

3.4.3: Measuring viral HA fluorescence via IFA at high magnification to further understand the effect of the compounds of interest on IAV entry

Given that blockade assays, time of addition assays, and HAI assays identified four candidate compounds that may be seasonal IAV entry inhibitors, further exploring their effect on attachment is needed. IFAs allow visualization of the attachment process on a cellular level, and these experiments were performed at a much higher magnification than past IFAs shown in this dissertation, to enable higher resolution of infection progression. IAV attachment occurs rapidly. Thus, for this immunofluorescence assay aiming to visualize attachment, observations were constrained to the first 90 minutes of infection. Attachment can occur within minutes after initial inoculation (when unaided by factors such as centrifugal force), and can take up to 2 hours depending on viral kinetics[215]. The pilot study showed similar fluorescence results between 15-minute interval test points during infection, so 30-minute intervals are shown for the final experiment to minimize redundancy. CellVue stain is a lipophilic compound that highlights the lipid membrane of MDCK cells so the outer periphery of the cell could be visualized.

The attachment assay aimed to visualize where the virus was localizing in the presence of proposed IAV entry inhibitors identified in previous experiments. By determining if the compound of interest limits entry of virus into the host cells or not, this can narrow down the possible mechanisms for further investigation. Past IFA experiments used protein-specific monoclonal antibodies to detect IAV proteins at various stages of infection during the first round of replication (8 hpi) and then one time point after multiple rounds of replication (24 hpi). This experiment utilized an HA-specific monoclonal antibody to fluorescently label HA (the primary viral protein involved in attachment). A lipophilic dye was used to fluorescently identify the surface of the host cell, which was not included in past experiments. This experiment was also

performed at a higher magnification (60X with oil, then zoomed in 4X further for clarity using Zeiss software) compared to the full image at 20X, shown in section 3.3.3. Prolong Gold mounting medium with DAPI was used to mount the coverslips and identified the host cell nucleus.

The CellVue stain indicates the cell membrane, and its absence in the center indicates the nucleus. Presence of CellVue allows some distinction of where cells are located in the pictured monolayer. However, there is some membrane staining from the overall membrane (including the top and bottom of the cell) which clouds the image, and some denser staining in panels where monolayer was denser such as the final timepoint of the infected, untreated control (see Figure 18a). Individual HA fluorescence has been brightened as far as possible without introducing excessive background not present in the initial image which can occur when the contrast is over-adjusted.

In the virus-infected, untreated control, clear fluorescence in the HA channel increases over time and eventually is very bright by the 90 mpi time point (see Figure 18a). By 90 mpi, HA fluorescence distribution is widespread and bright (see Figure 18a). In contrast, sodium aescinate and calycosin-7-glucoside showed less apparent HA fluorescence intensity than the virus control, but still contained visible HA fluorescence (see Figure 18b, Figure 18c, and Figure 18a, respectively). Oridonin showed bright HA fluorescence at specific points of the image, particularly where the MDCK cells were (i.e., detectable surface staining for viral HA that was added and had attached) (see Figure 18d). Dioscin showed less HA fluorescence than the virus-infected control, especially at the 60 and 90 mpi time points, but some potential toxicity (see Figure 18e). HA fluorescence was not as bright as in the virus-infected but untreated control (see Figure 18f and Figure 18a, respectively).

a)

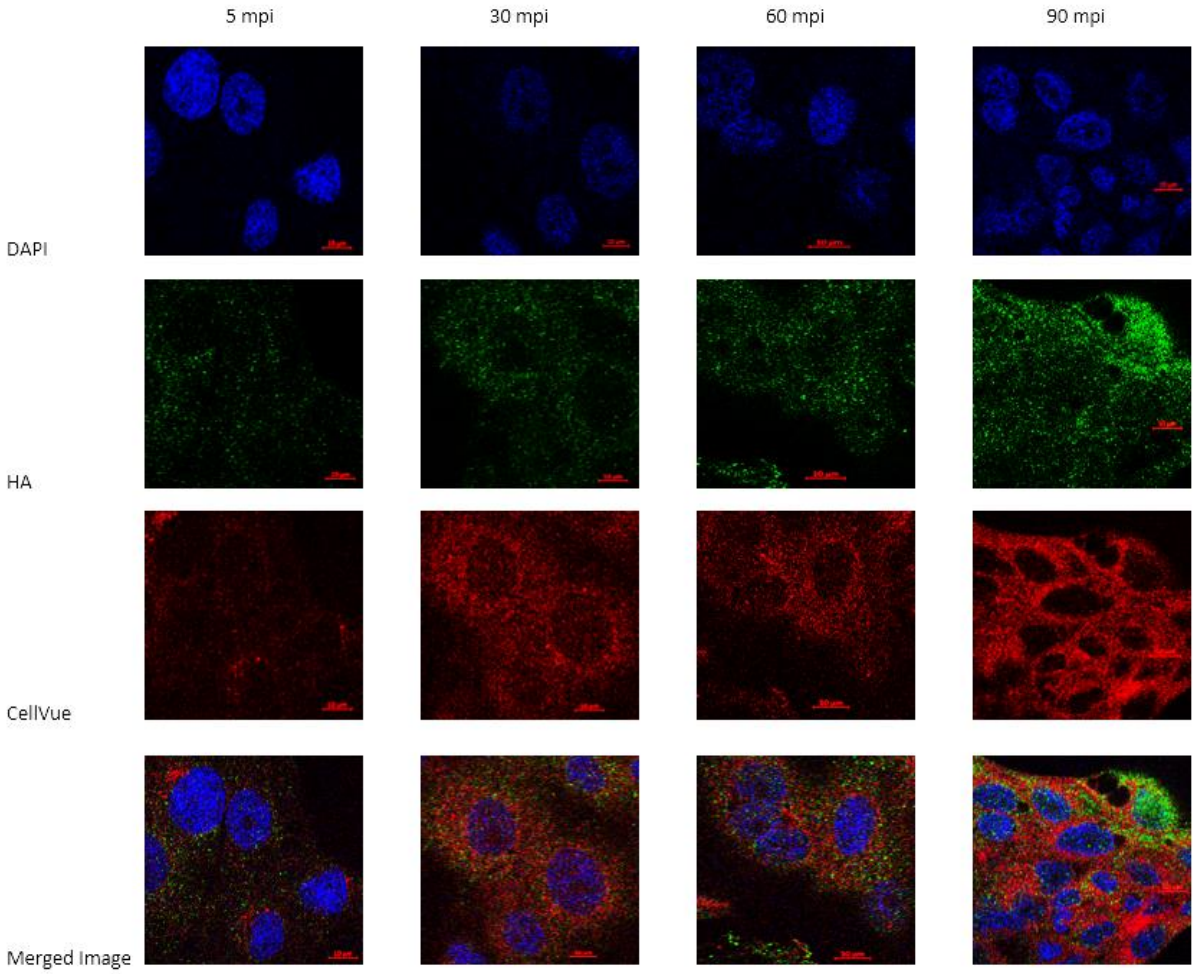

Figure 18a. Attachment immunofluorescence assay results for the untreated, infected cells. Images were taken on a Zeiss Confocal microscope at 60X. Scale bars indicate 10 µm. Infections were performed using 3 MOI of RV733, and treatment of $10IC_{95}$ was used. Blue represents DAPI, and green represents the viral protein indicated in the left margin. The result shown is of one independent representative experiment from a set of 2 biological replicates with 2 technical replicates in each.

b)

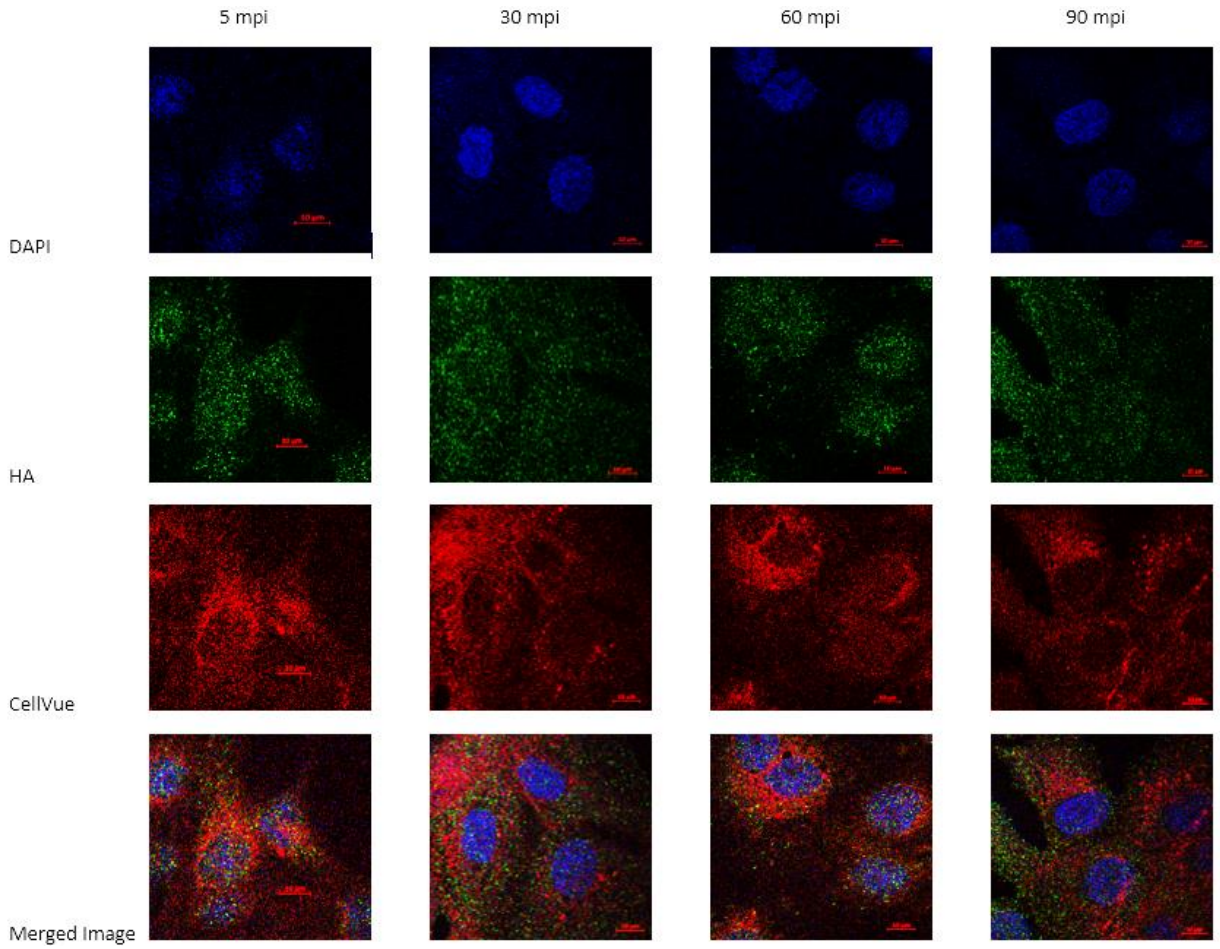

Figure 18b. Attachment immunofluorescence assay results for the sodium aescinate treated, infected cells. Images were taken on a Zeiss Confocal microscope at 60X. Scale bars indicate 10 µm. Infections were performed using 3 MOI of RV733, and treatment of $10IC_{95}$ was used. Blue represents DAPI, and green represents the viral protein indicated in the left margin. The result shown is of one independent representative experiment from a set of 2 biological replicates with 2 technical replicates in each.

c)

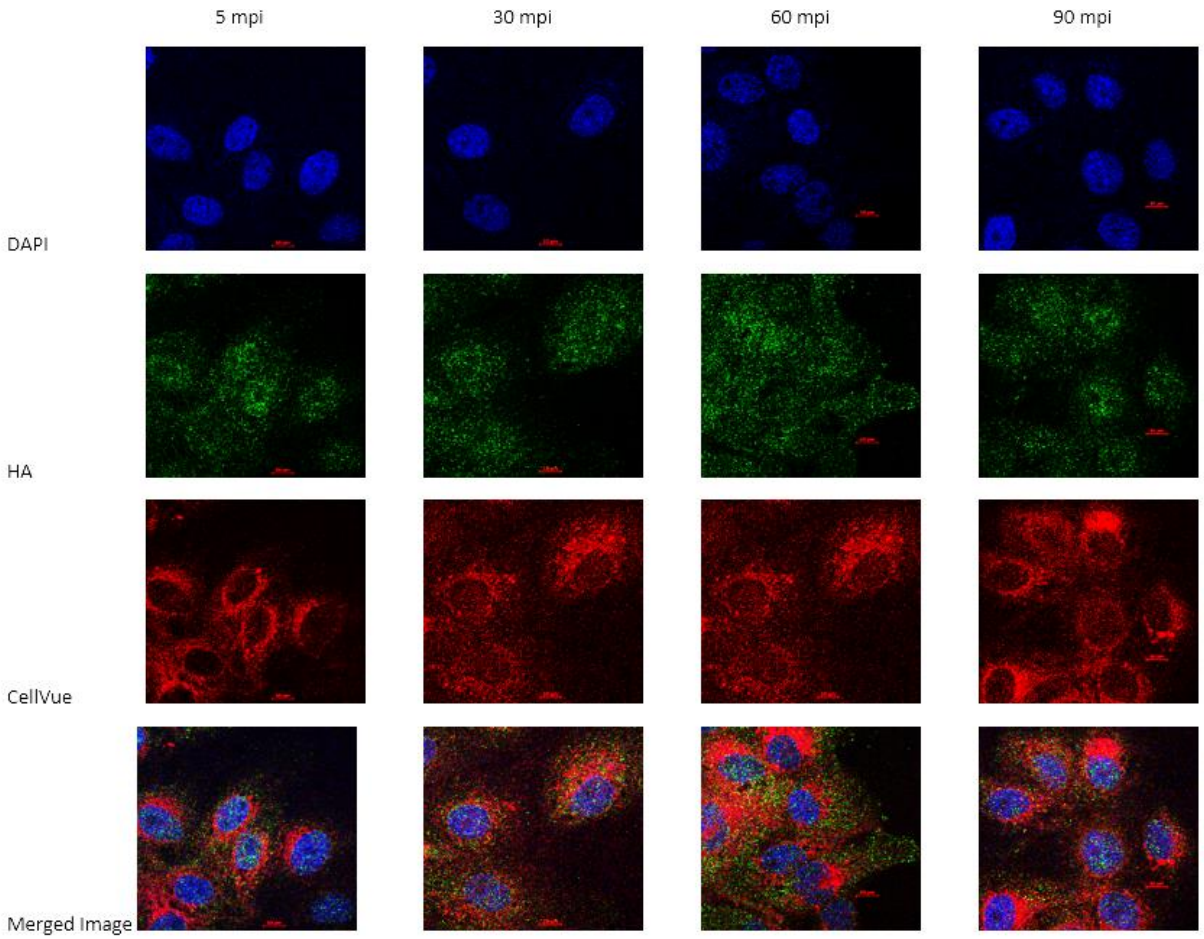

Figure 18c. Attachment immunofluorescence assay results for the calycosin-7-glucoside treated, infected cells. Images were taken on a Zeiss Confocal microscope at 60X. Scale bars indicate 10 µm. Infections were performed using 3 MOI of RV733, and treatment of $10IC_{95}$ was used. Blue represents DAPI, and green represents the viral protein indicated in the left margin. The result shown is of one independent representative experiment from a set of 2 biological replicates with 2 technical replicates in each.

d)

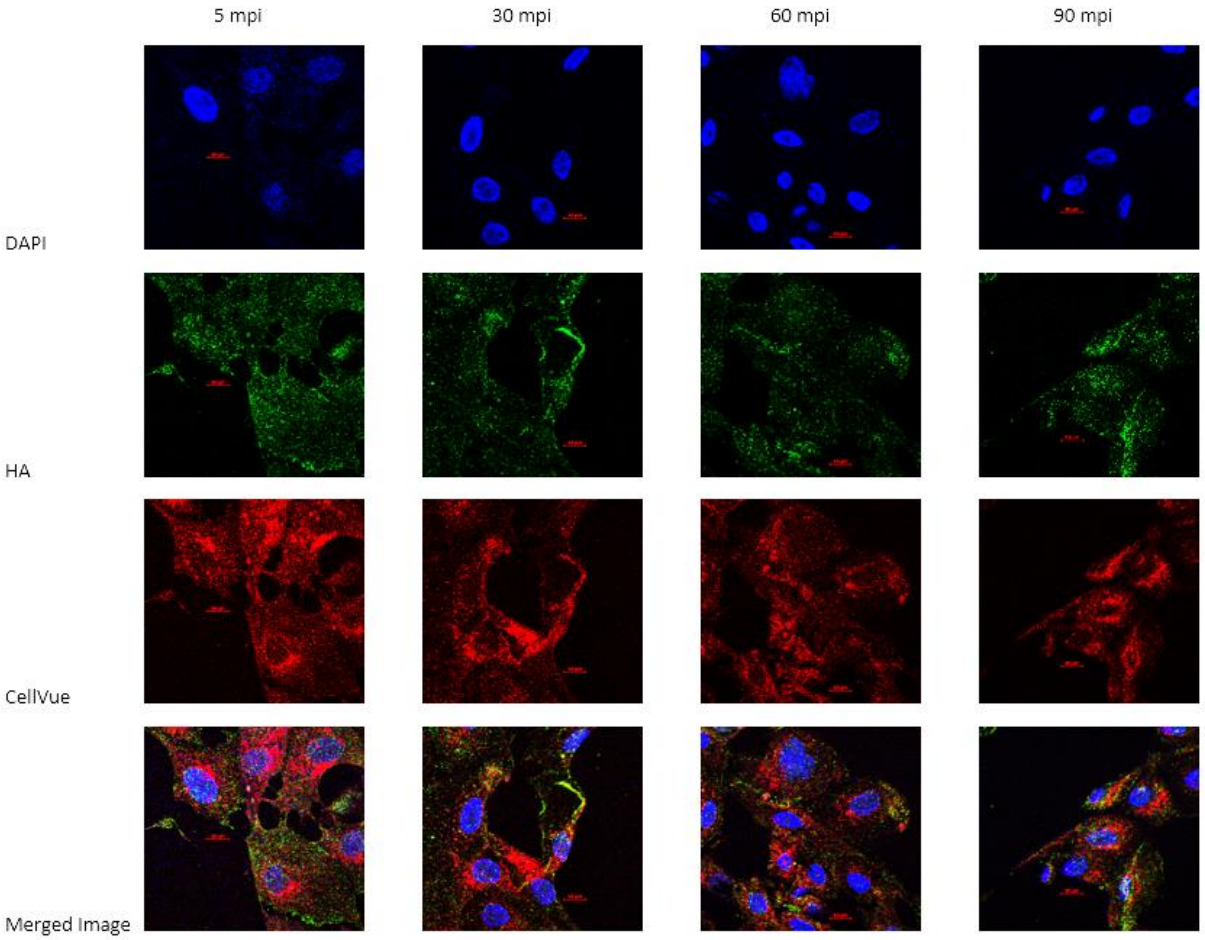

Figure 18d. Attachment immunofluorescence assay results for the oridonin treated, infected cells. Images were taken on a Zeiss Confocal microscope at 60X. Scale bars indicate 10 µm. Infections were performed using 3 MOI of RV733, and treatment of $10IC_{95}$ was used. Blue represents DAPI, and green represents the viral protein indicated in the left margin. The result shown is of one independent representative experiment from a set of 2 biological replicates with 2 technical replicates in each.

e)

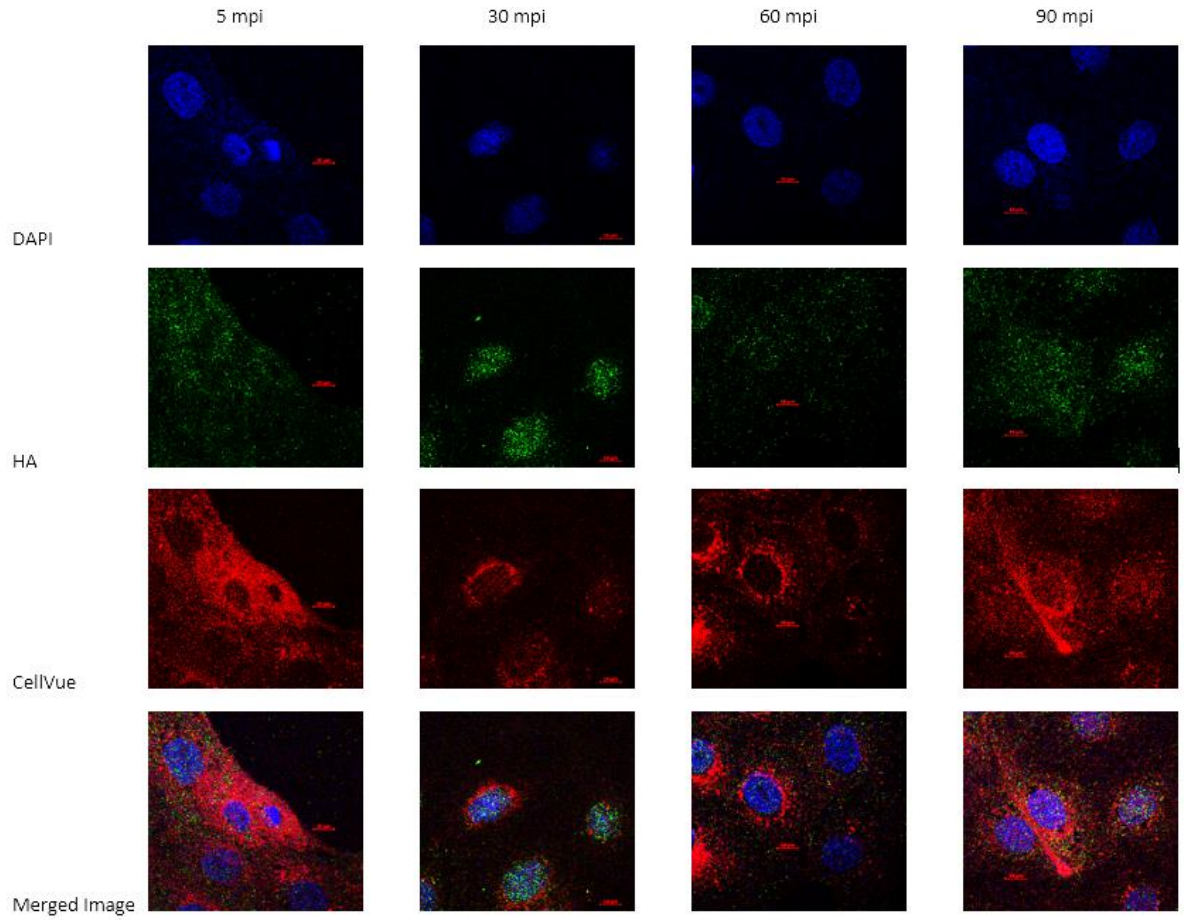

Figure 18e. Attachment immunofluorescence assay results for the dioscin treated, infected cells. Images were taken on a Zeiss Confocal microscope at 60X. Scale bars indicate 10 µm. Infections were performed using 3 MOI of RV733, and treatment of $10IC_{95}$ was used. Blue represents DAPI, and green represents the viral protein indicated in the left margin. The result shown is of one independent representative experiment from a set of 2 biological replicates with 2 technical replicates in each.

f)

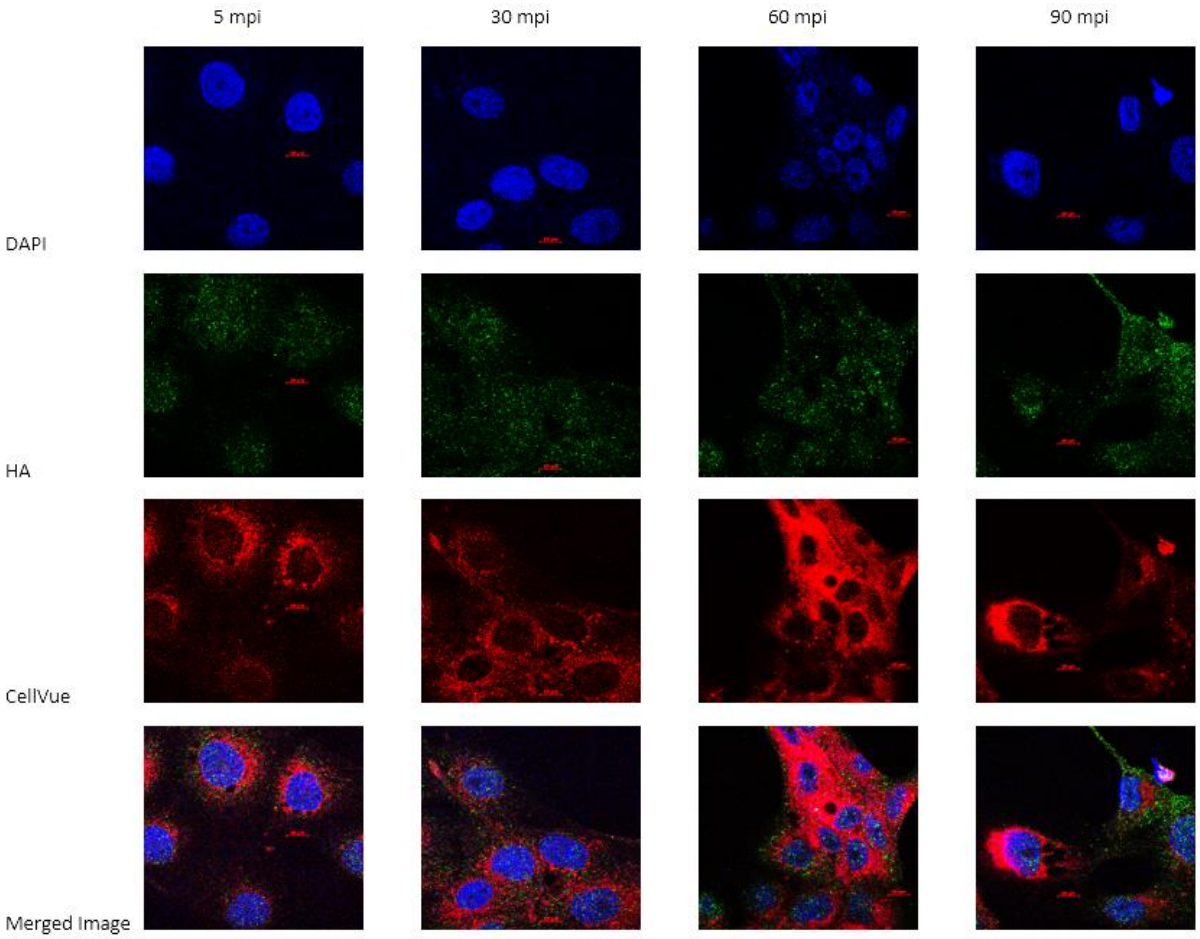

Figure 18f. Attachment immunofluorescence assay results for the virus control (a), sodium aescinate (b), calycosin-7-glucoside (c), oridonin (d), dioscin (e), and oseltamivir (f). MDCK cells grown to ~80% confluent were seeded in 24-well plates coated with poly-D-lysine 24 h prior to the assay. Each well contained 1 glass coverslip on which cells were grown. The following day, 10IC_{95} of the specified compound or 100 µM of oseltamivir was added to all wells at time -2 hpi, followed by 3 MOI of RV733 IAV at 0 mpi. The infection was then paused by removing the supernatant, fixing with 10% formalin, washing 3X with PBS, and adding fresh PBS at the specified time point (5, 30, 60, 90 mpi) until staining was performed at the end of the time course. Blue represents DAPI, green represents the virus protein (a monoclonal anti-HA antibody expressing green fluorescence), and red represents CellVue membrane stain, as indicated in the left margin. Images were taken on a Zeiss Confocal microscope at 60X with oil immersion. Scale bars represent 10 µm. The result shown is of one independent representative experiment from a set of 2 biological replicates with 2 technical replicates in each.

Previous data showed that dioscin inhibited viral replication, as evidenced by reductions in titers and CPE across multiple assays in this dissertation. However, HA immunofluorescence staining did not reflect this inhibitory effect, showing similar patterns in dioscin-treated cells and infected controls. Oseltamivir showed slightly less overall HA fluorescence at all time points compared to the untreated, infected control (see Figure 18f). The result from these IFAs did not show colocalization between HA and the outer membrane of the MDCK cells. Slides of uninfected MDCK cells were also processed with the previously described DAPI, HA, and CellVue fluorescent staining methods (see section 8.3). A Z-stack was performed, but was unsuccessful due to the size of the MDCK cells and limitations of the equipment used.

With the given adjustments made using Zen 2009 Light Edition software (Zeiss) to remove background fluorescence using the linear unmixing function and maximizing overall fluorescence for visibility, differences between the compound-treated panels and the virus-infected, untreated control were subtle. The results of this IFA experiment showed that while HA fluorescence indicated some possible accumulation of HA at the MDCK cell surface and slightly less overall HA fluorescence in the compound-treated experiments compared to the virus-infected, untreated control, the results between the treated panels and the untreated control panels were not significant. However, the results indicate a possible mode of action, which is discussed in section 4.5, particularly when past assay results including both IFA and $TCID_{50}$ data quantifications are taken into account.

The attachment and penetration blockades showed that sodium aescinate and calycosin-7-glucoside appear to block IAV penetration, while oridonin and dioscin appear to block IAV attachment. The IFA experiments shown in this section showed that the presence of sodium aescinate, calycosin-7-glucoside, dioscin, and oridonin subtly reduced the intensity of viral HA

fluorescence detected during infection, compared to the untreated, infected control, but did not show colocalization between HA and the outer membrane of the MDCK cells. These observations, along with the morphologically intact MDCK cells in the presence of the compounds, suggest that the presence of the compounds limited successful infection (quantified by viral titers in $TCID_{50}$ assays) and may have negatively impacted attachment and penetration of IAV (given the lack of a Z-stack, described in section 5.1 and presence of membrane permeabilization, it cannot be said whether the HA seen in the IFA experiments is inside of the MDCKs or dispersed outside of the cells).

3.5: Testing the *in vivo* Potential of Suspected Entry Inhibitors

To evaluate the in vivo potential of these compounds, I tested the highest dose found in the literature for alternative applications in mice (see Table 5)[130,132,133,216,217]. Notably, these compounds had not been tested for their antiviral effect against IAV at the time this dissertation research was performed. A murine-adapted HK68 (H3N2) virus was selected for these studies as this virus can provide a lethal infection model. A lethal model is advantageous because prevention of death indicates that the proposed antiviral is highly effective at combating a severe infection. Previous studies using these compounds in murine or rat studies did not identify toxicity concerns[130,132,133,216,217]. Previous work from this dissertation was performed exclusively *in vitro*, and there are many factors to consider when translating in vitro results to an *in vivo* model. These include biodistribution, the half-life of the compounds in the animal model, and the effective concentration of the compound communicated as dose per body weight. The mice received 10 mg/kg of oridonin, 80 mg/kg of dioscin, 2 mg/kg of sodium aescinate, or 100 mg/kg

of calycosin-7-glucoside daily for days -1 through 4 post-infection (with day -1 representing the day before infection) (see Table 5).

These doses were based on literature values used for other purposes, which provided the starting point for four compounds that had not previously been tested as an IAV therapeutic in mice, but showed potential *in vitro.* The dose and route of treatment for sodium aescinate was based on treatment of Sprague-Dawley rats for acute lung injury[169]. The dose and route of treatment strategy for calycosin-7-glucoside was based on treatment of male rats for reactive oxygen species sequestration[134]. The dosing and treatment strategy for dioscin was adapted from treatment of obese mice and pulmonary fibrosis treatment in a murine model[131,132]. The strategy for oridonin was based on treatment of asthmatic mice[130]. To adapt rat models (which were only adopted in the absence of available murine models) to murine models, the dose was corrected by body weight from the dose previously given to rats to that given to the mice in this study. These were the closest matches in the literature to the work performed in this dissertation, and provided a starting point for effective concentrations of these novel proposed antivirals.

Mice die of lethal infection (such as the $10LD_{50}$ dose used for this experiment) of MA-HK68 within 3-5 days, with symptoms beginning on day 3. The mice in this experiment progressively developed IAV symptoms and died of infection or reached the endpoint for humane termination between day 3-5 post-infection (see Figure 19 and section 8.1). These results indicate that these doses of the designated compound given for six days beginning the day before infection was insufficient to protect against a lethal HK68 infection.

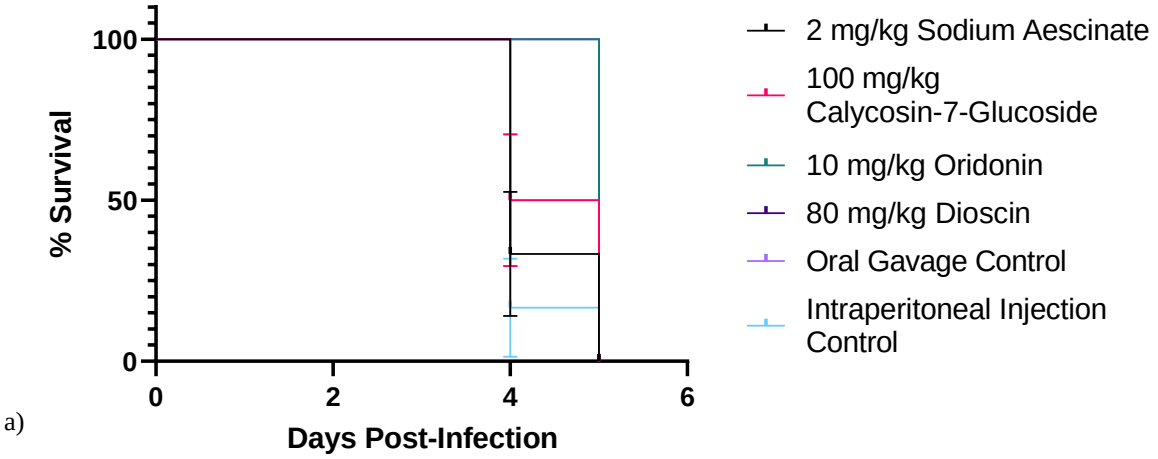

a)

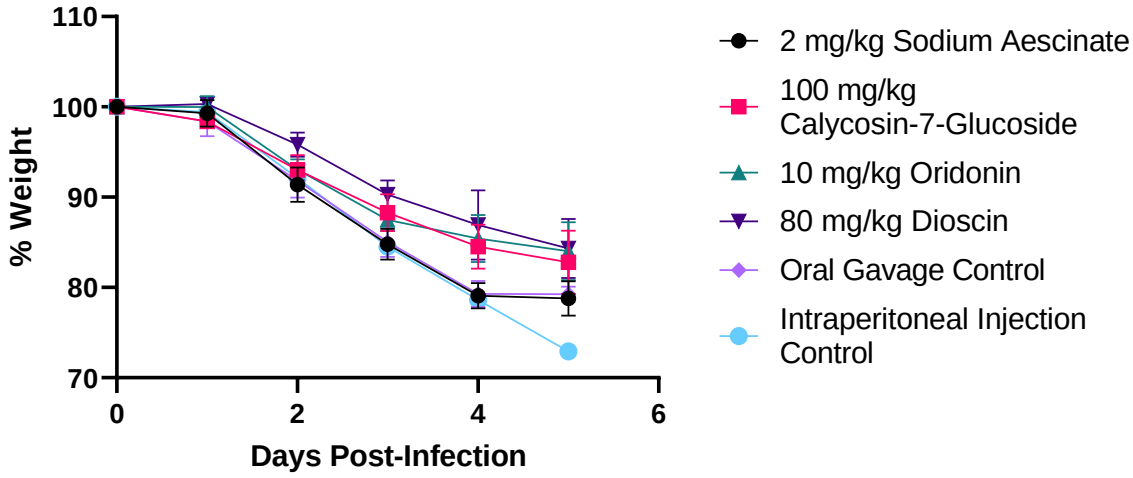

b)

Figure 19. Survival curves and weight loss trends *in vivo*. Mice were treated with the compound indicated in the legend on days -1 through 4 post-infection and were infected intranasally with $10LD_{50}$ of HK68 virus on day 0. Mock treatments of PBS were given by oral gavage or intraperitoneal injection, as indicated in the legend, using the same dosing strategy as the compounds. Weight loss is shown as a percentage of start weight prior to the experiment (b). Treatment groups were n=6 per compound, 3 male, 3 female. Post-infection, mice were observed for the duration of the experiment for clinical signs of disease and weight loss. Error bars represent ±SEM.

Chapter Four: Discussion

In this dissertation, I aimed to address the current shortage of seasonal IAV antiviral options by identifying novel IAV antivirals, followed by characterization of potential entry inhibitors. As described in my hypotheses and objectives (see section 1.5.2 and 1.5.3), this was achieved by screening libraries of compounds and further characterizing a subset of novel entry inhibitors to determine if IAV attachment or penetration specifically was inhibited *in vitro*. In total, 17 compounds that negatively impacted IAV replication but were not entry inhibitors were identified, addressing my first hypothesis. Of these, two attachment inhibitors and two penetration inhibitors for seasonal IAV were identified (addressing my second hypothesis). These compounds were tested for their ability to reduce viral titers and viral protein presence during infection while maintaining low toxicity, and were tested against multiple viruses *in vitro* (including non-IAV viruses and different subtypes of IAV) and two different cell lines. The project was concluded with a capstone *in vivo* assessment of the proposed antiviral candidates, addressing my third hypothesis.

4.1: The need for novel IAV antivirals: Providing options for inevitable future pandemics

In the post-Covid-19 world, there is no lack of appreciation regarding the toll pandemics can take. Pandemics of respiratory viruses with unknown and sometimes many natural reservoirs, such as Covid-19 and IAV, are impossible to eradicate. Multiple reservoirs and the ability to alter their genome, generating resistance to current treatments means that we must coexist with them, under the ever-present threat of another pandemic.

In addition to the historic IAVs listed in section 1.3 which have caused outbreaks over the last 100 years, there is a current outbreak of highly pathogenic avian influenza virus (HPAI) H5N1 virus wreaking havoc[218]. HPAIs like this are cause for great concern because of the risk of spillover to mammals, including humans. This H5N1 strain is currently being tracked by the CDC as novel lineages have been recently been observed to cause cattle and other mammalian infections in addition to the aquatic bird and poultry populations that have been affected for the last several decades by other lineages. This ongoing outbreak is thus negatively impacting the agricultural industry in addition to posing a potential public health crisis.

This Eurasian strain of H5N1 was recently identified in North America in late 2021, and the outbreak is continuing to cause infections in agricultural animals and some humans. The high death rate of cats who drank infected raw milk and reports of horizontal transmission of HPAI H5N1 between reservoir species and other mammals (including cats, ferrets, mink, etc.) are cause for concern as they indicate a higher risk of pandemic potential than other lower pathogenic strains of avian and other types of influenza[218].

For now, the human health risk remains low for HPAI. However, mutations in influenza and mammalian crossover events can happen rapidly. For this reason, it is essential to have effective treatments at the ready. Current treatments for IAV generate resistance quickly, and all must be used with caution. If widespread antiviral use is required (such as in the case of a pandemic), there are not enough options to serve healthcare systems and prevent disease if a mutation or spillover event causes sudden high rates of infections in the human population.

This dissertation shows a pipeline of experiments that can be used to identify potential novel entry inhibitors for influenza. There are no currently available and FDA-approved entry inhibitors for influenza. Entry inhibitors are an attractive option as they prevent infections before

they begin, quelling outbreaks. With this pipeline, I aim to identify novel treatment options beyond the currently available set of FDA-approved compounds (three quarters of which are NA inhibitors, putting substantial selective pressure on this viral protein), better preparing us for inevitable future IAV outbreaks, which are only a mutation away.

4.2: Screening compound libraries: A practical approach to novel antiviral discovery

Screening compound libraries presents an opportunity for identifying novel compounds that inhibit IAV replication. In this way, compounds that negatively impact viral replication can be identified. Compound library screening has been used by other groups successfully to identify potentially useful compounds against IAV[219,220]. The initial screening results of this dissertation identified 17 compounds as potential candidates for further studies against seasonal IAV, as they were highly effective at reducing CPE and viral titers, and had minimal toxicity. Initial screening identified several compounds that had been previously identified as potential IAV inhibitors, such as celestrol, showing the effectiveness of this strategy at identifying potential therapeutics (see section 3.1.1).

Once initial candidates had been selected from the FDA approved and natural source libraries offered by ApexBio, they were assessed for toxicity and inhibitory effect on replication measured by RV733 titers *in vitro* using a yield assay. Toxicity and antiviral efficacy could then be directly compared by calculating the SI. The higher the SI ratio (calculated by dividing the CC_{50} by the IC_{50}), the safer and more effective a compound will be for *in vivo* use, theoretically[221]. Thus, the SI quantifies which compounds have the most antiviral effectiveneness with limited toxicity. Compounds with low SI values driven by toxicity or lack of viral titer

reduction are not useful for further pursuit for ongoing study, mechanistic evaluation, and downstream cellular and animal model investigation including clinical trials because they are toxic or not effective enough as an antiviral to be useful for this application. SI values of one and below indicate compounds that are either not very effective at reducing viral titers or are toxic *in vitro,* while SI values of 10 or more indicate compounds of interest for further study[221]. All identified compounds of interest had SI values higher than 10.

An XTT cytotoxicity assay was selected for toxicity testing in this dissertation because of its high reported sensitivity and accuracy in addition to its high throughput design[222]. XTT is considered in some cases superior to MTT assays, which are of a similar design, because XTT salt is soluble (meaning uptake of XTT salt by living cells is possible, unlike MTT assays)[123]. The assay measures cell activity in a continuous living model rather than pausing the process and measuring the activity of lysed cells (whose structure is destroyed), as in MTT assays, making XTT a better selection for this project. Toxicity during *in vitro* testing helps to inform the dosage limits that can be used in a specific cell line, showing how much compound is damaging or even lethally toxic in a given cell model.

In reviewing the 17 compounds that were effective at reducing seasonal IAV titers, a recurring theme of the compounds isolated from the natural source compound library is that they had been tested against tumor cells or had been found to be anti-inflammatory, but the details of their specific effect and mechanism have not been described to date. For example, anti-inflammatory compounds including 3,3'-diindolylmethane, calycosin-7-glucoside and tumor reducing agents including 12-O-tetradecanoylphorbol-13-acetate all showed acceptable SI values indicating potential usefulness as a novel IAV antiviral candidate[177,184,223]. This suggests that the ability to reduce inflammation or negatively impact a pro-inflammatory response triggered by an

infection may be a useful means to predict compounds that are effective IAV antivirals. The identified compounds suggested in this stage had not been tested against seasonal IAV at the time they were performed, and making them novel antiviral candidates. These results also support my first experimental hypothesis which stated that because the compound libraries used for screening in this dissertation contain compounds thought or known to impact cellular processes, they present an excellent source of novel therapeutics for viral infectious agents such as IAV.

4.3: Testing potential antivirals against multiple cell types and viruses yields mechanistic details and suggests specificity of compound effectiveness

While MDCK cells are most permissible to IAV infection and form the foundation model for *in vitro* IAV studies, A549 cells are human lung epithelial cells, which may be a more accurate and representative cellular model of a human infection. Seeing that these compounds are largely effective in A549 cells in addition to the original MDCK model also shows the versatility of these compounds (see section 3.2.1), and confirms that the noted antiviral effects are not cell line specific, but showed some toxicity and antiviral efficacy discrepencies between the different cell lines used. MDCK cells, which were developed in 1958, are a transformed cancer cell line[224]. Despite being canine kidney cells, there are conflicting reports about what cancerous traits (such as tumorigenic capacity) the cells developed during transformation, and the ultimate impact of these changes, compared to wild type cells, in an experimental setting remains largely undocumented[224]. A549 cells, which were developed in the late 1980's, are also a transformed adenocarcinoma cell line[225]. These A549 cells retain many of the characteristics from the original cells (type II pneumocyte lung tumor cells), but have some architectural and

barrier properties that the original cells did not[225]. While these two cell lines have been extensively used for experiments such as those contained in this dissertation, they are immortalized cell lines, and may behave differently in some ways than untransformed, wild-type cells. Having said this, MDCK and A549 cells have been used for an extended period of time for influenza studies, and are considered standard cell lines for modeling IAV infection *in vitro*.

Broad activity of post-exposure treatments like antivirals is essential for IAV. As seen in section 3.2.2, several of the identified compounds of interest were effective against HK68, an H3N2 IAV, and Mx10, a pandemic H1N1 IAV, in addition to the 2007 seasonal H1N1 strain, RV733, used in the screening assays. This is an essential feature in an antiviral targeting seasonal IAV because many strains co-circulate seasonally and mutations can occur over time. Differences in effectiveness between RV733 and HK68, which were noted for several compounds including antazoline HCl and diosmetin, could be caused by interactions with HA or NA surface proteins, which differ between these viruses. However, there are many other differences between the these IAVs that could be driving changes in compound effectiveness. In addition, the lack of activity of some of the compounds seen in Table 10 suggest that follow up studies to determine the activity of these compounds compared to those designated as "N/D" which had a high level of antiviral activity at all doses tested, would be needed.

An interesting outcome of the work testing different IAVs was the variability of effectiveness between the different potential antivirals tested. While the HA and NA proteins differ between HK68 and the other two subtypes tested, RV733 and Mx10 were the same subtype. Because of this, I expected to see more broadly effective antiviral activity between RV733 and Mx10, and possibly HK68. Instead, many of the compounds tested showed different levels of antiviral activity between the viruses. Since all of these experiments were performed

with MDCK cells and utilized the same experimental setup, there may be differences between the functions of other highly related proteins or pathway differences not yet noted in the literature between these IAV subtypes.

I found that there were some cross-protective compounds particularly between subtypes of IAV, but the five potential entry inhibitors identified later in the project were not effective against Rhinovirus and were effective against VSV-MERS, with the exception of dioscin and kinetin (see section 3.2). VSV-MERS differs in structure and replication cycle from IAV, with the only similarity being that MERS (from which the VSV-MERS spike protein is derived) is also a respiratory virus. Considering that the replicative properties of VSV-MERS are derived from the VSV portion of this recombinant virus, this effect can likely be negated. VSV is an enveloped virus, like IAV, possessing different proteins from IAV as well as the MERS spike protein. Given the result that three of the five suspected IAV entry inhibiting compounds (sodium aescinate, oridonin, and calycosin-7-glucoside) were also effective against VSV-MERS, there appears to be some cross-protective potential of these compounds (their antiviral effectiveness is not exclusive to IAV). These cross-protective compounds may be having a similar inhibitory interaction with MERS spike protein and IAV HA during attachment to their respective host cell receptor. Unlike IAV, which targets sialic acid receptors, MERS targets the cellular receptor DPP4 to which the spike protein binds following proteolytic cleavage[226]. While IAV HA and MERS spike differ, the process of proteolytic processing, cellular attachment to their respective receptors, and fusion into the host cell do have their similarities. Depending on the mechanism of sodium aescinate, oridonin, and calycosin-7-glucoside, these similarities may be the cause of the noted cross-protection. The difference could also be due to the cellular

process hijacked by IAV and VSV. If it is a similar process or pathway, this could explain the cross-protected observed.

Testing the five proposed entry inhibiting compounds against a seasonal Rhinovirus showed they are ineffective against the strain tested (see Figure 13). Rhinoviruses do not possess an envelope and use a different mechanism of attachment than IAV and VSV, instead gaining entry to the host cell by using one of the following glycoproteins on human respiratory tract epithelium: intercellular adhesion molecule 1, low density lipoprotein receptor, or cadherin-related family member 3 glycoproteins[227]. This attachment of Rhinovirus to glycoproteins from a canyon in the VP1 protein of the icosahedral structure of the viral outer capsid is entirely different from the mechanism of seasonal IAV attachment[228]. IAV instead attaches by the globular head domain of the surface HA protein (embedded by the stalk in the viral envelope) which binds to the sialic acid of the host cell. However, upon entry into the cell the IAV and Rhinovirus infection cycles begin to align again starting with receptor-mediated endocytosis into host cell endosomes. Since the compounds tested at this stage of the project were the 5 identified as being potential entry inhibitors of seasonal IAV, this difference in surface composition and attachment mechanism may be part of the reason for the ineffectiveness against Rhinovirus for the two compounds ultimately identified as attachment inhibitors. However, other differences may be at play for the remaining compounds identified as penetration inhibitors, and this is a possible future direction of the project.

4.4: Discovering where in the viral replication cycle a compound is effective is a vital stage of novel antiviral characterization

Identifying the mechanism of action of a compound can be a monumental challenge because of the many factors that complicate infection (viral properties like the kinetics of infection driven by dissemination in medium, physical properties such as the half-life of compounds, and differences in cellular gene expression and function). Identifying compounds based on which stage of the viral replication cycle restricts the number of candidates later pursued in mechanism of action studies, simplifying downstream mechanism of action determination.

Sodium aescinate, calycosin-7-glucoside, oridonin, dioscin, and kinetin were the strongest IAV entry inhibitor candidates with downstream clinical potential that effectively reduced overall viral loads in past *in vitro* experiments. The virucidal assay was performed using plaque assay quantification and a flask experiment evaluating CPE from residual virus after compound treatment. The plaque assay experiment was designed to measure residual virus without amplifying surviving virus prior to titration. Plaque assays measure virus titer in terms of plaque forming units (PFUs). The plaque is the site of cell death in the monolayer, which is kept in place by the agar over the cells. A plaque results from an infectious virion that replicates and spreads progeny only to immediate neighbors because it is inhibited by the agar. The flask experiment was performed to ensure all residual virus could be evaluated and resultant CPE was present, as the full supernatant quantity was used for the assay, compared to 200 µL of the supernatent for the plaque assay. The flask experiment also confirmed that cell death observed was caused by viral replication, rather than compound toxicity.

Progesterone, which showed mixed results in previous assays in this dissertation showed some viral titer reduction in the virucidal assay (see section 3.3.1). It is possible that the compound made the MDCK cells less able to support replication, resulting in fewer plaques, but this would need further exploration to determine with certainty. Progesterone is complex because it is a hormone that affects many cellular pathways and biological phenomena[229]. While some *in vitro* studies have recently been performed have begin to delineate the complex interactions of progesterone during IAV infection, further research to fully understand these properties and the potential to exploit the benefits of progesterone without the negative side-effects noted will be key to determining its antiviral potential.

Domiphen bromide reduced viral titers by just over 40%, compared to the infected, untreated control in the virucidal assay (see section 3.3.1). Domiphen bromide is used as a quaternary ammonium disinfectant for sterilization in mouthwash, lozenges, and other products, so the apparent virucidal activity at high doses of this compound agrees with its current application[230]. Together, this information suggests that domiphen bromide may not be a good candidate as a novel antiviral, but if it is to be used for this purpose, toxicity and exposure time would need to be carefully monitored.

The unexpected results from the virucidal assay were the viral titer reductions seen in the presence of sodium aescinate, polyphyllin B, phloretin, and oridonin (see section 3.3.1). These compounds have little antiviral potential data known about them for any virus, but they showed promisingly low toxicity and high reduction of IAV titers when used at a much lower concentration. The virucidal potential of high concentrations was taken into consideration when framing later experiments for those compounds including sodium aescinate and oridonin, which remained of interest for further study.

To address the question of which viral replication stage the compounds of interest may be affecting, I performed a time of addition assay, which has previously been used for this purpose with other viruses[124,125,199]. Having used this experiment for several compounds during this dissertation project, I noted that it worked best for identifying entry inhibitors. Because this is a living system, discerning differences between all of the interactions that occur after entry but before exit is complex, and many stages of viral infection occur asynchronously because of the kinetic movement of viral particles. For example, the speed and ease at which virions travel through the medium, reach the host cells, and begin the attachment and entry process occurs at a different rate for each virion. This particular effect was minimized by incubating the cells on ice with the virus first, to allow distribution of the virus and localization to the host cell prior to beginning the infection at t=0. Differing viral kinetics does not take merit away from time of addition assays, which are useful for narrowing down what portion of the life cycle to try targeting first. But, when effects are seen throughout all time points of addition or in the midst of the time points selected, it can be difficult to draw a clear conclusion because of this overlap of different infection cycle stages. As well, after the first 8 hours of infection, it becomes difficult to interpret the effect of antiviral addition at a certain time point due to novel progeny virus presence. In short, I found that this approach was not ideal for identification of antivirals beyond entry inhibitors, and that the 1 MOI experiment was better at accurately identifying entry inhibitors than 0.001 MOI experiment, based on downstream results (see section 3.3.2 and 8.2). It could be that those compounds with reduced viral titers compared to the untreated, infected control only at later time points of addition (e.g., 2 hpi or later) are having an effect later in the infection cycle, but generation of novel viral proteins and progeny virus, the half-life of the proposed antivirals, and other factors cloud these results and complicate result interpretation.

Entry inhibitors are a clear target for further study for a number of reasons. Preventing the virus from entering the cell is an admirable goal of any novel antiviral because it would stop the infection before it begins. By narrowing down the search to entry inhibitors, I was able to further examine how the proposed antivirals may be binding to the virions, preventing entry by blocking attachment or penetration, forming a fundamental and essential part of the foundation research required for investigation of novel antiviral compounds.

IFAs were performed with several of the compounds of interest in this section of the dissertation, aimed at visualizing the infection process in real time, rather than relying on supernatant quantifications at specific points of infection. In addition to virus-infected and uninfected cellular controls, I ran a set of fluorescence controls for this and subsequent IFA experiments. By running single-fluorescent-dye-containing controls, then scanning each coverslip with all fluorescent channels being used, non-specific background staining was removed from the final images using the unmixing function in the free Zen 2009 Light Edition software (Zeiss). All IFA images shown in this dissertation have been processed in this manner in addition to having contrast adjustments made to the final images. Some of the compounds such as sodium aescinate that were most effective at reducing viral titers in past assays showed HA fluorescence by the end of the experiment. However, these two methods (analyzing live, replicating virus compared to fluorescently labeling viral proteins) are looking at very different aspects of an infection. This will be discussed in greater depth in section 4.6.

Phloretin, polyphyllin B, and 12-O-tetradecanoylphorbol-13-acetate were used at a concentration that was identified as toxic via XTT cytotoxicity assay during initial screening for those assays that utilized a dose of $10IC_{95}$ of compound. These compounds were only non-toxic at the lowest dose tested (3.9 μM) and resulted in a $10IC_{95}$ values above this concentration. All

three compounds were carried forward to the next stage to determine if the apparent toxicity remained when tested in other cell lines, which it did for 12-O-tetracanoylphorbol-13-acetate, eliminating this candidate from future study. Both phloretin and polyphyllin B showed a virucidal effect identified by viral titer reduction, but phloretin addition resulted in an intact monolayer at the end of the time period via IFA, despite high levels of HA fluorescence. The results of the XTT, virucidal, and IFA data together suggest that 110 µM ($10IC_{95}$) of polyphyllin B may have been too high a dose for this application, and 101 µM ($10IC_{95}$) of phloretin may still be useful but somewhat toxic in the cell lines used. The combination of results from these different assay measurements demonstrates the importance of utilizing a variety of assays that measure different viral parameters, as each approach has limitations. For example, the XTT cytotoxicity assay identified phloretin as toxic, but this dose did not destroy the monolayer, as observed in the IFA experiment. The cells may have been metabolically active but unable to digest the XTT salt in the medium, or the cells in the IFA-observed monolayer may have been dead and attached. In addition, metabolic activity is one of many factors that can indicate toxicity. Understanding how compounds are affecting a cell monolayer and virus interaction during infection requires a multifaceted approach using different quantification techniques.

As for the other compounds tested, other potential mechanisms may be occurring beyond entry inhibition. Phloretin, solamargine, mulberroside A, and polyphyllin B appear to affect a later stage of the IAV life cycle, such as transcription/translation or egress. While these compounds were not further tested during this project, they remain highly interesting candidates for future IAV antiviral application, as they were highly effective at reducing overall virus titers *in vitro*.

The identification of oridonin and sodium aescinate as potential IAV entry inhibitors in the time of addition assay, but with an apparent virucidal effect identified in the virucidal assay, may be explained by the design of the virucidal assay. By diluting the high amount of compound and virus previously incubated together for 2 h, if a compound is acting as an entry inhibitor by blocking the surface of the virus, it would appear as a virucidal compound in this assay due to the inability to form an attachment between the host cell and the virus. It may be that the action of oridonin, for example, involves blocking attachment by binding the surface of the virus, disallowing entry into the host cell, making them appear virucidal in this assay. The concentration of residual compound present in the flask after a 1:50 dilution would not fully inhibit IAV replication, based on past experimental results. For that reason, residual compound is not considered problematic in the virucidal assay, as complete inhibition of CPE and plaques were sought.

This dissertation work applied an approach of antiviral discovery by seeking out compounds that directly acted on viral proteins, rather than host cell proteins. Some studies undertake antiviral discovery by inhibiting cellular pathways which are also important for viral replication, rather than targeting viral proteins, for example, looking at host cell proteomic analysis, but this dissertation project instead aimed to discover novel IAV antivirals that blocked host interactions with the virus[231]. Additionally, the screening process was performed with compounds that had some known effects on various diseases. Taken together, although some of the compounds in the library are known to affect specific host cellular pathways, the screening results suggest that some of these compounds may also interact with viral proteins directly or indirectly, potentially inhibiting viral replication and enabling opportunities for drug repurposing., rather than compounds that had interactions with host proteins, or compounds that

had widespread destructive effects (like virucidal compounds). The benefit of this process is that many of the compounds were already FDA-approved, some of the compounds had at least one previously documented and known mechanism of action, and some had already undergone safety testing. The hindrance is that antiviral resistance may be more likely with the identified compounds because the discovery pipeline identified compounds that targeted a specific viral protein of interest.

While this approach provided a focused strategy for identifying antivirals that act directly on viral proteins, especially those with known safety profiles and mechanisms of action, it also introduced certain limitations. Among these is the fact that the strategy does not account for the complex interplay between the virus and host immune responses. Understanding how the host responds to influenza virus infection is critical, particularly when evaluating the broader therapeutic implications of candidate antivirals. When studying the efficacy of novel antivirals against IAV, focusing exclusively on viral components such as viral titers, replication kinetics, and protein expression offers valuable insights into direct antiviral activity. However, omitting the host response from such investigations can limit the interpretation and translational potential of the findings. The host immune response plays a central role in shaping the outcome of IAV infection and can profoundly influence the effectiveness of antiviral agents. For instance, certain antivirals may not only reduce viral replication but also modulate host pathways such as interferon signaling, inflammation, or apoptosis[232]. Without evaluating these host responses, potentially important mechanisms of action or side effects may be missed, which could lead to misinterpretation of a drug's full therapeutic potential or safety.

The host response to IAV is multifaceted, involving both innate and adaptive immune mechanisms. Early in infection, host cells recognize viral components through pattern

recognition receptors, triggering the production of proinflammatory cytokines[232]. These responses are crucial for limiting viral spread and activating downstream immune defenses. However, excessive or dysregulated host responses can lead to immunopathology, contributing to disease severity rather than protection[233]. Antiviral compounds may influence these pathways, either beneficially by tempering hyperinflammation or detrimentally by interfering with protective immunity. Thus, antiviral testing that does not assess the host's molecular and cellular responses may overlook key aspects of drug action or fail to predict *in vivo* outcomes accurately.

To more comprehensively assess the host response during antiviral testing, several methodologies could be employed. Proteomics, transcriptomics, and metabolomics provide broad views of cellular changes induced by infection and treatment[234]. Specifically, proteomic analyses can identify changes in host protein expression or post-translational modifications that occur during infection or in response to antiviral compounds. Transcriptomic profiling allows for the evaluation of immune gene expression, including interferon-stimulated genes, cytokines, and chemokines, which are crucial indicators of host antiviral activity and inflammation.

Thus, while plaque assays, qRT-PCR, and visualization of viral proteins are essential for understanding direct antiviral effects, they provide only a partial view of the complex virus-host interaction landscape. Incorporating analyses of the host response through modern -omics technologies and immunological assays can significantly enhance our understanding of antiviral efficacy, host protection, and potential adverse effects. Given that the ultimate goal of novel antivirals is to reduce pathogenesis rather than viral titers, these types of assays provide essential information beyond viral titer quantification reduction, which may or may not directly translate to reduced morbidity and mortality. As the field of antiviral development continues to evolve,

integrating host-directed data is increasingly recognized as essential for developing therapeutics with improved efficacy and safety profiles.

4.5: Oridonin and dioscin inhibit IAV attachment, while sodium aescinate and calycosin-7-glucoside inhibit IAV penetration

Past results suggested that sodium aescinate, calycosin-7-glucoside, oridonin, kinetin and dioscin may be having an impact early in the infectious cycle (i.e., attachment, penetration). Given that influenza virus attachment and entry occur in several steps beginning with the influenza HA surface protein binding to the sialic acid receptors on the surface of the host cell, I performed hemagglutination inhibition assays, attachment blockades, penetration blockades, and IFA staining to further delineate the effects of the novel proposed IAV entry inhibitors[235]. While hemagglutination inhibition assays have previously been applied primarily to antibody experiments, they are a functional way to determine the impact of any inhibitory substance on binding of surface receptors on RBCs[236,237]. Attachment and penetration blockades have previously been designed and tested for many viruses, including influenza, to determine which of these two stages of entry an inhibitory substance is potentially affecting[125].

The HAI assay requires many HA molecules on the surface of the IAV virus particles and many sialic acid receptors present on the surface of each of the RBC. Hemagglutination assays and hemagglutination inhibition assays are well-characterized assays that have long been used in diagnostic, clinical, and research settings to answer questions about IAV attachment and related antibody/antiviral mechanisms. This experiment clarifies whether attachment between the viral

HA and host cell sialic acid (as occurs during IAV infections) is impacted by the presence of the compound.

The presence of oridonin and dioscin was able to stop IAV virions from binding to the RBCs, even at a low concentration (195 and 98 nm, respectively), indicating an inhibitory interaction with the attachment process between the viral HA and sialic acid receptors of the RBCs (see section 3.4.1). The attachment blockade, in which the experimental compounds were only present during the attachment stage of infection, also suggested that these compounds are having an effect on attachment (see section 3.4.2). In comparison, sodium aescinate and calycosin-7-glucoside did not impact the ability of the viral HA to bind to the RBC sialic acid receptors, but showed an impact during the penetration blockade if they were only present during this step of infection (see section 3.4.1 and section 3.4.2). These experiments complement each other and provide strong evidence for the IAV attachment inhibition mechanism of oridonin and dioscin, and the IAV penetration inhibition mechanism of sodium aescinate and calycosin-7-glucoside.

The HAI assay also tested a higher dose of virus than previous experiments against these proposed novel antivirals, amounting to approximately $1.5x10^6$ $TCID_{50}$/mL of virus added to each well (taking 1 HA unit per well into account, given a 1:4 dilution of 4 HA units of virus in the final experiment). This indicates that the compounds of interest are active against a very high amount of seasonal IAV, providing further evidence for their effectiveness and potential as novel antivirals.

Together these results not only confirmed what previous experiments showed, which is that these compounds may be acting early in the IAV infectious cycle, but suggested more specifically that oridonin and dioscin appear to inhibit attachment, while sodium aescinate and

calycosin-7-glucoside inhibit penetration. These experiments provided another clue as to the mode of action for sodium aescinate, calycosin-7-glucoside, oridonin, and dioscin, which remain the top novel seasonal IAV entry inhibitors candidates identified in this project.

Given that the assays show blockage of attachment or penetration processes specifically of IAV, it is important to note that attachment of influenza may be negatively impacted by small molecules like these compounds in several different ways. Some compounds interfere with the amino acid residues or quaternery structures of hemagglutinin, preventing binding to the sialic acid receptor[238239]. Ultimately, preventing HA-sialic acid interactions is made more difficult because of the structure of the small, shallow sialic acid-binding pocket of HA[240]. Oridonin and dioscin may be blocking IAV entry by accumulating on the viral surface, binding to HA, preventing sialiac acid binding, or interfering with the binding pocket using a different mechanism.

Attachment inhibiting compounds will be defined in this dissertation as compounds that block the attachment of IAV to the sialic acid receptor of the host cell. Penetration blocking compounds will be defined in this dissertation as compounds that block the steps between attachment and fusion, entailing any blockade of entry into an endosome. Amantadine, for example, is well known for its ability to interfere with the M2 ion channel, required for viral uncoating once inside the endosome. Some other compounds have been noted as endosome acidification blocking compounds, which also effectively stops fusion from occurring, thus acting as a penetration blocking compound, according to the definition of penetration stated above[241]. The currently available, FDA-approved drugs for IAV are all either NA inhibitors (blocking viral exit), or polymerase inhibitors (blocking replication). Further mechanism of

action investigation of sodium aescinate, calycosin-7-glucoside, oridonin, and dioscin, which were identified as potential entry inhibitors, is a viable future direction for this project.

4.6: Understanding the differential results between virus quantification and IFA imagery

Attachment IFAs provided further viral protein load detail at higher magnification that previous IFAs performed, but failed to show specific membrane-virus interactions (see section 3.4.3). The IFAs showed less viral HA fluorescence intensity when the proposed entry inhibiting compounds were present during infection, and the morphology of the MDCK cells at the end of the experiment was slightly compacted but otherwise morphologically intact, compared to the virus-infected host cells which had lifted from the monolayer, indicating cell death.

The initial and attachment IFA results at first seem to contradict the findings of other *in vitro* experiments in the dissertation because there appears to be viral protein presence in experiments performed with the proposed attachment and penetration inhibitors. But, there is a substantial difference in what these assays quantified or showed via fluorescence. Partially formed, generated virus proteins, and defective virions (semi-infectious or non-infectious particles) would all be identified by fluorescence in IFAs, but not quantified in past experiments, which only quantified live, replicating virus.

The IFA results may be further explained by a phenomenon called the virus particle to PFU ratio. There are a number of situations during infection and replication that result in non-infectious viral particles[242]. Defective interfering particles are incomplete influenza particles that are unable to replicate independently due to lack of a complete genome, mutations, or other fundamental problems. These genomic deletions generate more detective interfering particles

when they co-infect with live, replication-competent IAV[242,243]. Conversely, semi-infectious particles are viral particles that have failed to contain one or more genomic segments essential for replication of infectious progeny[244]. When semi-infectious particles co-infect with another semi-infectious but replication-competent or fully competent IAV, the competent virus can supplement missing genomic segments for the non-infectious particles, generating replication-competent IAV, the same result as would be seen with an infectious particle alone. Co-infections with semi-infectious particles can thus result in IAV infections that produce the same result as fully infectious virus. The particle to PFU ratio refers to the presence of defective interfering particles or semi-infectious particles compared to infectious PFU-quantifiable (i.e., live) virus present during infection. In general, studies have shown that an estimated 90% or more of the particles in an IAV population are non-infectious[244].

The discrepancy between the presence of viral HA fluorescence in IFA and the absence of infectious virus in prior $TCID_{50}$ assays raises questions about the nature of the viral material being detected. One potential explanation is that background signal or incomplete entry could contribute to this observation, especially in the absence of Z-stack imaging or stringent controls to confirm intracellular localization of viral proteins. Additional controls and replicate experiments are necessary to rule out such possibilities.

That said, if further validation confirms that viral proteins are indeed being expressed within host cells despite an absence of infectious progeny, one possible hypothesis is that these compounds (particularly sodium aescinate, calycosin-7-glucoside, oridonin, and dioscin) may have dual effects. While they may function primarily as entry inhibitors, they could also interfere with downstream replication processes, such as RNA synthesis, assembly, or packaging, leading to the generation of non-infectious viral particles. Importantly, this is not to suggest that the

compounds are causing widespread or virus-specific mutagenesis, but rather that more nuanced disruptions in the replication cycle could be contributing to the observed phenotype. These possibilities remain speculative and would require further mechanistic investigation beyond the current scope of this work.

In the case of infectious virus (which may have been present in addition to non-infectious particles), results from the HAI assay and virus blockades suggest that the four identified entry inhibitors interfere with either the attachment or penetration steps of IAV infection. While the IFA experiments showed HA signal, they did not provide clear evidence of colocalization between viral HA and the MDCK cell membrane, due to limitations in imaging resolution and the absence of Z-stacking. Therefore, no definitive conclusion can be drawn from these images regarding whether the virus was attached to the cell surface or internalized.

However, based on reductions in quantifiable virus observed in the virucidal assay with oridonin and dioscin, it is plausible that these compounds may bind directly to the HA protein, thereby blocking entry. Sodium aescinate and calycosin-7-glucoside appear to inhibit penetration (see section 3.4.2), and given the lack of evidence for surface-bound HA in the IFA, these compounds may act during the fusion process within the endosome. This could account for the diffuse HA signal observed in IFA and the entry-inhibitory effects noted in functional assays.

It is also important to note the differences in MOI used for the IFA experiments compared to other assays performed in this dissertation. The difference in MOIs used may be responsible for the differences in semi- or noninfectious virus production versus the infectious virus seen and quantified in other assays shown in this dissertation. It is important to note that the IFA experiments were performed at a higher MOI of 3, whereas prior infectivity assays used lower MOIs of 0.001. This difference in MOI may contribute to the apparent discrepancy

between detectable viral HA signal in IFA and the lack of quantifiable infectious virus in $TCID_{50}$ assays. At higher MOIs, IAV is known to produce a greater proportion of defective interfering particles, which can express viral proteins but are non-infectious. While the IFA does not distinguish between infectious and non-infectious particles, this increased proportion of non-infectious particles at high MOI may partially explain why HA signal was observed despite an absence of infectious virus in parallel assays. For all past experiments, 0.001 MOI is a standard amount of virus to use because IAV replicates very quickly and overtakes a cellular monolayer, destroying any subtle changes being observed. For the IFA experiments, however, an MOI of 3 was used to ensure that enough virus was present to make the effect visible using fluorescence. A consideration to make with MOIs is that the addition of one MOI of virus is added to the cells does not mean that exactly one virus particle comes into contact with exactly one host cell. It is an estimated measure, but the kinetics and dynamics of infection rely on many factors. The Poisson Distribution equation articulates this problem, mathematically calculating the chance of a specific phenomenon to occur in a given time. The equation for the Poisson Distribution is as follows:

$$P(k) = e^{-m}m^{k}/k!$$

In the above equation, P(k) is the fraction of cells infected by k number of virus particles, and m represents the MOI. A higher MOI is required for many experiments because, given an example in which one million cells are infected with an MOI of one, only 37% of the cells receive one virion, 37% of the cells are uninfected, and 26% are multiply infected. This means that a low MOI of 0.001 for experiments spanning several days in which multiple rounds of

replication are occurring is ideal as many of the cells are left uninfected in the first round of replication, allowing multiple rounds of replication to occur. A slower progression of infection enables detection of viral titer changes that fall within the sensitivity of the assay, allowing accurate detection of viral titers during infection. However, for experiments performed over a shorter time or requiring the majority of cells to be successfully infected at the time of initial infection, a higher MOI is needed. In the case of these experiments, an MOI of three means that approximately 95% of the cells are will become infected. As the goal of IFA experiments is visibility of viral fluorescence, a higher MOI is needed. The MOI of three used in IFA experiments might have increased the amount of semi- or noninfectious virus present, compared to the 0.001 MOI used for other assays in this dissertation. This difference may have exacerbated the effect of observed, but potentially non-infectious viral proteins visible in the IFA experiments.

For past assays using 0.001 MOI, there are several host cells per virion, which is useful for a longer time span. This would more accurately reflect a natural infection in which a few virions make their way to the site of infection and spread. In summary, there are many experimental considerations to make when choosing the appropriate MOI to use for specific applications.

The anti-HA, anti-NA, and anti-NP monoclonal antibodies used in the IFA experiments were commercially sourced and validated by the manufacturers for immunofluorescence applications. These antibodies had also been previously validated for IFA and western blot use by a former student in our research group, and have since been used successfully by multiple group members, providing further support for their reliability. In my experiments, untreated infected samples exhibited an increase in viral protein signal (most notably HA) by 6 to 8 hpi in

both standard IFA and confocal experiments (see Section 8.3 and Figure 15), which is consistent with expected viral protein expression kinetics.

However, in Figure 18A, HA signal appears to increase as early as 30 to 90 minutes post-infection in the untreated control, which contradicts established influenza A virus replication timelines, where *de novo* viral protein synthesis is not expected that early. Upon review, this signal may be due to background or experimental noise rather than true HA expression. While key controls were included in the study, such as untreated infected samples, more comprehensive replication of early time point mock-infected controls across all experimental conditions would have strengthened the interpretation of early HA signal. Therefore, although validated antibodies and basic controls were used, the absence of full imaging controls across all conditions and time points restricts the confidence with which early HA signal can be interpreted.

A final consideration is the relatively high compound concentration used in most of the experiments presented in this dissertation. Specifically, a dose equivalent to 10 times the IC_{95} determined in early yield assays was applied in key assays such as TOA and attachment and penetration blockade experiments. For example, in the case of teriflunomide, the IC_{95} was calculated to be 2.8899 μM, resulting in a 10 times IC_{95} dose of 28.899 μM. While this concentration corresponds to approximately 8.6×10^{13} molecules per well (calculated from 5 μL of compound at this concentration, using Avogadro's number), this absolute molecule count should not be interpreted as a direct comparison to the number of virions or viral proteins present.

Rather than focusing solely on molecule-to-target ratios, it is more appropriate to consider the pharmacodynamic principles of drug-target interactions, such as binding affinity (KD), association/dissociation kinetics, and target occupancy. The biological efficacy of a

compound depends not just on its abundance, but also on how tightly and how long it binds to its target. For compounds hypothesized to act directly on viral proteins such as HA, binding kinetics are crucial, particularly in the competitive context of cell-free virus or virus-cell interactions.

Furthermore, *in vitro* infections at low MOI (e.g., 0.001) may involve not only infectious particles but also a large excess of non-infectious and defective interfering (DI) particles, which still carry viral proteins like HA. Because estimates suggest that non-infectious particles can greatly outnumber infectious particles, assumptions based solely on infectious titers underestimate the total number of potential binding targets for a given compound. For instance, with each virion carrying an estimated ~500 HA molecules.

4.7: The challenge of translating *in vitro* study to an *in vivo* model

Sodium aescinate, calyclsin-7-glucoside, oridonin, and dioscin were tested in a murine model in the final stage of this dissertation project, addressing the third hypothesis of determining *in vivo* potential. The outcome of this experiment showed that this dosing strategy (including timing of dosage and the amount of compound administered in each dose) was not sufficient to protect against a lethal infection of HK68 in mice, indicating that this model likely requires adjustment (see section 3.5 and section 5.1).

While many compounds look promising in *in vitro* models, they can be ineffective when translated to *in vivo* models due to added biological complexity (for example, the *in vivo* half-life of the compounds or their ability reach the active site). I tested the performance of these compounds at a single concentration in a murine model. The experiment was designed using a multi-dose system of a high concentration of compound to show maximum potential. This setup

makes the assumption that the dose and delivery method are both effective in our model, which was made based on previous studies not performed with IAV. The ineffectiveness of the compounds in mice in this experimental setup does not necessarily mean that these compounds are ineffective against IAV. Treatment of seasonal IAV may require a higher dose of compound, different route of delivery, or different animal model. A sub-lethal dose may solve the problem of the speed of the infection outpacing the action of the proposed antiviral. Because of these caveats, the compounds of interested tested remain of relevant interest for further investigation as novel seasonal IAV antivirals.

While this *in vivo* study was not successful, the host immune responses to influenza that may contribute to the outcome are also important to consider. *In vivo* studies offer critical insights into the complex interplay between IAV and the host immune system that cannot be fully captured through *in vitro* assays alone. While *in vitro* models are valuable for dissecting direct virus-cell interactions, they often lack the multicellular environment, systemic signaling, and tissue-specific context present in a living organism. Host immune regulation, including cytokine signaling, immune cell recruitment, and tissue remodeling, plays a role in determining both viral clearance and disease pathology.

However, it is important to recognize that host responses extend beyond immune factors and include physiological processes that directly affect drug bioavailability, pharmacokinetics, and overall antiviral efficacy. These host responses, such as metabolic processes, enzymatic degradation, and organ-specific distribution, are critical in determining how a compound is absorbed, distributed, metabolized, and excreted in the body. For example, factors like hepatic metabolism, renal clearance, and protein binding can limit the availability of a compound at the site of infection, which would influence its therapeutic potential. The tissue-specific

environment, including pH, cellular composition, and local inflammation, can also affect a drug's stability and activity, which are difficult to predict from *in vitro* data alone.

Moreover, adaptive immune responses such as T cell-mediated cytotoxicity and B cell-driven antibody production are critical components of *in vivo* viral control and long-term immunity. The timing, magnitude, and specificity of these responses can influence disease trajectory and treatment outcomes. Ignoring these host components may lead to incomplete or misleading conclusions, particularly in the evaluation of immunomodulatory therapies or interventions that interact with host signaling pathways. For these reasons, taking the immune response and protective immunity into account when interpreting these data is essential to put together the full story of antiviral effectiveness and potential.

Another factor that must be taken into account and can only be done using *in vivo* studies are sex differences between males and females. A recent study demonstrated that female mice generate stronger and more protective immune responses following both infection and vaccination compared to males, driven by higher titers of neutralizing antibodies, enhanced B cell activity, and more robust memory T cell responses[84]. These responses are modulated by sex-specific factors such as differential expression of TLR7, which is regulated epigenetically and contributes to enhanced antibody class switching and avidity in females.

In the context of novel antiviral development, such sex-based immunological variability can have considerable implications. An antiviral that appears effective in reducing viral load *in vitro* might perform differently *in vivo*, depending on how it interacts with or modulates the host immune system. For instance, compounds that indirectly enhance or suppress immune pathways may confer variable protection or pathology in male and female hosts. Without *in vivo* studies

that capture these dynamics, especially in both sexes, there is a risk of overlooking differential efficacy or toxicity that could manifest in clinical populations.

4.8: Conclusions and contributions: Building on what was known

Sodium aescinate has been previously identified as a useful pharmaceutical agent for its anti-inflammatory, swelling reduction, and vasoactive properties[246]. It has been used to treat some inflammatory conditions such as cerebral edema, and while some cellular changes in the presence of sodium aescinate have been noted, the mechanism of action remains largely unknown[247]. Calycosin-7-glucoside is a traditional Chinese medicine that has been tested as a treatment for conditions such as heat stroke, viral myocarditis, and, Coxsackie Virus B3 infection, but had not been tested against IAV[248]. Like sodium aescinate, specifics of the mechanism of action of calycosin-7-glucoside remain unknown. Oridonin is another traditional Chinese medicine, historically used for alleviating pain, improving blood circulation, and treatment of pharyngitis, tonsillitis, and bronchitis[249]. It has been observed to inhibit cellular proliferation by inducing apoptosis by inactivating Akt and activating p53, a pro-apoptotic protein[249]. Dioscin can associate with many essential immune response pathways such as complement, inflammation, DNA replication/repair, cell cycle signaling, apoptosis, protein modification, and adaptive and innate immunity-mediated cytotoxicity[250]. Like oridonin, it appears to impact apoptosis induction and cell cycle arrest[251]. All of these compounds were untested against IAV at the time of this dissertation. The literature shows that many of these compounds have interactions with different cellular processes involved during infection including inflammatory or immune-related pathways.

Given the viral protein fluorescence present in the IFAs performed on compound-treated, infected cells, the presence of these proposed entry inhibitors may be resulting in the production of a high number of non-infectious particles, reducing infectivity of progeny viruses. The IFAs performed did not distinguish whether the virus was inside or outside of the host cell, and the attachment and penetration blockade suggested the compounds of interest were blocking these respective processes. A possible conclusion from this study is that entry of the virus into the host cell is being limited by these proposed entry inhibitors, which may be simultaneously negatively impacting the ability of IAV to produce infectious progeny.

Together, I have addressed my three initial hypotheses, which aimed to utilize existing compound libraries to identify novel antiviral candidates, further characterize those antivirals that appeared to be IAV entry inhibitors, and test their *in vivo* potential. The compound libraries were a highly effective means of identifying novel antiviral candidates, four compounds were ultimately identified and characterized as IAV attachment or penetration inhibitors, and these were tested in a murine model.

This dissertation also highlights the importance of having a multi-faceted project that examines the presence of both viral protein and live virus. The project demonstrates a set of established protocols used to study novel IAV antivirals from screening to characterization using a variety of *in vitro* techniques, culminating in an *in vivo* experiment. This was the first time our research group demonstrated a complete antiviral discovery and characterization pipeline from initial screening identification to *in vivo* testing. This experimental approach could be effectively applied to future pathogen antiviral discovery and characterization projects.

I recommend sodium aescinate, calycosin-7-glucoside, oridonin, and dioscin as novel IAV antivirals for further *in vitro* and *in vivo* study to address the current shortage of antiviral

options against IAV. Given that there are only a select few pharmaceuticals currently on the market for IAV, and none that are entry inhibitors, these four compounds represent a promising potential addition to the existing pool of therapeutic options. These proposed antivirals also possess no known resistance concerns for IAV, unlike many currently available therapeutic options. This dissertation represents the foundation of work required for novel antiviral characterization prior to mechanism of action studies and animal models, identifying four novel IAV antiviral candidates that are highly effective *in vitro*. In addition, the specific mechanism of action has yet to be identified for these four novel candidates, and may present an antiviral option that does not pose the same mutation-driven antiviral resistance threats as other antivirals current availably for IAV.

It is a race against time to ensure that we have the treatments that will be necessary not if, but when, the next IAV pandemic begins. Covid-19 is proof that these outbreaks can occur without warning, and the current H5N1 outbreak is yet another testiment to the fact that we are never without the threat of an impending respiratory virus outbreak. During the "100 years since Spanish Influenza" campaign in 2018, researchers globally attested to the fact that we are not adequately prepared for the next influenza pandemic. It has been seven years and one global pandemic since then, and yet the question remains. Are we ready for the next influenza pandemic?

Chapter Five: Limitations and Future Directions

5.1: Limitations

Only one concentration of the candidate compounds (100 μM) was used to screen the FDA-approved library of compounds. Two concentrations (10 μM and 100 μM) were used to screen the natural source library, an adjustment based on my observations during the first screen of FDA-approved compounds that 100 μM may have been high enough to induce toxicity, ruling out good candidates. Rescreening both libraries using various concentrations could prove advantageous for identifying additional candidates of interest.

While MDCK and A549 cells were both used for this dissertation project, a more relevant addition could have been primary lung epithelial cells or other less dedifferentiated cell lines, as they are more physiologically relevant to the target tissue for influenza infection compared to the commonly used cancer-derived A549 cells. Throughout the experiments in this dissertation, small samples sizes were utilized. Future studies would benefit from expanding the sample sizes from duplicate and triplicate to n=6 for greater statistical power and reproducibility. While biological duplicates or triplicates are generally sufficient, any variation between replicates suggests the need for assay optimization and additional controls to ensure consistent results. For assays that showed high variation, such as the initial yield assays, additional experiments should have been performed to verify the reliability of the data. In addition, a control of a monoclonal antibody or other entry inhibitor may prove advantageous, which was not utilized in these studies as no FDA-approved antiviral that blocks entry is currently available. However, adding an improved control beyond oseltamivir (which targets NA, and is thus an entry inhibitor), virus-infected, untreated, and untreated, uninfected cell controls would strengthen future results.

Effective compounds may have been prematurely eliminated due to the nature of the selection process. In future studies, a wider dose range for testing would be more ideal for yield assays (see Figure 7 and 9). Some compounds tested produced the ideal "S-curve", which is the best model for antiviral research, as it provides the most accurate analysis potential when run through software like GraphPad Prism. In addition, diluting the compounds designated as "N/D" in Table 10 to determine their activity would be a useful future direction. The yield assay also did not include a positive treated control, only infected, untreated, and uninfected, untreated controls. In the case of the R-1644 and VSV-MERS experiments, a different cell line was used. The literature was consulted for potential toxicity differences, but these studies were not undertaken during the dissertation project. These experiments were performed to determine whether any cross-protection between the experimental compounds existed between these distinct viruses and IAV, at the range determined to be effective in IAV, the primary virus of concern for this dissertation.

It is important to note the difficulty in determining whether a compound is antiviral or virucidal. Given that an antiviral has an effect on a stage of the infection cycle and a virucidal is structurally destructive, other means of determining whether compounds were virucidal, such as rtPCR or IFAs, for residual protein or gene expression at various stages of infection may have been beneficial in determining whether the compounds were virucidal or not. Because antiviral compounds inhibit virus replication while virucidal agents destroy or alter structures, measuring viral replication by western blot or other method is an alternative way to determine whether or not compounds are antiviral or virucidal. However, to more confidently identify a compound as virucidal, a follow-up assay using a different virus or even bacteria could have been performed. Virucidal agents typically act non-specifically on biological proteins, lipids, and nucleic acids,

meaning they can kill a broad range of pathogens, whereas antiviral compounds tend to target specific viral mechanisms. This additional assay would provide further clarity on whether the compound's effect is virucidal or antiviral.

The time of addition assays were used to narrow down the viral replication cycle stage being affected, and downstream decisions of which compounds to investigate further hinged on the outcome and interpretation of this preliminary work. The problem with this approach is that if the experimental approach was flawed (though published examples from the literature which also utilized influenza were followed), the wrong compounds may have been pursued. The time of addition assay may also have benefitted from treatment controls known to affect specific portions of the IAV infection cycle, to clarify effectiveness of the assay, which were not used for this dissertation.

A limitation of the IFA experimental design in this dissertation is that the cells were permeabilized, and thus fluorescence inside and outside of the host cell could not be differentiated. If the cells are not permeabilized, only surface-bound viral HA will be visible, making it possible to assess attachment inhibition based on a decrease in HA signal. However, if the compound does not significantly reduce surface attachment, it would be difficult to distinguish the effects of the drug from the no-drug control. This means that a compound can only be considered an attachment inhibitor if there is a noticeable reduction in the HA signal at the cell surface. When investigating potential entry inhibitors, it was important to be able to fluorescently stain both intracelllular and extracellular environments, but this approach limited the information that can be taken from these assays.

Another element that may need to be taken into account for many of the experiments in this dissertation is the half-life of the experimental compounds. I did not supplement additional

compound over the duration of experiments, which is particularly noteworthy for those assays that spanned several hours to days.

In the IFAs performed, there is some background staining from DAPI evidenced by a blue haze in some of the images. These procedures were repeated several times in an attempt to reduce background staining, and the unmixing function in the Zen Blue program was also used to reduce background across images. A drawback to using the method of IFA staining on a glass coverslip is that background staining can occur. In this procedure, Prolong Gold with DAPI is dropped onto a glass microscope slide, and the glass coverslip is placed cell-side-down onto the glass microscope slide. While the cells were fixed, in some cases, some cells may have ruptured or become crushed when the two glass panes were squeezed together prior to imaging. Background staining is more prevalent when using the coverslip method because it requires adding different fluorescent dyes and fixing directly on the coverslip on which the cells were grown, leading to some nonspecific dye binding.

In the attachment IFA images, DAPI shows the location of the nucleus with CellVue showing the membrane around the cell. A Z-stack was performed as well, but because MDCKs are so thin, this did not clarify the images. The confocal microscope used to attain the images could not slice the images thin enough for a Z-stack to obtain only a slice of an MDCK cell without capturing any of the top or bottom of the cell, showing the membrane. This meant that the dye is more diffuse across the MDCK cells than it would be in a neat Z-stack slice. Instead, light CellVue dye is detected throughout the cell, binding to the top and bottom cell membranes as the light from the microscope sees the full plane of the cell from bottom to top. However, the edges of the cell can still be seen in red in the resultant images.

A final limitation to the IFA work performed in this dissertation was that only the oseltamivir and virus-infected control were included. No entry inhibitors for influenza are currently FDA-approved for useage, but using a monoclonal antibody or other entry-blocking substance would have strengthened the results of these experiments. In addition, while I included binding control for HA and the membrane stain (containing cells and dye only), I only performed these for the second set of IFA experiments examining the first 90 minutes post-infection, and did not include these controls for other dyes and time points included in the first 24 hpi IFA study shown in the dissertation.

Compounds and cells were pre-incubated for 1-2 h prior to infection to provide ideal conditions for the compounds to reach the host cells and become fully disseminated in the medium prior to introduction of the virus. However, for the penetration blockade, a pre-incubation was not possible because of the design of the experiment (compound was only to be present during the penetration stage of the infection cycle). This may have affected the ultimate result of this assay, as the compound may not have had time to reach the virions prior to infection of the cells.

5.2: Future Directions

There are several branches of future work to be done on this project. The first is further characterizing the suspected entry inhibitors *in vitro*. While these compounds appear to be entry inhibitors, specifically how they interact with host cells in order to limit IAV infection and virus titers (i.e., the mechanism of action) remains unknown. Delving into an intra-organelle level of analysis would be the next stage of depth looking at how these compounds may be having an

effect on IAV. There are many other analyses such as western blots that could yield further information about how these compounds are limiting IAV infection that were not performed during this dissertation project, but would be excellent future directions to discern the potential mechanism of action of these compounds.

In addition, proteomic analyses of how the host cell is responding may identify some of the alterations being induced by the proposed antiviral. This could also help to identify the different host pathways that are directly affected by the presence of the compound. In comparison to the virus-infected but untreated control, it would also be useful to see the different proteomic changes at various stages of infection to gain a full understanding of the effect of these proposed antivirals.

Following up on the IFA work performed in this disseration could also be achieved using Pulse-Chase S^{35} labeling to reveal temporal shifts in translational activity, showing when host protein synthesis declines or when viral protein synthesis dominates. IFAs do not differentiate between newly synthesized and pre-existing proteins, nor do they provide kinetic data about translation, and these gaps could be filled with Pulse-Chase S^{35} experiments.

There are also a number of antiviral options proposed in section 3.3.2 that appear to have activity against other stages of seasonal IAV replication. For the study of all viruses used for cross-reactivity testing in this section, it would be useful to follow-up on some of the compounds that were not further examined, but were effective at reducing viral titers and maintained low toxicity.

Another way to screen novel antivirals for influenza could involve the use of a reporter-based system utilizing GFP expression. This method could help identify compounds that

interfere with various stages of the viral life cycle, not just HA-mediated membrane fusion. By using a virus expressing a reporter gene, such as GFP, successful viral entry and replication would trigger GFP expression, while compounds that block viral replication at any stage would suppress the reporter signal. This approach would provide a functional, high-throughput means of identifying inhibitors across different antiviral mechanisms, complementing traditional CPE and viral load assays, and may offer an advantage by being less prone to resistance. The murine experiment conducted in this dissertation leaves substantial room for improvement and further investigation. One of the key reasons for the limited success of these experiments is the use of a literature-based drug dosage, which was originally established in a different animal model and for a distinct application. The lack of an appropriate dose-response curve is an additional limitation, as the doses used may not have been effective in achieving a therapeutic effect in this particular model. It is crucial to acknowledge that drug dosing plays a pivotal role in antiviral effectiveness, and without thorough optimization, conclusions about the compound's efficacy cannot be drawn with confidence.

To improve the outcomes of future *in vivo* studies, several key factors must be considered. First, a comprehensive range of doses should be tested, ideally covering both lower and higher doses to determine the optimal concentration for antiviral activity. Dosing should also take into account factors such as the compound's bioavailability, half-life, and potential off-target effects that could influence the results. The current model's drug delivery method, the route of administration, and the timing of dosing could all be refined to maximize the drug's exposure to the target tissue, such as lungs, the respiratory tract, or other sites of infection. Additionally, assessing different dosing schedules, particularly for compounds with shorter half-lives, may be essential to ensure sustained antiviral activity throughout the course of infection.

Another consideration is the virus strain used for infection. The use of a lethal viral dose may have overwhelmed the compounds' effectiveness, especially if the dosage or timing was not optimized. Non-lethal viral doses should be tested to better understand the antiviral potential of the compounds under more controlled and measurable conditions. It is also important to consider whether the model itself is fully representative of the human disease context, as the murine model used may not capture all aspects of the virus-host interaction. Exploring alternative small mammal models or different viral strains, including those that more closely mimic human influenza, could provide more accurate insights into the compounds' efficacy.

Additionally, bioavailability and targeting to the site of activity must be carefully addressed in future experiments. Issues such as tissue-specific drug distribution and the ability of the compound to cross biological barriers (e.g., the blood-brain barrier or lung tissue) can drastically impact the success of antiviral treatments. The physical properties of the compounds, including their solubility, stability, and ability to reach the target site, must be taken into account during dosing and experimental design.

In conclusion, future *in vivo* studies will need to systematically address the limitations observed in the current experiments. By refining drug dosing, optimizing delivery routes, using appropriate viral doses, and selecting the most suitable animal models, a more robust understanding of these compounds' antiviral potential can be gained. Additionally, careful consideration of factors such as bioavailability, drug half-life, and drug targeting to the infection site will be essential for improving the likelihood of successful outcomes in future antiviral studies.

Chapter Six: References

1. Palese P, Shaw ML. (2007). Orthomyxoviridae. In Fields Virology (5th ed., pp. 1647-1691). Lippincott Williams & Wilkins.
2. Hause BM, Collin EA, Liu R, *et al*. Characterization of a novel influenza virus in cattle and swine: Proposal for a new genus in the Orthomyxoviridae family. *mBio*. 2014;5(2). doi:10.1128/mBio.00031-14
3. Jang YH, Seong BL. Options and obstacles for designing a universal influenza vaccine. *Viruses*. 2014;6(8):3159-3180. doi:10.3390/v6083159
4. Webster RG, Bean WJ, Gorman OT, *et al*. Evolution and ecology of influenza A viruses. *Microbiol Rev.* 1992 Mar;56(1):152-79. doi: 10.1128/mr.56.1.152-179.1992
5. Tong S, Zhu X, Li Y, *et al*. New world bats harbor diverse influenza A viruses. *PLoS Pathog*. 2013;9(10). doi:10.1371/journal.ppat.1003657
6. Tong S, Li Y, Rivailler P, *et al*. A distinct lineage of influenza A virus from bats. *Proc Natl Acad Sci U S A*. 2012;109(11):4269-4274. doi:10.1073/pnas.1116200109
7. Bouvier NM, Palese P. The biology of influenza viruses. *Vaccine*. 2008;26(4):D49-D53. doi:10.1002/ejoc.201701499
8. Trifkovic S, Gilbertson B, Fairmaid E, *et al*. Gene segment interactions can drive the emergence of dominant yet suboptimal gene constellations during influenza virus reassortment. *Front Microbiol*. 2021;12. doi:10.3389/fmicb.2021.683152
9. Lamb RA, Lai CJ, Choppin PW. Sequences of mRNAs derived from genome RNA segment 7 of influenza virus: Colinear and interrupted mRNAs code for overlapping proteins. *Proc Natl Acad Sci U S A.* 1981 Jul;78(7):4170-4. doi: 10.1073/pnas.78.7.4170
10. O'neill RE, Talon J, Palese P. The influenza virus NEP (NS2 protein) mediates the nuclear export of viral ribonucleoproteins. *EMBO J*. 1998;17(1):288-96. doi: 10.1093/emboj/17.1.288
11. Chen W Calvo PA, Malide D, *et al*. A novel influenza A virus mitochondrial protein that induces cell death. *Nat Med*. 2001;7:1306-1312. doi: 10.1038/nm1201-1306
12. Wise HM, Foeglein A, Sun J, *et al*. A complicated message: Identification of a novel PB1-related protein translated from influenza A virus segment 2 mRNA. *J Virol*. 2009;83(16):8021-8031. doi:10.1128/jvi.00826-09
13. Jagger B, Wise H, Kash J, *et al*. An overlapping protein-coding region in influenza A virus segment 3 modules the host response. *Science (1979)*. 2012;337(6091):199-204. doi:10.1126/science.1219723
14. Kuchipudi S V., Nissly RH. Novel flu viruses in bats and cattle: "Pushing the envelope" of influenza infection. *Vet Sci*. 2018;5(3):1-10. doi:10.3390/vetsci5030071
15. Sreenivasan CC, Thomas M, Kaushik RS, *et al*. Influenza A in bovine species: A narrative literature review. *Viruses*. 2019;11(6). doi:10.3390/v11060561
16. Ferhadian D, Contrant M, Printz-Schweigert A, *et al*. Structural and functional motifs in influenza virus RNAs. *Front Microbiol*. 2018;9:1-11. doi:10.3389/fmicb.2018.00559
17. Honda A, Mizumoto K, Ishihama A. Minimum molecular architectures for transcription and replication of the influenza virus. *PNAS*. 2002;99(20):13166-13171. doi https://doi.org/10.1073/pnas.152456799
18. Webster R. *Textbook of Influenza*. 2nd ed. West Sussex, UK: Wiley-Blackwell; 2013.
19. Neumann G, Ozawa M, Kawaoka Y. Reverse genetics of influenza viruses. *Methods Mol Biol.* 2012;865:193-206. doi: 10.1007/978-1-61779-621-0_12

20. Nobusawa E, Sato K. Comparison of the mutation rates of human influenza A and B viruses. *J Virol*. 2006;80(7):3675-3678. doi:10.1128/jvi.80.7.3675-3678.2006
21. Badham MD, Rossman JS. Filamentous Influenza Viruses. *Curr Clin Microbiol Rep*. 2016;3(3):155-161. doi:10.1007/s40588-016-0041-7
22. Veit M, Thaa B. Association of influenza virus proteins with membrane rafts. *Adv Virol.* 2011;2011:370606. doi: 10.1155/2011/370606
23. Connor R, Kawaoka Y, Webster RG, *et al*. Receptor specificity in human, avian, and equine H2 and H3 influenza virus isolates. *Virology.* 1994;205(1):17-23. doi: 10.1006/viro.1994.1615
24. Nelli RK, Kuchipudhi SV, White GA, *et al.* Comparative distribution of human and avian type sialic acid influenza receptors in the pig. *BMC Vet Res*. 2010;6(4). doi:10.1186/1746-6148-6-4
25. Sriwilaijaroen N, Suzuki Y. Molecular basis of the structure and function of H1 hemagglutinin of influenza virus. *Proc Jpn Acad Ser B Phys Biol Sci*. 2012;88(6):226-249. doi:10.2183/pjab.88.226
26. Lofano G, Kumar A, Finco O, *et al*. B cells and functional antibody responses to combat influenza. *Front Immunol*. 2015;6:336. doi:10.3389/fimmu.2015.00336
27. Skehel JJ, Waterfield MD. Studies on the primary structure of the influenza virus hemagglutinin. *Proc Natl Acad Sci U S A.* 1975;72(1):93-7. doi: 10.1073/pnas.72.1.93
28. Lakadamyali M, Rust MJ, Zhuang X. Endocytosis of influenza viruses. *Microbes Infect*. 2004;6(10):929-936. doi:10.1038/jid.2014.371
29. Sieczkarski SB, Whittaker GR. Influenza virus can enter and infect cells in the absence of clathrin-mediated endocytosis. *J Virol*. 2002;76(20):10455-10464. doi:10.1128/jvi.76.20.10455-10464.2002
30. de Vries E, Tscherne DM, Wienholts MJ, *et al*. Dissection of the influenza a virus endocytic routes reveals macropinocytosis as an alternative entry pathway. *PLoS Pathog*. 2011;7(3). doi:10.1371/journal.ppat.1001329
31. Hay AJ, Lomniczi B, Bellamy AR, *et al*. Transcription of the influenza virus genome. *Virology.* 1977;83(2):337-55. doi: 10.1016/0042-6822(77)90179-9
32. Cros JF, García-Sastre A, Palese P, *et al*. An unconventional NLS is critical for the nuclear import of the influenza A virus nucleoprotein and ribonucleoprotein. *Traffic*. 2005;6:205-213. doi:10.1111/j.1600-0854.2004.00263
33. Koppstein D, Ashour J, Bartel DP. Sequencing the cap-snatching repertoire of H1N1 influenza provides insight into the mechanism of viral transcription initiation. *Nucleic Acids Res*. 2015;43(10):5052-5064. doi:10.1093/nar/gkv333
34. Reich S, Guilligay D, Pflug A, *et al.* Structural insight into cap-snatching and RNA synthesis by influenza polymerase. *Nature*. 2014;516(7531):361-366. doi:10.1038/nature14009
35. Luo G, Luytjes W, Enami M, *et al*. The polyadenylation signal of influenza virus RNA involves a stretch of uridines followed by the RNA duplex of the panhandle structure. *J Virol.* 1991;65(6):2861-7. doi: 10.1128/JVI.65.6.2861-2867.1991
36. Nayak DP, Hui EK, Barman S. Assembly and budding of influenza virus. *Virus Res.* 2004;106(2):147-65. doi: 10.1016/j.virusres.2004.08.012
37. Eisfeld AJ, Kawakami E, Watanabe T, *et al*. RAB11A Is essential for transport of the influenza virus genome to the plasma membrane. *J Virol*. 2011;85(13):6117-6126. doi:10.1128/jvi.00378-11

38. Kim P, Jang YH, Kwon S Bin, *et al*. Glycosylation of hemagglutinin and neuraminidase of influenza a virus as signature for ecological spillover and adaptation among influenza reservoirs. *Viruses*. 2018;10(4):1-18. doi:10.3390/v10040183
39. Veit M, Serebryakova M V., Kordyukova L V. Palmitoylation of influenza virus proteins. *Biochem Soc Trans*. 2013;41(1):50-55. doi:10.1042/BST20120210
40. Brown DA, Rose JK. Sorting of GPI-anchored proteins to glycolipid-enriched membrane subdomains during transport to the apical cell surface. *Cell*. 1992 Feb 7;68(3):533-44. doi: 10.1016/0092-8674(92)90189-j.
41. Rossman JS, Jing X, Leser GP, *et al*. Influenza virus M2 protein mediates ESCRT-independent membrane scission. *Cell*. 2010;142(6):902-913. doi:10.1016/jcell.2010.08.029
42. Iwatsuki-Horimoto K, Horimoto T, Noda T, *et al*. The cytoplasmic tail of the influenza A virus M2 protein plays a role in viral assembly. *J Virol*. 2006;80(11):5233-5240. doi:10.1128/jvi.00049-06
43. Rossman JS, Jing X, Leser GP, *et al*. Influenza virus M2 protein mediates ESCRT-independent membrane scission. *Cell*. 2010;142(6):902-913. doi:10.1038/jid.2014.371
44. Bouvier NM, Lowen AC. Animal models for influenza virus pathogenesis and transmission. *Viruses*. 2010;2(8):1530-1563. doi:10.3390/v20801530
45. Groves HT, McDonald JU, Langat P, *et al*. Mouse models of influenza infection with circulating strains to test seasonal vaccine efficacy. *Front Immunol*. 2018;9:1-11. doi:10.3389/fimmu.2018.00126
46. Enkirch T, von Messling V. Ferret models of viral pathogenesis. *Virology*. 2015;479-480:259-270. doi:10.1016/j.virol.2015.03.017
47. Lowen AC, Mubareka S, Tumpey TM, *et al*. The guinea pig as a transmission model for human influenza viruses. *Proc Natl Acad Sci U S A*. 2006;103(26):9988-92. doi: 10.1073/pnas.0604157103
48. Wantanabe T, Kawaoka Y. Pathogenesis of the 1918 pandemic influenza virus. *PLoS Pathog.* 2011;7(1):e1001218. doi: 10.1371/journal.ppat.1001218
49. Reid AH, Taubenberger JK, Fanning TG. The 1918 Spanish influenza: Integrating history and biology. *Microbes Infect*. 2001;3(1):81-87. doi:10.1016/S1286-4579(00)01351-4
50. Easterbrook JD, Kash JC, Sheng ZM, *et al*. Immunization with 1976 swine H1N1- or 2009 pandemic H1N1-inactivated vaccines protects mice from a lethal 1918 influenza infection. *Influenza Other Respir Viruses*. 2011;5(3):198-205. doi:10.1111/j.1750-2659.2010.00191.x
51. Pillet S, Kobasa D, Meunier I, *et al*. Cellular immune response in the presence of protective antibody levels correlates with protection against 1918 influenza in ferrets. *Vaccine*. 2011;29(39):6793-6801. doi:10.1016/j.vaccine.2010.12.059
52. Brown JN, Palermo RE, Baskin CR, *et al.* Macaque proteome response to highly pathogenic avian influenza and 1918 reassortant influenza virus infections. *J Virol*. 2010;84(22):12058-12068. doi:10.1128/jvi.01129-10
53. Kash JC, Tumpey TM, Proll SC, *et al*. Responses Induced By 1918 Influenza Virus. *Nature*. 2006;443:578-581. doi:10.1038/nature05181
54. Kobasa D, Jones SM, Shinya K, *et al.* Aberrant innate immune response in lethal infection of macaques with the 1918 influenza virus. *Nature*. 2007;445(7125):319-323. doi:10.1038/nature05495

55. Memoli MJ, Tumpey TM, Jagger BW, *et al*. Pathogenicity to the 1918 pandemic virus in ferrets and mice. *Virology*. 2009;393(2):338-345. doi:10.1016/j.virol.2009.08.021
56. Scholtissek C, Rohde W, Von Hoyningen V, *et al*. On the origin of the human influenza virus subtypes H2N2 and H3N2. *Virology*. 1978;87(1):13-20. doi: 10.1016/0042-6822(78)90153-8
57. Viboud C, Simonsen L, Fuentes R, *et al*. Global mortality impact of the 1957-1959 influenza pandemic. *J Infect Dis*. 2016;213(5):738-45. doi: 10.1093/infdis/jiv534
58. Gagnon A, Acosta E, Hallman S, *et al*. Pandemic paradox: Early life H2N2 pandemic influenza infection enhanced susceptibility to death during the 2009 H1N1 pandemic. *mBio*. 2018;9(1):1-15. doi:10.1128/mBio.02091-17
59. Honigsbaum M. Revisiting the 1957 and 1968 influenza pandemics. *The Lancet*. 2020;395(10240):1824-1826. doi:10.1016/S0140-6736(20)31201-0
60. Van Poucke S, Doedt J, Baumann J, *et al*. Role of substitutions in the hemagglutinin in the emergence of the 1968 pandemic influenza virus. *J Virol*. 2015;89(23):12211-12216. doi:10.1128/jvi.01292-15
61. Kawaoka Y, Krauss S, Webster RG. Avian-to-human transmission of the PB1 gene of influenza A viruses in the 1957 and 1968 pandemics. *J Virol*. 1989;63(11):4603-4608. doi:10.1128/jvi.63.11.4603-4608.1989
62. Wendel I, Rubbenstroth D, Doedt J, *et al*. The avian-origin PB1 gene segment facilitated replication and transmissibility of the H3N2/1968 pandemic influenza virus. *J Virol*. 2015;89(8):4170-4179. doi:10.1128/jvi.03194-14
63. Viboud C, Grais RF, Lafont BAP, *et al*. Multinational impact of the 1968 Hong Kong influenza pandemic: Evidence for a smoldering pandemic. *J Infect Dis.* 2005;192(2):233-248. doi:10.1086/431150
64. Nakajima K, Desselberger U, Palese P. Recent human influenza A (H1N1) viruses are closely related genetically to strains isolated in 1950. *Nature.* 1978;274(5669):334-9. doi: 10.1038/274334a0
65. Rozo M, Gronvall GK. The reemergent 1977 H1N1 strain and the gain-of-function debate. *mBio*. 2015;6(4):1-6. doi:10.1128/mBio.01013-15
66. Doshi P. Trends in recorded influenza mortality: United States, 1900-2004. *Am J Public Health*. 2008;98(5):939-945. doi:10.2105/AJPH.2007.119933
67. Girard MP, Tam JS, Assossou OM, *et al*. The 2009 A (H1N1) influenza virus pandemic: A review. *Vaccine*. 2010;28(31):4895-4902. doi:10.1016/j.vaccine.2010.05.031
68. Smith GJD, Vijaykrishna D, Bahl J, *et al.* Origins and evolutionary genomics of the 2009 swine-origin H1N1 influenza A epidemic. *Nature*. 2009;459(7250):1122-1125. doi:10.1038/nature08182
69. Dawood FS, Iuliano AD, Reed C, *et al*. Estimated global mortality associated with the first 12 months of 2009 pandemic influenza A H1N1 virus circulation: A modelling study. *Lancet Infect Dis*. 2012;12(9):687-695. doi:10.1016/S1473-3099(12)70121-4
70. Webster RG, Laver WG, Air GM, *et al*. Molecular mechanisms of variation in influenza viruses. *Nature.* 1982;296(5853):115-21. doi: 10.1038/296115a0.
71. Kawaoka Y, Krauss S, Webster RG. Avian-to-human transmission of the PB1 gene of influenza A virus in the 1957 and 1968 pandemics. *J Virol.* 1989;63(11):4603-4608. doi: https://doi.org/10.1128/JVI.63.11.4603-4608.1989

72. Banerjee S, De A, Kedia N, *et al*. The species-specific 282 residue in the PB2 subunit of the polymerase regulates RNA synthesis and replication of influenza A viruses infecting bat and nonbat hosts. *J Virol.* 2022;96(5):e0219021. doi: 10.1128/jvi.02190-21
73. Sun X, Shi Y, Lu X, *et al*. Bat-derived influenza hemagglutinin H17 does not bind canonical avian or human receptors and most likely uses a unique entry mechanism. *Cell Rep*. 2013;3(3):769-778. doi:10.1016/j.celrep.2013.01.025
74. Sandbulte MR, Spickler AR, Zaabel PK, *et al*. Optimal Use of Vaccines for Control of Influenza A Virus in Swine. *Vaccines (Basel).* 2015 Jan 30;3(1):22-73. doi: 10.3390/vaccines3010022
75. Centers for Disease Control. Disease Burden of Influenza. 2024. https://www.cdc.gov/flu-burden/php/about/index.html. Accessed July 2, 2024.
76. Government of Canada. Flu (Influenza): For Health Professionals. 2019. https://www.canada.ca/en/public-health/services/diseases/flu-influenza/health-professionals.html. Accessed September 29, 2019.
77. de Courville C, Cadarette SM, Wissinger E, *et al*. The economic burden of influenza among adults aged 18 to 64: A systematic literature review. *Influenza Other Respir Viruses*. 2022;16(3):376-385. doi:10.1111/irv.12963
78. Killingley B, Nguyen-Van-Tam J. Routes of influenza transmission. *Influenza Other Respir Viruses*. 2013;7:42-51. doi:10.1111/irv.12080
79. Chaves SS, Lynfield R, Lindegren M, *et al.* The US influenza hospitalization surveillance network. *Emerg. Infect. Dis*. 2015;21(9):1543-1550. doi:10.3201/eid2109.141912
80. Paget J, Spreeuwenberg P, Charu V, *et al*. Global mortality associated with seasonal influenza epidemics: New burden estimates and predictors from the GLaMOR Project. *J Glob Health.* 2019;9(2):1-12. doi:10.7189/jogh.09.020421
81. Ruf BR, Knuf M. The burden of seasonal and pandemic influenza in infants and children. *Eur J Pediatr.* 2014;173(3):265-76. doi: 10.1007/s00431-013-2023-6
82. Simon AK, Hollander GA, McMichael A. Evolution of the immune system in humans from infancy to old age. *Proc. Biol. Sci.* 2015;282(1821). doi:10.1098/rspb.2014.3085
83. Franceschi, C., Bonafè, M., & Valensin, S. Human immunosenescence: the prevailing of innate immunity, the failing of clonotypic immunity, and the filling of immunological space. *Vaccine*. 2000;*18*(16), 1717–1720. https://doi.org/10.1016/s0264-410x(99)00513-7
84. Fink AL, Engle K, Ursin RL, *et al*. Biological sex affects vaccine efficacy and protection against influenza in mice. *Proc Natl Acad Sci U S A*. 2018;115(49):12477-12482. doi:10.1073/pnas.1805268115
85. Putri WCWS, Muscatello DJ, Stockwell MS, *et al*. Economic burden of seasonal influenza in the United States. *Vaccine*. 2020;36(27):3960-3966. doi:10.1016/j.vaccine.2018.05.057
86. Hemmes J, Winkler K, Kool S. Virus survival as a seasonal factor in influenza and poliomyelitis. *Nature*. 1960;188(4748):430-431. doi: 10.1038/188430a0
87. Russell CA, Jones TC, Barr IG, *et al*. Influenza vaccine strain selection and recent studies on the global migration of seasonal influenza viruses. *Vaccine*. 2008;26:31-34. doi:10.1016/j.vaccine.2008.07.078
88. Ampofo WK, Azziz-Baumgartner E, Bashir U, *et al*. Strengthening the influenza vaccine virus selection and development process. Report of the 3rd WHO informal consultation for improving influenza vaccine virus selection held at WHO headquarters, Geneva,

Switzerland, 1-3 April 2014. *Vaccine*. 2015;33(36):4368-4382. doi:10.1016/j.vaccine.2015.06.090
89. Kim S, Chuang ESY, Sabaiduc S, *et al*. Influenza vaccine effectiveness against A(H3N2) during the delayed 2021/22 epidemic in Canada. *Eurosurveillance*. 2022;27(38). doi:10.2807/1560-7917.ES.2022.27.38.2200720
90. Hegde NR. Cell culture-based influenza vaccines: A necessary and indispensable investment for the future. *Hum Vaccin Immunother*. 2015;11(5):1223-1234. doi:10.1080/21645515.2015.1016666
91. Schickli JH, Flandorfer A, Nakaya T, *et al*. Plasmid-only rescue of influenza A virus vaccine candidates. *Philos Trans R Soc Lond B Biol Sci.* 2001;356(1416):1965-73. doi: 10.1098/rstb.2001.0979
92. Wiggins KB, Smith MA, Schultz-Cherry S. The nature of immune responses to influenza vaccination in high-risk populations. *Viruses.* 2021;13(6):1109. doi: 10.3390/v13061109
93. Turner JS, Zhou JQ, Han J, *et al*. Human germinal centres engage memory and naive B cells after influenza vaccination. *Nature*. 2020;586(7827):127-132. doi:10.1038/s41586-020-2711-0
94. Maassab H. Adaptation and growth characteristics of influenza virus at 25 degrees c. *Nature*. 1967;213(5076):612-4. doi: 10.1038/213612a0
95. Zhou B, Li Y, Speer SD, *et al*. Engineering temperature sensitive live attenuated influenza vaccines from emerging viruses. *Vaccine*. 2012;30(24):3691-3702. doi:10.1016/j.vaccine.2012.03.025
96. Mohn KGI, Zhou F, Brokstad KA, *et al*. Boosting of cross-reactive and protection-associated T cells in children after live attenuated influenza vaccination. *J Infect Dis*. 2017;215(10):1527-1535. doi:10.1093/infdis/jix165
97. Schmid P, Rauber D, Betsch C, *et al*. Barriers of influenza vaccination intention and behavior - A systematic review of influenza vaccine hesitancy, 2005 - 2016. *PLoS One.* 2017;12(1):e0170550. doi: 10.1371/journal.pone.0170550
98. Paules CI, Sullivan S, Subbarao K, *et al*. Chasing seasonal influenza - The need for a universal influenza vaccine. *N. Engl. J. Med*. 2018;378(1):7-9. doi:10.1056/NEJMp1709167
99. Crowe JE. Is it possible to develop a “universal” influenza virus vaccine? Potential for a universal influenza vaccine. *Cold Spring Harb Perspect Biol*. 2018;10(7). doi:10.1101/cshperspect.a029496
100. Allen UD, Aoki FY, Stiver HG. The use of antiviral drugs for influenza: Recommended guidelines for practitioners. *Can J Infect Dis Med Microbiol*. 2006;17(5):273-284. doi:10.1155/2006/165940
101. Wang C, Takeuchi K, Pinto LH, *et al*. Ion channel activity of influenza A virus M2 protein: characterization of the amantadine block. *J Virol*. 1993;67(9):5585-5594. doi:10.1128/jvi.67.9.5585-5594.1993
102. Cheng PKC, Leung TWC, Ho ECM, *et al.* Oseltamivir-and amantadine-resistant influenza viruses A (H1N1). *Emerg Infect Dis*. 2009;15(6):966-968. doi:10.3201/eid1506.081357
103. Tao J, Wang H, Wang W, *et al*. Binding mechanism of oseltamivir and influenza neuraminidase suggests perspectives for the design of new anti-influenza drugs. *PLoS Comput Biol*. 2022;18(7). doi:10.1371/journal.pcbi.1010343
104. Pinilla LT, Holder BP, Abed Y, *et al*. The H275Y neuraminidase mutation of the pandemic A/H1N1 influenza virus lengthens the eclipse phase and reduces viral output of

infected cells, potentially compromising fitness in ferrets. *J Virol*. 2012;86(19):10651-10660. doi:10.1128/jvi.07244-11
105. Jin Z, Smith LK, Rajwanshi VK, Kim B, *et al*. The ambiguous base-pairing and high substrate efficiency of T-705 (favipiravir) ribofuranosyl 5′-triphosphate towards influenza A virus polymerase. *PLoS One*. 2013;8(7). doi:10.1371/journal.pone.0068347
106. Goldhill DH, Te Velthuis AJW, Fletcher RA, *et al*. The mechanism of resistance to favipiravir in influenza. *Proc Natl Acad Sci U S A*. 2018;115(45):11613-11618. doi:10.1073/pnas.1811345115
107. Heneghan CJ, Onakpoya I, Thompson M, *et al*. Zanamivir for influenza in adults and children: Systematic review of clinical study reports and summary of regulatory comments. *BMJ*. 2014;348:1-16. doi:10.1136/bmj.g2547
108. Hurt AC, Holien JK, Parker M, *et al*. Zanamivir-resistant influenza viruses with a novel neuraminidase mutation. *J Virol*. 2009;83(20):10366-10373. doi:10.1128/jvi.01200-09
109. Yoo JW, Choi SH, Huh JW, *et al*. Peramivir is as effective as oral oseltamivir in the treatment of severe seasonal influenza. *J Med Virol*. 2015;87(10):1649-1655. doi:10.1002/jmv.24232
110. Arya V, Carter WW, Robertson SM. The role of clinical pharmacology in supporting the emergency use authorization of an unapproved anti-influenza drug, peramivir. *Clin Pharmacol Ther*. 2010;88(5):587-589. doi:10.1038/clpt.2010.187
111. O'Hanlon R, Shaw ML. Baloxavir marboxil: The new influenza drug on the market. *Curr Opin Virol*. 2019;35:14-18. doi:10.1016/j.coviro.2019.01.006
112. Takashita E, Kawakami C, Ogawa R, *et al*. Influenza A (H3N2) virus exhibiting reduced susceptibility to baloxavir due to a polymerase acidic subunit I38T substitution detected from a hospitalised child without prior baloxavir treatment, Japan, January 2019. *Euro Surveill*. 2019;24(12):1-4. doi:10.2807/1560-7917.ES.2019.24.12.1900170
113. Wouters OJ, McKee M, Luyten J. Estimated research and development investment needed to bring a new medicine to market, 2009-2018. *JAMA*. 2020;323(9):844-853. doi:10.1001/jama.2020.1166
114. Hughes JP, Rees SS, Kalindjian SB, *et al*. Principles of early drug discovery. *Br J Pharmacol*. 2011;162(6):1239-1249. doi:10.1111/j.1476-5381.2010.01127
115. Gubareva L, Mohan T. Antivirals targeting the neuraminidase. *Cold Spring Harb Perspect Med*. 2022;12(1). doi:10.1101/cshperspect.a038455
116. Loregian A, M Mercorelli B, Nannetti G, *et al*. Antiviral strategies against influenza virus: Towards new therapeutic approaches. *Cellular and Molecular Life Sciences*. 2014;71(19):3659-3683. doi:10.1007/s00018-014-1615-2
117. Green DVS. Virtual screening of virtual libraries. *Prog Med Chem*. 2003;41:61-97. doi: 10.1016/s0079-6468(02)41002-8
118. Pizzorno A, Terrier O, de Lamballerie CN, *et al*. Repurposing of drugs as novel influenza inhibitors from clinical gene expression infection signatures. *Front Immunol*. 2019;10(JAN). doi:10.3389/fimmu.2019.00060
119. Rajasekaran D, Palombo EA, Yeo TC, *et al*. Identification of traditional medicinal plant extracts with novel anti-influenza activity. *PLoS One*. 2013;8(11):1-15. doi:10.1371/journal.pone.0079293
120. Ping J, Dankar SK, Forbes NE, *et al*. PB2 and hemagglutinin mutations are major determinants of host range and virulence in mouse-adapted influenza A virus. *J Virol*. 2010;84(20):10606-10618. doi:10.1128/jvi.01187-10

121. Niwa H, Yamamura K, Miyazaki J. Efficient selection for high-expression transfectants with a novel eukaryotic vector. *Gene.* 1991;108(2):193-9. doi: 10.1016/0378-1119(91)90434-d
122. Lei C, Yang J, Hu J, *et al*. On the calculation of TCID50 for quantitation of virus infectivity. *Virol Sin*. 2021;36(1):141-144. doi:10.1007/s12250-020-00230-5
123. Thermo Fisher Scientific. CyQUANT ™ XTT Cell Viability Assay. 2018. www.thermofisher.com/us/en/home/global/terms-and-conditions.html. Accessed January 10 2018.
124. Furuta Y, Takahashi K, Kuno-Maekawa M, *et al*. Mechanism of action of T-705 against influenza virus. *Antimicrob Agents Chemother*. 2005;49(3):981-986. doi:10.1128/AAC.49.3.981-986.2005
125. Aoki-Utsubo C, Chen M, Hotta H. Time-of-addition and temperature-shift assays to determine particular step(s) in the viral life cycle that is blocked by antiviral substance(s). *Bio Protoc*. 2018;8(9):1-12. doi:10.21769/bioprotoc.2830
126. Kelava T, Ćavar I, Čulo F. Biological actions of drug solvents. *Period Biol*. 2011;113(3):311-320. WOS:000298216300005
127. Fujita E, Nagao Y, Node M, *et al.* Antitumor activity of the isodon diterpenoids: Structural requirements for the activity. *Experientia*. 1976;32(2):203-206. doi:10.1007/BF01937766
128. Khushboo M. Sanjeev S, Murthy MK, *et al*. Dietary phytoestrogen diosgenin interrupts metabolism, physiology, and reproduction of Swiss albino mice: Possible mode of action as an emerging environmental contaminant, endocrine disruptor and reproductive toxicant. *Food Chem Toxicol.* 2023;176:113798. doi: 10.1016/j.fct.2023.113798
129. Federal Register. Dimethyl Sulfoxide; Exemption From the Requirement of a Tolerance. 2022. https://www.federalregister.gov/documents/2022/10/12/2022-22129/dimethyl-sulfoxide-exemption-from-the-requirement-of-a-tolerance. Accessed February 2 2022.
130. Wang J, Li F, Ding J, Tian G, *et al*. Investigation of the anti-asthmatic activity of oridonin on a mouse model of asthma. *Mol Med Rep*. 2016;14(3):2000-2006. doi:10.3892/mmr.2016.5485
131. Liu M, Xu L, Yin L, *et al*. Potent effects of dioscin against obesity in mice. *Sci Rep*. 2015;5:7973. doi:10.1038/srep07973
132. Li C, Lu Y, Du S, *et al*. Dioscin exerts protective effects against crystalline silica-induced pulmonary fibrosis in mice. *Theranostics*. 2017;7(17):4255-4275. doi:10.7150/thno.20270
133. Wei T, Tong W, Wen-Ping S, *et al*. The impact of sodium aescinate on acute lung injury induced by oleic acid in rats. *Exp Lung Res*. 2011;37(10):585-599. doi:10.3109/01902148.2011.622426
134. Fu S, Gu Y, Jiang JQ, *et al*. Calycosin-7-O-β-d-glucoside regulates nitric oxide/caveolin-1/matrix metalloproteinases pathway and protects blood-brain barrier integrity in experimental cerebral ischemia-reperfusion injury. *J Ethnopharmacol*. 2014;155(1):692-701. doi:10.1016/j.jep.2014.06.015
135. Yang H, Sun PS, Jung ES, *et al.* Nilotinib-induced immune-mediated liver injury: Corticosteroid as a possible therapeutic option. *Pharmacology of Anti-Cancer Drugs.* 2020;10. doi: https://doi.org/10.3389/fonc.2020.01160
136. Sadiq S, Owen E, Foster T, *et al*. Nilotinib-induced metabolic dysfunction: insights from a translational study using in vitro adipocyte models and patient cohorts. *Leukemia*. 2019;33(7):1810-1814. doi:10.1038/s41375-018-0337-0

137. Hamedani MP, Kashi MA, Goodarzi S, *et al*. Elucidation of flavonoids from potent Iranian Scutellaria species against Influenza A (H1N1) virus. *Iran J Basic Med Sci*. 2023;26(1):76-84. doi:10.22038/IJBMS.2022.66255.14553
138. Ho JY, Chang HW, Lin CF, *et al*. Characterization of the anti-influenza activity of the Chinese herbal plant Paeonia lactiflora. *Viruses*. 2014;6(4):1861-1875. doi:10.3390/v6041861
139. Yang Z, Liu N, Huang B, *et al*. Effect of anti-influenza virus of Arctigenin in vivo. *Zhong Yao Cai.* 2005;28(11):1012-4. PMID: 16514891
140. Yang X, Long F, Jia W, *et al*. Artesunate inhibits PDE4 leading to intracellular cAMP accumulation, reduced ERK/MAPK signaling, and blockade of influenza A virus vRNP nuclear export. *Antiviral Res*. 2023;215. doi:10.1016/j.antiviral.2023.105635
141. Arm JA, Froelich EJ. Inactivation of viruses by benzalkonium chloride. *Appl Microbiol*. 1964;12(2):132-7. doi: 10.1128/am.12.2.132-137
142. Shin HB, Choi MS, Ryu B, *et al*. Antiviral activity of carnosic acid against respiratory syncytial virus. *Virol J*. 2013;10. doi:10.1186/1743-422X-10-303
143. de Oliveira PG, Termini L, Durigon EL, *et al*. Diacerein: A potential multi-target therapeutic drug for COVID-19. *Med Hypotheses*. 2020;144. doi:10.1016/j.mehy.2020.109920
144. Pizzorno A, Terrier O, de Lamballerie CN, *et al*. Repurposing of drugs as novel influenza inhibitors from clinical gene expression infection signatures. *Front Immunol*. 2019 Jan 29;10:60. doi: 10.3389/fimmu.2019.00060.
145. Rauš K, Pleschka S, Klein P, *et al*. Effect of an Echinacea-Based Hot Drink Versus Oseltamivir in Influenza Treatment: A Randomized, Double-Blind, Double-Dummy, Multicenter, Noninferiority Clinical Trial. *Curr Ther Res Clin Exp*. 2015;77:66-72. doi:10.1016/j.curtheres.2015.04.001
146. Ho JY, Chang HW, Lin CF, *et al*. Characterization of the anti-influenza activity of the Chinese herbal plant Paeonia lactiflora. *Viruses*. 2014;6(4):1861-1875. doi:10.3390/v6041861
147. Wee JJ, Mee Park K, Chung AS. Biological Activities of Ginseng and Its Application to Human Health. In: Benzie IFF, Wachtel-Galor S, editors. Herbal Medicine: Biomolecular and Clinical Aspects. 2nd ed. Boca Raton (FL): CRC Press/Taylor & Francis; 2011. Chapter 8. PMID: 22593942
148. Moradi MT, Karimi A, Fotouhi F, *et al*. In vitro and *in vivo* effects of *Peganum harmala* L. seeds extract against influenza A virus. *Avicenna J Phytomed*. 2017 Nov-Dec;7(6):519-530. PMID: 29299435
149. Hegazy A, Mahmoud SH, Elshaier Yamm, *et al*. Antiviral activities of plant-derived indole and β-carboline alkaloids against human and avian influenza viruses. *Sci Rep*. 2023;13(1). doi:10.1038/s41598-023-27954-0
150. Ding Y, Cao Z, Cao L, *et al*. Antiviral activity of chlorogenic acid against influenza A (H1N1/H3N2) virus and its inhibition of neuraminidase. *Sci Rep*. 2017;7. doi:10.1038/srep45723
151. Wang Z, Sun L, Zhao H, *et al*. Inhibition Effects and Mechanisms of Marine Compound Mycophenolic Acid Methyl Ester against Influenza A Virus. *Mar Drugs*. 2024;22(5). doi:10.3390/md22050190

152. Qin Y, Yang J, Li H, *et al*. Recent advances in the therapeutic potential of nobiletin against respiratory diseases. *Phytomedicine*. 2024;128. doi:10.1016/j.phymed.2024.155506
153. Fan Y, Zhang Q, Zhang W, *et al*. Inhibitory effects of Patchouli alcohol on the early lifecycle stages of influenza A virus. *Front Microbiol*. 2023;13. doi:10.3389/fmicb.2022.938868
154. Dong W, Farooqui A, Leon AJ, *et al*. Inhibition of influenza A virus infection by ginsenosides. *PLoS One.* 2017;12(2). doi:10.1371/journal.pone.0171936
155. Zhang Y, Han H, Qiu H, *et al*. Antiviral activity of a synthesized shikonin ester against influenza A (H1N1) virus and insights into its mechanism. *Biomed. Pharmacother*. 2017;93:636-645. doi:10.1016/j.biopha.2017.06.076
156. Wei X, Lan Y, Nong Z, *et al*. Ursolic acid represses influenza A virus-triggered inflammation and oxidative stress in A549 cells by modulating the miR-34c-5p/TLR5 axis. *Cytokine*. 2022;157. doi:10.1016/j.cyto.2022.155947
157. Maria Jancy Rani J, Kalaimathi K, Prabhu S, *et al*. Unravelling the influenza virus inhibitory potential: Ligand-based docking, pharmacophore, MM-GBSA, and molecular dynamic simulation of phytochemicals and cyanobacteria metabolites. *Intelligent Pharmacy*. 2024;2(1):83-93. doi:10.1016/j.ipha.2023.10.011
158. Redfield DC, Richman DD, Oxman MN, *et al*. Psoralen inactivation of influenza and herpes simplex viruses and of virus-infected cells. *Infect Immun.* 1981 Jun;32(3):1216-26. doi: 10.1128/iai.32.3.1216-1226.1981
159. Robinson DP, Lorenzo ME, Jian W, *et al*. Elevated 17β-estradiol protects females from influenza a virus pathogenesis by suppressing inflammatory responses. *PLoS Pathog*. 2011;7(7). doi:10.1371/journal.ppat.1002149
160. O'connor P, Wolinsky JS, Confavreux C, *et al*. Randomized trial of oral teriflunomide for relapsing multiple sclerosis. *N Engl J Med.* 2011 Oct 6;365(14):1293-303. doi: 10.1056/NEJMoa1014656
161. European Medicines Agency. 2013. https://www.ema.europa.eu/en/documents/assessment-report/aubagio-epar-public-assessment-report_en. Accessed August 10 2021.
162. Miller J, Wolf EH. Antazoline phosphate and naphazoline hydrochloride, singly and in combination for the treatment of allergic conjunctivitis-a controlled, double-blind clinical trial. *Ann Allergy.* 1975 Aug;35(2):81-6. PMID: 1096685
163. Aaronson JK. *Meyler's Side Effects of Drugs.* 16th ed. Oxford, UK: Elsevier; 2016.
164. Chen H, Hu P, Liu H, *et al*. Combining with domiphen bromide restores colistin efficacy against colistin-resistant Gram-negative bacteria in vitro and in vivo. *Int J Antimicrob Agents*. 2024;63(2). doi:10.1016/j.ijantimicag.2023.107066
165. An S, Cha HJ, Ko JM, *et al*. Kinetin improves barrier function of the skin by modulating keratinocyte differentiation markers. *Ann Dermatol*. 2017;29(1):6-12. doi:10.5021/ad.2017.29.1.6
166. Rivera C. *Progesterone: Functions, Uses and Research Insights*. New York: Nova Science Publishers, Inc; 2017.
167. Campagnoli C, Clavel-Chapelon F, Kaaks R, *et al*. Progestins and progesterone in hormone replacement therapy and the risk of breast cancer. *J Steroid Biochem Mol Biol*. 2005;96(2):95-108. doi:10.1016/j.jsbmb.2005.02.014

168. Zhang Z, Cao G, Sha L, *et al*. The efficacy of sodium aescinate on cutaneous wound healing in diabetic rats. *Inflammation*. 2015;38(5):1942-1948. doi:10.1007/s10753-015-0174-5
169. Wei T, Tong W, Wen-Ping S, *et al*. The impact of sodium aescinate on acute lung injury induced by oleic acid in rats. *Exp Lung Res*. 2011;37(10):585-599. doi:10.3109/01902148.2011.622426
170. World Intellectual Property Organization. Prodrug of Green tea Epigallocatechin-3-Gallate (Pro-ECGC) for Use in the Treatment of Endometriosis. 2013. https://patentimages.storage.googleapis.com/fe/1a/53/b8e24881def083/WO2014029327A1. Accessed August 10 2021.
171. Palhano FL, Lee J, Grimster NP, *et al*. Toward the molecular mechanism(s) by which EGCG treatment remodels mature amyloid fibrils. *J Am Chem Soc*. 2013;135(20):7503-7510. doi:10.1021/ja3115696
172. Rajoria S, Suriano R, Parmar PS, *et al*. 3,3′-diindolylmethane modulates estrogen metabolism in patients with thyroid proliferative disease: A pilot study. *Thyroid*. 2011;21(3):299-304. doi:10.1089/thy.2010.0245
173. Ghumatkar PJ, Patil SP, Jain PD, *et al*. Nootropic, neuroprotective and neurotrophic effects of phloretin in scopolamine induced amnesia in mice. *Pharmacol Biochem Behav*. 2015;135:182-191. doi:10.1016/j.pbb.2015.06.005
174. Chang WT, Huang WC, Liou CJ. Evaluation of the anti-inflammatory effects of phloretin and phlorizin in lipopolysaccharide-stimulated mouse macrophages. *Food Chem*. 2012;134(2):972-979. doi:10.1016/j.foodchem.2012.03.002
175. Moon SH, Mistry B, Kim DH, *et al*. Antioxidant and anticancer potential of bioactive compounds following UV-C light-induced plant cambium meristematic cell cultures. *Ind Crops Prod*. 2017;109:762-772. doi:10.1016/j.indcrop.2017.09.024
176. Fu R, Wang X, Hu Y, *et al*. Solamargine inhibits gastric cancer progression by regulating the expression of lncNEAT1_2 via the MAPK signaling pathway. *Int J Oncol*. 2019;54(5):1545-1554. doi:10.3892/ijo.2019.4744
177. Yan X, Yu A, Zheng H, *et al*. Calycosin-7-O-β-D-glucoside attenuates OGD/R-induced damage by preventing oxidative stress and neuronal apoptosis via the SIRT1/FOXO1/PGC-1α Pathway in HT22 Cells. *Neural Plast*. 2019;8798069. doi:10.1155/2019/8798069
178. Wang CP, Zhang LZ, Li GC, *et al*. Mulberroside A protects against ischemic impairment in primary culture of rat cortical neurons after oxygen-glucose deprivation followed by reperfusion. *J Neurosci Res*. 2014;92(7):944-954. doi:10.1002/jnr.23374
179. Saghaei E, Nasiri Boroujeni S, Safavi P, *et al*. Diosmetin mitigates cognitive and memory impairment provoked by chronic unpredictable mild stress in mice. *Evid Based Complement Alternat Med*. 2020;2020:5725361. doi: 10.1155/2020/5725361
180. Yang L, Ren S, Xu F, *et al*. Recent advances in the pharmacological activities of dioscin. *Biomed Res Int*. 2019. doi:10.1155/2019/5763602
181. Kang N, Cao SJ, Zhou Y, *et al.* Inhibition of caspase-9 by oridonin, a diterpenoid isolated from Rabdosia rubescens, augments apoptosis in human laryngeal cancer cells. *Int J Oncol*. 2015;47(6):2045-2056. doi:10.3892/ijo.2015.3186
182. Xu J, Wold EA, Ding Y, *et al*. Therapeutic potential of oridonin and its analogs: From anticancer and antiinflammation to neuroprotection. *Molecules*. 2018;23(2). doi:10.3390/molecules23020474

183. Hu C, Zu D, Xu J, *et al.* Polyphyllin B suppresses gastric tumor growth by modulating iron metabolism and inducing ferroptosis. *Int J Biol Sci*. 2023;19(4):1063-1079. doi:10.7150/ijbs.80324
184. Zhu G, Chen Y, Zhang X, *et al*. 12-O-tetradecanoylphorbol-13-acetate (TPA) is anti-tumorigenic in liver cancer cells via inhibiting YAP through AMOT. *Sci Rep*. 2017;7:44940. doi: 10.1038/srep44940
185. Uchide N, Toyoda H. Antioxidant therapy as a potential approach to severe influenza-associated complications. *Molecules*. 2011;16(3):2032-2052. doi:10.3390/molecules16032032
186. Thacker H. Antiviral Activity of Doxycycline. *JIMA*. 2024;72(2):10-11. doi:10.59556/japi.72.0463
187. Khalili N, Karimi A, Moradi MT, *et al*. In vitro immunomodulatory activity of celastrol against influenza A virus infection. *Immunopharmacol Immunotoxicol*. 2018;40(3):250-255. doi:10.1080/08923973.2018.1440591
188. Wang H, Jia X, Zhang M, *et al*. Isoliquiritigenin inhibits virus replication and virus-mediated inflammation via NRF2 signaling. *Phytomedicine*. 2023;114. doi:10.1016/j.phymed.2023.154786
189. Benet LZ, Hosey CM, Ursu O, *et al*. BDDCS, the Rule of 5 and drugability. *Adv Drug Deliv Rev*. 2016;101:89-98. doi:10.1016/j.addr.2016.05.007
190. Fan S, Zhang C, Luo T, *et al*. Limonin: A review of its pharmacology, toxicity, and pharmacokinetics. *Molecules*. 2019;24(20). doi:10.3390/molecules24203679
191. Chen Z, Duan H, Tong X, *et al*. Cytotoxicity, Hemolytic Toxicity, and Mechanism of Action of Pulsatilla Saponin D and Its Synthetic Derivatives. doi:10.1021/acs.jnat-prod.7b00578
192. Danenberg HD, Ben-Yehuda A, Zakay-Rones Z, *et al*. Dehydroepiandrosterone (DHEA) treatment reverses the impaired immune response of old mice to influenza vaccination and protects from influenza infection. *Vaccine.* 1995;13(15):1445-8. doi: 10.1016/0264-410x(95)00063-7
193. Reed LJ, Muench H. A simple method of estimating fifty percent endpoints. *Am. J. Hyg.* 1938;27. 493-497
194. Indrayanto G, Putra GS, Suhud F. Validation of in-vitro bioassay methods: Application in herbal drug research. *Profiles Drug Subst Excip Relat Methodol*. 2021;46:273-307. doi: 10.1016/bs.podrm.2020.07.005
195. Yahalom-Ronen Y, Tamir H, Melamed S, *et al*. A single dose of recombinant VSV-ΔG-spike vaccine provides protection against SARS-CoV-2 challenge. *Nat Commun*. 2020;11(1):1-13. doi:10.1038/s41467-020-20228-7
196. Chiba S. Effect of early oseltamivir on outpatients without hypoxia with suspected COVID-19. *Wien Klin Wochenschr*. 2021;133(7-8):292-297. doi:10.1007/s00508-020-01780-0
197. Song EJ, Español E, Shim SM, *et al*. Inhibitory effects of aprotinin on influenza A and B viruses in vitro and in vivo. *Sci Rep*. 2021;11(1). doi:10.1038/s41598-021-88886-1
198. Amy G, Craun G, Craun GF, Siddiqui M. EHC 216: Disinfectants and Disinfectant By-products. *Environmental Health Criteria*. 2004;216.
199. Zhang W, Chen ST, He QY, *et al.* Asprellcosides B of ilex asprellainhibits influenza a virus infection by blocking the hemagglutinin-mediated membrane fusion. *Front Microbiol*. 2019;10. doi:10.3389/fmicb.2018.03325

200. Duwe S. Influenza viruses - antiviral therapy and resistance. *GMS Infect Dis.* 2017;5. doi: 10.3205/id000030
201. Davies BE. Pharmacokinetics of oseltamivir: An oral antiviral for the treatment and prophylaxis of influenza in diverse populations. *J Antimicrob Chemother*. 2010;65:5-10. doi:10.1093/jac/dkq015
202. Renzette N, Caffrey DR, Zeldovich KB, *et al*. Evolution of the influenza A virus genome during development of oseltamivir resistance *in vitro*. *J Virol*. 2014;88(1):272-281. doi:10.1128/jvi.01067-13
203. Gao R, Du N, Liu D, *et al*. Oseltamivir inhibits both viral entry and release but enhances apoptosis of cells infected with influenza A H1N1. *Biochem Biophys Res Commun*. 2013;431(4):788-795. doi:10.1016/j.bbrc.2013.01.019
204. Matrosovich MN, Matrosovich TY, Gray T, *et al*. Neuraminidase is important for the initiation of influenza virus infection in human airway epithelium. *J Virol*. 2004;78(22):12665-12667. doi:10.1128/jvi.78.22.12665-12667.2004
205. Hamilton BS, Whittaker GR, Daniel S. Influenza virus-mediated membrane fusion: Determinants of hemagglutinin fusogenic activity and experimental approaches for assessing virus fusion. *Viruses*. 2012;4(7):1144-1168. doi:10.3390/v4071144
206. Byrd-Leotis L, Galloway SE, Agbogu E, *et al*. Influenza hemagglutinin (HA) stem region mutations that stabilize or destabilize the structure of multiple HA subtypes. *J Virol*. 2015;89(8):4504-4516. doi:10.1128/jvi.00057-15
207. Benton DJ, Wharton SA, Martin SR, *et al*. Role of neuraminidase in influenza A(H7N9) virus receptor binding. *J Virol*. 2017;91(11). doi:10.1128/jvi.02293-16
208. Li J, Yu M, Zheng W, *et al*. Nucleocytoplasmic shuttling of influenza a virus proteins. *Viruses*. 2015;7(5):2668-2682. doi:10.3390/v7052668
209. Neumann G, Castrucci MR, Kawaoka Y. Nuclear import and export of influenza virus nucleoprotein. *J Virol*. 1997;71(12):9690-9700. doi:10.1128/jvi.71.12.9690-9700.1997
210. Resa-Infante P, Jorba N, Coloma R, *et al.* The influenza virus RNA synthesis machine. *RNA Biol*. 2011;8(2):207-215. doi:10.4161/rna.8.2.14513
211. Zeng H, Yang L, Zhang X, *et al*. Dioscin prevents LPS-induced acute lung injury through inhibiting the TLR4/MyD88 signaling pathway via upregulation of HSP70. *Mol Med Rep*. 2018;17(5):6752-6758. doi:10.3892/mmr.2018.8667
212. Zhao Y, Jin H, Lei K, *et al.* Oridonin inhibits inflammation of epithelial cells via dual-targeting of CD31 Keap1 to ameliorate acute lung injury. *Front Immunol*. 2023;14. doi:10.3389/fimmu.2023.116339
213. Spackman E, *Animal Influenza Virus.* 3rd ed. New York, NY: Humana New York;2020.
214. Ovsyannikova IG, White SJ, Albrecht RA, *et al*. Turkey versus guinea pig red blood cells: Hemagglutination differences alter hemagglutination inhibition responses against influenza A/H1N1. *Viral Immunol*. 2014;27(4):174-178. doi:10.1089/vim.2013.0111
215. Hahon N, Booth JA, Eckert HL. Cell attachment and penetration by influenza virus. *Infect Immun*. 1973;7(3):341-351. doi:10.1128/iai.7.3.341-351.1973
216. Yan H, Xie Y, Sun S, *et al*. Chemical analysis of Astragalus mongholicus polysaccharides and antioxidant activity of the polysaccharides. *Carbohydr Polym*. 2010;82(3):636-640. doi:10.1016/j.carbpol.2010.05.026
217. Zhang L, Fei M, Wang H, *et al*. Sodium aescinate provides neuroprotection in experimental traumatic brain injury via the Nrf2-ARE pathway. *Brain Res Bull*. 2020;157:26-36. doi:10.1016/j.brainresbull.2020.01.019

218. Burrough ER, Magstadt DR, Petersen B, *et al*. Highly Pathogenic Avian Influenza A(H5N1) Clade 2.3.4.4b Virus Infection in Domestic Dairy Cattle and Cats, United States, 2024. *Emerg Infect Dis*. 2024;30(7):1335-1343. doi:10.3201/eid3007.240508
219. Olszewski D, Georgi F, Murer L, *et al*. High-content, arrayed compound screens with rhinovirus, influenza A virus and herpes simplex virus infections. *Sci Data*. 2022;9(1). doi:10.1038/s41597-022-01733-4
220. Severson WE, McDowell M, Ananthan S, *et al*. High-throughput screening of a 100,000-compound library for inhibitors of influenza a virus (H3N2). *J Biomol Screen*. 2008;13(9):879-887. doi:10.1177/1087057108323123
221. Indrayanto G, Putra GS, Suhud F. Validation of in-vitro bioassay methods: Application in herbal drug research. *Profiles Drug Subst. Excip. Relat. Methodol*. Vol 46. Academic Press Inc.; 2021:273-307. doi:10.1016/bs.podrm.2020.07.005
222. Aslantürk ÖS. In Vitro Cytotoxicity and Cell Viability Assays: Principles, Advantages, and Disadvantages. 2018. https://www.intechopen.com/chapters/57717. Accessed March 19 2018.
223. Cho HJ, Seon MR, Lee YM, *et al*. 3,3'-Diindolylmethane suppresses the inflammatory response to lipopolysaccharide in murine macrophages. *J Nutr*. 2008;138(1):17-23. doi: 10.1093/jn/138.1.17
224. Omeir RL, Teferedegne B, Foseh GS, *et al*. Heterogeneity of the tumorigenic phenotype expressed by Madin-Darby canine kidney cells. *Comp Med*. 2011;61(3):243-250. PMID: 21819694
225. Swain RJ, Kemp SJ, Goldstraw P, *et al*. Assessment of cell line models of primary human cells by raman spectral phenotyping. *Biophys J*. 2010;98(8):1703-1711. doi:10.1016/j.bpj.2009.12.4289
226. Park JE, Li K, Barlan A, *et al*. Proteolytic processing of middle east respiratory syndrome coronavirus spikes expands virus tropism. *Proc Natl Acad Sci U S A*. 2016;113(43):12262-12267. doi:10.1073/pnas.1608147113
227. Bochkov YA, Gern JE. Rhinoviruses and their receptors: Implications for allergic disease. *Curr Allergy Asthma Rep*. 2017;16(4):30. doi:10.1007/s11882-016-0608-7
228. Shukla SD, Shastri MD, Vanka SK, *et al*. Targeting intercellular adhesion molecule-1 (ICAM-1) to reduce rhinovirus-induced acute exacerbations in chronic respiratory diseases. *Inflammopharmacology*. 2022;30(3):725-735. doi:10.1007/s10787-022-00968-2
229. Li M, Li A, Huang H, *et al*. Impact of progesterone on innate immunity and cell death after influenza A virus H1N1 2009 infection of lung and placental cells in vitro. *Front Virol*. 2022;2:953208. doi: 10.3389/fviro.2022.953208
230. Bährle-Rapp M. *Springer Lexikon Kosmetik und Körperpflege*. Berlin, Germany; 2007.
231. Cakir M, Obernier K, Forget A, *et al*. Target Discovery for Host-Directed Antiviral Therapies: Application of Proteomics Approaches. *mSystems*. 2021;6(5). doi:10.1128/msystems.00388-21
232. Iwasaki A, Pillai PS. Innate immunity to influenza virus infection. *Nat Rev Immunol*. 2014;14(5):315-328. doi:10.1038/nri3665
233. Guo X zhi J, Thomas PG. New fronts emerge in the influenza cytokine storm. *Semin Immunopathol*. 2017;39(5):541-550. doi:10.1007/s00281-017-0636-y
234. Söderholm S, Fu Y, Gaelings L, et al. Multi-omics studies towards novel modulators of influenza a virus-host interaction. *Viruses*. 2016;8(10). doi:10.3390/v8100269

235. Luo M. Influenza virus entry. *Adv Exp Med Biol*. 2012;726:201-221. doi:10.1007/978-1-4614-0980-9_9
236. Kirchenbaum GA, Sautto GA, Richardson RA, Ecker JW, Ross TM. A Competitive Hemagglutination Inhibition Assay for Dissecting Functional Antibody Activity against Influenza Virus. *J Virol*. 2021;95(23). doi:10.1128/jvi.02379-20
237. Shi WZ, Jiang LZ, Song GP, Wang S, Xiong P, Ke CW. Study on the antiviral activities and hemagglutinin-based molecular mechanism of novel chlorogenin 3-O-β-chacotrioside derivatives against H5N1 subtype viruses. *Viruses*. 2020;12(3). doi:10.3390/v12030304
238. Sacramento CQ, Marttorelli A, Fintelman-Rodrigues N, et al. Aureonitol, a fungi-derived tetrahydrofuran, inhibits influenza replication by targeting its surface glycoprotein hemagglutinin. *PLoS One*. 2015;10(10). doi:10.1371/journal.pone.0139236
239. Meng L, Su Y, Yang F, et al. Design, synthesis and biological evaluation of amino acids-oleanolic acid conjugates as influenza virus inhibitors. *Bioorg Med Chem*. 2019;27(23). doi:10.1016/j.bmc.2019.115147
240. Weis W, Brown JH, Cusack S, Paulsont JC, Skehel JJ, Wiley DC. *Structure of the Influenza Virus Haemagglutinin Complexed with Its Receptor, Sialic Acid*.; 1988.
241. Jang Y, Shin JS, Yoon YS, et al. Salinomycin Inhibits Influenza Virus Infection by Disrupting Endosomal Acidification and Viral Matrix Protein 2 Function. *J Virol*. 2018;92(24). doi:10.1128/jvi.01441-18
242. Bhat T, Cao A, Yin J. Virus-like Particles: Measures and Biological Functions. *Viruses*. 2022;14(2). doi:10.3390/v14020383
243. Huang AS, Baltimore D. Defective Viral Particles and Viral Disease Processes. *Nature Publishing Group NATURE*. 1970;226:325-327.
244. Brooke CB, Ince WL, Wrammert J, et al. Most Influenza A Virions Fail To Express at Least One Essential Viral Protein. *J Virol*. 2013;87(6):3155-3162. doi:10.1128/jvi.02284-12
245. Mancini N, Solforosi L, Clementi N, De Marco D, Clementi M, Burioni R. A potential role for monoclonal antibodies in prophylactic and therapeutic treatment of influenza. *Antiviral Res*. 2011;92(1):15-26. doi:10.1016/j.antiviral.2011.07.013
246. Huang S, Wang X, Liu M, et al. Modification of sodium aescinate into a safer, more stable and effective water-soluble drug by liposome-encapsulation: an in vitro and in vivo study. *Drug Deliv*. 2022;29(1):1132-1141. doi:10.1080/10717544.2022.2058114
247. Huang XJ, Wang DG, Ye LC, et al. Sodium aescinate and its bioactive components induce degranulation via oxidative stress in RBL-2H3 mast cells. *Toxicol Res (Camb)*. 2020;9(4):413-424. doi:10.1093/TOXRES/TFAA042
248. Zhu H, Zhang Y, Ye G, Li Z, Zhou P, Huang C. In vivo and in vitro antiviral activities of calycosin-7-o- β-D-glucopyranoside against coxsackie virus B3. *Biol Pharm Bull*. 2009;32(1):68-73. doi:10.1248/bpb.32.68
249. Li X, Zhang CT, Ma W, Xie X, Huang Q. Oridonin: A Review of Its Pharmacology, Pharmacokinetics and Toxicity. *Front Pharmacol*. 2021;12(July). doi:10.3389/fphar.2021.645824
250. Bandopadhyay S, Anand U, Gadekar VS, et al. Dioscin: A review on pharmacological properties and therapeutic values. *BioFactors*. 2022;48(1):22-55. doi:10.1002/biof.1815
251. Xu P, Yu B. *Chemical Synthesis of Saponins: An Update*. Vol 79. 1st ed. Elsevier Inc.; 2021. doi:10.1016/bs.accb.2021.11.001

Chapter Seven: Copyright Authorization

Figure 1: Covered by Creative Commons Attribution License (CC BY). Veterinary and Biomedical Sciences: MDPI. Author authorization attached.

Figure 2: No authorization needed. Public domain work from Eurosurveillance.

Figure 3: Covered by Creative Commons Attribution License (CC BY). Vaccines: MDPI. Author authorization attached.

Figure 4: Covered by Creative Commons Attribution License (CC BY). Frontiers in Microbiology. Author authorization attached.

Figure 5: Covered by Creative Commons Attribution License (CC BY). Frontiers in Immunology. Author authorization attached.

Re: Seeking Copyright Permission

Kuchipudi, Suresh Varma <svk11@psu.edu>
Tue 8/23/2022 2:39 PM

To: Marnie Willman <hustinsm@myumanitoba.ca>

Hi Marnie,
Thanks for reaching out; I am okay with using this image for the stated purpose. However, I suggest you also check with the journal if they have any restrictions
Thank you
Suresh

Suresh V Kuchipudi, DVM, MVSc, PhD, FHEA, DACVM, MBA
Dorothy Foehr Huck and J. Lloyd Huck Chair in Emerging Infectious Diseases,
Clinical Professor and Interim Director, Animal Diagnostic Lab,
Department of Veterinary and Biomedical Sciences,
Huck Institutes of the Life Sciences,
224, Huck Life Sciences Building,
Penn State University, University Park, PA 16802-1110,
Phone: 814-863-5737; Fax: 814-865-3907
Email: skuchipudi@psu.edu
Research Innovator of the Year Award-2022
Web page: http://vbs.psu.edu/directory/svk11
Kuchipudi lab: http://vbs.psu.edu/research/labs/kuchipudi
LinkedIn: https://www.linkedin.com/in/suresh-v-kuchipudi-03607a18b/

"The way to get started is to quit talking and begin doing" - Walt Disney

---

From: Marnie Willman <hustinsm@myumanitoba.ca>
Date: Tuesday, August 23, 2022 at 8:54 AM
To: Kuchipudi, Suresh Varma <svk11@psu.edu>
Subject: Seeking Copyright Permission

I'm finishing a PhD in Medical Microbiology at the University of Manitoba in Canada. I am seeking copyright permission to use Figure 1 from your 2018 publication entitled "Novel Flu Viruses in Bats and Cattle: "Pushing the Envelope" of Influenza Infection" for my written thesis. The work is academic, non-profit, and will be available in both print and electronic format. The figure legend and all associated bodies of writing will cite the image.

Much appreciated,

Marnie Hustins, B.Sc.
PhD Candidate
High Risk Respiratory Pathogens, Special Pathogens
National Microbiology Laboratory | Laboratoire national de microbiologie
Public Health Agency of Canada | Agence de la santé publique du Canada

Re: Seeking Copyright Permission

Sylvie Bertholet <sylvie.c.bertholet-girardin@gsk.com>
Tue 8/23/2022 9:37 AM
To: Marnie Willman <hustinsm@myumanitoba.ca>

Dear Marnie,
This is fine as long as you follow the guidelines below.
Kind regards,
Sylvie

From: Marnie Willman <hustinsm@myumanitoba.ca>
Date: Tuesday, August 23, 2022 at 9:02 AM
To: Sylvie Bertholet <sylvie.c.bertholet-girardin@gsk.com>
Subject: Seeking Copyright Permission

EXTERNAL

I'm finishing a PhD in Medical Microbiology at the University of Manitoba in Canada. I am seeking copyright permission to use Figure 1 from your 2015 publication entitled "B Cells and Functional Antibody Responses to Combat Influenza" for my written thesis. The work is academic, non-profit, and will be available in both print and electronic format. The figure legend and all associated bodies of writing will cite the image.

Much appreciated,

Marnie Hustins, B.Sc.
PhD Candidate
High Risk Respiratory Pathogens, Special Pathogens
National Microbiology Laboratory | Laboratoire national de microbiologie
Public Health Agency of Canada | Agence de la santé publique du Canada
Canadian Science Centre for Human and Animal Health | Centre scientifique canadien de la santé humaine et animale
Winnipeg, Canada R3E 3P6
marnie.hustins@canada.ca
Telephone | Téléphone 204-789-5066
Government of Canada | Gouvernement du Canada

Re: Seeking Copyright Permission

Roland Marquet <r.marquet@ibmc-cnrs.unistra.fr>

Tue 8/23/2022 8:26 AM

To: Marnie Willman <hustinsm@myumanitoba.ca>

Dear Marnie,

You are welcome to reuse Figure 1 of our paper as long as complete reference to our paper is given in the figure legend and in the section of the text mentioning the figure.

Best wishes with your PhD,

Roland

Roland Marquet
Deputy Director, UPR 9002 CNRS - ARN
Co-PI, Viral Ribonucleoprotein, Genome Incorporation & Assembly laboratory
IBMC - CNRS - Université de Strasbourg
2, Allée Conrad Roentgen
67084 Strasbourg cedex, France

Tel: +33 3 88 41 70 54
e-mail: r.marquet@ibmc-cnrs.unistra.fr
website: https://ibmc.cnrs.fr/en/laboratoire/arn/equipes/viral-ribonucleoproteins-incorporation-of-the-genome-and-assembly/

> Le 23 août 2022 à 15:00, Marnie Willman <hustinsm@myumanitoba.ca> a écrit :
>
> I'm finishing a PhD in Medical Microbiology at the University of Manitoba in Canada. I am seeking copyright permission to use Figure 1 from your 2018 publication entitled "Structural and Functional Motifs in Influenza Virus RNAs" for my written thesis. The work is academic, non-profit, and will be available in both print and electronic format. The figure legend and all associated bodies of writing will cite the image.
>
> Much appreciated,
>
> Marnie Hustins, B.Sc.
> PhD Candidate
> High Risk Respiratory Pathogens, Special Pathogens
> National Microbiology Laboratory | Laboratoire national de microbiologie
> Public Health Agency of Canada | Agence de la santé publique du Canada
> Canadian Science Centre for Human and Animal Health | Centre scientifique canadien de la santé humaine et animale
> Winnipeg, Canada R3E 3P6
> marnie.hustins@canada.ca
> Telephone | Téléphone 204-789-5066
> Government of Canada | Gouvernement du Canada

Re: Seeking Copyright Permission

SG APD <samgan@apdskeg.com>
Sat 3/9/2024 10:37 PM
To:Marnie Willman <hustinsm@myumanitoba.ca>

Hello,

Since it is an academic work, so long proper academic citation follows the image, you are free to use it.

Rgds
Samuel

From: Marnie Willman <hustinsm@myumanitoba.ca>
Sent: Tuesday, February 27, 2024 7:02 AM
To: samgan@apdskeg.com <samgan@apdskeg.com>
Subject: Seeking Copyright Permission

I'm finishing a PhD in Medical Microbiology at the University of Manitoba in Canada. I am seeking copyright permission to use Figure 2 from your 2021 publication entitled "Peering into Avian influenza A(H5N8) for a Framework towards Pandemic Preparedness" for my written thesis. The work is academic, non-profit, and will be available in both print and electronic format. The figure legend and all associated bodies of writing will cite the image.

Much appreciated,

Marnie Hustins, B.Sc.
PhD Candidate
High Risk Respiratory Pathogens, Special Pathogens
National Microbiology Laboratory | Laboratoire national de microbiologie
Public Health Agency of Canada | Agence de la santé publique du Canada
Canadian Science Centre for Human and Animal Health | Centre scientifique canadien de la santé humaine et animale
Winnipeg, Canada R3E 3P6
hustinsm@myumanitoba.ca
Telephone | Téléphone 204-789-5066
Government of Canada | Gouvernement du Canada

Chapter Eight: Appendix

8.1: Clinical scoring criteria for Influenza A infection in mice

points	Clinical signs
0	No symptoms
1	Slightly ruffled fur, less activity
2	Above signs plus any of the following: Slightly hunched posture, very ruffled fur, weight loss 10-15%
3	Above signs plus any of the following: Very hunched posture, Laboured or rapid breathing, weight loss 16-20%
4	Above signs plus any of the following: Loss of righting reflex, unresponsive, weight loss greater than 20%, paralysis (full or partial)
5	death

8.2: Time of addition results using 1 MOI of RV733.

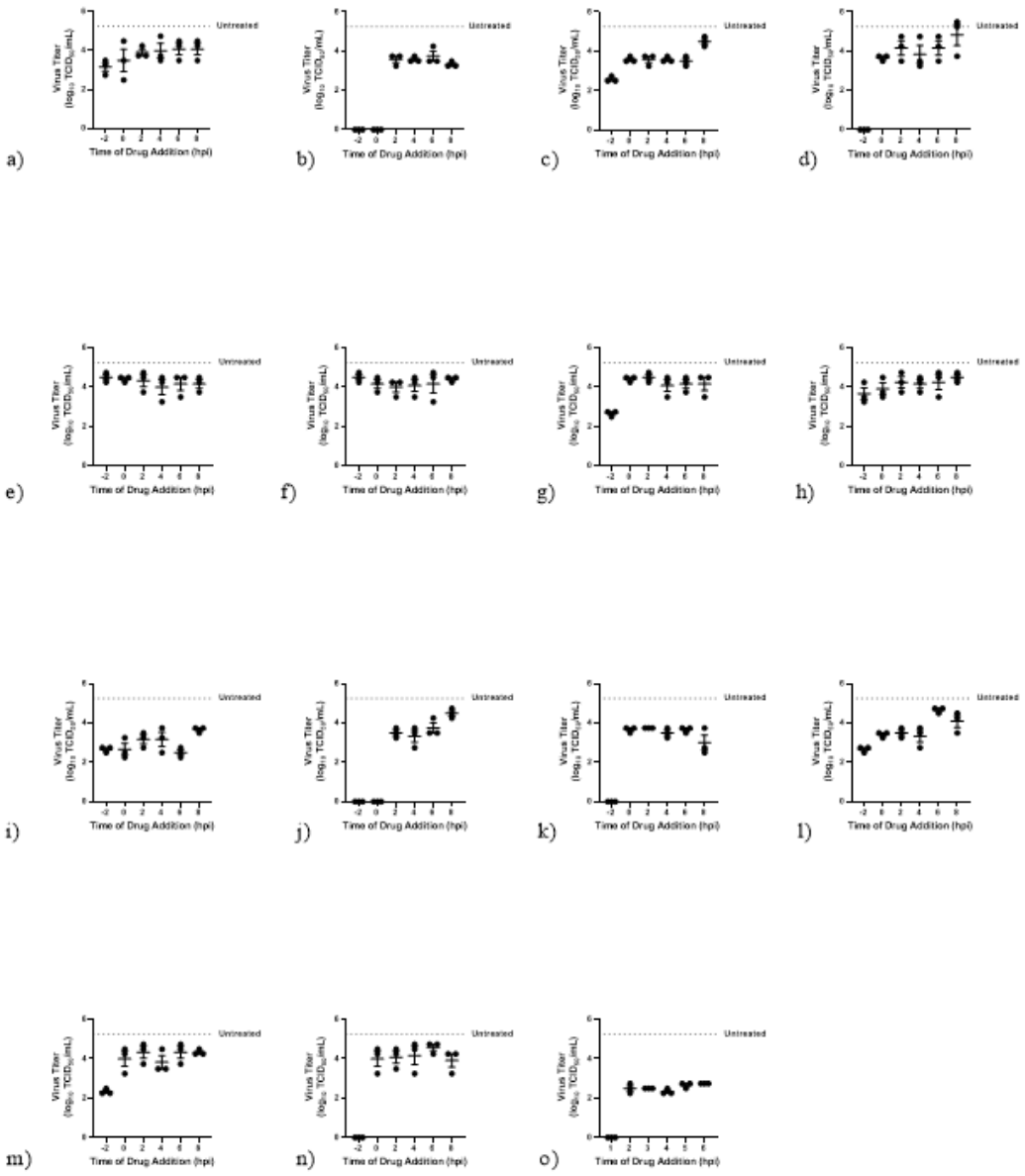

Time of addition assay results for teriflunomide (a), antazoline HCl (b), domiphen bromide (c), sodium aescinate (d), phloretin (e), solamargine (f), calycosin-7-glucoside (g), mulberroside A (h), diosmetin (i), dioscin (j), oridonin (k), polyphyllin B (l), kinetin (m), progesterone (n), and oseltamivir (o). Data points represent the means of biological triplicates, each containing 2 technical replicates, and error bars indicate SEM. MDCK cells grown to ~80% confluent were seeded in 12-well plates 24 h prior to the assay. The following day, 1 MOI of RV733 IAV was allowed to pre-adsorb on ice for 1 h, after which the cells were washed 3X with PBS and incubated at 37º. Subsequently, $10IC_{95}$ of the specified compound (determined by yield assay results) was then added at the specified time point (-2 to 0, 0 to 2, 2 to 4, 4 to 6, 6 to 8, 8 to 10 hpi), after which the well was washed with PBS and incubated until 24 hpi had been reached. The supernatants were then harvested, and stored at -80°C until quantification. Viral titers were determined by titration of samples in a standard $TCID_{50}$ assay and titers calculated using the method of Reed and Muench for estimating 50% endpoints[193]. Virus control wells contained virus added for an adsorption step of -1 – 0 hpi.

8.3: Uninfected, Dye IFA Controls

a) b) c) d)

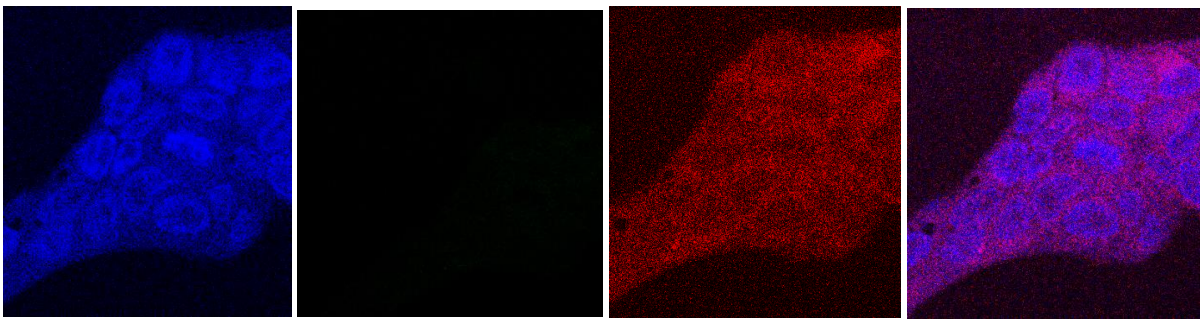

Immunofluorescence assay results for uninfected cells stained with HA antibody and CellVue membrane dye. Panel A shows the DAPI nuclear stain, panel B shows HA antibody fluoresence, panel C shows CellVue membrane dye, and panel D presents the merged image of all three channels. Images were acquired using a Zeiss confocal microscope at 20X magnification, displaying a field of view of approximately 0.9 mm. The image set was captured at 90 mpi.